ÉCOLE DE TECHNOLOGIE SUPÉRIEURE
UNIVERSITÉ DU QUÉBEC

MANUSCRIPT-BASED THESIS PRESENTED TO
ÉCOLE DE TECHNOLOGIE SUPÉRIEURE

IN PARTIAL FULFILMENT OF THE REQUIREMENTS
FOR THE DEGREE OF DOCTOR OF PHILOSOPHY
Ph. D.

BY
Amir MOFIDI

SHEAR STRENGTHENING OF REINFORCED-CONCRETE BEAMS USING
ADVANCED COMPOSITE MATERIALS

MONTRÉAL, 31 JULY 2012

THIS THESIS HAS BEEN EVALUATED

BY THE FOLLOWING BOARD OF EXAMINERS

Dr. Omar Chaallal, Thesis Supervisor
Department of Construction Engineering, École de Technologie Supérieure

Dr. Marie-José Nollet, Member of the Board of Examiners
Department of Construction Engineering, École de Technologie Supérieure

Dr. Vladimir Brailovsky, President of the Board of Examiners
Department of Mechanical Engineering, École de Technologie Supérieure

Dr. Yixin Shao, External Member of the Board of Examiners
Department of Civil Engineering, McGill University

THIS THESIS WAS PRESENTED AND DEFENDED

BEFORE A BOARD OF EXAMINERS AND PUBLIC

18 JULY 2012

AT ÉCOLE DE TECHNOLOGIE SUPÉRIEURE

ACKNOWLEDGMENTS

There are many people I must thank for their various forms of support and appreciation towards me.

First of all, I thank my family. Their love, support and encouragement were essential for the completion of my Ph.D. program.

I offer my sincere gratitude to my Ph.D. advisor, Professor Omar Chaallal. His excellent advice, support and friendship have been invaluable on both an academic and a personal level, for which I am extremely grateful.

I very much appreciate the efficient collaboration of Mr. John Lescelleur (senior technician) and Mr. Juan Mauricio Rios (technician) at ÉTS structural laboratory, in conducting the experimental tests.

SHEAR STRENGTHENING OF REINFORCED-CONCRETE BEAMS USING ADVANCED COMPOSITE MATERIALS

Amir MOFIDI

ABSTRACT

This Doctorate program focuses on the shear strengthening of reinforced concrete (RC) beams using fibre-reinforced polymers (FRP) composites. Several research problems related to shear strengthening still linger and therefore require further research studies to be entirely solved. The main objective of this program is to experimentally and analytically study the FRP strengthening methods of full-scale RC T-section beams in shear. During this Ph.D. program major aspects related to shear strengthening of RC beams with fibre-reinforced polymers (FRP) sheets and rods are investigated as follows: 1) Shear strengthening of RC beams with externally-bonded (EB) FRP-Influencing factors and conceptual debonding model: On the basis of this effort, a new design approach is proposed to calculate the shear contribution of the FRP considering the effect of the transverse steel (among other influencing parameters) on the FRP contribution in shear resistance. The proposed model shows the best correlation with experimental results in comparison with the current design codes and guidelines; 2) Performance of end-anchorage systems for RC beams strengthened in shear with epoxy-bonded FRP composites: The results of this study reveal that specimens retrofitted with EB FRP methods and properly designed end-anchorage systems can achieve a superior contribution to shear resistance compared to specimens strengthened using EB FRP with no anchorage and Near-Surface Mounted (NSM) rebar method; 3) Shear strengthening of RC beams with EB FRP- Effect of strip-width to strip-spacing ratio: An experimental and analytical investigation with emphasis on the effect of strip-width to strip-spacing ratio on the contribution of FRP (V_f) in shear strengthened of RC beams with EB FRP strips is carried out; and 4) Behaviour of RC beams strengthened in shear using embedded through-section (ETS) FRP rods method: A newly developed shear strengthening method is investigated Embedded through-section (ETS) FRP rod method is a promising method for strengthening RC beams in shear using FRP rods. In the ETS method, FRP rods are epoxy-bonded to pre-drilled holes through the cross section of the RC beams. The test results not only confirmed the feasibility of the ETS method, but also revealed that the performance of the beams strengthened using this method is significantly superior to that of the beams strengthened with EB FRP and NSM FRP methods.

RENFORCEMENT EN CISAILLEMENT DES POUTRES BÉTON ARMÉ À L'AIDE DE MATÉRIAUX COMPOSITES AVANCÉS

Amir MOFIDI

RÉSUMÉ

Cette thèse de doctorat traite du renforcement en cisaillement de structures en béton armé (BA) à l'aide de matériaux composites en polymère renforcé de fibres (PRF). De nombreuses problématiques de recherche reliées au renforcement en cisaillement n'ont pas encore été résolues à ce jour. L'objectif principal du présent est d'étudier expérimentalement et analytiquement les méthodes de renforcement en cisaillement de poutres de section en Té en BA à l'aide de PRF. Le programme considère plusieurs aspects majeurs reliés au renforcement en cisaillement de poutres en BA à l'aide de tissus et de tiges en PRF, comme suit: 1) Renforcement en cisaillement de poutres en BA à l'aide de PRF collé en surface (EB: *Externally Bonded*) – Facteurs d'influence et modèle conceptuel de délamination: Sur la base des résultats obtenus, une nouvelle approche de design est proposée pour le calcul de la contribution au cisaillement du PRF tenant compte de l'influence de l'acier transversal (entre autres) sur la contribution du PRF à la résistance globale. Le modèle proposé montre une meilleure corrélation avec les résultats expérimentaux en comparaison aux codes et guides en vigueur; 2) Performance de systèmes d'ancrage pour poutres en BA renforcées à l'aide de PRF collé en surface: Les résultats de cette étude révèlent que les spécimens renforcés par la méthode PRF EB avec des ancrages adéquatement conçus peuvent atteindre des contributions à la résistance en cisaillement supérieures á ceux sans système d'ancrage et ceux renforcés à laide de la méthode NSMR (*Near-Surface Mounted Rebar*) ; 3) Renforcement en cisaillement de poutres en BA à l'aide de PRF EB: Effet du rapport largeur sur espacement des bandes en PRF : Investigation expérimentale et analytique investigation avec emphase sur l'effet du rapport largeur sur espacement des bandes en PRF sur la contribution du PRF (V_f) dans les poutres renforcées en cisaillement à l'aide de bandes en PRF EB est menée ; et 4) Comportement des poutres en BA renforcées à l'aide de la méthode ETS (*embedded through-section*) : Une méthode novatrice développée pour le renforcement en cisaillement est explorée. Cette méthode est très prometteuse pour le renforcement en cisaillement. Dans cette méthode, des tiges en PRF sont insérées et scellées à l'aide d'époxy dans des trous préalablement percés à travers l'âme de la poutre en BA. Les résultats d'essais ont confirmé la faisabilité de la méthode ETS, mais aussi révélé que la performance des poutres renforcées à l'aide de cette méthode est substantiellement supérieure à celle des poutres renforcées à l'aide de PRF EB et NSMR.

Mots clés: Polymère renforcé de fibres, Poutre béton, Renforcement, Résistance au cisaillement

TABLE OF CONTENTS

Page

LIST OF TABLES

LIST OF FIGURES

Page

LIST OF SYMBOLS

A_f	Area of the cross-section of an FRP sheet or strip $= 2n.t_f.w_f$
A_{fv}	Area of the cross-section of an FRP sheet or strip $= 2n.t_f.w_f$
A_s	Area of the cross-section of steel stirrup
b	Width of the concrete-beam cross-section
b_c	Width of concrete member
b_f, b_p	Width of bond area
b_w	Concrete section web width
c_f	Constant determined using the results of shear tests
d	Effective depth of the concrete beam
d_f	Distance from the extreme compression fibre to the centroid of tension reinforcement
D_f	Stress distribution factor
E_f	Elastic modulus of FRP in the principal fibre-orientation direction
f'_c, f_{ck}, f_{cm}	Cylindrical compressive strength of concrete
f_{ctm}	Average surface tensile strength of concrete
f_{fd}	Design value for the ultimate FRP stress
f_{fdd}	Design value for the FRP debonding stress
$f_{fd,\text{mam}}$	Maximum design stress in FRP
f_{fe}	Effective stress of FRP
f_{fed}	Design value for the FRP effective stress
f_{fu}	Ultimate FRP tensile stress

f_{ct}	Concrete tensile strength
G_{fk}	Bonded joint specific fracture energy
h_{fe}	Effective height of the bonded reinforcement
h_w	Concrete cross section web height
k_1	Concrete-strength modification factor
k_2	Wrapping-scheme modification factor
k_b	Covering / scale coefficient
k_p	Factor related to the width of the bonded plate and the width of the concrete member
L	FRP fiber length
L_e	Effective anchorage length of FRP
L_{max}	Maximum available bond length
n_f	Number of FRP layers
P_{bond}	Bond shear force in the equivalent rectangular area
P_{fe}	Effective resisting force in the FRP
P_{max}	Force that can be developed in the sheet on one side of the beam
P_u	Ultimate bond strength
r_c	Corner rounding radius
R_L	Ratio of FRP effective width to total FRP width
R^2	Coefficient of determination
R^*	Reduction factor, a function of $E_s A_s / E_f A_f$
s_f	Spacing between FRP strips

s_{uf}	FRP slip at debonding (0.20mm)
t_f	Thickness of FRP composite
V_c	Contribution of concrete to shear
V_f	Contribution of FRP to shear as defined in ACI 440 2R-08 and CSA-S806
V_{frp}	Contribution of FRP to shear as defined in CSA-S06
$V_{f\,cal}$	Contribution of FRP to shear as calculated by models
$V_{f\,exp}$	Experimental contribution of FRP to shear
V_n	Nominal shear resistance at the ultimate limit state
V_s	Contributions of internal steel reinforcement to shear
w_f	Width of an FRP strip
w_{fe}	Effective FRP width
α	Angle of inclination of the FRP fibres
β	Shear-slip coefficient (set equal to 0.315 times the 95th percentile characteristic value of the bond strength proposed by Chen and Teng (2001))
β_c	Concrete-cracking coefficient based on transverse-steel and FRP rigidity values
β_L	Coefficient to compensate for insufficient FRP anchorage length
β_w	FRP-width-to-spacing-ratio coefficient
γ_{fd}	Partial safety factor depending on the application quality
γ_{rd}	Partial factor for the resistance model (1.2)
ε_{fe}	Effective strain of FRP
ε_{fu}	Maximum strain of FRP
ϕ_R	Reduction factor due to local stress in corners

κ_v	Bond-reduction coefficient
λ	Normalized maximum bond length
θ	Angle of concrete shear crack
ρ_f	FRP strengthening ratio $= (2n.t_f/b).(w_f/s_f)$
ρ_s	Transverse-steel ratio $= A_v/b_w.s$
ρ_{tot}	Total shear-reinforcement ratio $= n.\rho_f + \rho_s$
τ_{eff}	Average bond shear stress at failure

INTRODUCTION

A large number of aging civil infrastructures are known to be structurally deficient at the present time. Three decades of delayed maintenance work have created a situation where if the deterioration is not halted, the associated costs will escalate exponentially (Mofidi 2008). Structural deficiencies in bridge girders are usually the result of deterioration caused by ageing, exposure to harsh environments, and higher traffic demands.

During last decades, Fibre-Reinforced Polymers (FRP) have received much attention for a variety of applications in strengthening of defective structures due to their technical and economical advantages. The outstanding mechanical characteristics of FRP combined with its high strength-to-weight ratio, corrosion resistance and easiness of handling and application make the FRP composites a variable strengthening alternative material.

The area of advanced composites in strengthening structures has been one of the fastest growing areas within civil engineering during the decade. Much focus and effort has been placed on understanding the behaviour of the concrete structures strengthened with FRP. Common structural deficiencies of deteriorated bridge girders are their inadequate shear strength or their low flexural and displacement ductility capacities. Strengthening of beams and slabs in flexure and confinement of columns are well documented. However, a review of research studies on shear strengthening reveals that experimental investigations are still needed to encompass T-section beams and joints. Most of the few research studies that have been performed in strengthening RC beams in shear were conducted on rectangular RC sections. The previous tests were mostly conducted on small size beams that may perform differently from Full-scale girder in several aspects. Besides, FRP debonding failure mode that leads to a premature beam failure in a brittle manner is still a disadvantage for the beams strengthened with FRP. This doctorate study is aimed to address these shortcomings.

CHAPTER 1

RESEARCH FOCUS AND OBJECTIVES

1.1 Problem definition

In Quebec and Canada, many of the ageing reinforced concrete (RC) infrastructures suffer from serious degradation of materials. This degradation, which is severe in Quebec's bridges, is due to the effect of steel reinforcement corrosion, the action of freeze-thaw cycles and increased use of de-icing salts. The degradation of the bridges combine with structural deficiencies due to changes in operating loads and more stringent new design codes has created a critical situation for the bridge inventory in Quebec and Canada.

According to Statistics Canada (2012), the useful life of a bridge in Canada is set at 43.3 years. The average age of bridges in Canada is 24.5 years compared to 31 years in Quebec. In addition, 57% and 72% (the highest ratio in the nation) of bridges in Canada and Quebec respectively have exceeded their useful life.

In Quebec and Canada, many girders were designed on the basis of the pre-1970s codes and standards. In fact, about 80 per cent of Quebec roads and bridges were built in the 1950s and 1960s. Several researchers pointed out that previous design provisions did not have a comprehensive understanding of the shear behaviour. As a result, pre-1970s designs might be deficient in shear according to current codes. Such deficient beams, would fail suddenly and without warning, even before the element reaches its full capacity in flexure, once their shear capacity is reached. The collapse of "de la Concorde" overpass in Laval is a tragic example of sudden and without warning shear failure in concrete bridges that led to loss of life and significant economic disruption. In this respect, Mr. Sam Hamad, former Minister of Transportation of Quebec, noted that the "de la Concorde" overpass did not meet the load capacity for modern trucks. So far, there is no statistical data on the number of deficient bridges in shear in Quebec. However, it may be instructive to consider that in the province of

Alberta among 5000 bridges that required strengthening, more than 3000 (60%) showed deficiency in shear.

Since the "de la Concorde" overpass collapse, Premier Jean Charest's government has earmarked $21 billion for infrastructure. Following the incident, 135 bridges and overpasses were inspected in recent months after being identified for potential safety risks. The transport ministry decided to replace 28 bridges and overpasses conduct extensive repairs on 25 more, and reinforce four bridges from the list of 135. Replacing a large number of the deficient bridges at the same time requires enormous Federal and Provincial investments. Rehabilitation of those bridges seems to be a better alternative as it is faster, safer and more economical. According to recently published report on Champlain bridge by Ministère des Transports du Québec (2011), the estimated cost for a new bridge to replace the current Champlain bridge is $1.282 billion. Federal Canadian government issued $5 billion to replace the existing Champlain bridge. Whereas, prolonging the life of the current Champlain Bridge would only cost as much as $25 million a year for the next decade.

Historically, concrete members have been repaired by post-tensioning or jacketing with new concrete in conjunction with a surface adhesive (Klaiber et al. 1987). Since the mid 1960s epoxy-bonded steel plates have been used to retrofit flexural members (Dussek 1980). Steel plates have a durability problem inherent to this technique, because corrosion may occur along the adhesive interface. This type of corrosion adversely affects the bond at the steel plate/concrete interface and is difficult to monitor during routine inspection. Additionally, special equipment is required to install the heavy plates.

Recently FRP composites have been increasingly used in rehabilitation and strengthening of concrete structures. The advantages of using composites are mainly due to their high modulus of elasticity, lightness, corrosion resistance, and adaptable electromagnetic properties. To date, various FRP rehabilitation methods are being applied in practice for strengthening and improvement of RC concrete beams. Although the technique of using FRP in structural rehabilitation has proven its feasibility and viability during the last two decades, more comprehensive research studies in some specific areas are still in need.

1.2   Scope of work and objectives

Scope of work

This PhD program deals with the shear strengthening of RC beams using fibre-reinforced FRP composites. Due to its complexity, the shear strengthening of RC members with externally bonded (EB) FRP still has numerous research problems that require further investigation to be completely solved (e.g., accurate analytical models; FRP debonding; effect of transverse steel). Recent findings have highlighted major influencing parameters related to shear strengthening with EB FRP that have still not been captured by existing theoretical predictive tools (e.g., effect of transverse steel among others), including the codes and guidelines. A new design method is proposed in this PhD program to consider the effect of transverse steel in addition to other influencing factors on the shear contribution of FRP. The accuracy of the proposed equations has been verified by predicting the shear strength of experimentally tested RC beams using data collected from the literature. On the other hand, current methods in shear strengthening of RC beams with FRP present shortcomings such as: (i) concrete strata; (ii) surface preparation; (iii) protection (vandalism /fire); (iv) debonding. In this PhD program new shear retrofitting methods has been developed to increase the shear capacity of RC beams. The new methods present many advantages over existing methods such as EB FRP sheet method and near-surface mounted (NSM) FRP rod method. Unlike the current methods where the FRP relies on the concrete cover of RC beams, in the new methods FRP relies on the concrete core of the RC beam which offers a greater confinement and hence improves bonding performance. The proposed methods to prevent FRP debonding in this program are: (1) Embedded through-section (ETS) FRP rods method; (2) New end-anchorage systems for FRP U-jackets. The results of the analytical and experimental research studies reveal that the performance of the beams strengthened using these methods are far more superior to that of the beams strengthened with EB FRP and NSM FRP methods.

The results of this Ph.D program are reported in five published articles in international refereed journal papers and three articles in press.

Objectives

The main objective of this program is to study the behaviour of RC beams strengthened with FRP material in shear.

The specific objectives are:

a) to experimentally and analytically study different rehabilitation methods of full-scale RC T-section beams in shear using FRP sheets, strips and rods;

b) to investigate the design procedures in the guidelines to evaluate the shear contribution of EB FRP in the shear resistance of retrofitted RC beams. To review existing design proposals and to highlight their deficiencies;

c) to study the effect of certain parameters which have been proven to influence the shear resistance of EB FRP, but which have not been sufficiently documented in the guidelines (e.g., cracking pattern; FRP anchorage length; FRP strip width to spacing ratio etc.);

d) to better understand the interaction between internal transverse steel and external FRP reinforcement. To realize the effect of the steel and FRP transverse reinforcement on concrete cracking pattern and FRP debonding;

e) to develop a transparent, rational, and evolutionary design model for the shear resistance of FRP-strengthened beams which fail by FRP debonding. It is thought that such a design proposal will offer an improvement to the current debonding design equations in the guidelines;

f) to analyze the behaviour of RC beams strengthened in shear with the ETS FRP rods by varying the influencing parameters;

g) to identify different failure modes in beams strengthened with the ETS method;

h) to study the mechanics of interaction between the concrete and the FRP rod in the RC beams strengthened in shear using the ETS FRP rod method;

i) to propose a rational design approach to calculate the shear contribution of FRP for the RC beams strengthened in shear with the ETS method;

j) to study the feasibility and effectiveness of new rehabilitation methods of strengthening beams in shear to prevent FRP debonding;

k) to study the feasibility and practicality of new mechanical end-anchorage systems in FRP U-jackets.

1.3 Research significance

Most of the research activities on the use of FRP in strengthening RC beams were directed to enhancing their flexural capacity. For the few research studies that have been undertaken in strengthening RC beams in shear, most of the researches were conducted on RC rectangular sections (Bousselham and Chaallal 2004). Despite the fact that RC T-section and AASHTO type are the most popular shape of girders used in bridges. Research data on shear strengthening is very limited, and often times produced conflicting conclusions. In addition, such research is often limited to small-size rectangular beams. Experimental research data is not available for large-scale girders deficient in shear and retrofitted with FRP. Moreover, recent findings revealed that major aspects related to shear strengthening of RC beams with EB FRP are still not captured by the existing theoretical predictions (Bousselham and Chaallal 2008).

The results of this Ph.D. program will provide us with a better understanding of the behaviour of shear deficient beams in bridges that will be strengthened with FRP sheets, strips and rods. The effect of various influencing parameters will be considered on the strengthened beams. Moreover, this research consolidates the scientifically progressive position of the research in this innovative area in Québec and Canada. Especially since several companies in Québec and Canada work or commercialize composite materials inside or outside the nation. This study can provide guidance to the structural engineers and

companies when using different strengthening methods using FRP composites in future projects.

In the first part of this Ph.D program, a transparent and rational design model for the shear resistance of FRP-strengthened RC beams, the failure of which is by FRP sheet debonding, was proposed. This research was initiated with a comprehensive literature review on the previous research studies in this area. It has been realized that the effect of transverse steel on the shear contribution of FRP for RC beams strengthened in shear with FRP is already established but is not considered by any existing international or national codes or guidelines. In addition, the major factors influencing the shear contribution of EB FRP and the role of these factors in the current design guidelines were collected. Finally, a new design approach for calculating the shear contribution of FRP, taking into consideration the effect of transverse steel on the EB FRP contribution in shear was proposed. The effectiveness of the proposed method was verified using experimental results available in the literature. The accuracy of the proposed model was superior compared to available design codes and guidelines. The results of this research were published in the forms of journal article and conference papers. The mentioned article, "Shear strengthening of RC beams with EB FRP-influencing factors and conceptual debonding model" in published to Journal of Composites for Construction, ASCE, which is one of the most prominent journals that deals with the use of FRP materials in construction.

In the second part of this Ph.D program, a series of exploratory tests on RC beams strengthened in shear using the Embedded Through-Section (ETS) FRP rods were conducted. The effectiveness of the newly developed strengthening method was compared with EB FRP sheet and NSM FRP rod shear strengthening methods. The outcome of the tests were analysed and published in the form of a journal article called, "Embedded through-section FRP rod method for shear strengthening of RC beams: performance and comparison with existing techniques". The article is also published in the Journal of Composites for Construction, ASCE.

In the third part of this doctorate program, the available equations in current international design codes which consider the effect of strip-width to strip-spacing of FRP strips in RC

beam strengthened in shear were critically reviewed. Current equations used in codes and guidelines to consider the effect of strip-width to strip-spacing of FRP strips are proposed based on FRP-to-concrete direct pull-out tests on FRP strips bonded to concrete blocks. The applicability of the mentioned equations for RC beams strengthened in shear with FRP strips was not validated. The results of this study reveals that previous equations do not predict accurate results when the strip-width to strip-spacing ratio is greater than 0.5. More accurate equations were proposed where the effect of strip-width and strip-spacing of FRP strips is taken into account. To check the accuracy of the equations in predicting the contribution of CFRP strips to the shear resistance of beams strengthened with CFRP strips, the results of the experimental part of this study on beams strengthened with CFRP strips were considered. The study showed that the predictions based on the proposed equations were more accurate than those based on the design guidelines. The findings of this research can be incorporated into the codes and standards to better predict the shear contribution of FRP in RC beams strengthened in shear. The outcome of the research was published as a journal article in Journal of Composites for Construction, ASCE. The title of the article is, "Shear strengthening of RC beams with externally bonded FRP composites: effect of strip-width to strip-spacing ratio".

In the fourth part of this doctorate program, an experimental investigation on the performance of full-scale RC T-girders strengthened in shear using EB FRP U-jackets end-anchored with different systems was conducted. Debonding of FRP, particularly in shear, is a major failure mode when using FRP sheets to strengthen concrete structures. Design code provisions and guidelines related to shear strengthening of RC beams using EB FRP suggest the use of end-anchorage systems to prevent FRP debonding. However, no guidelines are available to design effective end-anchorage systems. The main objective of this study is to evaluate the effectiveness of different end-anchorage systems for RC beams strengthened using EB FRP methods. The results of this study are published in the form of a journal article entitled, "Performance of end-anchorage systems for RC beams strengthened in shear with epoxy-bonded FRP".

At the end of this doctorate program, an analytical and experimental investigation was conducted to better understand the behaviour of RC T-beams strengthened in shear with ETS FRP rods by varying different parameters. The ETS FRP rod method was proven to be a promising method to increase the shear strength of RC beams. The parameters considered were: (i) the effect of the surface coating on the FRP bars; (ii) the effect of internal transverse-steel reinforcement on the FRP shear contribution; (iii) the effect of FRP bar spacing; (iv) the effect of FRP rod diameter; and (v) the efficiency of the embedded through-section FRP rod method. New design equations were proposed to calculate the shear contribution of FRP for beams strengthened using the ETS FRP method. The design equations were validated against results obtained from the experimental part of the research study.

The promising results of this study were shared with the Ministère des Transports du Québec (MTQ) by Prof. Omar Chaallal, Ph.D supervisor, and with the shear sub-committee of Canadian Standard CSA-S806 that he presides. Positive feedbacks were received in all the mentioned cases.

As this method develops, the structural behaviour of RC beams strengthened with the ETS method needs to be thoroughly characterized and the influencing parameters addressed. The new method can be used to rehabilitate the RC beams and bridge girders in a safer, faster and more economical way. Comprehensive analytical and experimental investigations are still required to completely understand the behaviour or RC beams strengthened with the ETS FRP rod method.

1.4 Outline of thesis

The research work in this study is reported in seven chapters. Chapter 1 provides a brief introduction and discusses the objectives and scope of the research work. Chapter 2 provides a literature review of the previous research topics related to the current work. Chapter 3 presents the first published article in this Ph.D program. The article is titled "Shear strengthening of RC beams with EB FRP-influencing factors and conceptual debonding model". Chapter 4 titled,

"Performance of end-anchorage systems for RC beams strengthened in shear with epoxy-bonded FRP", presents the published article based on the exploratory tests on the RC beams strengthened with the ETS method. Chapter 5 presents the third article published during this Ph.D program. The article is titled "Shear strengthening of RC beams with externally bonded FRP composites: effect of strip-width to strip-spacing ratio". Chapter 6 titled, "Performance of end-anchorage systems for RC beams strengthened in shear with epoxy-bonded FRP", presents the published article based on the experimental tests on the RC beams strengthened with end anchored EB FRP sheets. Chapter 7 presents the fifth article published during this Ph.D program. The article is titled "Experimental tests and design model for RC beams strengthened in shear using the embedded through-section FRP method". Finally, conclusions and recommendations for future work are provided.

CHAPTER 2

BACKGROUND AND LITERATURE REVIEW

2.1 Utilization of FRP sheets and rods in shear strengthening of reinforced-concrete (RC) beams

Recently researchers paid more attention to the potential applications and benefits of using FRP in retrofitting RC elements. This is due to the attractive characteristics of FRP, such as its high strength to density ratios, corrosion resistance and high fatigue performance. The area of advanced composites in strengthening structures has been one of the fastest growing areas within civil engineering during the last decade. Much focus and effort has been placed on understanding the behaviour of the concrete structures strengthened with FRP. Strengthening of beams and slabs in flexure and confinement of columns have been well documented. However, a review of research studies on shear strengthening reveals that experimental investigations are still needed to encompass T-section beams. Most of the few research studies that have been performed in strengthening RC beams in shear were conducted on rectangular RC sections. The previous tests were mostly conducted on small size beams that may perform differently from full-scale girders in several aspects.

2.2 Externally-bonded (EB) FRP sheets strengthening method

As it was mentioned previously, most of the research activities on the use of FRP in strengthening RC beams were directed to enhancing their flexural capacity. For the few research studies on strengthening RC beams in shear, most of them were conducted on RC rectangular sections. This is not representative of the fact that most RC beams would have a T-section due to the presence of top slab. To date, most of the research conducted on strengthening RC T-beams in shear focused on enhancing the shear strength of the beam by utilizing the contribution of the FRP through bond with the exterior faces of the beam.

Different shear strengthening configuration using FRP are categorized as: complete FRP wraps covering the whole cross section (i.e., complete wrapping, valid only for rectangular sections), FRP U-jackets covering the two sides of the tension face (i.e., U-jacketing) and FRP sheets glued only onto the two sides of the beam (i.e., side bonding).

By 2004, the most effective FRP strengthening configuration for T-section beams were proven to be FRP U-Jackets (Bousselham and Chaallal 2004). This section provides a comprehensive review of all the papers related to reported experimental investigations on shear strengthening with externally bonded FRP. The review is presented in a chronological order, to allow a better understanding on the evolution of the findings of the research effort, as well as the issues involved as the research progressed. For each paper, the review provides information on the objectives, the methodology, the experimental program, the test method, the FRP used and its orientation, as well as the strengthening scheme (FRP configuration) used.

Berset (1992)

The first study of shear strengthening with FRP was carried out by Berset (1992). Through a series of tests, he examined the shear behaviour of reinforced concrete beams retrofitted with GFRP composite. Six rectangular beams with dimensions 102 mm × 114 mm × 600 mm were tested, targeting the following two parameters: (i) the thickness of the GFRP composite and (ii) the effect of transverse steel. The GFRP composite fabric used was bonded onto the beam sides at an angle of 45°. The beams with no transverse steel, retrofitted with FRP, failed in shear with debonding of the FRP composite. The gain in shear obtained was a function of the FRP thickness and a 33% to 66% improvement was attained. By contrast, the beams containing transverse steel failed in flexure. The model developed by the author is based on the truss analogy. The maximum FRP strain, which is an important variable in the model, is drawn from these tests. This investigation, recognized by the author as exploratory, showed that the FRP retrofit technique may result in an enhancement of shear resistance. In its conclusions, the author drew attention to the scale effect, particularly for small specimens such as the ones considered in this study.

Uji (1992)

Uji (1992) tested eight rectangular concrete beams of dimensions 100 mm × 200 mm × 1300 mm, strengthened with CFRP composite. The investigation targeted the following parameters: (i) the strengthening scheme, i.e., wrapped versus bonded on the sides and (ii) the effect of transverse steel (by studying sections with and without transverse steel reinforcement). The shear ratio (a/d) was fixed at 2.5. The predominant failure mode of the test beams was by debonding of the composite. The latter never reached more than 30% to 50% of its ultimate resistance. The author observed that the FRP strains were greater than those of transverse steel and therefore concluded that the shear capacity is governed by the bonding mechanism at the concrete-FRP interface.

Al Sulaimani et al. (1994)

Al Sulaimani et al. (1994) investigated the behaviour of concrete beams that were pre-cracked before being retrofitted in shear with GFRP. Two series of tests were performed, one series with and the other without additional strengthening with GFRP in flexure. Each series included eight rectangular beams of dimensions 150 mm × 150 mm × 1250 mm and considered the following composite configurations: (a) composite in two forms, strips or continuous fabric and (b) composite bonded on the sides or wrapped in a U-configuration.

It was observed that the beams retrofitted with GFRP strips or continuous GFRP fabric without additional strengthening in flexure failed by debonding. The remaining specimens failed in flexure. The cracks developed followed the same crack pattern initiated during the pre-cracking phase. To evaluate the contribution of the composite, the authors considered the average shear stress at the concrete-FRP interface, which was determined to be 1.2 MPa in the case of strips and 0.8 MPa in the case of continuous fabric. The authors concluded that the U-shaped wrap is more effective in preventing debonding.

Chajes et al. (1995)

Chajes et al. (1995) tested twelve T-section beams of dimensions 63 mm × 190 mm, having a span of 1220 mm, with no transverse steel reinforcement. Three types of FRP were used:

glass, aramid, and carbon. The FRP fabric was wrapped around the web in a U-shape over the entire beam length, at two different angles (0°and 90°) with respect to the longitudinal axis. In the case of CFRP, two more wrap angles were tested: 45° and 135°. The specimens were subjected to four-point loads with a shear ratio a/d of 2.7. All the specimens failed in shear and no debonding of the FRP was observed in any of the specimens. The shear resistance increased by 60% to 150% and the strain measured at failure was approximately ε = 0.005. The latter observation was used by the authors to evaluate the contribution of FRP to shear resistance. No distinction was made between the different types of FRP fibres or their orientations.

Sato et al. (1996)

Sato et al. (1996) carried out a series of tests on ten rectangular concrete beams of dimensions 200 mm × 300 mm × 2200 mm, retrofitted in shear with CFRP. The following parameters were studied: (i) the influence of the FRP strengthening scheme, i.e., bonded on the sides versus wrapped in a U pattern, and FRP strips versus continuous fabric, and (ii) the influence of the transverse steel reinforcement.

The test results indicated that the specimens with no transverse steel reinforcement failed by debonding of FRP. They also indicated that the gain in resistance due to U-wrapping of FRP is 60% greater compared to FRP bonded onto the sides. In the model presented, the authors refer to the bonding mechanism at the concrete-FRP interface to describe the failure mode by debonding.

Miyauchi et al. (1997)

Miyauchi et al. (1997) presented the results of tests performed on a series of seventeen beams strengthened in shear with CFRP. The specimens had a rectangular section of 125 mm × 200 mm and a span between supports of 1400 mm. The experimental program considered the following parameters: (i) the strengthening scheme (CFRP strips with three different spacings versus continuous fabric with one or two layers) and the FRP ratio, (ii) the content

ratio of the transverse steel reinforcement, and (iii) the shear length ratio which varied between 1.0 and 3.0.

On the basis of these tests, the authors concluded that the rate of increase in the strain on CFRP was greater than that of the strain on steel and proposed a relation which describes the observed interaction. To calculate the contribution of FRP to shear resistance, they adopted the truss analogy by applying a reduction factor of 0.507 to the ultimate FRP stress.

It should be noted that only three of the FRP-retrofitted specimens without transverse steel failed in shear. The remaining specimens failed in flexure. Yet the authors developed their calculations on the basis of these latter specimens, which does not appear to be rational.

Taerwe et al. (1997)

Taerwe et al. (1997) present results of tests conducted on a series of seven rectangular concrete beams of dimensions 200 mm × 450 mm × 4000 mm, strengthened in shear with CFRP. The following parameters were targeted: (i) the influence of the strengthening scheme (U-wrap versus full wrap), (ii) the spacing of the strengthening additions, and (iii) the influence of the transverse steel ratio.

The tests showed that all but one of the strengthened specimens failed by debonding. In the specimen that did not fail by debonding, the FRP wrap fractured after crushing of concrete. Gains in capacity of 20% were achieved. The authors concluded that the contribution of FRP to the shear resistance can be calculated using the truss analogy.

Umezu et al. (1997)

Umezu et al. (1997) conducted a large experimental program on the use of FRP for shear strengthening and retrofit. Twenty-six rectangular concrete beams of various dimensions were tested. For all these tests, the shear ratio was kept constant and equal to 3.

Fourteen specimens were retrofitted with aramid (AFRP) and the rest with carbon (CFRP). The full-wrap composite was either continuous or in strip form and was applied over the entire shear length.

The authors observed two modes of failure: (i) failure of FRP after crushing of concrete and (ii) simultaneous rupture of FRP and concrete. As observed by the authors, the latter mode tends to occur with small FRP ratio. In addition, on the basis of the observation that the FRP never reached its full capacity, the authors proposed to apply a reduction factor to the tension resistance of FRP before using the truss analogy model. This factor, which represents the ratio of the resistance obtained by tests over the resistance obtained with the truss model, assuming that the full capacity of the FRP is attained, decreased when the FRP ratio increased. A maximum value of 0.4 is suggested by the authors for the reduction factor.

Funakawa et al. (1997)

Funakawa et al. (1997) tested five rectangular concrete beams of dimensions 600 mm × 510 mm × 5060 mm. Three specimens were retrofitted with one, two, or three layers of CFRP fabric full-wrapped over the entire shear length. A fourth specimen was strengthened with AFRP. The last specimen was maintained as control.

The specimens strengthened with one and two layers of FRP failed by fracture of the FRP, whereas with three layers the fracture of the FRP occurred well after rupture of the concrete in compression. From these results, it could be concluded that the FRP contribution to shear resistance increased with the number of FRP layers, and that the combination of aramid and carbon fibres can be effective for enhancing the stiffness of a retrofitted member.

Araki et al. (1997)

Araki et al. (1997) conducted an experimental program on a series of nine rectangular concrete beams of dimensions 200 mm × 400 mm × 3400 mm. They tested two parameters: (i) the FRP ratio and (ii) the type of fibres, i.e., aramid versus carbon. All the strengthened specimens, when tested, reached the maximum load without fracture of the FRP. Specimens showed shear tension failure mode. In this failure mode, the expansion of shear cracks due to the yielding of stirrups caused failure. In all specimens strengthened with the sheets, rupture of sheets could not be observed when the maximum load was achieved. Fracture occurred after failure of the specimen. FRP strain reached approximately two-thirds of the ultimate

strain capacity. The load-deflection curves show that after the formation of the first cracks, the smaller the FRP ratio, the greater was the loss of rigidity. To determine the FRP contribution to shear resistance, the authors used the truss analogy by reducing the tensile resistance of the FRP by an estimated factor of 0.60 for carbon and 0.45 for aramid.

Kamiharako et al. (1997)

Kamiharako et al. (1997) presented results of tests carried out on eight rectangular beams. Two series were considered, depending on the dimensions of the specimens: 250 mm × 400 mm × 3000 mm in Series 1, and 400 mm × 600 mm × 3000 mm in Series 2. The parameters studied were: (i) the rigidity of the FRP, which was applied as a full wrap and consisted either of aramid or carbon fibres, (ii) the influence of the resin used; the FRP was applied without resin in two specimens in Series 1, and (iii) specimen size. The beams were tested under three-point loads. The a/d ratio depends on the height of the specimen, since the shear length was kept constant at 1000 mm.

All the tested beams failed in diagonal tension. The gains in capacity due to FRP varied between 31% and 93%, depending on the rigidity of the FRP and the size of the specimens. As for rigidity, the reported values were greater for carbon than for aramid fibres. Regarding specimen size, the reported gains were greater in beams of Series 2 (height = 700 mm) than for beams of Series 1. However, it must be noted that the a/d ratio for Series 1 (2.5) is different from that of Series 2 (1.7). This would certainly influence the behaviour of the beams, particularly in terms of ultimate resistance. Therefore, the conclusions related to specimen size must be used with caution. Finally, concerning the influence of resin, the reported results indicated that the gains in capacity due to FRP are nil when the FRP is applied without resin.

Täljsten et al. (1997)

Täljsten et al. (1997) conducted a series of tests on eight concrete rectangular beams of dimensions 180 mm × 500 mm × 4500 mm. One of the objectives of the program was to study the shear behaviour before and after retrofit with CFRP. To this end, two of the three

control specimens were first tested to failure, then retrofitted, and then loaded again. The CFRP composite was applied onto the sides of the beams at an angle of 45°. The second objective was to evaluate three FRP application systems: (i) hand lay-up, (ii) pre-impregnation in combination with vacuum and heat, and (iii) vacuum injection. The distance between the applied loads was varied so as to ensure rupture by shear.

Only three tests out of ten were valid. For example, the specimens which were highly strengthened (two layers of FRP) failed by flexure, which was attributed by the authors to an underestimation of the shear capacity and a resulting under-design of the beams in flexure. The control specimens which were tested to failure before retrofit ruptured by debonding of the FRP at the FRP-concrete interface. The gain in shear resistance reached 100%. In the third beam, fracture of FRP and rupture of concrete occurred simultaneously. Finally, the authors noted that although the hand lay-up method of FRP application was easier and more convenient, the pre-impregnation and vacuum injection systems achieved better quality control.

Chaallal et al. (1998)

Chaallal et al. (1998-a) studied the performance of concrete beams under-designed in shear and retrofitted with CFRP strips bonded onto the sides of the beams. The experimental investigation included a series of eight beams, of rectangular cross section with dimensions 150 mm × 250 mm × 1300 mm. The parameter studied was the angle of orientation of the CFRP strips: 90° versus 135° with respect to the longitudinal axis.

The strengthened specimens failed by debonding of the CFRP strips. The CFRP did not have any effect on the rigidity of the beams in the initial phase of loading. However, their effect became apparent at the formation of the first cracks and increased with increasing applied load. In their conclusions, the authors noted that shear strengthening enhanced not only the shear capacity, but also the overall rigidity of the retrofitted beams, by inhibiting the propagation of cracks.

Mitsui et al. (1998)

Mitsui et al. (1998) investigated the influence of the shear length ratio a/d on the shear capacity of concrete beams retrofitted with FRP. They tested six rectangular beams with a cross section of 150 mm × 250 mm, strengthened with a full wrap of CFRP fabric.

Two parameters were examined: (i) the a/d ratio (two values were considered, 1.14 and 1.59) and (ii) the state of the beams. The latter parameter refers to the following three cases: Pre-loaded beam, lightly cracked and then retrofitted beam pre-loaded to failure, after which the cracks were repaired with epoxy injection before retrofitting of the beam with FRP. Beams strengthened with FRP with no pre-loading: No debonding was observed in any of the specimens. In all the specimens, the FRP fractured as the beam failed. The measured gain in the shear resistance varied between 30% and 80%. The specimens that were lightly pre-cracked and then retrofitted featured two cracking patterns: one corresponds to the cracks which occurred during the first pre-loading prior to the retrofit and the second corresponding to the cracks due to the second loading after the retrofit. It was also concluded that the contribution of FRP to the resistance tends to increase with the shear length ratio a/d.

Triantafillou (1998)

Triantafillou (1998) proposed a model to determine the contribution of FRP to the shear resistance of reinforced concrete beams. The model is based on the truss analogy by adopting the euro-code format. It was obtained by calibration of data collected by the author from the literature and from his own test results. The latter were obtained from a series of tests performed on rectangular concrete beams of dimensions 70 mm × 110 mm × 1000 mm, without transverse steel, strengthened in shear with CFRP strips. Two variables were tested: the FRP thickness and the angle of orientation (90° and 45°) with respect to the longitudinal axis.

In this model, the FRP strain, ε_{FRP}, constitutes the main variable. It is deduced, using the truss analogy, from the measured FRP contribution and then expressed in terms of the axial rigidity of the FRP, $\rho_{FRP}E_{FRP}$. The author noted in particular that the FRP strain decreased as

the rigidity increased. He also noted that the gain due to the FRP varies linearly with the rigidity up to an optimum value corresponding to $\rho_{FRP}E_{FRP}$= 0.4 GPa, after which it remains constant. The author suggested that this threshold be used as a design criterion.

However, the drawback of this model is that it covers two distinct modes of failure: fracture of FRP and debonding. In addition, the model fails to take concrete resistance into consideration (Khalifa et al. 1998).

Khalifa and Nanni (1999)

Khalifa and Nanni (1999) tested a series of twelve concrete rectangular beams of dimensions 150 mm × 305 mm × 3050 mm, strengthened in shear with FRP. The objective of the study was to study the influence of the following parameters: (i) the presence of internal transverse steel reinforcement, (ii) the shear length ratio a/d (at values of 3 and 4), and (iii) the strengthening configuration. This last parameter referred to the following schemes: (a) unidirectional U-shaped strips with two different widths, (b) unidirectional U-shaped continuous fabric, and (c) bidirectional continuous fabric bonded onto the sides of the beam only. The objective of comparing unidirectional with bidirectional FRP was to evaluate the effect of horizontal fibres on the shear resistance of FRP.

The specimens failed in shear by debonding of FRP. Examination of the test results confirmed that the contribution of FRP stabilized beyond a certain level of FRP axial stiffness. In some specimens, a 250% increase in the FRP ratio enhanced the total shear capacity by merely 10%. In the beams with transverse steel, given the applied load, comparison of CFRP strains with corresponding transverse steel strains shows that in presence of CFRP, the steel is less strained. As for the influence of the shear length ratio a/d, only two tests were valid, and these indicated a slight increase in shear capacity as the a/d ratio increased.

Khalifa et al. (1999)

Khalifa et al. (1999) tested nine continuous rectangular beams with a cross section of 150 mm × 305 mm and a span of 2 × 2290 mm, strengthened with CFRP. The parameters of the

study included the transverse steel ratio, the FRP ratio, the strengthening configuration, and the orientation of the fibres (unidirectional versus bi-directional).

The modes of failure obtained from the tests were in most cases out of target, since most of the specimens failed by slippage of the longitudinal steel reinforcement or by flexure. Failure by debonding occurred only in two specimens. The latter specimens were both without transverse steel; one was strengthened with a U-shaped CFRP wrap and the other with CFRP strips. However, a significant contribution from CFRP, 83% and 135% respectively, was recorded for these cases. Examination of the load-deflection curves of the two valid tests reveals that the effect of the FRP configuration on the contribution of FRP to the shear resistance became apparent only after a certain level of loading was reached. The U-shaped wrap exhibited better performance in providing rigidity. The authors also introduced a small modification to their model describing the debonding mode of failure, first published in Khalifa et al. (1998), to take into consideration the work by Miller (1999) on the FRP-concrete bonding mechanism. The merit of this study stems from its establishment of the fact that, contrary to the case of simple spans (the majority of tests), the strengthened zones of continuous beams experience maximum shear and maximum moment simultaneously.

Khalifa and Nanni (2000)

Khalifa and Nanni (2000) studied the behaviour of concrete T-beams without transverse steel reinforcement, retrofitted in shear with different configurations of externally-bonded CFRP. Six 150 mm × 405 mm × 3050 mm beams were tested. The strengthened beams failed predominantly by debonding. However, the specimen strengthened with a U-wrap anchored to the compression table by means of an FRP bar failed in flexure. The increase in measured shear capacity was between 35% and 145%. Moreover, the results indicated that the horizontal fibres had no significant effect on the capacity gain, at least in the case of failure by debonding. However, the authors added that such an effect is not to be excluded in the case of deep beams. The following conclusions were drawn from the study: (1) The contribution of FRP to the shear resistance was significant, particularly when adequate anchorage is provided; (2) The U-wrap configuration was more effective compared to FRP bonded onto the sides compared to FRP strips, continuous fabric covered larger areas that

could be subject to cracking; and (3) The horizontal fibres did not play a significant role in shear resistance.

Khalifa et al. (2000)

Khalifa et al. (2000-b) investigated the influence of concrete surface roughness on the shear performance of reinforced-concrete (RC) beams strengthened in shear with externally-bonded FRP. A series of five 150 mm × 305 mm × 3050 mm T-section beams was retrofitted with a U- wrapped CFRP fabric. Different levels of concrete surface roughness were tested. The beams were tested under four-point loads with a shear length ratio a/d = 3.0.

All the specimens ruptured forcefully by debonding of the FRP. This was accompanied by delamination of the concrete substrate; the higher the surface roughness, the more dramatic was the delamination. The results showed that the capacity gains due to FRP averaged 75%, including all the specimens with different concrete surface treatments. The authors concluded that additional concrete surface roughness beyond that normally prescribed by the manufacturer does not influence the shear capacity of the strengthened beams.

Deniaud and Cheng (2001)

Deniaud and Cheng (2001) explored the behaviour in shear of T-beams strengthened in shear with CFRP. Eight 140 mm × 600 mm × 3700 mm beams were tested. The following parameters were considered: (i) the spacing of the stirrups, (ii) the type of fibre (carbon versus glass), and (iii) the orientation of the fibres: 90°, 45°/90°, and tri-axial 0°/60°/-60°.

In order to collect as large a quantity of data as possible, the tests performed on the specimens were carefully instrumented. All the specimens failed by debonding. They also featured similar load-deflection response curves: neither the internal transverse steel reinforcement nor the external FRP affected the initial overall rigidity of the beam. In contrast, both the ultimate capacity and the ductility are clearly influenced by the FRP and the transverse steel ratios. In this context, the authors noted that the contribution of FRP decreased as the transverse steel ratio increased. Therefore, there is an interaction between internal reinforcement and external strengthening.

Li et al. (2001)

Li et al. (2001) studied the influence of the strengthened height of the beam on the shear capacity. Five rectangular beams with dimensions 130 mm × 200 mm × 1350 mm were tested. Shear strengthening was implemented using CFRP continuous fabric bonded to the sides of the beam at different heights. CFRP composite was also bonded onto the soffit of the beam. The specimens were carefully prepared before strengthening. The strains were measured at different locations. No failure by debonding was observed. According to the authors, this is attributable to the high quality of the bonding glue. The load-deflection response curves featured two distinct phases. The curves corresponding to the different configurations are quasi-identical in the first phase of loading, which shows that the configuration has no effect on the load.

The curves intersected each other as the load increased. However, it was interesting to observe that there was no noticeable difference between the different FRP configurations in the ultimate load that was reached. On the basis of this result, the authors suggest that there is no need for the FRP to be applied over the entire height of the web. However, the authors did not give an indication on the minimum FRP height required to ensure shear strengthening effectiveness.

Pellegrino and Modena (2002)

Pellegrino and Modena (2002) studied the influence of transverse steel on the contribution of FRP. To this end, they tested a series of eleven rectangular beams with dimensions 150 mm × 250 mm × 2700 mm. The parameters studied were: (i) the presence of transverse steel (sections with and without) and (ii) the CFRP ratio. The CFRP fabric used was applied onto the sides of the beams in one, two, or three layers.

All the specimens failed in shear by delamination of the CFRP composite. In the beams without transverse steel, the presence of FRP modified the cracking pattern that is usually observed: near the support, the cracks were inclined more or less horizontally, whereas near the load point, they were inclined at 45°. In the beams containing transverse steel,

delamination was more severe and cracks were inclined at angles less than 45°. The authors concluded that in the presence of transverse steel, the contribution of FRP decreased. To take this interaction into consideration, they suggested a partial modification of the model proposed by Khalifa (1999), based on their test results. This modification is a function of the rigidity of the transverse steel rather than of the FRP ratio.

Chaallal et al. (2002)

Chaallal et al. (2002) has presented the results of an experimental program including twenty-eight tests performed on fourteen T-section beams with dimensions 130 mm × 450 mm × 6000 mm. Two parameters were considered in this study: (i) the spacing of the stirrups and (ii) the number of CFRP layers. The CFRP fabric was applied as a U wrap over the web. The specimens tested had an a/d ratio of 2 and therefore may be classified as deep beams.

The strengthened specimens exhibited rupture of the compression struts followed by rupture of the CFRP near the supports. Such behaviour is characteristic of deep beams. In fact, as the CFRP fabric was removed, it was observed that the concrete underneath was completely pulverized. It was clear that enhancing the confinement of concrete in compression was the main role played by the FRP in this case. The shear capacity, on the other hand, increased with the number of FRP layers. However, this increase is linked to the transverse steel ratio, as clearly demonstrated by the test results: the higher the ratio, the less significant is the contribution of the FRP to the shear resistance. This result led the authors to propose an expression for FRP strain as a function of the global shear reinforcement ratio, that is, including both steel and FRP. The proposed expression was used along with the truss analogy to evaluate the contribution of FRP. Moreover, to extend the expression to the case of slender beams, the authors proposed an additional factor to take into account the shear length ratio, a/d, as well as the global reinforcement ratio.

Micelli et al. (2002)

Micelli et al. (2002) tested beams extracted from an existing concrete building constructed in 1964. The merit of the study stems from the fact that it considered the performance of FRP

used to strengthen an existing structure. Twelve T-beams, two of which were maintained as a control, were tested. The beams had the following dimensions: 152 mm × 381 mm × 2743 mm. They were retrofitted with U-wrapped continuous FRP fabric in one or two layers with and without anchorage. Of the ten strengthened beams, eight were retrofitted with CFRP and the remainder with aramid composite. For the anchorage, the authors used the technique described by Khalifa et al. (2000). In addition, the small longitudinal steel reinforcement ratio led the authors to strengthen the beams in flexure in order to inhibit any premature failure in flexure. The flexural strengthening was applied to both critical positive and critical negative moment regions. The beams were tested under three-point loads with the load applied at distance 2.4 m from the support. In the beams with no anchorage, failure occurred by premature debonding of the FRP, accompanied by severe delamination. The gain in shear resistance was 11% to 16%, depending on the number of FRP layers. The beams with anchored FRP achieved higher gains, ranging from 35% to 27%, depending on the number of FRP layers. Failure in this case was caused by loss of anchorage. The addition of a second CFRP layer to the specimens with anchorage did not result in a capacity increase. The authors noted that the gains achieved are small compared to those predicted by theory. This behaviour was attributed to deep beam action by the authors, who strongly recommended further investigation into this phenomenon. It must be said that an a/d ratio of 2.4 is at the upper limit of what can be considered as a deep beam. It must also be noted that the resistance of concrete in compression was around 20 MPa. The quality of the concrete substrate could also explain the results obtained. In this context, it would have been interesting to know more details on the state of the concrete substrate and on the surface preparation prior to application of FRP.

Li et al. (2002)

Li et al. (2002) carried out a series of tests on 16 rectangular concrete beams with dimensions 130 mm × 280 mm × 2700 mm, strengthened in shear with CFRP. The following parameters were studied: (i) the configuration of FRP, which was applied discontinuously over the length on the sides of the beams at different heights, (ii) the spacing of the stirrups, and (iii) the longitudinal steel reinforcement ratio. The strains were measured at various locations

(CFRP, transverse steel, concrete and longitudinal steel). The beams were tested under three-point loads with an a/d ratio of 2.9. All the beams ruptured by crushing of concrete, under two failure modes: in shear and in flexure. The gains due to CFRP varied between 25% and 115%. These gains were proportional to the area of the strengthened surface (the height of the CFRP bonded onto the sides of the beams was one of the parameters studied). The results showed that the presence of transverse steel resulted in a reduction of strength gains. These gains also decreased as the longitudinal reinforcement ratio increased. However, the results which led to this last conclusion are based on specimens which failed in two different modes: in shear and in flexure.

Lees et al. (2002)

Lees et al. (2002) investigated the feasibility of a new strengthening system with FRP, specifically pre-stressed carbon-FRP straps. This full-wrap system is innovative in the sense that the FRP contributes to strength starting from the first stage of loading. In comparison, other strengthening systems, including those with FRP, are passive systems and, therefore, do not influence the shear behaviour and particularly concrete contribution before the formation of diagonal cracks. For this investigation, the authors tested two T-beams, one of which was a control beam, with dimensions 150 mm × 430 mm × 2700 mm. The beams were tested under four-point loads. The strengthened beam ruptured by fracture of the strap. In addition to the gain in capacity (33%) due to the use of this system, the results also included a gain in overall rigidity compared to the control beam. In conclusion, the authors recognized that further work was required to investigate the influence of loading arrangement, pre-stress level, and strap arrangement on the behaviour of a strengthened beam.

Czaderski (2002)

Czaderski (2002) tested six T-beams strengthened with L-shaped CFRP plates. The dimensions of the specimens were 150 mm × 430 mm × 3500 mm. The parameters studied were: (i) the type of loading (static loading versus pre-loading with subsequent static loading versus fatigue with subsequent static loading) and (ii) the presence of internal steel stirrups. Two failure modes were observed: (i) shear rupture of the strengthened beam without

transverse steel; and (ii) crushing of concrete after yielding of longitudinal steel reinforcement. The latter mode involved the strengthened beams containing transverse steel reinforcement, regardless of the type of applied load. These beams featured a slight increase of 5% in capacity, in contrast to the strengthened beams with no transverse steel, where the gain due to FRP was as high as 95%. The study also presented numerous results on different factors related to strains in CFRP and transverse steel.

Diagana et al. (2003)

Diagana et al. (2003) have presented the results of tests conducted on a series of ten rectangular concrete beams with dimensions 130 mm × 425 mm × 2200 mm. The parameters tested are closely related to the properties of FRP composites: (i) the orientation of the fibres (45° versus 90°) with respect to the beam longitudinal axis, (ii) the configuration of FRP: U-wrap versus full wrap, and (iii) the spacing of the FRP composite application. The composite was made of carbon fibres and was applied discontinuously onto the beam. The beams were tested under three-point loads, with an a/d ratio of 2.1.

The gains in capacity due to the CFRP varied between 18% and 61%, depending on the configuration of the FRP and the orientation of the fibres. These gains were greatest for FRP with fibres perpendicular to the plane of cracking and applied in a U-shaped configuration. Two failure modes were observed: debonding of the FRP for U-wrap configuration and fracture of FRP for full wrap.

Täljsten (2003)

Täljsten (2003) tested a series of seven rectangular concrete beams with dimensions 180 mm × 500 mm × 4500 mm, strengthened in shear with FRP. The beams had no transverse steel. CFRP fabric was used for retrofit and was U-wrapped around the web. The parameters studied included the fibre orientation (45°, 90° and 0°) and FRP thickness. The concrete resistance in compression ranged from 59 to 71 MPa. The beams were tested under four-point loads with an a/d ratio of 2.7. The gains in capacity due to the CFRP were exceptionally high, ranging from 100% to 170%. Only the specimen with the fibres oriented

longitudinally to the beam axis recorded a relatively small gain (24%). Most of the beams failed by concrete crushing. One focus of the study was the vertical distribution of the strains in the CFRP composite within the test zone. The author noted that the maximum strain was reached at mid-height of the beam.

Hsu et al. (2003)

Hsu et al. (2003) explored, through a series of five tests, the behaviour of rectangular beams with no transverse steel, strengthened in shear with CFRP. The dimensions of the beams were 152 mm × 165 mm × 1070 mm. All the tested parameters were related to the external FRP configuration, as follows: (i) inclination of the CFRP strips (90° versus 45°), (ii) continuous wrap (fabric) versus discontinuous (strips) and (iii) bonding of the FRP composite up to midheight onto the sides of the beams. The strengthened beams failed in shear by debonding of the FRP. Indeed, except for the beam that was strengthened with FRP fabric wrap, which ruptured by fracture of the FRP, all three other beams failed due to debonding of the CFRP. The gains in capacity due to CFRP varied with the configuration of the FRP. The strips oriented at an angle of 45° showed the best performance improvement (80%), compared to 60% for the strips oriented at an angle of 90° and 33% for the continuous fabric. In this context, it may be worth noting that the FRP strip ratio used was approximately 50% greater than that of the CFRP fabric. As for the FRP partially bonded up to the beam mid-height, the results indicated a capacity gain of 16% due to FRP.

Adhikary et al. (2004)

Adhikary et al. (2004) performed a series of tests on nine rectangular beams with dimensions 300 mm × 245 mm × 3500 mm, strengthened in shear with CFRP. The parameters of the study are related to the FRP configuration and the fibre type, as follows: (i) types of fibres (carbon versus aramid), (ii) wrapping layout (U-wrap versus full wrap) and (iii) anchorage length (anchorage was provided by bonding a certain length of sheet to the top face of the beam). The beams were tested under four-point loads with an a/d ratio of 4.1. With the exception of the beams strengthened with full wrap, which failed in flexure, all the other beams (six in total) failed in shear by debonding of FRP or by spalling of concrete. As for

resistance, the reported results revealed that the capacity gains due to CFRP and AFRP reached 123% and 118%, respectively. It was concluded that the full-wrap configuration outperformed the U-wrap.

Zhang et al. (2004)

Zhang et al. (2004) studied the behaviour of deep beams strengthened in shear with CFRP. They conducted an experimental program of 16 tests on rectangular concrete beams with dimensions 102 mm × 203 mm × 760 mm. The objectives of the research study were: (i) to evaluate the influence of the a/d ratio on the performance of shear strengthening with FRP and (ii) to compare the performance of different FRP configurations. The following configurations were successively examined: (a) continuous versus discontinuous (fabric versus strips), (b) fibre orientation (45° versus 90° versus 0°) and (c) FRP application pattern (on the sides only versus U-wrap). The beams were tested under four-point bending with a shear length ratio a/d=1.25, and under three-point bending with an a/d ratio of 1.88. The results showed that, for a given a/d ratio, the gains in capacity due to strengthening depend strongly upon the configuration. Indeed, the beams strengthened with CFRP strips inclined at a 45° angle recorded the highest capacity gains, compared to strips applied at 90°, that is, 200% compared to 179% for a/d = 1.89. Moreover, the beams strengthened with CFRP fabric generally outperformed the beams strengthened with CFRP strips in terms of capacity gain. As for the influence of the a/d ratio, the results showed that the gains were greater for a/d = 1.25, compared to a/d = 1.88. In terms of failure modes, the study indicated that delamination of the CFRP laminates from underneath the concrete surface is the dominant failure mode for all CFRP-strengthened beams.

Cao et al. (2005)

Cao et al. (2005) presented the results of an experimental program encompassing 18 tests, six of which were used as a control. The objective of the investigation was to study the phenomenon of debonding of FRP strips, which can be observed particularly in critical regions of shear strengthening. The beams tested had a rectangular cross-section with the following dimensions: 150 mm × 222 mm × 1700 mm (or 1600 mm for 6 specimens). The

parameters studied were: (i) the a/d ratio, considering the following values: 2.9; 2.7; 2.5; 1.8; 14 and (ii) the rigidity of the beam, investigated by varying the spacing and the width of the strips, as well as the type of FRP (carbon or glass). Note also that the test beams were pre-loaded under four-point bending until a diagonal shear crack became apparent, and then fully unloaded. The beams were next strengthened by wrapping FRP strips around the entire cross-section within the test shear span and loaded again up to failure.

In general, all test beams exhibited a similar failure process. Local debonding of some FRP strips was initiated at or near the critical shear crack. At a sufficiently high load level, the most highly-stressed strip debonded completely from the side of the beam, although it remained bonded to the top and bottom surfaces of the beam. In terms of capacity gains due to CFRP, the results showed a variation between 18 and 80%, depending on the a/d ratio and the CFRP content. The measuring devices used in the study, particularly those placed on the CFRP strips to measure the strains, yielded interesting conclusions with regards to the strain distribution in the strips located in the critical sections for shear. This distribution was confirmed to be non uniform, which, according to the authors, must be taken into account for the prediction of CFRP contribution to shear resistance.

Carolin and Täljsten (2005-b)

Carolin and Täljsten (2005b) tested a series of 23 rectangular concrete beams having the following dimensions: 180 mm × 440 mm × 4000 mm, strengthened in shear with CFRP. The objective of the study was to examine the influence of CFRP thickness, fibre orientation, and FRP configuration (U-wrap versus full wrap) on the performance of strengthened beams. Some of the beams were pre-cracked before strengthening was applied. Other beams were subjected to fatigue loading after strengthening had been applied. The beams were tested under four-point bending with an a/d ratio of 2.8. The specimens failed in shear according to different modes, depending on FRP configuration, FRP thickness, and fibre orientation. For example, debonding failure was observed for the cases where the fibres were oriented at a 90° angle, whereas FRP fracture failure occurred when fibres were oriented at 45°. This last failure mode was often associated with a loss of anchorage. The test results also showed that the beams that have been pre-loaded, unloaded, then strengthened and loaded again, achieved

a performance comparable to the strengthened pristine beams, i.e., those which did not have to go through the pre-loading phase. As for fatigue, the results indicated that fatigue-loaded beams tend to have a higher load-bearing capacity when tested to failure, compared to beams without a fatigue history.

Monti et al. (2006)

Monti et al. (2005) have presented the results of an experimental investigation involving a series of 24 tests performed on rectangular concrete beams with dimensions 250 mm × 410 mm × 2800 mm, strengthened in shear with CFRP. A number of different configurations of the composite were tested: (i) surface-bonded FRP versus U-wrap versus full wrap, (ii) fibre orientation (90° versus 45°) and (iii) continuous FRP versus strips at different spacings. The beams were tested under three-point bending with a shear length ratio a/d = 3.4. The tests showed that rupture by debonding was the predominant mode of failure, accompanied in some cases by opening of a stirrup overlap. The results showed that the gains in shear capacity due to the FRP were greater for a 45° fibre orientation and increased as the spacing of strips was reduced or with a continuous FRP composite. Thus, for example, the beam strengthened with U-shaped FRP strips inclined at an angle of 45° and spaced at only 225 mm achieved a capacity gain of 190%. By comparison, for the beam strengthened with FRP strips bonded onto the sides of the beam at an angle of 90°, the gain obtained was only 5%. In parallel to the experimental study described above, the authors proposed a model for prediction of the contribution of FRP strengthening to shear resistance. The model describes a scenario through which debonding occurs. It is based on the concept of effective bond length and requires a number of factors related to parameters such as FRP configuration. The proposed model was validated with test results achieved by the authors in this study and in other studies reported in the literature.

Bousselham and Chaallal (2006-a)

Bousselham and Chaallal (2006-a) presented results of 22 tests performed on RC T-beams retrofitted in shear with CFRP layers. The dimensions of the tested specimens are as follows: 152 mm × 350 mm × 3110 mm. The following parameters are investigated: (i) the CFRP

ratio (i.e., the number of CFRP layers), (ii) the internal shear steel reinforcement ratio (i.e., spacing), and (iii) the shear length to the beam's depth ratio, *a/d* (i.e., deep beam effect). All the tested specimens failed in shear, except those of series SB-S2 (slender beams, with steel stirrups spaced at *s = d/4*), which failed in flexure. No specimen failed by debonding, delamination or fracture of the CFRP. The shear failure occurred by crushing of the concrete struts. The results showed that the contribution of the CFRP to the shear resistance is not in proportion to the CFRP thickness (i.e., the stiffness) provided, and depends on whether the strengthened beam is reinforced in shear with internal transverse steel reinforcement. Results also confirmed the influence of the ratio *a/d* on the behaviour of RC beams retrofitted in shear with external FRP.

Bousselham and Chaallal (2006-b)

Bousselham and Chaallal (2006-b) present results of an experimental investigation involving twelve tests on T-beams (95 mm × 175 mm × 1584 mm) strengthened in shear with CFRP fabrics. The main objective of this study was to evaluate the effect of the following parameters on the shear performance of strengthened RC beams: (i) the CFRP ratio, (ii) the transverse steel reinforcement ratio, and (iii) the type of beams (deep versus slender). All the test specimens failed in shear. No specimen failed by premature debonding, delamination or fracture of the CFRP. The shear failure, which occurred by crushing of concrete struts, was accompanied with a wide open crack in the compression table. The results clearly indicated that: (i) the gain in shear capacity was significant in slender beams whereas it was very modest in deep beams; (ii) the increase of the CFRP thickness (1L to 2L) achieved an additional gain in capacity for slender specimens, particularly those pertaining to specimens without transverse steel. In deep specimens no noticeable gain was achieved; and (iii) the addition of internal transverse steel resulted in a significant decrease of the gain in the slender specimens. The existence of an interaction between the internal transverse steel and the externally applied CFRP was showed in terms of the gain in the shear capacity as well as of the strains.

Hassan Dirar et al. (2006)

Hassan Dirar et al. (2006) tested four T-beams, three of which (B2, B3, and B4) were retrofitted with CFRP straps and one (B1) maintained as a control. The dimensions of the beams were 105 mm × 210 mm × 2500 mm. The objective of the study was to examine the effect, if any, of existing cracks on the shear performance of beams retrofitted in shear with FRP. To this end, the authors proceeded as follows: (i) in one beam among the three to be retrofitted, pre-stress was activated in the straps, with no loading (beam B2); (ii) the two other beams (B3 and B4) were submitted to a pre-loading of 70% of the load capacity, which had been obtained by testing the control beam (B1). They were then unloaded down to 40% of their capacity. The pre-stress load was then activated in the straps before the beams were finally tested up to failure. In addition, in beam B4, to evaluate the combined effect of pre-loading and a/d ratio, the load, which was applied after the pre-stress had been activated, was moved gradually from a shear length a = 410 mm to a = 820 mm. As far as the failure modes are concerned, the results obtained indicated that the specimen B3 suffered a shear failure due to a set of parallel shear cracks emerging from and above the support. This was accompanied by significant damage both to the flange and to the end of the beam. In specimen B4, the major shear crack emanated from the outer strap pad at an angle of approximately 34° and ran towards the flange, crossing the middle strap just under the flange. The flange suffered less damage in this specimen than in B3. As for capacity gains, the results yielded values of 46% and 22% for B3 and B4, respectively. The authors attributed this difference in gain to the more detrimental loading scheme used with B4. As for the influence of pre-loading on shear performance, the results showed that the loading history did not seem to have a pronounced effect on the behaviour of RC beams strengthened with CFRP straps.

Pellegrino and Modena (2006)

Pellegrino and Modena (2006) tests involved 12 full-scale rectangular beams specimens. The tests were developed with a simply supported load scheme and with a continuous load scheme in which maximum shear and maximum bending moment were simultaneously acting at the support. The control specimens (not strengthened) were labelled U0, whereas

the specimens strengthened with CFRP sheets were labelled U1 or U2 (continuous U-jacketing with one or two bonded layers is used). The letters S and C were used for the simply supported and continuous schemes, respectively. FRP-reinforced beams failed in shear always with peeling off. Longitudinal cracks were often present at the upper surface of the beam. Cracks started near the location of the applied load and extended towards the support. Concrete cover splitting developed along the entire height of the beam. Results confirmed the presence of an interaction between the internal transverse steel reinforcement and the external FRP strengthening also for U-wraps.

Hassan Dirar et al. (2007)

Hassan Dirar et al. (2007) tested four pre-cracked T-section RC beams. The control specimen was referred to as *CB*. The other three beams are designated $\rho_1 d_1$, $\rho_1 d_2$ and $\rho_2 d_1$ according to their longitudinal reinforcement ratio and effective depth. The beams were tested in four-point bending. Each specimen had a 1000mm long central (moment) region. The two shear spans were varied with the change in effective depth, so as to maintain a shear span to depth ratio of 3.8 in all beams. Specimens *CB* and $\rho_1 d_1$ had two 25mm and two 16mm bars as longitudinal (flexural) reinforcement, whereas beams $\rho_1 d_2$ and $\rho_2 d_1$ had two 20mm and two 16mm bars. The goal of the research study was to examine the effect of the effective depth and the longitudinal steel ratio on the shear capacity of a pre-cracked T-beam strengthened in shear with CFRP composites.

The percentage gains in shear force when compared with equivalent unstrengthened beams, for the strengthened beams $\rho_1 d_1$ and $\rho_1 d_2$ were 26.2% and 15.9%, respectively. Hence, the fabric strengthening was more effective when the effective depth was increased from 215mm to 295mm. This increase in effectiveness was due mainly to the increased bond area made available in $\rho_1 d_1$. The reduction in longitudinal steel ratio from 4.47% in $\rho_1 d_1$ to 3.33% in $\rho_2 d_1$ changed the mode of failure from shear to flexure. The shear force enhancement was 19kN in $\rho_2 d_1$ compared to 28kN in $\rho_1 d_1$.

2.3   End-anchorage systems for EB FRP sheet method

So far, different anchorage systems have been proposed to prevent pre-mature FRP debonding for shear strengthening of RC beams using EB FRP sheets or strips. A review of experimental studies on shear strengthening of RC beam with end-anchored EB FRP sheets is presented as follows:

Sato et al. (1997)

Sato et al. (1997) explored the possibility of utilizing a mechanical anchorage system to address the problem of FRP debonding. Three T-section beams of dimensions 150 mm × 300 mm × 2000 mm were tested: the first was kept aside as a control specimen, while the two others were strengthened with a U-wrapped CFRP fabric applied over the entire shear length. The mechanical anchorage system provided in one of the two specimens consisted of a 50-mm wide metal plate fixed to the web by means of screws spaced at 50 mm.

In both cases, failure occurred by delamination of the FRP. In terms of shear capacity, the gains achieved were 12% and 33% for specimens without and with a mechanical anchorage system, respectively. In other words, the use of a mechanical anchorage system resulted in a gain of 18%. However, the authors believe that the presence of a mechanical anchorage enhances the resistance at the FRP-concrete interface and thereby enhances the shear resistance.

Khalifa and Nanni (2000)

Khalifa and Nanni (2000) investigated a form of bonded anchored U-jacketing FRP application. The anchor consisted of a bent portion of the end of the FRP reinforcement embedded into a preformed groove in concrete. The experimental program consisted of six full-scale reinforced concrete T-beams. The specimens were reinforced with longitudinal steel bars with no transverse reinforcement. In their experimental program, the selected parameters were: CFRP quantity and configuration (continuous sheets versus strips); bond surface (side-bonded versus U-wrap); fibre direction; end anchorage (U-wrap without end anchor versus with end anchor). It has been concluded that the proposed U-anchor system

can significantly improve the shear resistance of EB FRP sheets for RC beams strengthened with FRP.

Schuman (2004)

Schuman (2004) used GFRP/steel anchorage systems for FRP-concrete double-shear bond test series. The test specimens used in Schuman (2004) study were designed after a bridge that is currently in need of strengthening. The specimens were rehabilitated using mechanically-anchored CFRP sheets. Overall, seven test specimens were prepared. The main variables of their study were the mechanical anchorage system used. It has been concluded that the anchorage depth, diameter and location plays an important role in the ultimate and service response of the test specimens.

Eshwar et al. (2008)

Eshwar et al. (2008) investigated the performance of spike anchors and near-surface mounted (NSM) end-anchorage systems in a series of FRP-concrete shear bond tests. The experimental test of Eshwar et al. (2008) study consisted of ten reinforced concrete beams. A spike anchor consists of a bundle of carbon or glass fibres. One end of the fibres takes the form of a fan which is sandwiched between the two FRP sheets to be anchored. The other end of the bundle is fully bonded and inserted into a hole through the RC beam. In a research study by Eshwar et al. (2008), many of the spike anchors failed prematurely and did not add to the FRP-concrete bond resistance. The NSM end-anchorage system used by Eshwar et al. (2008) was similar to one proposed by Khalifa and Nanni (2000) and had been successfully tested in FRP- concrete shear bond tests.

Ceroni et al. (2008)

Ceroni et al. (2008) investigated the effectiveness of different anchorage systems in a series of double-tension tests on CFRP sheets epoxy-bonded to T-shaped concrete specimens. The experimental program consisted of 14 specimens to study the efficiency of different end-anchorage systems for FRP sheets. The specimens were T-shape beam-column joints. Each specimen was made by two concrete blocks with 300 mm spacing. Steel stirrups were

vertically placed with 60 mm spacing in the greater part of the T-block and horizontally in the web with 130 mm spacing. The specimens were strengthened using carbon sheets on two opposite sides of the specimens with 100 mm spacing.

Among the different anchorage systems considered in their research study, EB FRP laminates, EB steel plates, and NSM FRP end-anchorage systems showed superior performance.

Mofidi (2008)

Mofidi (2008) conducted a research study on a total of three RC T-beams with shear span-to-depth ratio of 2.0 tested under increasing monotonic load untill failure. The beams were tested in four-point bending. The total length of the beams was 2.4 m, with a shear span of 575 mm resulting in a shear span-to-depth ratio of 2.0. 10M U-shaped stirrups, with 11.3 mm (7/16 in.) nominal diameter, at a spacing of 250 mm were used. The pilot tests were done as a proof-of-concept of the effectiveness of the proposed method in increasing the shear capacity of the RC T-beams. The first T-beam, which was tested as the control beam, failed in shear. The second beam was strengthened by using a U-shaped CFRP sheet that was externally bonded to the web of the beam in the shear zones. The third beam was strengthened by using anchored U-shaped dry CF sheet. The test results showed that the beam strengthened by the new mechanically anchored dry CF had about 48% increase in shear capacity as compared to the control beam and 16% increase in shear capacity as compared to the beam strengthened by CFRP epoxy-bonding method. Results confirmed that the mechanically anchored dry CF U-jackets can increase the ultimate shear strength of RC T-beams and slightly improve the flexural stiffness.

2.4   Near-surface mounted (NSM) FRP rod strengthening method

Very limited experimental and analytical studies are conducted to date on the use of NSM FRP rods for shear strengthening of RC beams. A review of experimental studies on shear strengthening of RC beam with NSM FRP rod is reported as follows:

De Lorenzis and Nanni (2001)

De Lorenzis and Nanni (2001) studied the performance of RC beams strengthened in shear with NSM CFRP rods. A total of 8 T-beams were tested. The cross-sectional dimensions of the beams were 152 mm × 355 mm and the span was 3000 mm. The parameters studied were: (i) spacing of rods, (ii) inclination of rods, (iii) presence of an anchorage in the flange, and (iv) presence of internal steel stirrups. The specimens were tested under four-point loads with a shear length ratio a/d=3. With the exception of the specimen with transverse steel, which failed in flexure, all the specimens strengthened in shear with FRP NSM rods failed in shear. Failure was due either to bonding failure of one or more NSM rods, or to splitting of the concrete cover of the longitudinal reinforcement. The results showed that the gains in capacity due to external strengthening can be as high as 106%. The shear capacity of the strengthened beams can be increased by decreasing the spacing of the NSM rods, by anchoring the rods into the flange, or by changing the inclination of the rods from vertical to 45 degrees. This work shows that the use of NSM FRP rods is an effective technique to enhance the shear capacity of RC beams.

De Lorenzis and Nanni (2002)

De Lorenzis and Nanni (2002) investigated the bond between NSM FRP rods and concrete. The test variables were the bonded length, diameter of the FRP rod, type of FRP material, surface finish of the rod and size of the groove. Twenty two specimens were tested to investigate the effect of the mentioned factors on the bond behavior.

Barros and Dias (2005)

Barros and Dias (2005) presented results of tests carried out on twelve RC T-beams. An experimental program composed of RC T-beams, with a certain percentage of steel stirrups, was carried out to evaluate the effectiveness of NSM with CFRP laminates as a shear strengthening technique. The effect of the percentage and the inclination of CFRP are discussed. Besides, the main results and failure modes are presented and analyzed. According

to the results of their study, the configuration with laminates at 60° was the most efficient among other shear strengthening arrangements.

De Lorenzis and Teng (2007)

De Lorenzis and Teng (2007) provided a critical review of existing research in NSM strengthening subject, identifying gaps of knowledge, and outlines directions for further research. De Lorenzis and Teng (2006) focused on research work on the structural aspects of NSM strengthening of concrete structures.

Rizzo and De Lorenzis (2009)

Rizzo and De Lorenzis (2009) conducted a research program on shear strengthening of RC beams with NSM reinforcement. A total of nine, 2.0 m-long RC beams with a rectangular 200 mm×210 mm cross-section were tested to analyze the influence on the structural behaviour and failure mode of selected test parameters, i.e. type of NSM reinforcement (round bars and strips), spacing and inclination of the NSM reinforcement, and mechanical properties of the groove-filling epoxy. One beam strengthened in shear with externally bonded FRP laminates was also tested for comparison purposes. All beams had internal steel flexural and shear reinforcement, designed to ensure that unstrengthened and shear-strengthened beams would all fail in shear. The steel tension and compression reinforcement consisted respectively of four and two steel deformed bars with 22 mm nominal diameter. The steel shear reinforcement consisted of closed double-legged stirrups. One half of each beam starting from mid-span was taken as the "test side", while the other half was designed as the "strong side". Only the test side was strengthened in shear with FRP systems and appropriately instrumented with strain gages to monitor the strain distribution in the internal steel stirrups and in the shear strengthening system, as detailed later. CFRP ribbed round bars in epoxy-filled grooves were used as NSM shear reinforcement. The test variables included bar spacing and inclination angle, and anchorage of the bars in the flange. The NSM reinforcement produced a shear strength increase which was as high as 106% in the absence of steel stirrups, and still significant in presence of a limited amount of internal shear reinforcement. Overall, the increase in shear capacity was about 16% for the beam

strengthened with externally bonded U-wrapped laminate, and ranged between 22% and 44% for the beams strengthened with NSM reinforcement.

Dias and Barros (2008)

Dias and Barros (2008) conducted an experimental test series on T cross-section RC beams, with different percentages of steel stirrups. The influence of both the percentage and the CFRP strip inclination was discussed. The experimental program consisted of 12 RC T beams. The beams were reinforced to guarantee shear failure mode for all the tested specimens. Beams were tested under three point load configuration to limit shear failure in only one of the beam shear spans. The experimental program consisted of one beam without any transverse steel reinforcement; one beam with transverse steel reinforcement of $\phi 6$ spaced at 300 mm; one beam with transverse steel reinforcement of $\phi 6$ spaced at 130 mm; and nine FRP strengthened beams with transverse steel reinforcement of $\phi 6$ spaced at 300 mm. The FRP strengthened beams included different CFRP percentages of CFRP laminate on the tested shear span. For RC beams with each of the three percentages of CFRP laminates there were three inclinations for the laminates equal to 90°, 60°, and 45°.

2.5 Embedded through-section (ETS) FRP rod strengthening method

FRP rods can be epoxy-bonded to vertical holes drilled into concrete to strengthen RC beams in shear. Until now, very few experimental studies are carried out on the use of ETS FRP rods for shear strengthening of RC beams. A review of experimental studies on shear strengthening of RC beam with ETS FRP rod is reported as follows:

Valerio et al. (2009)

An experimental test series on 10 FRP strengthened pre-stressed small-scale concrete bridges was performed by Valerio et al. (2009). The small-scale specimens were designed to match the average values in the shear zone of the real pre-stressed bridge girders. The percentage of transverse reinforcement equals 0.175% in the shear spans. The beams were 110 mm wide, 190 mm deep and 3000 mm long. The longitudinal reinforcement consisted of four 7 mm

wires (only the upper two were pre-tensioned) and 3 mm-diameter mild steel bars at 100 mm spacing in the shear zone as transverse steel reinforcement. The specimens were tested under four-point loading configuration to provide constant shear within the shear spans. Based on results reported by Valerio et al. (2009), the proposed shear strengthening method was concluded feasible and effective for both pre-stressed and RC beams even in the presence of transverse steel reinforcement.

CHAPTER 3

SHEAR STRENGTHENING OF RC BEAMS WITH EB FRP-INFLUENCING FACTORS AND CONCEPTUAL DEBONDING MODEL

Amir Mofidi and Omar Chaallal

Department of Construction Engineering, École de Technologie Supérieure 1100 Notre-Dame Ouest, Montréal, Québec, Canada H3C 1K3

3.1   Abstract

This paper deals with the shear strengthening of reinforced concrete (RC) beams using externally bonded (EB) fibre-reinforced polymers (FRP). Current code provisions and design guidelines related to shear strengthening of RC beams with FRP are discussed in this paper. The findings of research studies, including recent work, have been collected and analyzed. The parameters that have the greatest influence on the shear behaviour of RC members strengthened with EB FRP and the role of these parameters in current design codes are reviewed. This study reveals that the effect of transverse steel on the shear contribution of FRP is important and yet is not considered by any existing codes or guidelines. Therefore, a new design method is proposed to consider the effect of transverse steel in addition to other influencing factors on the shear contribution of FRP (V_{frp}). Separate design equations are proposed for U-wrap and side-bonded FRP configurations. The accuracy of the proposed equations has been verified by predicting the shear strength of experimentally tested RC beams using data collected from the literature. Finally, comparison with current design guidelines has shown that the proposed model achieves a better correlation with experimental results than current design guidelines.

3.2 Introduction

In recent years, an outstanding research effort has been undertaken with a view to understand the behaviour of EB FRP used for strengthening and retrofitting concrete structures. As a result, numerous aspects of the subject have been addressed, and many codes and design guidelines (hereafter called "the guidelines") for concrete structures strengthened with EB FRP have been published worldwide (e.g., ACI 440.2R 2008, CAN/CSA S806 2002, CAN/CSA S6 2006, European *fib*-TG 9.3 2001). The use of FRP reinforcement for strengthening RC beams and slabs in flexure and for confinement of columns is well established. However, because of its complexity, the shear strengthening of RC members with EB FRP is still a research problem and requires further investigation to be completely solved (Bousselham and Chaallal 2004). Between 1992 and 2008, numerous research studies on the shear strengthening of RC beams with EB FRP composites were carried out (e.g., Uji 1992; Al-Sulaimani et al. 1994; Chaallal et al. 1998; Triantafillou 1998; Khalifa et al. 1998; Pellegrino and Modena 2002; Chen and Teng 2003; Monti and Liotta 2006; Bousselham and Chaallal 2008). The results of these studies led to several design equations and analytical models that were implemented in a code format to predict the shear contribution of EB FRP. However, recent findings have highlighted major influencing parameters related to shear strengthening with EB FRP that have still not been captured by existing theoretical predictive tools, including the codes and guidelines (Bousselham and Chaallal 2008). Although experimentally observed and quantified, these parameters remain insufficiently documented, and many questions about them remain unanswered.

One category of these parameters is related to the formulation of effective FRP strain. In this context, all the guidelines use the same FRP effective-strain value for RC beams both with and without transverse steel. However, does the FRP effective strain remain unchanged whether or not the RC beam has internal transverse steel reinforcement? Recent research studies (Chaallal et al. 2002; Pellegrino and Modena 2002; Bousselham and Chaallal 2004) have revealed that the contribution of FRP to shear resistance (that is, the effective FRP strain) decreases as the internal steel-reinforcement ratio increases. However, whether or not

there exists a quantitative relationship between transverse-shear steel reinforcement and FRP shear contribution, in particular with FRP effective strain, remains to be demonstrated.

A second category of parameters is related to FRP debonding models. These models have been incorporated into the design equations of some major guidelines for shear strengthening of RC beams with FRP (e.g., ACI 440.2R 2008, CAN/CSA S6 2006). How do the predictions of these bond models compare with the results of pure research studies on FRP-to-concrete bonding (Holzenkämpfer 1994, Neubauer and Rostásy 1997, Chen and Teng 2001)? In addition, all the design guidelines that use this approach assume a single-line cracking pattern to model FRP-to-concrete bonding. However, is the single-line assumption reasonably representative of reality despite the rather distributed concrete-cracking patterns observed in recent research studies (Chaallal et al. 2002; Pellegrino and Modena 2002; Carolin and Täljsten 2005)? Is the cracking pattern an influencing parameter on FRP debonding of beams strengthened in shear with FRP? Does the presence of transverse internal steel or external FRP have any effect on the shear cracking pattern or angle?

These and other legitimate questions have provided the main impetus to carry out this study, the objectives of which are as follows:

- to investigate the design procedures recently introduced into the guidelines to evaluate the shear contribution of EB FRP to the shear resistance of retrofitted RC beams. To review briefly existing design proposals and to highlight their deficiencies;

- to understand better the interaction between internal transverse steel and external FRP reinforcement and the effect of these two components on concrete-cracking patterns and FRP debonding;

- to study the effect of certain parameters which have been proven to influence the shear resistance of EB FRP, but which have not been sufficiently documented in the guidelines;

- to develop a transparent, rational, and evolutionary design model for the shear resistance of FRP-strengthened beams which fail by FRP debonding. It is thought that such a

design proposal will offer an improvement to the current debonding design equations in the guidelines.

The present research study does not address every aspect of shear strengthening with EB FRP. However, ongoing research at the University of Quebec, École de technologie supérieure in Montreal is aimed at developing comprehensive design procedures for shear strengthening with FRP.

3.3 Contribution of EB FRP to shear resistance

The nominal shear resistance at the ultimate limit state, V_n, of RC beams retrofitted in shear with EB FRP is generally calculated simply by adding the contribution of FRP to the shear resistance, V_f, to that of concrete, V_c, and of steel, V_s, as follows:

$$V_n = V_c + V_s + V_f \tag{3.1}$$

The contributions of concrete and transverse steel are calculated using the design guidelines for non-strengthened RC structures, assuming that the FRP strengthening does not influence the shear contribution of the concrete or of the transverse steel reinforcement. To calculate the FRP contribution to shear resistance, most guidelines use the same truss analogy as that used to calculate steel stirrups. Thus, the shear contribution of FRP is obtained by multiplying the ultimate vertical stress in the FRP strips by the area of the FRP sheet that crosses a potential shear crack. All the FRP strips that are intersected by the selected shear crack are assumed to contribute the same FRP effective strain (hereafter called "effective strain"). Most of the design guidelines and analytical models basically use a similar design analogy with different definitions of effective strain.

3.4   **Current design guideline provisions**

The objective of this section is to review the design provisions of the latest versions of the major design guidelines related to shear strengthening of RC beams with FRP.

3.4.1   **CAN/CSA-S806 2002**

In the CSA-S806 (2002) design guidelines, the contribution of FRP is given by:

$$V_f = \frac{A_f.E_f.\varepsilon_{fe}.d_f}{s_f} \qquad (3.2)$$

where $A_f = 2n.t_f.w_f$ is the area of the cross-section of the FRP sheet or strip. V_f is calculated based on the 45°-truss analogy. The effective strain, ε_{fe}, is limited to 4000 µɛ for U-shaped FRP wraps and 2000 µɛ for FRP side-bonded to the concrete web.

3.4.2   *fib*-**TG 9.3 2001**

The *fib*-TG 9.3 (2001) provisions on shear strengthening of RC beams are based on the regression of experimental results carried out by Triantafillou and Antonopoulos (2000). In the *fib* 2001 model, the contribution of the FRP shear reinforcement is given by:

$$V_f = \rho_f.E_f.\varepsilon_{fe}.b.d.(\cot\theta + \cot\alpha)\sin\alpha \qquad (3.3)$$

In the *fib* model, the effective strain is governed by the FRP strengthening configuration and the FRP material type. The guidelines states that the effective strain is a function of the axial rigidity of FRP ($E_f.\rho_f$) and the compressive strength of concrete, as follows:

for full carbon-FRP (CFRP) wraps,

$$\varepsilon_{fe} = 0.17 \left(\frac{f_{cm}^{2/3}}{E_f \rho_f} \right)^{0.30} \varepsilon_{fu} \qquad (3.4)$$

for side-bonded or U-shaped CFRP jackets,

$$\varepsilon_{fe} = \min \left[0.65 \left(\frac{f_{cm}^{2/3}}{E_f \rho_f} \right)^{0.56} .10^{-3}; \ 0.17 \left(\frac{f_{cm}^{2/3}}{E_f \rho_f} \right)^{0.30} \varepsilon_{fu} \right] \qquad (3.5)$$

and for full Aramid-FRP wraps,

$$\varepsilon_{fe} = 0.048 \left(\frac{f_{cm}^{2/3}}{E_f \rho_f} \right)^{0.47} \varepsilon_{fu} \qquad (3.6)$$

where E_f is in GPa and f_{cm} is the cylindrical compressive strength of concrete in MPa.

3.4.3   ACI 440.2R 2008

The ACI 440.2R-08 (2008) provision is based on a research study by Khalifa et al. (1998). In the ACI code, the FRP contribution is given by:

$$V_f = \frac{A_{fv}.f_{fe}.(\sin \alpha + \cos \alpha).d_{fv}}{s_f} \qquad (3.7)$$

The effective strain limit for full-wrap FRP systems is based on limiting the crack opening to ensure proper aggregate interlocking of the concrete, whereas the effective strain for the bonded U-wraps and side-bonded FRP systems is calculated based on the FRP-to-concrete bond mechanism, as follows:

for full FRP wraps,

$$\varepsilon_{fe} = 0.004 \leq 0.75 \varepsilon_{fu} \qquad (3.8)$$

and for side-bonded or U-shaped FRP jackets,

$$\varepsilon_{fe} = \kappa_v \varepsilon_{fu} \leq 0.004 \tag{3.9}$$

$$\kappa_v = \frac{k_1 k_2 L_e}{11900\varepsilon_{fu}} \leq 0.75; \quad L_e = \frac{23300}{(n_f t_f E_f)^{0.58}} \tag{3.10}$$

$$k_1 = \left(\frac{f_{cm}}{27}\right)^{2/3}; \quad k_2 = \begin{cases} \dfrac{d_f - L_e}{d_f} & \text{(U-jacketing),} \\ \dfrac{d_f - 2L_e}{d_f} & \text{(side-bonding),} \end{cases} \tag{3.11}$$

3.4.4   CAN/CSA-S6 2006

The CAN/CSA-S6 (2006) standard has adopted design provisions similar to those in ACI 440 2R-08. The differences between the CSA-S6 and ACI codes are: (1) CSA-S6 uses the variable-truss-angle analogy instead of the 45°-truss-angle analogy used by ACI. The FRP contribution according to CSA-S6 is therefore given by:

$$V_f = \frac{A_f . E_f . \varepsilon_{fe} . d_f (\cot\theta + \cot\alpha).\sin\alpha}{s_f} \tag{3.12}$$

(2) Given the possibility for side-bonded EB FRP RC beams that $d_f < 2L_e$ (Eq. 3.13), which would lead to a negative value for k_2 when using the ACI 440 model, CSA-S6 uses a single equation for both U-wrap and side-bonded FRP for the bond-reduction factor, k_2. That is:

$$k_2 = \frac{d_f - L_e}{d_f} \tag{3.13}$$

3.4.5   CNR-DT200 2004

The Italian CNR-DT200 (2004) guidelines provisions are based on a research study by Monti and Liotta (2006). In the CNR guidelines, the FRP contribution related to each of the FRP strengthening configurations is given by:

(i) for a full FRP wrap configuration,

$$V_{fd} = \frac{1}{\gamma_{rd}} \cdot 0.9d \cdot f_{fed} \cdot 2t_f \cdot (\cot\theta + \cot\alpha) \cdot \frac{w_f}{s_f} \tag{3.14}$$

$$f_{fed} = f_{fdd} \cdot \left[1 - \frac{1}{6} \cdot \frac{L_e \cdot \sin\alpha}{\min\{0.9d\,;h_w\}}\right] + \frac{1}{2}\left(\phi_R f_{fd} - f_{fdd}\right)\left[1 - \frac{L_e \cdot \sin\alpha}{\min\{0.9d\,;h_w\}}\right] \tag{3.15}$$

$$\phi_R = 0.2 + 1.6\frac{r_c}{b_w} \;;\quad 0 \le \frac{r_c}{b_w} \le 0.5 \tag{3.16}$$

$$L_e = \sqrt{\frac{E_f \cdot t_f}{2 \cdot f_{ctm}}} \;;\quad f_{fdd} = \frac{0.80}{\gamma_{fd}} \cdot \sqrt{\frac{2 \cdot E_f \cdot G_{fk}}{t_f}} \tag{3.17}$$

$$G_{fk} = 0.03\,k_b \cdot \sqrt{f_{ck} \cdot f_{ctm}} \;;\quad k_b = \sqrt{\frac{2 - w_f / s_f}{1 + b_f / 400}} \ge 1 \tag{3.18}$$

(ii) for a U-shaped FRP configuration,

$$f_{fed} = f_{fdd} \cdot \left[1 - \frac{1}{3} \cdot \frac{L_e \cdot \sin\alpha}{\min\{0.9d\,;h_w\}}\right] \tag{3.19}$$

(iii) for a side-bonded configuration,

$$V_{fd} = \frac{1}{\gamma_{rd}} \cdot \min\{0.9d\,;h_w\} \cdot f_{fed} \cdot 2 \cdot t_f \cdot \frac{\sin\alpha}{\sin\theta} \cdot \frac{w_f}{s_f} \tag{3.20}$$

$$f_{fed} = f_{fdd} \cdot \frac{Z_{red,eq}}{\min\{0.9d\,;h_w\}} \cdot \left[1 - 0.6 \cdot \sqrt{\frac{L_{eq}}{Z_{red,eq}}}\right]^2 \tag{3.21}$$

where,

$$Z_{red,eq} = Z_{red} + L_{eq} \tag{3.22}$$

$$Z_{red} = \min\{0.9d; h_w\} - L_e \cdot \sin\alpha \tag{3.23}$$

$$L_{eq} = \frac{s_{uf}}{f_{fdd} / E_f} \cdot \sin\alpha \tag{3.24}$$

3.4.6   HB 305-2008

The Australian guidelines (2006) provisions on shear strengthening of RC beams are based on a research study carried out by Chen and Teng (2003). In the HB 305-2008 model, the contribution of the FRP shear reinforcement is given by:

$$V_f = 2f_{fed} \cdot t_f \cdot \frac{w_f}{s_f} \cdot h_{fe} \cdot (\cot\theta + \cot\alpha) \cdot \sin\alpha \tag{3.25}$$

$$h_{fe} = z_b - z_t \; ; \; z_b = 0.9d - d_{fb} \; ; \; z_t = d_{ft} \tag{3.26}$$

$$f_{fed} = D_f \cdot f_{fd,\max} \tag{3.27}$$

(i) for a full FRP wrap configuration,

$$f_{fd,\max} = \begin{cases} \dfrac{1}{\gamma_f} \cdot \phi_{R'} \cdot f_{fu} \; ; & \varepsilon_f \leq 1.5\% \\ \dfrac{1}{\gamma_f} \cdot \phi_{R'} \cdot E_f . \varepsilon_f \; ; & \varepsilon_f > 1.5\% \end{cases} \tag{3.28}$$

$$D_f = 0.5\left(1 + \frac{z_t}{z_b}\right) \tag{3.29}$$

(ii) for U-shaped and side-bonded configurations,

$$D_f = \begin{cases} \dfrac{2}{\pi \cdot \lambda} \cdot \dfrac{1 - \cos\left(\dfrac{\pi}{2} \cdot \lambda\right)}{\sin\left(\dfrac{\pi}{2} \cdot \lambda\right)} \; ; & \lambda = \dfrac{L_{\max}}{L_e} \leq 1 \\ 1 - \dfrac{\pi - 2}{\pi \cdot \lambda} \; ; & \lambda = \dfrac{L_{\max}}{L_e} > 1 \end{cases} \tag{3.30}$$

$$L_{max} = \begin{cases} \dfrac{h_{fe}}{\sin \alpha} & \text{(U-shaped)} \\ \dfrac{h_{fe}}{2\sin \alpha} & \text{(Side bonded)} \end{cases} \quad ; \quad L_e = \sqrt{\dfrac{E_f \cdot t_f}{\sqrt{f_{ck}}}} \quad (3.31)$$

$$f_{fd,max} = \min \begin{cases} \dfrac{1}{\gamma_f} \cdot \phi_{R'} \cdot f_{fu} \\ \dfrac{1}{\gamma_f} \cdot 0.35 \cdot \beta_L \cdot \beta_w \cdot \sqrt{\dfrac{E_f \cdot \sqrt{f_{ck}}}{t_f}} \end{cases} \quad (3.32)$$

$$\beta_L = \begin{cases} \lambda & , & \lambda \le 1 \\ 1 & , & \lambda > 1 \end{cases} \quad ; \quad \beta_w = \sqrt{\dfrac{2 - w_f / (s_f \cdot \sin \alpha)}{1 + w_f / (s_f \cdot \sin \alpha)}} \quad (3.33)$$

where $\phi_{R'} = 0.80$ and $\gamma_f = 1.25$.

3.5   Factors influencing FRP debonding in shear

Debonding of FRP is the most likely governing failure mode for RC beams shear-strengthened with EB FRP. This is particularly true for the side-bonded and U-jacket FRP configurations. Over the past twenty years, several research studies (e.g., Triantafillou 1998; Khalifa et al. 1998; Chaallal et al. 2002; Pellegrino and Modena 2002; Chen and Teng 2003; Bousselham and Chaallal 2004; Monti and Liotta 2006) have been conducted to explore the factors influencing the FRP debonding failure mode for RC beams strengthened in shear with EB FRP. These studies have identified several major parameters which affect the shear contribution of FRP to shear resistance. Some of these parameters have been code-formatted and successfully introduced into the guidelines. However, as can be clearly seen in Table 3.1, which lists the major influencing factors and the status of their consideration by the current design guidelines, there are still many important parameters that have not yet been captured by the guidelines.

Table 3.1   Status of influencing factors on shear strengthening
of RC beams in the current design guidelines

FRP design guidelines	Latest revisio	Bond mode	Effective strain	Anchorage length	w_f/s_f	Crack angle	Crack pattern	Effect of transverse
ACI 440-2R	2008	✓	✓	✓	✗	✗	✗	✗
CSA-S6	2006	✓	✓	✓	✗	✓	✗	✗
CSA-S806	2002	✗	✓	✗	✗	✗	✗	✗
fib-TG 9.3	2001	✗	✓	✗	✗	✓	✗	✗
CNR-DT 200	2004	✓	✓	✓	✓	✓	✗	✗
CIDAR	2006	✓	✓	✓	✓	✓	✗	✗

It may be argued that some of these parameters are not yet fully understood and need further research. Nevertheless, it is believed that an inclusive, rational, and evolutionary model is attainable given the body of research in the field. Before developing such a conceptual model, it was deemed useful to provide a brief review of the influencing parameters (see Table 3.1) in the following sections.

3.5.1   Bonding model

To study the mechanism of FRP debonding from concrete, a reliable bonding model is required. Several researchers have proposed various bonding models based on experimental research studies (Hiroyuki and Wu 1997; Tanaka 1996; Maeda et al. 1997; Holzenkämpfer 1994 and Neubauer and Rostásy 1997). The bonding models proposed by Hiroyuki and Wu (1997) and Tanaka (1996) calculated the average bond shear at failure, τ_{eff}, as a function of the bonding length, L. Those models did not fit well with experimental data. They generated a very large scatter in the results. This may be attributed to the failure of these models to take into consideration the effective bond length (Chen and Teng 2001).

Maeda et al. (1997) demonstrated that, beyond a certain FRP bond-length threshold (effective bond length), increasing bond length does not result in an increase in the ultimate bond strength.

Therefore, they introduced an FRP rigidity factor into their equation for τ_{eff}. Khalifa et al. (1998) modified the model proposed by Maeda et al. (1997) to be used in design by including involving the effect of concrete strength. The model proposed by Khalifa et al. (1998) showed a good correlation with experimental results in predicting the bond strength, P_u. However, it failed to predict accurately the effective bond length and the shear stress at failure when these were considered separately (Chen and Teng 2001). This might be due to the fact that L_e in the Khalifa et al. (1998) model has an inverse relationship with $E_f \cdot t_f$, whereas experimental research studies (e.g. Bizindavyi and Neale 1999; Brosens and Van Gemet 1999) have proved that the effective bond length has a direct relationship with $E_f \cdot t_f$.

Some researchers have related the effective bond strength to the concrete-surface tensile strength (Holzenkämpfer 1994, Neubauer and Rostásy 1997). Chajes et al. (1995) experimentally observed that the ultimate bond strength is proportional to $\sqrt{f'_c}$. This observation was later confirmed by Chen and Teng (2001), who expressed shear-slip properties in terms of concrete strength as follows:

$$\tau_{eff} = \beta \sqrt{f'_c} \qquad (3.34)$$

Karbhari et al. (2006) evaluated the performance of some of the models described above in predicting bond strength by comparing their predictions with experimental results available in the literature. The models of Neubauer and Rostásy (1997) and Chen and Teng (2001) showed good correlation with experimental results in predicting effective bond length, L_e. However, unlike the Neubauer and Rostásy (1997) model, the Chen and Teng (2001) model, although accurate in predicting L_e, produced conservative results on the bond strength, P_u. The Holzenkämpfer (1994) model showed a good correlation with experimental results for concrete-to-steel bonding in predicting the bond strength, P_u (Blaschko et al. 1998). On the other hand, the Holzenkämpfer (1994) model produced conservative results in predicting the effective bond length with concrete in FRP bonding experimental tests (Chen and Teng 2001).

3.5.2 Effective strain

Assuming that the external FRP reinforcement carries only normal stresses in the principal FRP material direction, FRP may be treated by analogy to internal steel. In this case, all the FRP strips intersected by the selected shear crack are assumed to contribute the same FRP effective strain. The effective strain, ε_{fe}, in the principal material direction is in general less than the tensile strain at failure, ε_{fu}. Hence, the FRP contribution to shear resistance can be written in the following form (ACI 440.2R-08):

$$V_f = \frac{A_{fv}.f_{fe}.(\sin\alpha + \cos\alpha).d_f}{s_f} = \rho_f.E_f.\varepsilon_{fe}.b.d_f.(\sin\alpha + \cos\alpha) \qquad (3.35)$$

In recent years, researchers have proposed various equations to calculate ε_{fe}. Chaallal et al. (1998) suggested, on the basis of the truss model, that the maximum FRP strain be limited by a maximum allowable shear strain between FRP and concrete. Triantafillou (1998) proposed a truss model in which the effective strain in the FRP is calculated using empirical equations with terms representing the FRP bonding configuration, the FRP axial rigidity, and the compressive strength of concrete. Khalifa et al. (1998) modified Triantafillou's model by calculating the effective strain using Maeda's (1997) modified bonding model. In addition, they recommended a strain limitation due to the shear-crack width and the loss of aggregate interlocking.

Basically, the effective strain in the FRP can be calculated using the equilibrium conditions in the FRP sheet. Before debonding, the force in the FRP is equal to the maximum bonding force between the FRP and the concrete surface. The force that can be developed in the sheet on one side of the beam, P_{max}, can be calculated using one of the proposed bonding models. The effective strain can be determined from the following equations:

$$P_{max} = A_f.f_{fe} \qquad (3.36)$$

$$L_e.w_f.\tau_{eff} = t_f.w_f.E_f.\varepsilon_{fe} \qquad (3.37)$$

It follows that:

$$\varepsilon_{fe} = \frac{\tau_{eff}.L_e}{t_f.E_f} \leq \varepsilon_{fu} \tag{3.38}$$

3.5.3   FRP effective anchorage length

Empirically, for an FRP sheet bonded with an FRP anchorage length greater than the effective anchorage length, the ultimate tensile force is limited to the force corresponding to the effective anchorage length. In the early phase of loading, the load is sustained by the bond resistance developed in an area whose dimensions are the FRP effective anchorage length and the FRP width. Local FRP debonding and concrete-cover delamination (debonding due to concrete failure beneath the FRP-to-concrete interface) in the active bonded zone take place as the load increases. Therefore, the active bond area shifts to the nearest inactive bonded zone. This migration of the bonded zone continues until total FRP debonding occurs. This implies that bond strength does not increase steadily and constantly with bond length. This also explains the rationale behind the important concept of effective bond length, defined as the length beyond which the bond strength remains constant.

Maeda et al. (1997) proposed an empirical equation to calculate effective bond length. This equation is a function of $t_f{\cdot}E_f$ of the FRP sheet, expressed as:

$$L_e = e^{6.134 - 0.58\ln(t_f \cdot E_f)} \tag{3.39}$$

Equation (3.39) is currently in use to calculate the effective anchorage length of an FRP sheet bonded to a concrete surface in the ACI 440.2R-08 and CAN/CSA S6-06 design guidelines.

Holzenkämpfer (1994) studied the bond strength between steel plates and concrete using nonlinear fracture mechanics (NLFM). The modified form of NLFM as developed by Neubauer and Rostásy (1997) calculates the bond strength, P_u, as:

$$P_u = \begin{cases} 0.64 \cdot k_p \cdot b_f \sqrt{E_f t_f f_{ct}} & \text{for } L \geq L_e \\ 0.64 \cdot k_p \cdot b_f \sqrt{E_f t_f f_{ct}} \dfrac{L}{L_e}\left(2 - \dfrac{L}{L_e}\right) & \text{for } L < L_e \end{cases}$$

(3.40)

where the effective bond length, L_e, is given by:

$$L_e = \sqrt{\frac{E_f t_f}{2 f_{ct}}} \text{ (mm)}$$

(3.41)

The NLFM equations for predicting the FRP anchorage length were later modified by many researchers (Chen and Teng (2001) and Monti et al. (2003) among others). The modified NLFM is currently used to calculate the effective anchorage length of an FRP sheet bonded to a concrete surface in the Italian CNR-DT200 (2004) and Australian HB 305-2008 design guidelines, which are respectively based on the Monti et al. (2003) and Chen and Teng (2001) research studies.

Meanwhile, the maximum bond stress in the FRP sheets intersected by the critical shear crack may be obtained from one of the proposed bond models. Clearly, the maximum FRP stress occurs in those fibres that have a bond length at least equal to the effective bond length. Assuming that the critical shear crack is a single line, for an FRP U-jacket, the only side of the FRP where the bond length is at least equal to the effective bond length is the side above the crack line. In contrast, for side-bonded FRP sheets, effective bond lengths should be sought on both sides of the crack line to ensure a successful bond. Therefore, the maximum available bond length, L_{max}, is given by:

$$L_{max} = \begin{cases} \dfrac{d_f}{sin\,\alpha} & \text{for U-jackets} \\ \dfrac{d_f}{2\,sin\,\alpha} & \text{for side plates} \end{cases}$$

(3.42)

In beams with a maximum available anchorage length, L_{max}, shorter than L_e, a decreasing β_L coefficient ($0 < \beta_L < 1$) has been proposed by some researchers (Holzenkämpfer 1994,

Neubauer and Rostásy 1997, Chen and Teng 2001) to represent the effect of FRP sheets having an anchorage length shorter than L_e (Figure 3.1). According to the models proposed by Holzenkämpfer (1994) and Neubauer and Rostásy 1997, β_L can be determined using the following equation:

$$\beta_L = \begin{cases} 1 & \text{if } \lambda \geq 1 \\ (2-\lambda).\lambda & \text{if } \lambda < 1 \end{cases} \qquad \lambda = \frac{L_{max}}{L_e} \tag{3.43}$$

Note that Chen and Teng (2001) also proposed an equation for β_L as follows:

$$\beta_L = \begin{cases} 1 & \text{if } \lambda \geq 1 \\ sin\dfrac{\pi\lambda}{2} & \text{if } \lambda < 1 \end{cases} \qquad \lambda = \frac{L_{max}}{L_e} \tag{3.44}$$

A comparison of Eq. (3.43) with Eq. (3.44) is provided in Figure 3.1.
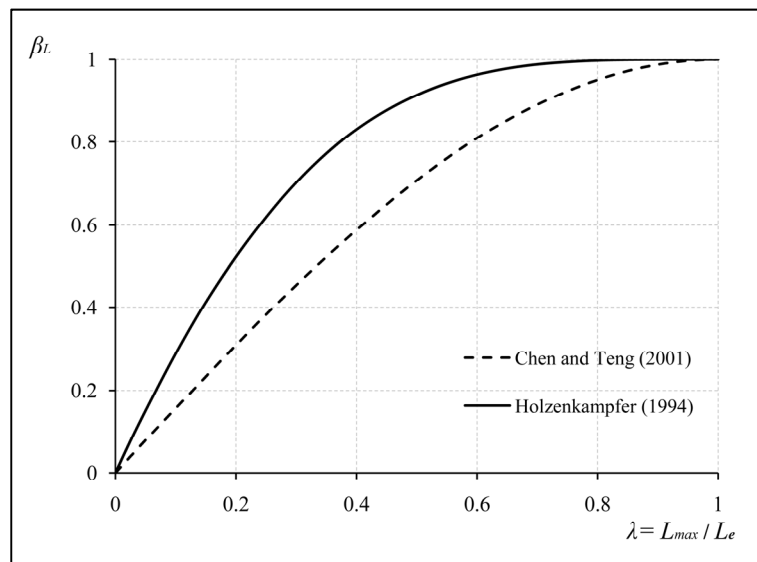
Figure 3.1   FRP effective anchorage length ratio β_L versus λ according to Holzenkämpfer (1994) and Chen and Teng (2001).

3.5.4 FRP effective width

After a major shear crack propagates through a beam's cross section, only the FRP fibres that have an anchorage length greater than the FRP effective length remain adequately anchored and capable of carrying a shear force in proportion to their width. Above the crack line, the strips closest to the web-flange corner (for U-jacket FRP) have a small anchorage length. Therefore, they can transfer only a reduced bond force in comparison to those strips that have longer anchorage lengths. The overall FRP shear resistance is then redistributed to the remaining strips. Therefore, it has been suggested that the width of the FRP sheet, w_f, be replaced by an effective width, w_{fe}. Khalifa et al. (1998) proposed equations to calculate the effective width based on the shear-crack angle (assumed to be 45°) and the bonded-surface configuration (Figure 3.2), as follows:

$$w_{fe} = d_f - L_e \qquad \text{for sheets in the form of U-jackets} \qquad (3.45)$$
$$w_{fe} = d_f - 2L_e \qquad \text{for sheets bonded to the sides of the beam} \qquad (3.46)$$
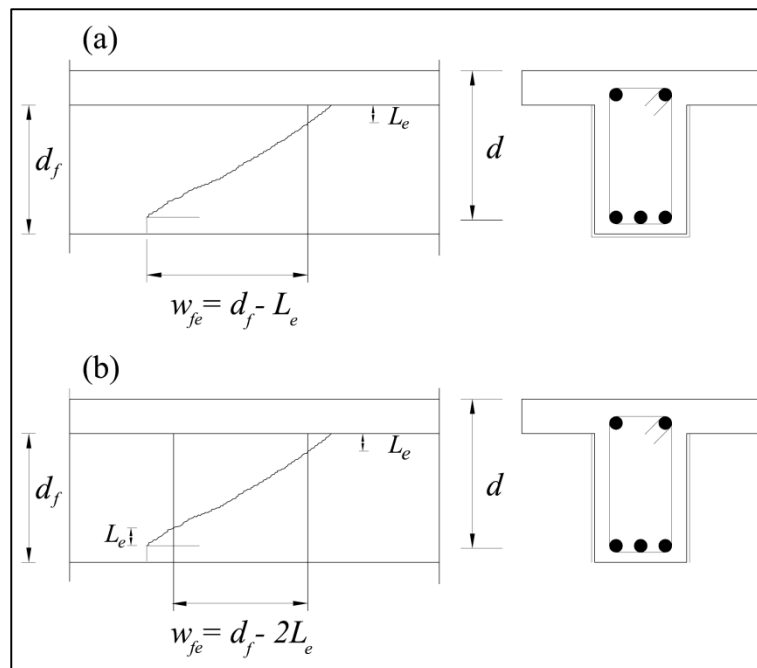
Figure 3.2   Effective width of FRP sheets for: a) U-jacket
and b) side-bonded installations.

Current models for calculating w_{fe} are based on one major 45° shear crack. However, this might not be a realistic assumption for RC beams that are internally or externally reinforced in shear because these show a more complex cracking pattern, as discussed further below.

3.5.5 Strip-width to spacing ratio

Results from previous FRP-to-concrete direct pull-out tests have shown that the width of the FRP sheets bonded to a concrete block has a significant effect on the maximum bond strength of the FRP. If the width of the bonded plate is smaller than that of the concrete member, the force transferred from the plate to the concrete leads to a non-uniform stress distribution across the width of the concrete member. In fact, as the FRP sheets become narrower, the bond strain increases. Kamel et al. (2000) observed that FRP strain values are substantially greater at the edge than at the center of a sheet. They also observed that the difference between the strain values (edge versus center) increased as the load approached its ultimate value. Therefore, the maximum load per unit width of the FRP strip can be considerably decreased in wide FRP sheets because of strain concentrations at the edges. In contrast, it is believed that the strain distribution across the width is likely to be fairly uniform for narrow FRP sheets.

Holzenkämpfer (1994) and Neubauer and Rostásy (1997) introduced the term k_p to express this phenomenon:

$$k_p = \sqrt{1.125 \times \frac{2 - \dfrac{b_p}{b_c}}{1 + \dfrac{b_p}{400}}} \tag{3.47}$$

The effect of this phenomenon was later extended to RC beams strengthened in shear using bonded strips when Holzenkämpfer's equation was modified by Chen and Teng (2001). In this equation, b_p is replaced by w_f and b_c by s_f. That is:

$$\beta_w = \sqrt{\dfrac{2 - {w_f}/{s_f}}{1 + {w_f}/{s_f}}} \qquad\qquad (3.48)$$

Note that the coefficient β_w is derived from direct pull-out test results. Therefore, the validity of this multiplier for RC beams strengthened in shear with FRP remains to be evaluated for members subjected to shear and for different combinations of w_f and s_f. Work on this problem is being pursued in the ETS laboratory of the University of Quebec.

3.5.6   Cracking angle

It has been established that the concrete-cracking angle affects neither the FRP effective strain nor the FRP effective width. According to Deniaud and Cheng (2004), the effective FRP strain, ε_{fe}, and the ratio, R_L (FRP effective width over total FRP width), are independent of the concrete-cracking angle, θ. However, the load carried by the FRP sheet is assumed to be a function of the concrete-cracking angle when the truss analogy with a variable strut angle is used. Most of the design guidelines recommend that θ be conservatively set equal to 45° when calculating V_f. Although in most usual cases θ is less than 45°, there are some particular cases, where very closely spaced transverse reinforcement is used, for which $\theta >$ 45°. Note that the truss model with 45° cracks is conservative only for normally reinforced beams strengthened in shear with FRP. With a relatively large amount of transverse reinforcement the crack may require less energy to pass through the cross-section with an inclination greater than 45° than with a crack inclination less than 45 °. In this way, the crack «chooses» to pass through less transverse reinforcement with a higher inclination (Carolin and Täljsten 2005).

On the basis of this discussion, the authors believe that it is appropriate to use a variable crack angle in the V_f equation, as follows:

$$V_f = \frac{A_{fv}.f_{fe}.(\cot\theta + \cot\alpha).\sin\alpha.d_f}{s_f} = \rho_f.E_f.\varepsilon_{fe}.b.d_f.(\cot\theta + \cot\alpha).\sin\alpha \quad (3.49)$$

3.5.7   Cracking pattern

Experimental observations clearly showed that in RC beams with transverse reinforcement the shear-crack pattern tends to be distributed over a large width compared with the pattern in RC beams with no or less shear reinforcement (Pellegrino and Modena 2002). Figures 3.3(a) to 3.3(d) (taken from an ongoing experimental research study carried out by the authors) illustrate the effect of transverse steel and EB FRP on the cracking pattern. These figures show four similar RC beams with different shear-reinforcement ratios. These beams failed in shear under similar loading and support conditions. The beam in Figure 3.3(a), with no shear reinforcement, failed along a single crack line. The beam in Figure 3.3(b), with transverse steel reinforcement, failed with one major shear crack and a few minor shear cracks. The beam in Figure 3.3(c) was reinforced in shear only with externally bonded FRP sheets. This beam failed with one major shear crack and two additional surface shear cracks (in the concrete cover) that joined the major shear crack in the concrete core. This led to debonding of FRP attached to a large chunk of concrete. The beam in Figure 3.3(d) was reinforced with both transverse internal steel and externally bonded FRP sheets. It can be seen that the beam failed with a distributed shear multi-crack pattern.

On the other hand, it can also be said that a more distributed cracking pattern can accelerate FRP debonding and lead to premature shear failure. The debonding process generally starts from a shear crack in the cracked zone, because bonding shear stresses become too high at the crack and the anchorage is reduced. Eventually, the stress concentration moves outward from the crack, and the anchorage failure propagates until the final debonding failure occurs (Carolin and Täljsten 2005).
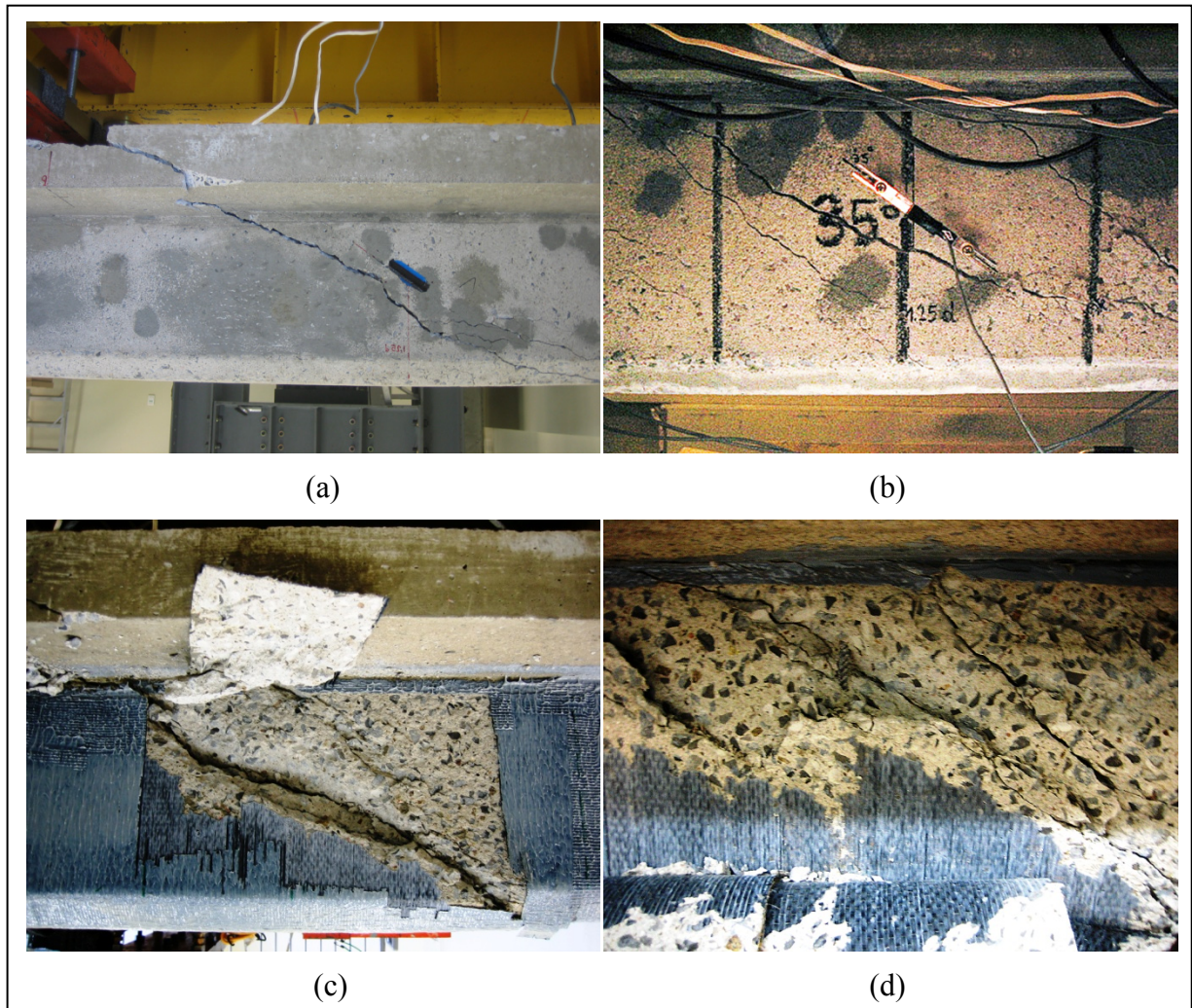
Figure 3.3   Effect of transverse steel and epoxy-bonded FRP on cracking pattern: a) unreinforced unstrengthened RC beam; b) reinforced unstrengthened RC beam; c) unreinforced strengthened RC beam; and d) reinforced strengthened RC beam.

It is believed that cracking affects the debonding process because it results in a loss of bond in the crack vicinity. This initiates debonding of the fibres that bridge the cracks. In addition, a beam with a more distributed cracking pattern tends to have FRP fibres with smaller anchorage lengths compared with the fibres on a beam with a single-line crack pattern.

As was discussed earlier, assuming a single-crack line pattern, some of the fibres that have an anchorage length less than L_e debond earlier than the rest of the fibres. These fibres should be

disregarded from the V_f calculations. Therefore, an effective width, w_{fe}, for a single-crack line pattern was proposed. In the present article, to extend this phenomenon to the multi-shear-crack pattern, a β_c coefficient is introduced. In a multi-line cracking pattern, multi-shear-crack lines intersect the FRP fibres in several points. According to Carolin and Taljsten (2005), each FRP fibre/crack intersection causes stress concentration in the fibres at that point. This leads to shorter FRP anchorage lengths for FRP fibres, which eventually leads to premature debonding. Therefore, assuming a multi-line cracking pattern, the anchorage lengths of the FRP fibres cannot be warranted using the proposed equations for a single-line crack pattern. Because there are several irregular intersections of fibres with a multi-shear-crack pattern, it is not easy to determine a bonding area containing FRP fibres that have the minimum effective anchorage length.

The coefficient β_c transforms a bonding area of a beam with a multi-line cracking pattern to the equivalent bonding area of a beam with a 45º single-line cracking pattern using a newly proposed FRP effective width.

3.5.8   Transverse steel

Experimental tests have revealed that FRP composites are less effective when beams are heavily reinforced with internal shear-steel reinforcement (Chaallal et al. 2002, Pellegrino and Modena 2002, Bousselham and Chaallal 2004). It has been clearly established that the effectiveness of the strengthening contribution of FRP to shear resistance depends on the amount of internal shear-steel reinforcement. However, as can be observed in Table 3.1, none of the guidelines has yet considered the effect of transverse steel on V_f in their formulae. Two models have been proposed to predict the effect of transverse steel on FRP shear contribution. Chaallal et al. (2002) proposed an equation to calculate the effective strain of FRP based on the total shear-reinforcement ratio, $\rho_{tot} = n.\rho_f + \rho_s$. This model yielded promising results within a limited range of shear reinforcement values. Pellegrino and Modena (2002) modified the model of Khalifa et al. (1998) by adding an R^* reduction factor to take into account the effect of transverse-steel reinforcement. The R^* reduction factor is a function of $E_s \cdot A_s / E_f \cdot A_f$. Note that

this model did not consider the effect of the spacing between internal steel stirrups or external FRP strips.

On the basis of the various studies discussed in the previous sections, the authors believe that the effectiveness of FRP shear strengthening is predominantly governed by the effectiveness of the bond between FRP and concrete, which in turn is highly dependent on the anchorage length as a proportion of the effective length of the FRP fibres. Moreover, as discussed earlier, the greater the amount of transverse reinforcement (steel + FRP), the more distributed is the cracking pattern and the shorter is the available anchorage length. Consequently, the bond force and hence the EB FRP contribution to the shear resistance decrease.

3.6   Proposed conceptual model

Figure 3.4(a) shows a typical configuration of a beam strengthened in shear with a bonded FRP U-jacket. According to experimental observations (e.g., those shown in Figure 3.3(c)), it can be assumed that the effective debonded FRP is defined by a trapezoidal area as shown by the hatched area in Figure 3.4(a) for U-jacket and Figure 3.4(c) for side bonded FRP. This typical configuration is based on the assumption of multi-shear crack pattern. Note that the effect on bond of several cracks intersecting the FRP is not well documented. However, one way of taking into account the effect of multi-crack pattern is to substitute the trapezoidal bonding area by an equivalent rectangular area, the dimensions of which are the effective length (L_e) and the effective width (w_{fe}) [Figures 3.4(b) and 3.4(d)].

The effective length can be calculated using Neubauer and Rostásy (1997) equation:

$$L_e = \sqrt{\frac{E_f t_f}{2 f_{ct}}} \ \text{(mm)} \tag{3.50}$$

where f_{ct} is the concrete tensile strength. However, if f_{ct} is not available, it can be calculated as a function of f'_c (Mirza et al. 1979). That is:

$$f_{ct} = 0.53\sqrt{f'_c}$$
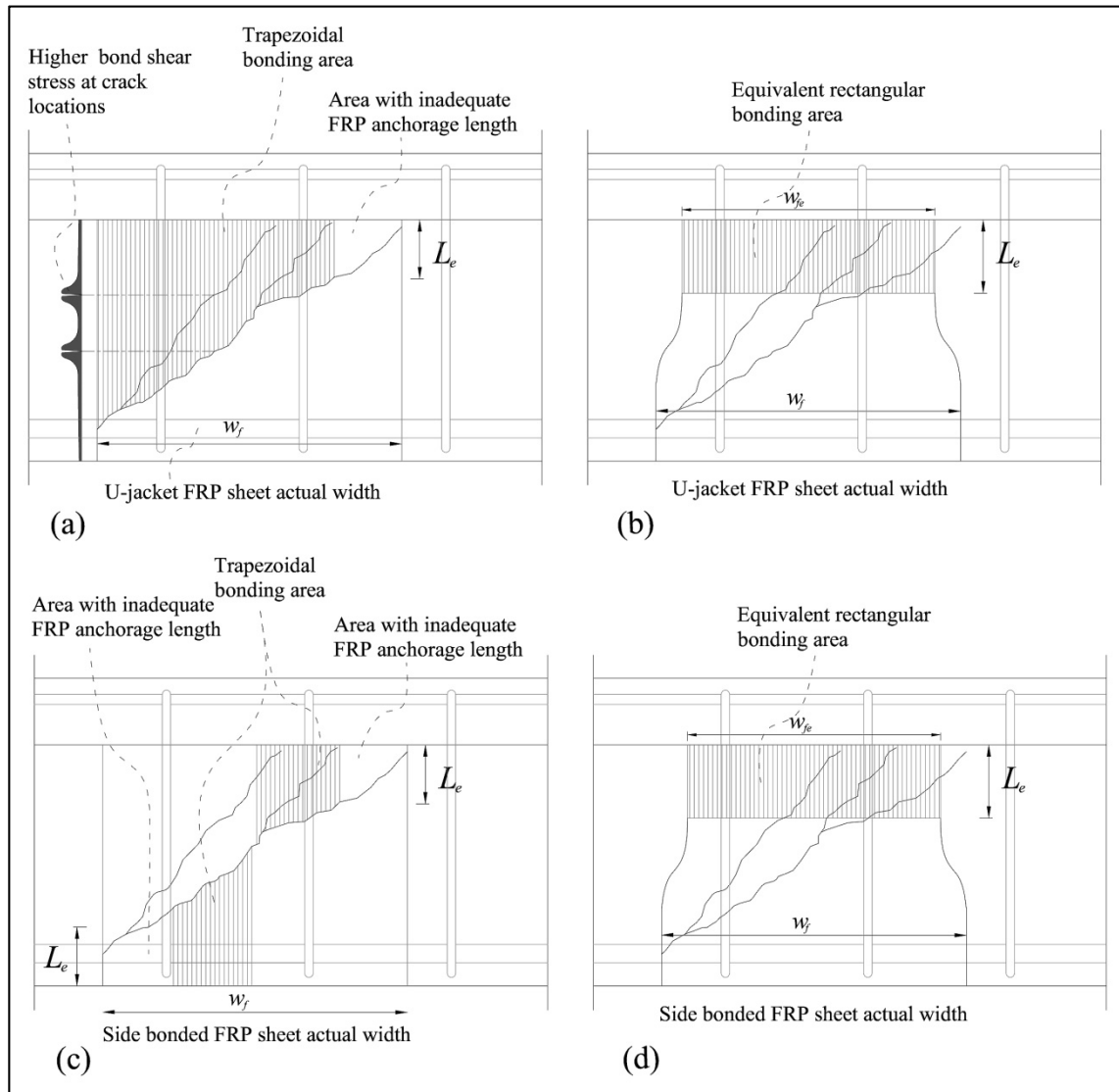
Figure 3.4 Typical configuration of effective FRP width in beams strengthened in shear with EB continuous FRP sheet: a) actual bonding area for U-jacket; b) equivalent bonding area for U-jacket; c) actual bonding area for side-bonded FRP; and d) equivalent bonding area for side-bonded FRP.

In the calculation of w_{fe}, it is assumed that the cracking pattern changes with the amount of internal steel and external FRP shear reinforcement as measured by their respective rigidities. In addition, the cracking pattern affects the anchorage length of the fibres. As the cracking pattern becomes more distributed, fewer fibres will offer full effective anchorage length. Consequently, the effective width, that is the width of the fibres long enough to achieve the effective anchorage length, decreases. Using a computational analysis based on test results available in the literature (see Bousselham and Chaallal (2004) for the database) the effective width is defined as a function of the sum of the rigidity of transverse steel reinforcement and that of transverse FRP sheets (see Figures 3.5 and 3.6).
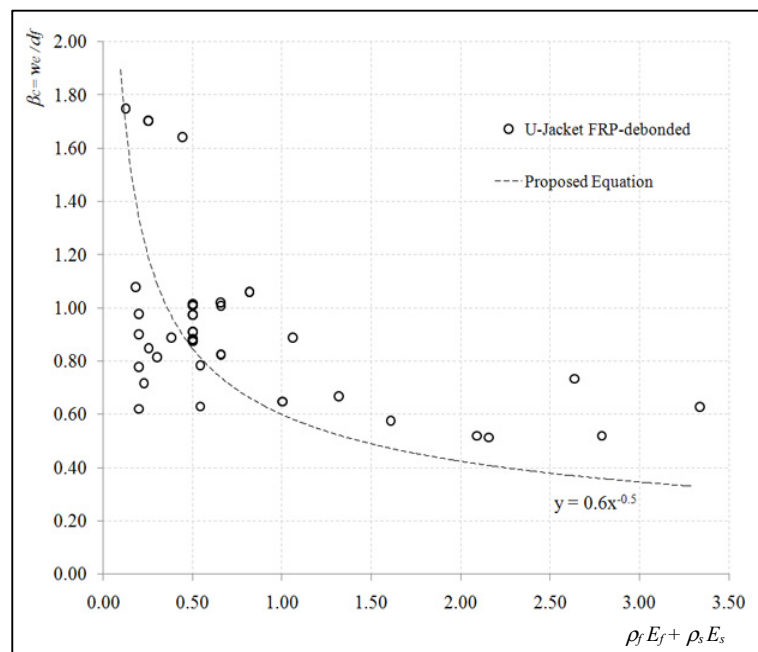
Figure 3.5 $\beta_c = w_{fe} / d_f$ ratio versus FRP rigidity plus transverse-steel rigidity for bonded U-jacket configuration.
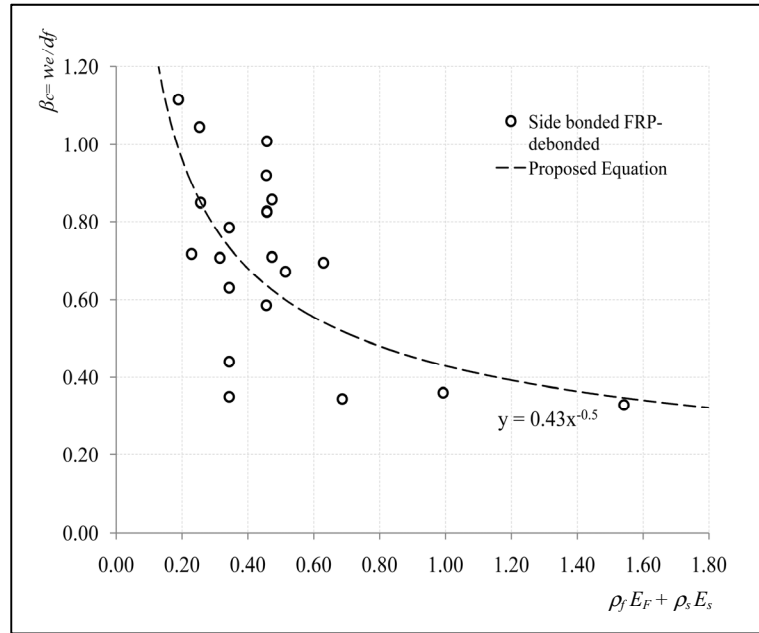
Figure 3.6 $\beta_c = w_{fe}/d_f$ ratio versus FRP rigidity plus transverse-steel rigidity for side-bonded configuration.

In this analysis, the coefficient β_c and the proposed w_{fe} are calculated based on the strut-and-tie model as follows (assuming a cracking angle $\theta = 45°$):

$$V_f = 2\beta_c \cdot t_f \cdot \varepsilon_{fe} \cdot E_f \cdot (\sin\alpha + \cos\alpha) \cdot d_f \times \frac{w_f}{s_f} \qquad (3.52)$$

Using the equilibrium conditions in the FRP sheet (Eq. 3.37), w_{fe} can be calculated using the following equation:

$$w_{fe} = \frac{V_f}{2L_e \cdot \tau_{eff}} \times (\sin\alpha + \cos\alpha) \times \frac{w_f}{s_f} \qquad (3.53)$$

Based on the results calculated above, Equation 3.54 is calibrated using available experimental results to calculate the effective width, w_{fe}, as a function of $\rho_f.E_f + \rho_s.E_s$ for beams strengthened with a continuous U-jacket configuration (E_f and E_s are in GPa). Similarly, Eq. 3.55 is calibrated for a side-bonding configuration:

$$w_{fe} = \frac{0.6}{\sqrt{\rho_f \cdot E_f + \rho_s \cdot E_s}} \times d_f \quad \text{for U-Jacket} \tag{3.54}$$

$$w_{fe} = \frac{0.43}{\sqrt{\rho_f \cdot E_f + \rho_s \cdot E_s}} \times d_f \quad \text{for side bonded} \tag{3.55}$$

with w_{fe} defined, the cracking modification factor can then be calculated as β_c, i.e.,

$$\beta_c = \frac{w_{fe}}{d_f} = \frac{0.6}{\sqrt{\rho_f \cdot E_f + \rho_s \cdot E_s}} \quad \text{for U-Jackets} \tag{3.56}$$

$$\beta_c = \frac{w_{fe}}{d_f} = \frac{0.43}{\sqrt{\rho_f \cdot E_f + \rho_s \cdot E_s}} \quad \text{for side bonded} \tag{3.57}$$

The bond shear force can be calculated by multiplying the proposed rectangular bond area by the bond shear stress, τ_{eff}, as calculated using Eq. 3.34. The effects of β_L for beams with an anchorage length less than the effective length and of β_w to incorporate the w_f / s_f ratio of the FRP strips are considered in the equation for effective strain:

$$P_{bond} = P_{fe} \tag{3.58}$$

$$\beta_c \, \beta_L \, \beta_w \, L_e \, w_{fe} \, \tau_{eff} = t \cdot w_{fe} \cdot E_f \cdot \varepsilon_{fe} \tag{3.59}$$

and hence:

$$\varepsilon_{fe} = \frac{\beta_c \cdot \beta_L \cdot \beta_w \cdot \tau_{eff} \cdot L_e}{t_f \cdot E_f} = 0.31 \beta_c \cdot \beta_L \cdot \beta_w \sqrt{\frac{\sqrt{f_c'}}{t_f E_f}} \leq \varepsilon_{uf} \tag{3.60}$$

Note that β_L and β_w can be calculated using Eqs. (3.43) and (3.47). In addition, V_f can be calculated as a function of ε_{fe} using the following equation that accounts for the effect of the cracking angle, θ:

$$V_f = \frac{2t_f \cdot w_f \cdot \varepsilon_{fe} \cdot E_f \cdot (\cot\theta + \cot\alpha).\sin\alpha.d_f}{s_f} = \rho_f \cdot E_f \cdot \varepsilon_{fe} \cdot b.d_f \cdot (\cot\theta + \cot\alpha).\sin\alpha \tag{3.61}$$

It should be noted that in the case of a continuous FRP sheet, the FRP width, w_f, and the spacing, s_f, can be assumed equal to one. For an FRP strip configuration, the effective width can be calculated as the sum of the FRP strip widths within the effective width zone. It should be remembered that the proposed model is not valid for RC members strengthened with a full wrap configuration.

3.7 Validation of the design proposal

To assess the validity of the proposed theoretical predictions, test results from other research studies were used. A database representing 75 RC beams strengthened in shear with U-jacket and side-bonded FRP that failed exclusively in FRP debonding was collected from published literature (Uji 1992, Al-Sulaimani et al. 1994, Sato et al. 1996, Taerwe et al. 1997, Chaallal et al. 1998, Taljsten 1998, Triantafillou 1998, Khalifa et al. 2000-a, Khalifa et al. 2000-b, Deniaud and Cheng 2001, Pellegrino and Modena 2002, Micelli et al. 2002, Diagana et al. 2003, Hsu et al. 2003, Adhikary et al. 2004, Zhang et al. 2004, Monti and Liotta 2005). The contribution of FRP to shear was calculated using the proposed model and compared with the values given by the ACI 440.2R 2008, *fib* -TG 9.3 2001, CAN/CSA-S806 2002, HB 305-2008, and CNR-DT200 2004 guidelines. Figures 3.6(a) to 3.6(f) show the $V_{f\,cal}$ values calculated using the proposed model and each of the guidelines versus the experimental values of $V_{f\,exp.}$

Table 3.2, which presents the coefficients of determination (R^2) between the calculated $V_{f\,cal}$ from each of the models and the experimental $V_{f\,exp.}$, clearly shows that the proposed model ($R^2 = 0.61$) is superior to the available design guidelines. To check the sensitivity of the proposed model to the effect of the transverse steel (cracking coefficient β_c), the model was compared with the experimental results assuming β_c equal to one (i.e., the effect of transverse steel not considered). This resulted in a considerable scatter in the proposed model's predictions of V_f and a significant drop in R^2 ($R^2 = 0.37$).
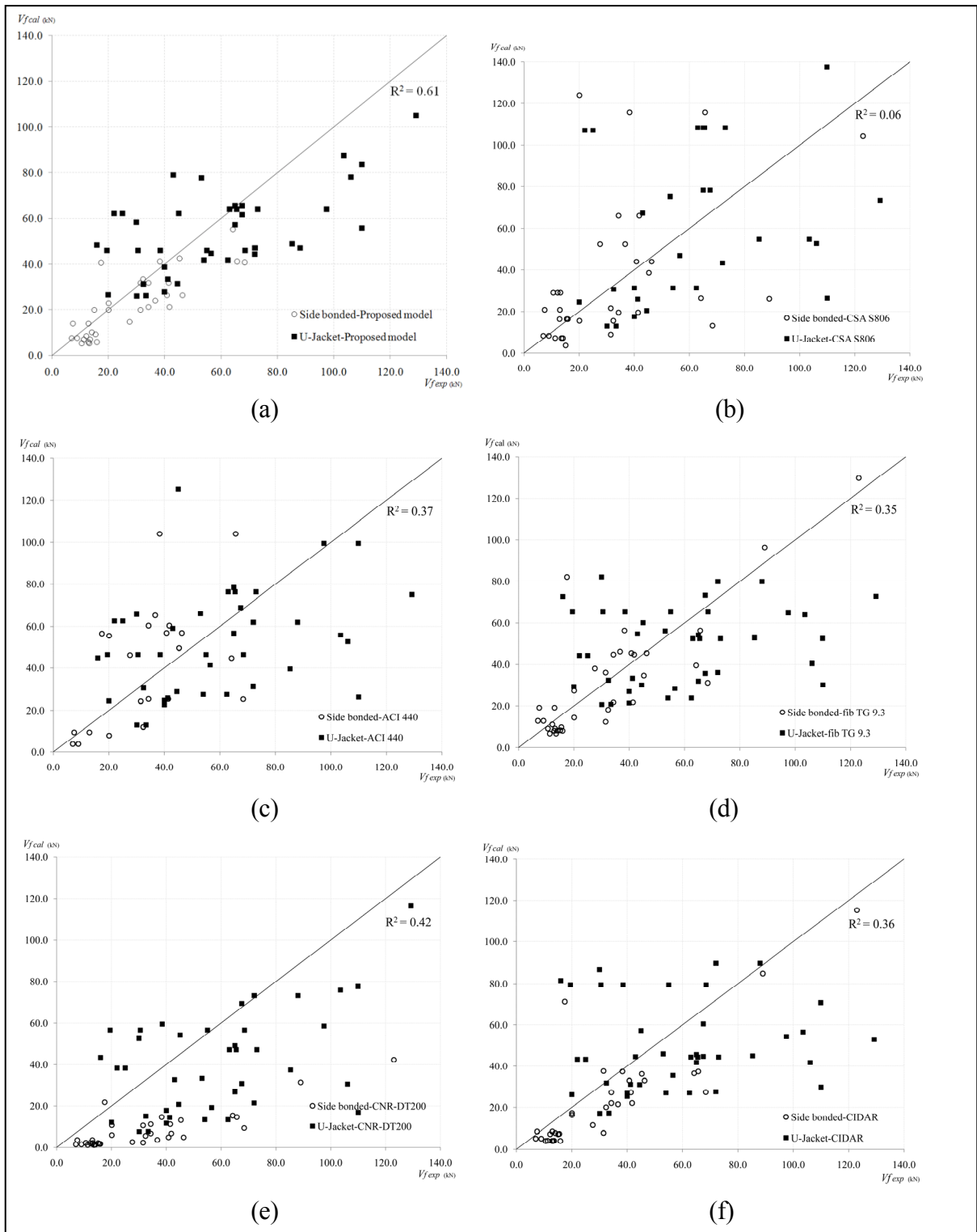
Figure 3.7   Predicted versus experimental FRP contribution for U-jacket and side-bonded FRP calculated using a) the proposed model, b) CSA S806, c) ACI 440 2R, d) *fib* TG 9.3, e) CNR DT-200, and f) CIDAR.

On the other hand, it was deemed instructive to evaluate the effect of β_c (dimensionless coefficient) on the predicted results of other codes. Multiplying β_c by V_{fcal} using the ACI 440.2R 2008, *fib* -TG 9.3 2001, CAN/CSA-S806 2002, HB 305-2008, and CNR-DT200 2004 guidelines resulted in a significant improvement on the accuracy of the calculated results for all the mentioned guidelines (Table 3.2). This shows the relevance of considering β_c into the V_f equation.

Table 3.2   Coefficient of determination (R^2) between the calculated
V_{fcal} of each of the guidelines and the experimental V_{fexp}.

FRP design model	Year	R^2 (with β_c)	R^2 (without β_c)
Proposed model	-	0.61	0.37
CSA-S806	2002	0.14	0.06
ACI 440-2R	2008	0.42	0.37
fib-TG 9.3	2001	0.49	0.35
CNR-DT 200	2004	0.51	0.42
CIDAR	2006	0.58	0.36

3.8   Conclusions

The major factors influencing the shear contribution of EB FRP and the role of these factors in the current design guidelines are studied and discussed in this paper. On the basis of this effort, a new design approach has been proposed for calculating the shear contribution of FRP, taking into consideration the effect of transverse steel on the EB FRP contribution in shear. The effectiveness of the proposed method has been validated using experimental results available in the literature. The proposed model showed the best correlation with experimental results in comparison with the current guidelines. From this research study, the following conclusions can be drawn:

- the influence of conventional transverse-steel reinforcement on the contribution of FRP to shear resistance has been proved to be significant. However, none of the studied

models and guidelines explicitly considers this parameter when calculating the FRP contribution to shear;

- a new FRP effective width, w_{fe}, is defined to transform a bonding area of a beam with multi-line cracking pattern to an equivalent bonding area of a beam with a single-line cracking pattern;

- to address the effect of transverse steel on V_f, a coefficient β_c has been introduced. The sum of transverse-steel rigidity and FRP rigidity shows a good correlation with β_c.

The coefficient β_c can add the effect of transverse steel to the V_f design equations of other models. Applying β_c to the design equations of other guideline models resulted in a better correlation of the experimental results with the design equations results for all guidelines.

3.9   References

Adhikary, B.B., Mutsuyoshi, H., and Ashraf, M. (2004). Shear strengthening of reinforced concrete beams using fibre-reinforced polymer sheets with bonded anchorage. *ACI Struct. J.* 101(5), pp. 660–668.

American Concrete Institute (ACI) (2008). *Guide for the Design and Construction of Externally Bonded FRP Systems for Strengthening Concrete Structures.* Report No. 440 2R-08, Farmington Hills MI.

Al-Sulaimani, G.J., Sharif, A.M., Basunbul, I.A., Baluch, M.H., and Ghaleb, B.N. (1994). Shear repair for reinforced concrete by fibreglass plate bonding. *ACI Struct. J.* 91(3), pp. 458–464.

Berset, J.-D. (1992). *Strengthening of Reinforced Concrete Beams for Shear Using FRP Composites.* MSc Thesis, Department of Civil and Environmental Engineering, Massachusetts Institute of Technology, Boston MA USA: 105 pp.

Bizindavyi, L. and Neale, K. W. (1999). Transfer lengths and bond strengths for composites bonded to concrete, *J. Compos. Constr.* 3(4), pp. 153–160.

Blaschko, M. Niedermeier, R. and Zilch, K. (1998). Bond failure modes of flexural members strengthened with FRP. *Proceedings Fibre Compos. in Infrastruct., 2nd Int. Conf. on Compos. In Infrastruct.*, Tucson. Arizona, pp. 315–327.

Bousselham, A. and Chaallal, O. (2004). Shear strengthening reinforced concrete beams with fibre-reinforced polymer: assessment of influencing parameters and required research. *ACI Struct. J.* 101(2), pp. 219–227.

Bousselham, A. and Chaallal, O. (2008). Mechanisms of shear resistance of concrete beams strengthened in shear with externally bonded FRP. *J. Compos. Constr.* 12(5), pp. 499–512.

Brosens, K. and Van Gemert, D. (1999). Anchorage design for externally bonded carbon fibre polymer laminates, *Proceedings of the 4th International Symposium on Fibre Reinforced Polymer Reinforcement for Concrete Structures*, Baltimore, MD, pp. 635–645.

CAN/CSA-S806-02 (2002). *Design and construction of building components with fibre-reinforced polymer.* Canadian Standards Association, Rexdale, Canada.

CAN/CSA-S6-06 (2006). *Canadian Highway Bridge Design Code.* Canadian Standards Association, Mississauga, Canada.

Carolin, A. and Täljsten, B. (2005). Theoretical study of strengthening for increased shear bearing capacity. *J. Compos. Constr.* 9(6), pp. 497–506.

Chaallal, O., Nollet, M.J., and Perraton, D. (1998). Strengthening of reinforced concrete beams with externally bonded fibre-reinforced-plastic plates: design guidelines for shear and flexure. *Can. J. Civil Eng.* 25(4), pp. 692–704.

Chaallal, O., Shahawy, M., and Hassan, M. (2002). Performance of reinforced concrete T-girders strengthened in shear with CFRP fabrics. *ACI Struct. J.* 99(3), pp. 335–343.

Chajes, M.J., Januszka, T.F., Mertz, D.R., Thomson, T.A. Jr., and Finch W.W. Jr. (1995). Shear strengthening of reinforced concrete beams using externally applied composite fabrics. *ACI Struct. J.* 92(3) pp. 295–303.

Chen, J.F. and Teng, J.G., (2001). Anchorage strength models for FRP and steel plates bonded to concrete. *J. Struct. Eng.* 127(7) pp. 784–791.

Chen, J.F. and Teng, J.G. (2003). Shear capacity of FRP-strengthened RC beams: FRP debonding. *Construction and Building Materials* 17(1), pp. 27–41.

CNR-DT200 (2004). *Guidelines for Design, Execution, and Control of Strengthening Interventions by means of Fibre-Reinforced Composites.* National Research Council, Italy.

Deniaud, C. and Cheng, J.J.R. (2001). Shear behavior of reinforced concrete T-beams with externally bonded fibre-reinforced polymer sheets. *ACI Struct. J.* 98(3), pp. 386–394.

Deniaud, C. and Cheng, J.J.R. (2004). Simplified shear design method for concrete beams strengthened with fibre-reinforced polymer sheets. *J. Compos. Constr.* 8(5), pp. 425–433.

Diagana, C., Li, A., Gedalia, B., and Delmas, Y. (2003). Shear strengthening effectiveness with CFRP strips. *Engineering Structures* 25(4), pp. 507–516.

fib-TG 9.3 (2001). *Externally Bonded FRP Reinforcement for RC Structures.* International Federation for Structural Concrete, Lausanne, Switzerland.

Hiroyuki, Y. and Wu, Z. (1997). *Analysis of Debonding Fracture Properties of a CFS-Strengthened Member Subject to Tension.* Japan Concrete Institute, Sapporo, Japan: pp. 287–294.

Holzenkämpfer, P. (1994). *Ingenieurmodelle des Verbundes Geklebter Bewehrung für Betonbauteile.* Dissertation, TU Braunschweig, Germany.

Hsu, C.T.T., Punurai, W., and Zhang, Z. (2003). *Flexural and Shear Strengthening of RC Beams Using Carbon Fibre Reinforced Polymer Laminates.* SP 211-5, ACI, pp. 89–114.

Kamel, A.S., Elwi, A.E., and Cheng, J.J.R. (2000). Experimental study of the behavior of CFRP sheets bonded to concrete. *Proceedings, 3rd Int. Conf. on Advanced Composite Materials for Bridges and Structures*, Canadian Society for Civil Engineering, Ottawa, pp. 61–68.

Karbhari, V. M., Niu, H., and Sikorsky, C. (2006). Review and comparison of fracture mechanics-based bond strength models for FRP-strengthened structures. *J. Reinf. Plastics Compos.* 25, pp. 17.

Khalifa, A., Gold, W.J., Nanni, A., and Aziz, A. (1998). Contribution of externally bonded FRP to shear capacity of RC flexural members. *J. Compos. Constr.* 2(4), pp. 195–203.

Khalifa, A. and Nanni, A. (2000-a). Improving shear capacity of existing RC T-section beams using CFRP composites. *Cem. Concr. Compos.* 22, pp. 165–174.

Khalifa, A., Nanni, A., and De Lorenzis, L. (2000-b). FRP composites for shear strengthening of RC beams. *Proceedings, 3rd Int. Conf. on Advanced Compos. Materials in Bridges and Structures (ACMBS)*, Ottawa, Canada, pp. 137–144.

Maeda, T., Asano, Y., Sato, Y., Ueda, T., and Kakuta, Y. (1997). A study on bond mechanism of carbon fibre sheet. Maeda, T., Asano, Y., Sato, Y., Ueda, T., and Kakuta, Y. (1997). *Proc. of the 3rd Int. Symp. on Non-Metallic (FRP) Reinforcement for Concrete Structures*, Sapporo, Japan, 1, 279-286. pp. 279–285.

Micelli, F., Annaiah, R.H., and Nanni, A. (2002). Strengthening of short shear span reinforced concrete T-joists with fibre-reinforced plastic composites. *J. Compos. Constr* 6(4), pp. 264–271.

Mirza, S., MacGregor, J., and Hatzinikolas, M. (1979). Statistical descriptions of strength of concrete. *J. Struct. Div.* 105(6), pp. 1021–1037.

Monti, G., Renzelli, M. and Luciani, P. (2003). FRP Adhesion in uncracked and cracked concrete zones. *FRPRCS-6*, Singapore, pp. 183-192.

Monti, G. and Liotta, M. (2006). Tests and design equations for FRP strengthening in shear. *Construction and Building Materials* 21, pp. 799–809.

Neubauer, U. and Rostásy, F.S. (1997). *Design Aspects of Concrete Structures Strengthened with Externally Bonded CFRP Plates.* ECS Publications, Edinburgh: pp. 109–118.

Pellegrino, C. and Modena, C. (2002). Fibre reinforced polymer shear strengthening of RC beams with transverse steel reinforcement. *J. Compos. Constr.* 6(2), pp. 104–111.

Oehlers, D.J., Seracino, R. and Smith, S.T. (2008) *Design Guideline for RC Structures Retrofitted with FRP and Metal Plates: Beams and Slabs*, HB 305-2008, Standards Australia, Sydney, Australia, ISBN 0 7337 7831 3, 73 pp.

Sato, Y., Ueda, T., Kakuta, Y., and Tanaka, T. (1996). Shear reinforcing effect of carbon fibre sheet attached to side of reinforced concrete beam. *Proceedings, 2nd Int. Conf. on Advanced Compos. Materials in Bridges, ACMBS II*, Montreal, Canada, pp. 621–637.

Taerwe, L., Khalil, H., and Matthys, S. (1997). Behaviour of RC beams strengthened in shear by external CFRP sheets. *Proceedings, 3rd Int. Symp. on Non-Metallic (FRP) Reinforcement for Concrete Structures*, Sapporo, Japan, Vol. 1, pp. 507–514.

Tanaka, T. (1996). *Shear-Resisting Mechanism of Reinforced Concrete Beams with CFS as Shear Reinforcement.* Graduation thesis, Hokkaido University, Japan.

Täljsten, B. (1997). Strengthening of concrete structures for shear with bonded CFRP fabrics. *Proceedings, US-Canada-Europe Workshop on Bridge Engineering,* organized by EMPA, Zurich, Switzerland, pp. 57–64.

Triantafillou, T.C. (1998). Shear strengthening of reinforced concrete beams using epoxy-bonded FRP composites. *ACI Struct. J.* 95(2), pp. 107–115.

Triantafillou, T.C. and Antonopoulos, C.P. (2000). Design of concrete flexural members strengthened in shear with FRP. *J. Compos. Constr.* 4(4), pp. 198–205.

Uji, K. (1992). Improving shear capacity of existing reinforced concrete members by applying carbon fibre sheets. *Trans. Jpn. Concr. Institute* 14(253), pp. 66.

Zhang, Z., Hsu, C.-T., and Moren, J. (2004). Shear strengthening of reinforced concrete deep beams using carbon fibre reinforced polymer laminates. *J. Compos. Constr* 8(5), pp. 403–414.

CHAPTER 4

EMBEDDED THROUGH-SECTION FRP ROD METHOD FOR SHEAR STRENGTHENING OF RC BEAMS: PERFORMANCE AND COMPARISON WITH EXISTING TECHNIQUES

Omar Chaallal and Amir Mofidi

Department of Construction Engineering, École de Technologie Supérieure 1100 Notre-Dame Ouest, Montréal, Québec, Canada H3C 1K3

4.1 Abstract

Embedded through-section technique (ETS) is a recently developed method to increase the shear capacity of reinforced concrete (RC) using fiber reinforced polymer (FRP) rods. The ETS method presents many advantages over existing methods such as externally bonded FRP sheets (EB FRP) and near surface mounted FRP rods (NSM FRP). Unlike EB and NSM methods where the FRP relies on the concrete cover of RC beams, in the ETS method the FRP relies on the concrete core of the RC beam which offers a greater confinement and hence improves bonding performance. Additionally, the ETS method requires less concrete preparation compared to EB and NSM methods. The objective of this paper is to present results of an experimental investigation which studies the effectiveness of the ETS method and compares the performance of the ETS method with both EB and NSM methods.

In total, 12 tests are performed on 4520 mm-long T-beams. The parameters investigated are as follows: 1) the effectiveness of the ETS method, compared to EB FRP sheet and NSM FRP rod methods; 2) the presence of the internal steel and 3) the internal transverse steel

reinforcement ratio (i.e., spacing). The test results confirm the feasibility of the ETS method and reveal that the performance of the beams strengthened in shear using this method is significantly superior compared with that of the beams strengthened with EB and NSM methods.

4.2 Introduction

In the last two decades the use of externally-bonded (EB) fiber-reinforced polymer (FRP) composites has gained acceptance in the construction engineering community, particularly in the rehabilitation of reinforced concrete (RC) structures. As a result, numerous research studies on different aspects of the subject have been conducted and different techniques have been used with success in field strengthening and rehabilitation projects involving RC beams and girders. Currently, to increase the shear resistance of RC beams, FRP sheets are generally applied on the side surface of the beams to be strengthened. This method is called the externally bonded (EB) method. Numerous research studies confirm that the shear capacity of RC beams can be increased using the EB FRP method (Uji 1992; Al-Sulaimani et al. 1994; Triantafillou 1998; Khalifa et al. 1998; Chaallal et al. 1998; Pellegrino and Modena 2002; Bousselham and Chaallal 2004). Some argue that the method presents shortcomings such as: (i) quality of the concrete strata; (ii) surface preparation; (iii) lack of protection (vandalism /fire); and (iv) debonding. The near surface mounted (NSM) FRP rebar method is another technique successfully used to increase the shear resistance of RC beams. In the NSM method, FRP rods are embedded into grooves intentionally prepared on the concrete cover of the side faces of RC beams. Research has shown that a significant increase in shear resistance of RC beams is reachable using the NSM FRP method (De Lorenzis and Nanni 2001 and Barros and Dias 2005). However, the surface (groove) preparation as well as adhesive and FRP installation are tedious. In addition, debonding of FRP rods is still inevitable. Thus, the debonding problem remains the main disadvantage for EB FRP and NSM methods. This is due to the relatively low tensile strength of the concrete surface that limits the bonding force between the FRP and concrete (Mofidi and Chaallal 2011-a). This results on premature debonding of the FRP, limiting thereby the maximum FRP strain to a

value well below its ultimate strain and hence the efficiency of these FRP strengthening systems. Moreover, FRP or steel bars can be epoxied to vertical holes drilled into concrete to strengthen RC beams in shear (Valerio and Ibell 2003). The proposed technique is shown to be feasible, successful and potentially more effective than other shear strengthening approaches (Valerio et al. 2009).

4.3   Research significance

The current FRP strengthening methods in shear, although efficient to some extent, present numerous shortcomings. The high potential for debonding, the need for surface preparation, the uncertainty in the FRP/concrete bond and interface characteristics and the protection against vandalism and fire are examples of these shortcomings. The advantages of the ETS method over current FRP strengthening methods for RC beams is that the application of the ETS method is less time consuming, needs less adhesive and does not require surface preparation or skilled workers to install. Moreover, the application of FRP rods (instead of steel rods) prevents possible corrosion of the strengthening rods. The objective of this collaborative research study between École de Technologie Supérieure of Montreal and University of Sherbrooke is to examine the effectiveness of the ETS strengthening method in increasing the shear capacity of RC beams compared to the current shear strengthening methods using FRP.

4.4   Test program

The experimental program (Table 4.1) involves 12 tests performed on 6 full-scale RC T-beams. The control specimens, not strengthened with Carbon FRP (CFRP), are labeled CON, whereas the specimens retrofitted with one layer of EB CFRP sheet are labeled EB. The specimens strengthened with NSM FRP rods are labeled NSM and the specimens strengthened with the ETS FRP method are labeled ETS. Series S0 consists of specimens with no internal transverse steel reinforcement (that is, no stirrups). Series S1 and S3

correspond to specimens with internal transverse steel stirrups, hereafter called transverse steel, spaced at $s = d/2$ for S1 and $s= 3d/4$ for S3, where $d = 350$ mm and represents the effective depth of the cross section of the beam (Figure 4.1). It may be worth noting that S2 series is not part of the current research study. Thus, for instance, Specimen S0-ETS features a beam retrofitted with the ETS method and with no transverse steel. The specimen details are provided in Table 4.1, together with the identification codes used hereafter.
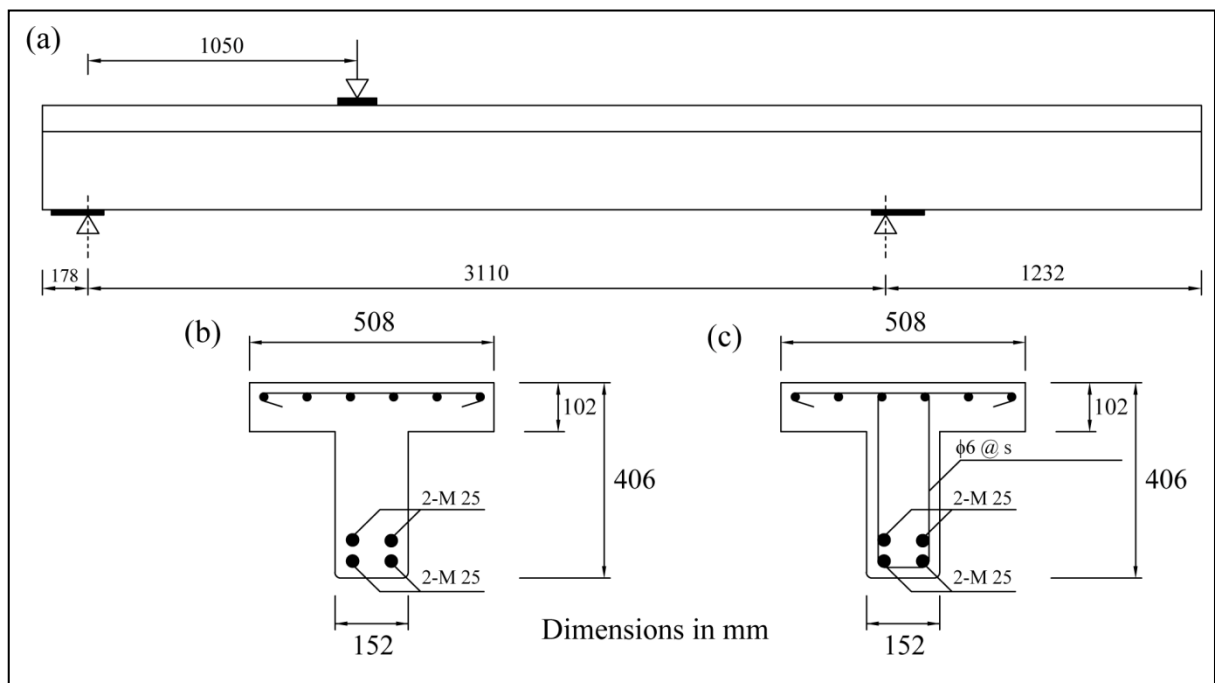
Figure 4.1   Details of concrete beams: a) elevation; b) cross section with no transverse steel; and c) cross section with transverse steel.

Table 4.1   Experimental program matrix

Beam name / Series	S0 Series	S1 Series	S3 Series
Control beam	S0-CON	S1-CON	S3-CON
EB FRP method	S0-EB	S1-EB	S3-EB
NSM FRP method	S0-NSM	S1-NSM	S3-NSM
ETS FRP method	S0-ETS	S1-ETS	S3-ETS

4.4.1   Description of specimens

The T-beams are 4520 mm long. The T-section has overall dimensions of 508 mm (width of flange) by 406 mm (total depth). The width of the web and the thickness of the flange are 152 and 102 mm, respectively (Figure 4.1). It should be noted that the web is chamfered at the outer corners for the beams strengthened with the EB FRP method, thereby easing the high stress concentration in the CFRP at those sharp locations. The longitudinal steel reinforcement consists of four 25M bars (diameter of 25.2 mm, area of 500 mm^2) laid in two layers at the bottom and six 10M bars (diameter of 10.3 mm, area of 100 mm^2) laid in one layer at the top (see Figure 4.1). The bottom bars are anchored at the support with 90 degree hooks to prevent premature anchorage failure. The internal steel stirrups (where applicable) are 8 mm in diameter (area of 50 mm^2).

The variables to be examined in the experimental test matrix are as follows:

- effectiveness of strengthening methods. This is measured by comparing the gain achieved by each strengthening method for an equivalent amount of FRP to carry shear loads;

- presence of internal steel stirrups. Three series of beams are considered: S0 with no transverse steel and S1 and S3 with steel stirrups spaced at 175 mm and 260 mm, respectively;

- spacing of the steel stirrups. Two different spacings were examined: 175 mm and 260 mm.

4.4.2   Materials

A commercially available concrete is used in this project; it is delivered to the laboratory by a local supplier. The average concrete strength on three 152 mm diameter by 305 mm concrete cylinders is 25 MPa for S0 and S1 series and 35 MPa on average for S3 series. The internal

flexural steel have a nominal yield strength of 470 MPa for S0 and S1 series and 650 MPa for S3 series. The shear reinforcement has a nominal yield strength of 540 MPa for S0 and S1 and 650 MPa for S3 series. Sand coated CFRP rods manufactured by Pultrall inc., with a nominal diameter of 9.5 mm (area: 71 mm^2) and 12.7 mm (area: 127 mm^2), are used for NSM and ETS strengthening methods, respectively. The tensile strength and modulus of elasticity of the CFRP rods are determined according to the test method B2 in ACI 440.3R-04. The average resulting values are 1870 MPa and 143.9 GPa, respectively. A commercially available epoxy paste is used for embedding the rods. Its mechanical properties, as specified by the manufacturer, are: 21 MPa bond strength, 1% elongation at break, 75 MPa compressive strength and 3656 MPa compressive modulus. The CFRP sheet used for EB series is a unidirectional carbon fiber fabric. It is applied continuously over the test zone in a U-shape envelope around the web. The continuous composite material is selected as it is well suited for intercepting diagonal cracks, which may occur and propagate over a large area within the test zone. The CFRP fabric (SikaWrap Hex 230C) is bonded to the beam surface with an adhesive made of a resin and a hardener, both of which are specially engineered for structural applications and supplied by the CFRP manufacturer. Table 4.2 provides the mechanical and elastic properties of the CFRP fabric and rods as provided by the manufacturers.

Table 4.2   Mechanical properties of CFRP sheets and rods used

Property	Dry fiber sheet	9.5mm diameter CFRP rod	12.7 mm diameter CFRP rod
Modulus of elasticity, GPa	231	148	140
Ultimate elongation, %	1.40	1.27	1.33
Ultimate stress, MPa	3650	1885	1855

4.4.3   Test setup and procedure

The beams are tested in three-point load flexure. This type of loading is chosen as it allowed two tests to be performed on each specimen: (a) one beam end zone is first tested keeping the other overhung and unstressed (Figure 4.1). The load is applied at a distance $a = 3d$ from the

nearest support, which corresponds to a slender beam test and (b) the other beam end zone is tested, but this time it is the end zone already tested that is overhung and unstressed.

To meet the objective and the scope of the study, a very comprehensive and carefully engineered measuring scheme is adopted for the project (Figure 4.2 a-d). The vertical displacement is measured at the position under the applied load and at the mid-span using linear displacement sensors. The latter are also installed at each side of the supports perpendicular to the flange plan to control any undesired sway or tilt effects. Strain gauges are glued on the transverse steel and CFRP rods to measure stirrup deformations during the different loading stages and to monitor any yielding in steel and measure the CFRP rod maximum strain. The deformations experienced by the CFRP U-jacket are measured using displacement sensors known as crack gauges. These gauges are fixed vertically on the lateral faces of the specimens at the same positions along the longitudinal axis as the strain gauges on the stirrups. Thus, the CFRP and the transverse steel responses can be conveniently compared at the same positions during the different stages of loading. Likewise, strain gauges are also installed in parallel on the longitudinal steel bars, in the concrete, on the strengthening CFRP rods, and on the CFRP U-jacket at the tension zone of the specimens.

The load is applied using a 2000 kN capacity MTS hydraulic jack. All the tests are performed under displacement control conditions at 2 mm/minute. The signals from the gauges and the displacement sensors are captured and monitored using an automatic data acquisition system.

4.4.4 Strengthening systems

Three different strengthening systems are used in this research study. The EB FRP, NSM FRP and ETS FRP strengthening techniques are illustrated in Figure 4.2 b to d. To apply the EB FRP strengthening system, the following procedures are implemented: (1) the area of the beam where the continuous CFRP sheet is to be glued, is sand blasted to remove the superficial cement paste and to round out the beam edges; (2) the bond area is grinded to remove any possible irregularities and achieve a desirable smooth bond surface ; (3) the

residues are removed by compressed air; and (4) a layer of U-shape continuous CFRP sheet is glued to the bottom and to the lateral faces of the RC beam, using a two component epoxy resin.

(a)	(b)
(c)	(d)
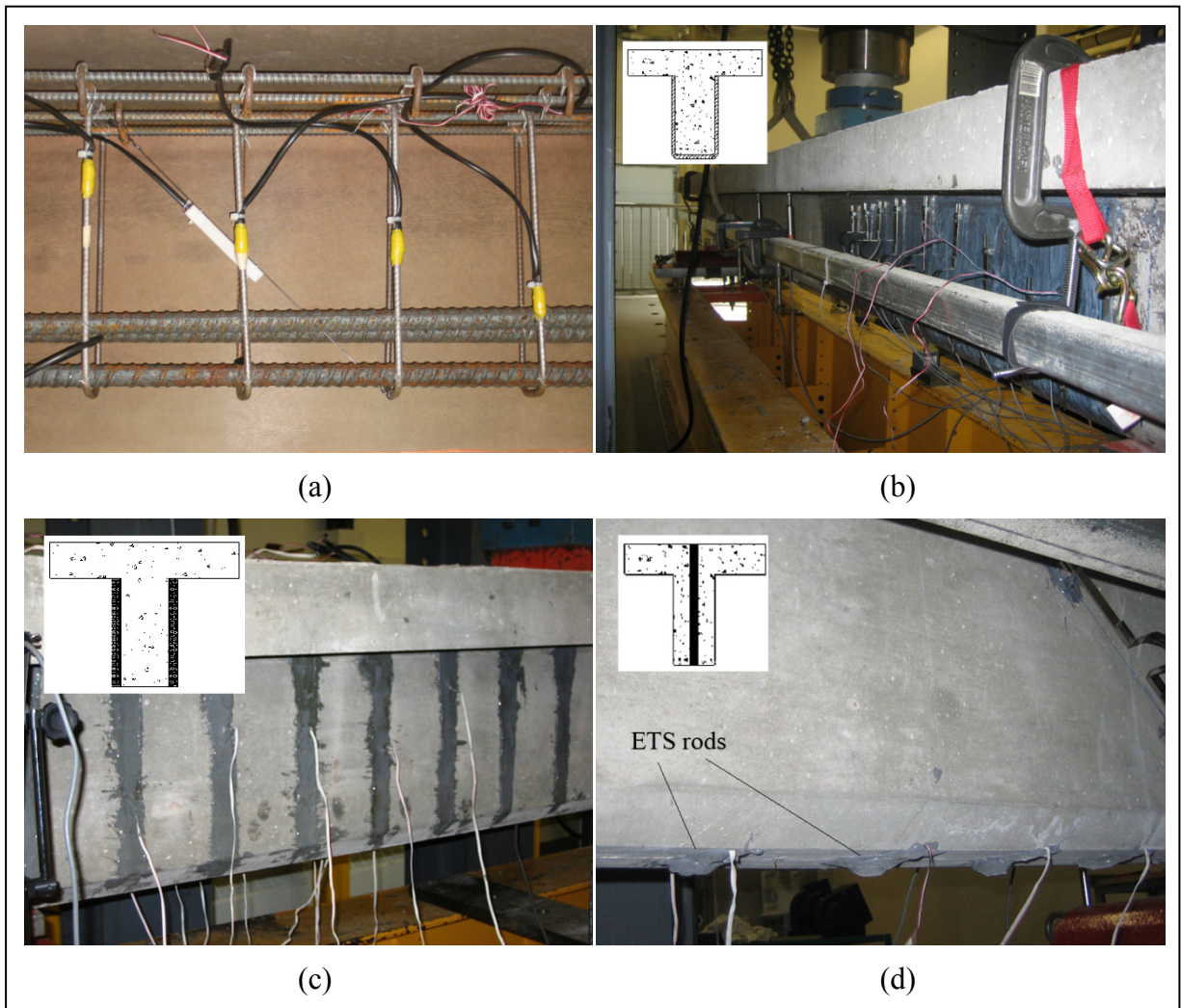
Figure 4.2 Instrumentation: a) strain gauges on transverse steel and embedded in concrete; b) crack gauges on CFRP sheets and LVDT in mid-span and under loading point; c) strain gauges on NSM rods; and d) strain gauges on ETS rods and concrete crack gauge.

To apply the NSM FRP strengthening system, the following steps are performed: (1) grooves of 15 mm width and 15 mm depth and spaced at 130 mm (that is equal to s/2 in S3 series) are made on the both lateral sides of the beam. (2) the grooves are cleaned by compressed water

and air; (3) the grooves are filled with 2/3 of the epoxy adhesive volume required blended according to the supplier's recommendations; (4) a thin layer of supplier's epoxy adhesive is applied around the 9.5 mm-diameter CFRP rods; (5) the 9.5 mm-CFRP rods are installed into the groove on the both sides of the beam; and (6) the excess epoxy adhesive is removed. For the ETS FRP strengthening system, the following application steps are carried out: (1) 18 mm-diameter vertical holes spaced at 130 mm are made through the middle of the cross-section of the RC beam and the beam's longitudinal axis ; (2) the holes are cleaned by compressed water ; (3) one end of the holes is blocked using epoxy and the holes are filled with 2/3 of the needed epoxy adhesive volume required; (4) a thin layer of one epoxy adhesive is applied around the 12.7 mm-diameter CFRP rods (the cross section area of 12.7 mm-diameter rod is approximately equal to the cross section area of the two 9.5 mm-diameter rod used in the NSM method); (5) the 12.7 mm CFRP rods are installed into the holes; and the excess epoxy adhesive is removed.

4.5   Presentation of results

4.5.1   Overall response

Table 4.3 summarizes the average experimental results obtained from the tests for all the test series. The results are presented in terms of the loads attained at failure; the experimental shear resistance due to concrete, due to the transverse steel, and due to the CFRP; as well as the shear capacity gain due to the CFRP. It should be mentioned that the shear contribution of the concrete and the steel are calculated based on the results gained from the unstrengthened specimens. Note that some of the values provided in Table 4.3 are derived on the basis of the following assumptions implicitly admitted in the guidelines: a) the shear resistance due to concrete is the same whether the beam is retrofitted in shear with FRP or not and whether the retrofitted beam is reinforced with transverse steel or not; and b) the contribution of the transverse steel is the same for both strengthened and un-strengthened beams.

Table 4.3 Experimental results

Strength ening method	Series	Specim en	Load at rupture kN	Total shear resistan ce kN	Resistance due to concrete kN	Resistance due to steel kN	Resistance due to CFRP kN	Gain due to CFRP %	Deflection at load point mm	Failure mode
Control	S0	S0-CON	122.7	81.3	81.3	0.0	0.0	0	2.6	Shear
	S1	S1-CON	350.6	232.2	81.3	150.9	0.0	0	11.9	Shear
	S3	S3-CON	294.0	194.7	96.2	98.5	0.0	0	11.2	Shear
EB	S0	S0-EB	181.2	120.0	81.3	0.0	38.7	48	4.2	Shear
	S1	S1-EB	378.5	250.7	81.3	150.9	18.5	8	14.5	Shear
	S3	S3-EB	335.2	222.0	96.2	98.5	27.3	14	11.3	Shear
NSM	S0	S0-NSM	198.0	131.1	81.3	0.0	49.8	61	6.1	Shear
	S1	S1-NSM	365.0	241.7	81.3	150.9	9.5	4	13.1	Shear
	S3	S3-NSM	380.0	251.6	96.2	98.5	56.9	29	11.7	Shear
ETS	S0	S0-ETS	273.0	180.8	81.3	0.0	99.5	122	9.9	Shear
	S1	S1-ETS	397.0	262.9	81.3	150.9	30.7	13	15.9	Flexure
	S3	S3-ETS	425.5	281.8	96.2	98.5	87.1	45	15.2	Flexure

The results show that the shear capacity gain due to the CFRP for the specimens with no transverse steel strengthened by the ETS method is 122%, compared to 48% and 61% for the corresponding specimens strengthened with EB and NSM methods, respectively. For the specimens with transverse steel, these gains drastically decrease for all the strengthening methods, to reach an average of 29% for S1-ETS and S3-ETS specimens, 11% for S1-EB and S3-EB specimens and 17% for S1-NSM and S3-NSM specimens. This clearly confirms the observations made in earlier studies (Chaallal et al. 2002; Pellegrino and Modena 2002; Bousselham and Chaallal 2004) that the contribution of FRP to the shear resistance of a beam with transverse steel differs from that of the same beam but with no transverse steel. This holds true regardless of the strengthening technique used. This is in agreement with the hypothesis of the effect of cracking pattern on the bond force (Mofidi and Chaallal 2011-a), since generally the cracking pattern on the surface of the beams strengthened with FRP is more distributed than within the concrete core of those beams (Figures 4.3a and 4.3b).

4.5.2   Presentation of results by series

S0 Series—Series S0 consisted of four beams with no steel stirrups, one control beam and three beams strengthened using EB, NSM and ETS strengthening methods. During loading of beam S0-CON, diagonal shear cracks formed at a load of 78.8 kN. The shear cracks initiated at the center of the shear span. As the load increased, one crack widened and propagated until failure, which occurred at a load of 122.7 kN.

| (a) | (b) |
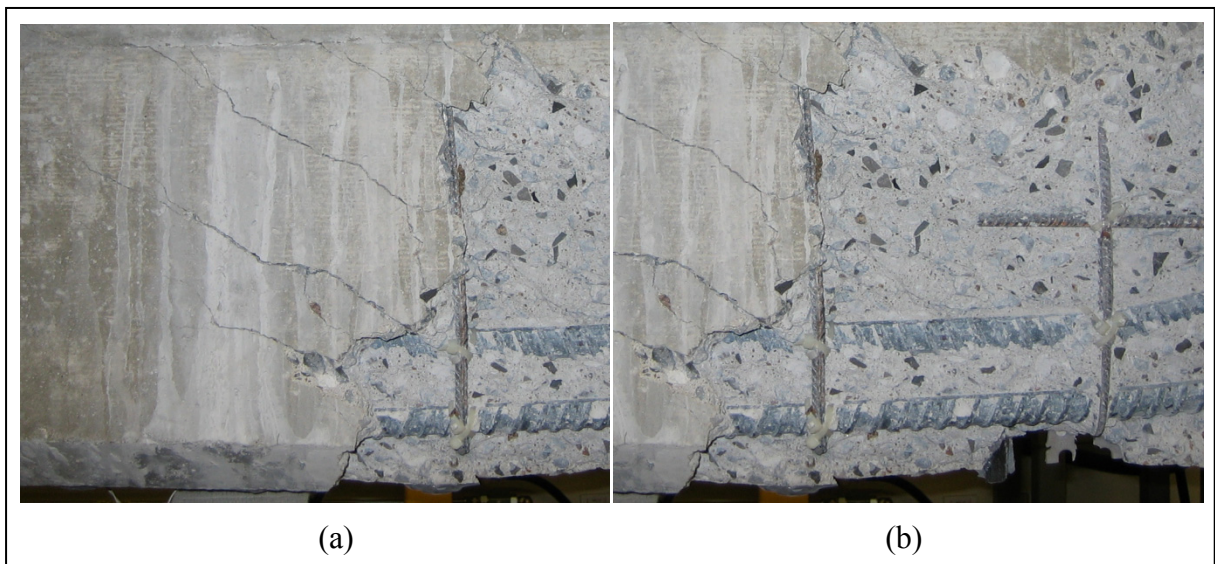
Figure 4.3   Cracking pattern of specimen S1-ETS: a) on the surface (left side of the picture) and b) on the concrete core (right side of the picture).

In specimen S0-EB, failure was initiated by debonding of the CFRP sheets (with a layer of concrete adhered to them) over the main shear crack which occurred at the same location as the control beam S0-CON. The CFRP debonding was followed by shear compression failure at a load of 181.2 kN, which corresponded to a 48% increase in the shear capacity due to FRP.

In specimen S0-NSM, retrofitted with 9.5 mm diameter NSM vertical rods spaced of 130 mm, failure occurred at a load of 198.0 kN. This corresponds to an increase in shear capacity of 61% with respect to control beam S0-CON. Diagonal shear cracks also formed in this beam, and widened and propagated as the applied load was increased. A popping noise throughout the test revealed the progressive cracking of the epoxy adhesive in which the

CFRP rods were embedded. Failure eventually occurred due to splitting of the concrete cover. The shear cracks could not pass the RC beam's surface due to the presence of the NSM CFRP rods. Therefore, the cracks avoided the NSM rods by passing around the NSM CFRP rods towards the concrete cover. This resulted in 2 thick layers of concrete cover (including the NSM FRP rods) split from the beam's sides (Figures 4.4). Losing the strengthening CFRP NSM rods the RC beam failed in a diagonal tension failure mode. The highest longitudinal strain reached in the rods was approximately equal to 1920 $\mu\varepsilon$, which corresponds to 15% of the reported ultimate strain of the CFRP. It must be pointed out that this strain value and all those reported herein are the maximum measured values, but not necessarily the absolute maximum values experienced by the FRP. This is the case where the strain gauges did not intercept the main cracks.

In specimen S0-ETS, retrofitted with 12.7 mm embedded through-section vertical rods spaced at 130 mm, diagonal shear cracks formed in this beam at a relatively higher load (86.3 kN) in comparison to S0-EB and S0-NSM. Failure occurred at a load of 273.0 kN, which corresponded to a 122% increase in shear capacity with respect to the control beam. Failure eventually occurred by concrete crushing (shear diagonal compression failure). The highest longitudinal strain in the rods was approximately equal to 2286 $\mu\varepsilon$, which corresponds to 17% of the ultimate strain of the CFRP rod.

(a)   (b)

Figure 4.4   Common failure mode in beams strengthened with NSM method:
a) Cracking pattern and b) detachment of concrete cover.

S1 Series—Beam S1-CON with steel stirrups spaced at 175 mm, developed diagonal shear cracks at a load approximately equal to the load at which the shear crack initiated in S0-CON (78.2 kN). Failure of specimen S1-CON occurred at a load of 350.6 kN and was due to rupture of the third stirrup located at 438 mm from the support.

Beam S1-EB had the same transverse steel as the control specimen S1-CON, but was externally strengthened with one layer of continuous EB CFRP U-jacket. The ultimate load attained at 378.5 kN, that is, 8% greater than the ultimate capacity of S1-CON. The S1-EB specimen failed by concrte cover rip-off and hence debonding of the FRP. However, unlike S0-EB, concrete cover did not spall completely, due to the restraining action of the steel stirrups. The highest longitudinal strain in CFRP sheet was approximately equal to 3950 με, which corresponds to 28% of the reported ultimate strain of the CFRP sheet.

Beam S1-NSM had the same transverse steel as beam S1-CON, but externally strengthened with NSM vertical rods, spaced at 130 mm. The ultimate load achieved was 365.0 kN, that is, 4% greater than the capacity of the control beam S1-CON. The final failure mode was by splitting of the concrete cover. The highest longitudinal strain in the rods was approximately equal to 2112 με, which corresponds to 17% of the reported ultimate strain of the CFRP rod.
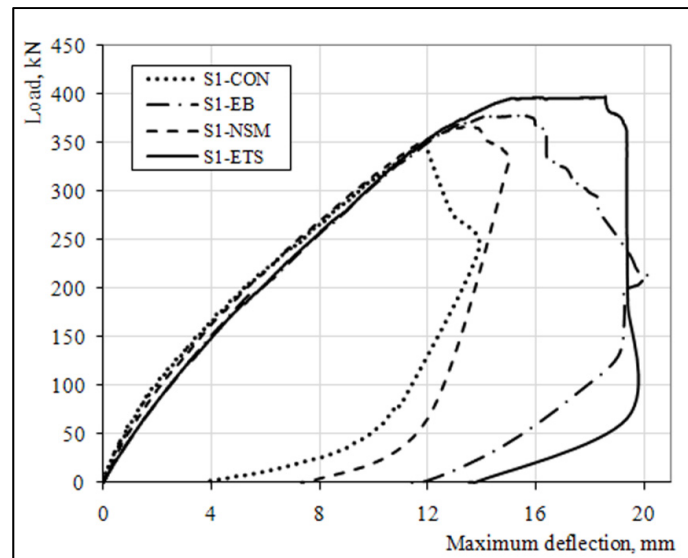
Figure 4.5   Load versus maximum deflection – Series S1.

Beam S1-ETS had the same transverse steel as beam S1-CON but was strengthened with 12.7 mm ETS vertical rods spaced at 130 mm. The ultimate load attained was 397.0 kN, that is, 13% greater than the shear capacity of control beam S1-CON. Specimen S1-ETS failed by flexure as evidenced by the plateau featured in the load versus mid-span deflection diagram (Figure 4.5), accompanied with a major shear crack. The final shear failure did not occur. The highest longitudinal strain in the rods was approximately equal to 2882 $\mu\varepsilon$, which corresponds to 22% of the reported ultimate strain of the CFRP rod.

S3 Series—In Beam S3-CON with steel stirrups spaced at 260 mm, diagonal shear cracks formed at a load (79.2 kN) similar to the load at which the shear crack appeared in S0-CON. Eventually, failure occured at a load of 294.0 kN and was due to rupture of the third stirrup located at 650 mm from the support.

Beam S3-EB had the same transverse steel as S3-CON, but was externally strengthened with EB CFRP U-jacket. The ultimate load was obtained 335.2 kN, that is, 14% greater than the capacity of the control beam S3-CON. Specimen S3-EB failed by concrete cover rip-off and debonding of the FRP sheet, likewise beam S0-EB described earlier. However, unlike the beam S0-EB, the concrete cover did not spall completely in S3-EB, due to the restraining action of the steel stirrups. The highest longitudinal strain in the CFRP sheet was approximately equal to 4050 $\mu\varepsilon$, which corresponds to 29% of the reported ultimate strain of the CFRP sheet.

Beam S3-NSM had the same transverse steel as beam S3-CON, but was externally strengthened with NSM vertical rods spaced at 130 mm. The ultimate load was 380.0 kN, that is, 29.2% greater than the capacity of control beam S3-CON. The final failure was triggered by splitting of the concrete cover as previously described for beam S0-NSM and resulted in the beam's shear diagonal tension failure. The highest longitudinal strain in the rods was approximately equal to 2640 $\mu\varepsilon$, which corresponded to 21% of the reported ultimate strain of the CFRP rod.

Beam S3-ETS had the same transverse steel as S3-CON, but was strengthened with ETS vertical rods spaced at of 130 mm. The ultimate load obtained was 425.5 kN, that is, 45%

greater than the shear capacity of control beam S3-CON. The failure occurred by longitudinal steel yield, as clearly evidenced by the plateau in the load versus mid-span deflection diagram (Figure 4.6). The highest longitudinal strain in the rods was approximately equal to 3767 με, which corresponds to 28% of the reported ultimate strain of the CFRP rod.

4.5.3 Deflection response

Figures 4.5, 4.6 and 4.7 show the curves representing the load versus the mid-span deflection for Series S1, S3 and S0, respectively. Each figure provides the total applied load versus mid-span deflection for the control beam as well as for the three beams strengthened with the different retrofitting techniques for comparison. The quasi-linear behaviour of the curves is characteristic of a shear failure (except for the beams S1-ETS and S3-ETS that failed in flexure). Figure 4.6 reveals that S3-NSM and S3-ETS specimens showed a greater overall stiffness, in comparison to the control and S3-EB beams (Figure 4.6).
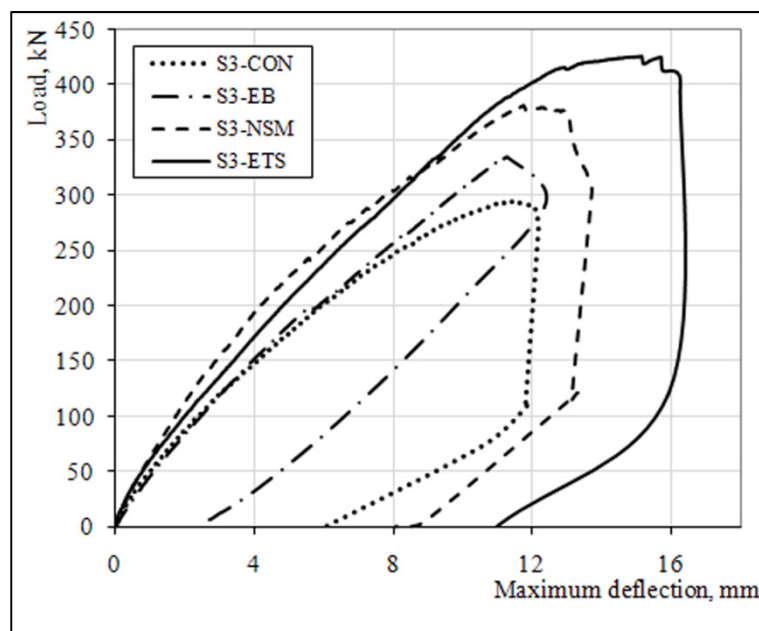
Figure 4.6   Load versus maximum deflection – Series S3.

Specimens S1-ETS and S3-ETS, which reached their flexural capacity limit (Figures 4.5 and 4.6), failed in a more ductile manner compared to other strengthened and unstrengthened specimens. Note that the maximum load at failure and the maximum deflection attained at the loading point for each specimen are provided in Table 4.3.

ETS specimens exhibited a higher deflection at the loading point and maximum load at failure compared with other strengthened and unstrengthened specimens of other series (Table 4.3). It can be seen that the embedded through-section technique greatly enhanced the overall behaviour of the RC beams since it resulted in higher load at failure and greater maximum deflection than other specimens (Figures 4.5 to 4.7). For example, in S3 series (Figure 4.6), the deflection under the point load of the beam S3-ETS at the maximum load was 1.30 times that of S3-NSM beam at the maximum load (15.2 mm at load 425.5 kN versus 11.7 mm at 380.0 kN) and 1.34 times that of S3-EB beam at the maximum load (15.2 mm at load 425.5 kN versus 11.3 mm at 335.2 kN), whereas the control S3-CON beam achieved the smallest deflection at the maximum load (11.2 mm at 294.0 kN).
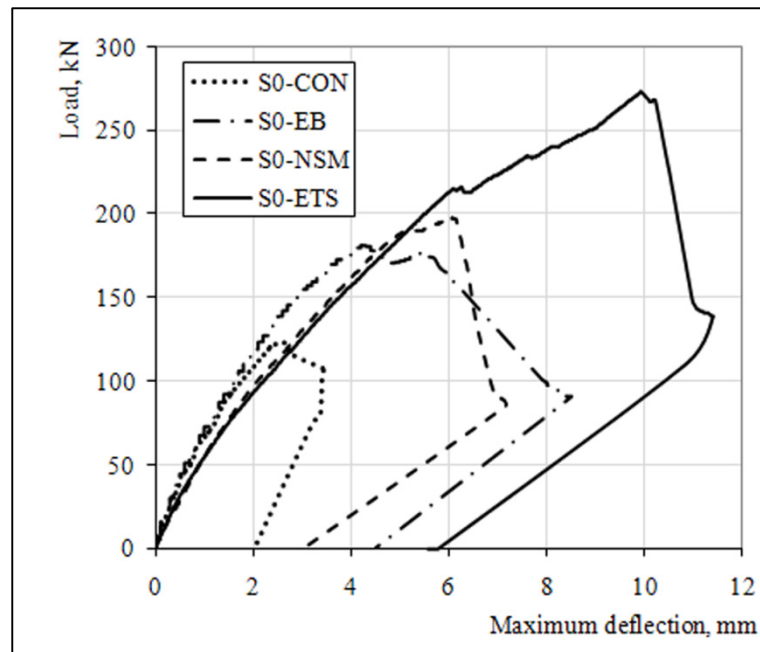
Figure 4.7   Load versus maximum deflection – Series S0.

All the beams in S3 series, except S3-ETS, exhibited a brittle type of behaviour, characterized by a sudden drop in the load-displacement curves after the peak load. In contrast, beam S3-ETS showed a ductile behaviour and failed in flexure.

4.5.4 Strain response

This part of the study examines the behaviour of the CFRP and the transverse steel for the three CFRP strengthening methods. As mentioned earlier, extensive instrumentation for strain monitoring was carefully engineered to obtain valuable information and data much needed for the understanding of the shear resistance mechanism involved in beams retrofitted with FRP using different strengthening methods.

CFRP strain—Figures 4.8, 4.9 and 4.10 present the curves of the load versus the strains in the CFRP strengthening material (sheets and rods) for series S0 with no transverse steel, S1 with transverse steel spaced at $s = d/2$ and S3 with transverse steel spaced at $s = 3d/4$. It is observed that the curves have the same tendency and feature three phases. In the initial stage of loading, the CFRP does not contribute to the load-carrying capacity. In the second stage, the CFRP begins to strain at an applied load of approximately 100 kN for all the three series. The CFRP strain continues to increase under increasing applied load up to a certain threshold, the level of which differs from one specimen to another depending on the strengthening method. In S1 specimens for instance (Figure 4.9), the maximum strain attains 3950 $\mu\varepsilon$ and 2112 $\mu\varepsilon$ in specimens S1-EB and S1-NSM, respectively. In the third stage, the CFRP strain starts to decrease, drastically at times, as the load increases. This is shown by the reversing of the curves in Figures 4.8 to 4.10 and can be explained as follows. Although no sign of debonding was observed during the course of the test, the few crackling noises heard in the beam lead to believe that local debonding could have occurred and may explain the CFRP strain decrease. Incidentally, this decrease has no impact on the applied loading, which in fact continues to increase. This phenomenon, called the migration of the bond zone, is fully described in Mofidi and Chaallal (2011-a). FRP rods pertaining to specimens S1-ETS

and S3-ETS does not show any sign of FRP debonding, and maintained the strain as they were loaded up to failure (Figures 4.8 and 4.9).

Transverse steel strain—Figures 4.11 and 4.12 present for respectively S1 and S3 specimens, the curves of the applied load versus the strains in the transverse steel for each of the strengthening method. These curves indicate that the behaviour of the transverse steel go through three phases during loading. In the first initial phase, no noticeable contribution of the transverse steel to the resistance is observed. In the second phase, the first diagonal cracks initiate and the transverse steel start to strain. In series S3, for instance, this phase starts at an average applied load of approximately 75 kN for the control specimens, and 100 kN for the retrofitted specimens.
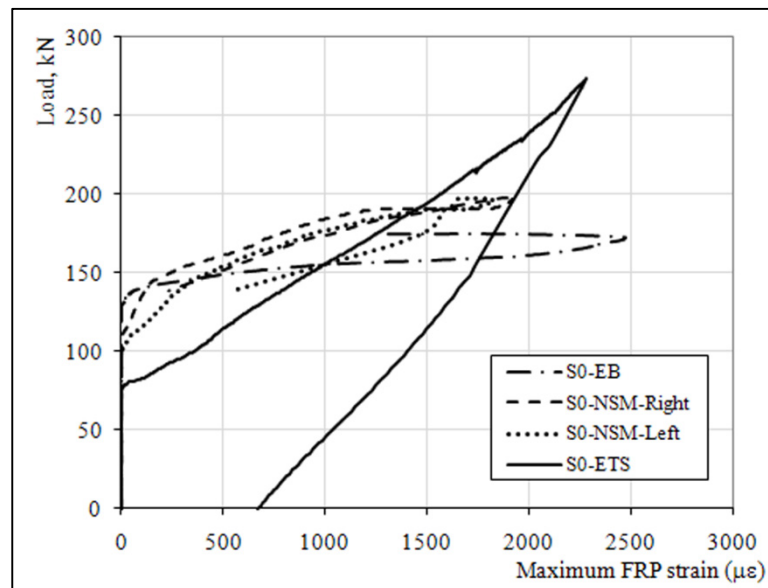
Figure 4.8   Load versus maximum strain in FRP – Series S0.
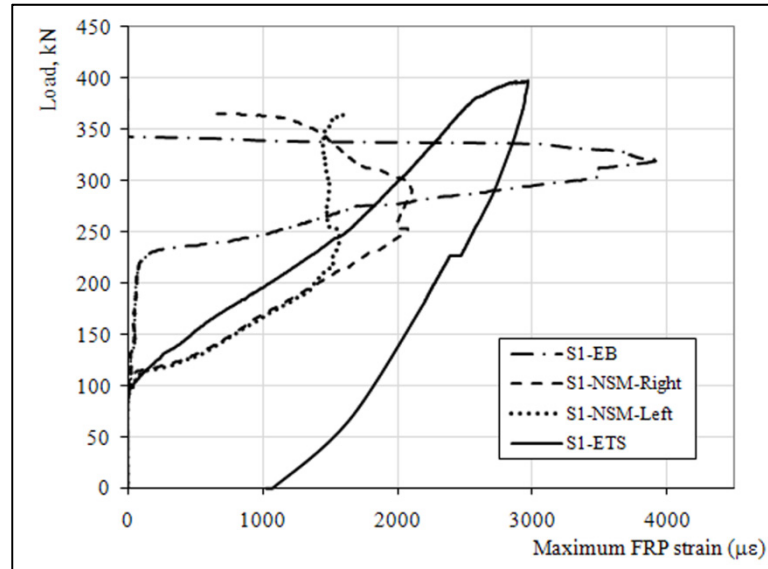
Figure 4.9   Load versus maximum strain in FRP – Series S1.

In the third stage, the transverse steel strain continues to increase with increasing load until either the transverse steel yields or rupture of the specimen occurs. The transverse steel that yields is easily identified by the large ductility plateau featured in the corresponding shear force strain curves.

Given the applied load, the strain in the transverse steel is substantially greater in specimens with no CFRP (Figures 4.11 and 4.12). Thus, it can be seen that the presence of CFRP eased the strains in the transverse steel. Also, the yielding of the transverse steel occurs earlier in specimens with no CFRP in comparison to corresponding retrofitted specimens. It must be noted, however, that yielding of transverse steel is achieved in most cases, which is in agreement with the assumptions of the design guidelines (ACI 440.2R-08; CSA S806-02; *fib* TG 9.3-01).

4.6   Discussion of results

Table 4.3 shows that the shear-strengthened beams experienced significant increase in capacity with respect to the control beams. In average, the beams strengthened with EB CFRP U-jacket sheet and NSM were about 23% and 31% stronger than the corresponding

control beams, respectively. For the beams strengthened with ETS method, these numbers jump to 60% over the control beam in average. This confirms that ETS FRP outperformed the other two retrofitting techniques and can be a cost-effective method for strengthening RC beams deficient in shear.
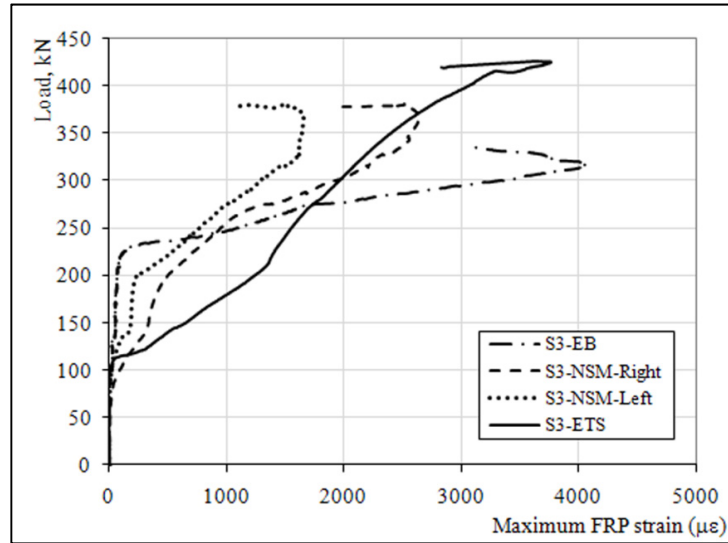
Figure 4.10 Load versus maximum strain in FRP – Series S3.
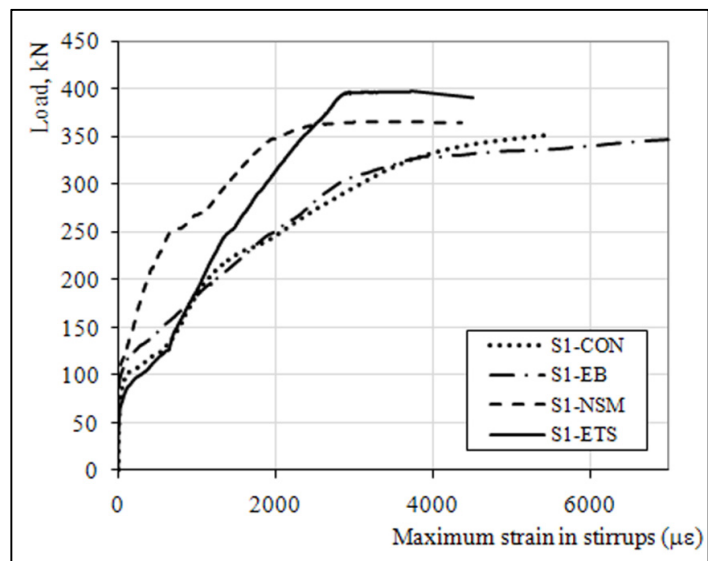
Figure 4.11   Load versus maximum strain in steel stirrup – Series S1.
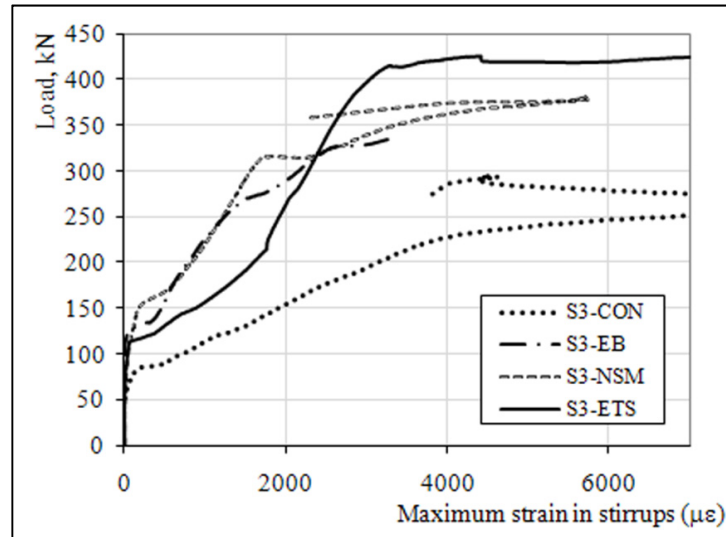
Figure 4.12   Load versus maximum strain in steel stirrup – Series S3.

Effect of transverse steel - As previously established (Chaallal et al. 2002; Pellegrino and Modena 2002 and Bousselham and Chaallal 2006), the presence of transverse steel resulted in a significant gain decrease for the beams strengthened with EB FRP method. Thus, the gain in the specimen S0-EB with no transverse steel is 48%, compared to 8% and 14.0% for beams S1-EB (spacing = 175 mm) and S3-EB (spacing = 260 mm). It should be noted that the difference in the concrete strength is considered for the calculation of V_f and of the gain due to FRP strengthening.

In the beams strengthened with the NSM method the presence of transverse steel resulted in a drastic decrease in the shear contribution of the FRP to the shear resistance. Thus, the gain drops from 61% for S0-NSM to 4% and 29% for beams S1-NSM and S3-NSM, respectively. This is attributed to the vertical legs of the steel stirrups which create two vertical planes of weakness (Figure 4.4), facilitating thereby the spalling of the side concrete cover (Rizzo and De Lorenzis 2009).

In the beams strengthened with the ETS method the presence of transverse steel also decreased the shear contribution of the FRP. The gain due to FRP attained 122% in beam S0-ETS, compared to 13% and 45% for beams S1-ETS and S3-ETS, respectively. However, it

should be noted that beams S1-ETS and S3-ETS reached their ultimate. Therefore, the gain due to ETS strengthening method in the beams with stirrups would have been higher, had failure did not occur by flexure or concrete cross section limitations. In addition, it should be noted that the resistance due to FRP has not significantly changed in the specimens with transverse steel strengthened with ETS method. This shows that the effect of transverse steel in inhibiting the effectiveness of FRP is less pronounced in the ETS method in comparison to EB method and NSM method.

This is in agreement with the theory of the effect of cracking pattern on the bond force (Mofidi and Chaallal 2011-a). Generally the cracking pattern is more spread on the surface of beams strengthened with FRP than in the beams' confined core. When the cracks pass the FRP fibers, the FRP bond length and hence the bond force decreases. It follows that debonding happens at a lower force compared to a concrete cross-section with less spread cracking pattern. Therefore, the ETS method where FRP is embedded in a less cracked concrete core is less prone to FRP debonding failure than EB and NSM methods.

Internal transverse steel reinforcement ratio (spacing) - Series S1 and S3 differed by the spacing of the transverse steel reinforcement: *d/2* for S1 and *3d/4* for S3 series. In EB specimens, as the spacing of the transverse steel reinforcement decreases, the gain due to FRP drops. This is attributed to the fact that the cracking pattern became more distributed as the spacing of the steel striups was reduced resulting thereby in a decrease in the bond force in the FRP fibers. Therefore, the specimen S1-EB started debonding at a lower FRP strain than S3-EB. It follows that the gain in S1-EB is lower than that of S3-EB specimen.

In NSM strengthened specimens, decreasing the spacing of the transverse steel reinforcement resulted in a lower gain for the S1-NSM compared to S3-NSM specimen. As the spacing of the steel stirrups was reduced, the effect of steel stirrup vertical legs, causing the side concrete of RC beam to detach, increased. Therefore, the specimen S1-NSM started debonding at a lower FRP strain than S3-NSM. It follows that, the gain in the S1-NSM is lower than that of S3-NSM specimen. Similar failure effect has been reported by De Lorenzis and Nanni (2001).

In the specimens strengthened using ETS method, it seems that decreasing the spacing of the transverse steel resulted in a lower resistance gain due to FRP. However, the failure modes of S1-ETS and S3-ETS beams were governed by flexure. Therefore, S1-ETS and S3-ETS beams did not reach their maximum shear capacity and hence the effect of transverse steel for these specimens could not be analyzed.

4.7 Efficiency of the ETS method

The effectiveness of the ETS method compared to EB FRP sheet method and NSM FRP rod method considering the amount of FRP per unit length is discussed in this section. The section area of the CFRP per meter of shear span used in all beams strengthened with EB, NSM and ETS methods was equal to 214 mm^2/m, 1090 mm^2/m and 974 mm^2/m, respectively. The ultimate tensile capacity per unit length of the strengthening systems in the same beams was equal to 781, 2055 and 1807 kN/m, respectively (Table 4.4).

Table 4.4   Efficiency of the FRP in different strengthening methods

Strengthening method	Series	Specimen	Area of dry fiber used, mm^2/m	Ultimate tensile capacity per unit length kN/m	V_f, kN	ψ_f, Efficiency of FRP %
EB	S0	S0-EB	214	781	38.7	5.0
	S1	S1-EB	214	781	18.5	2.3
	S3	S3-EB	214	781	27.3	3.5
NSM	S0	S0-NSM	1090	2055	49.8	2.4
	S1	S1-NSM	1090	2055	9.5	0.5
	S3	S3-NSM	1090	2055	56.9	2.7
ETS	S0	S0-ETS	974	1807	99.5	5.5
	S1	S1-ETS	974	1807	30.7	1.7
	S3	S3-ETS	974	1807	87.1	4.8

It should be noted that the CFRP characteristics are calculated based on the dry fiber material characteristics. The efficiency of the FRP strengthening system (ψ_f) for each specimen is

defined as the FRP contribution to the shear capacity, V_f, for each specimen divided by the ultimate tensile capacity per unit length of FRP used in each specimen for each specimen. Table 4.4 shows the efficiency of the FRP strengthening methods for each specimen. It can be seen that in average the ETS method efficiency for all series of transverse reinforcement is 1.1 and 2.1 times greater than that of EB method and NSM method respectively. This indicates the superior cost-effectiveness of the ETS FRP strengthening over the other methods.

4.8 Conclusions

Based on results of the present investigation, the following main conclusions can be drawn:

- FRP systems and, in particular, ETS FRP strengthening system can significantly enhance the shear capacity of RC beams even in presence of a limited amount of transverse steel reinforcement. In this study, the average increase in shear capacity reached 23% for the beam strengthened with EB U-jacket sheet, 31% for the beams strengthened with NSM FRP rods and 60% for the beams strengthened with ETS FRP rods. The ETS technique was more efficient in terms of developing FRP tensile strength potential before the final failure happens;

- beams strengthened with EB failed by FRP sheet debonding, whereas beams strengthened with NSM failed by separation of the side concrete covers at the internal steel stirrups. The failure in the beams strengthened with ETS FRP rods was mainly in flexure (S1 and S3 series);

- the presence of the transverse steel resulted in a decrease of the contribution of FRP to the shear resistance for the beams strengthened with EB and NSM methods. The contribution of FRP did not significantly decrease with the presence of transverse steel reinforcement in the specimens strengthened with the ETS method. This is attributed to the confined concrete core of the RC beam where the rods are embedded, which is less

cracked in comparison to the concrete cover which is the substrate for the FRP in the EB and NSM methods;

- given the load, the strain in the transverse steel was significantly greater in specimens with no CFRP. Nevertheless, the transverse steel yielded in most cases, as assumed by design codes and standards;

- ETS method is very promising. Therefore, further research is needed to address other important aspects such as the effect of spacing, cross section area and different types of FRP rods, and ultimately develop design models for professorial designers.

4.9   References

American Concrete Institute (ACI) (2008). *Guide for the Design and Construction of Externally Bonded FRP Systems for Strengthening Concrete Structures.* Report No. 440 2R-08, Farmington Hills MI.

American Concrete Institute (ACI) (2004). *Guide Test Methods for Fiber-Reinforced Polymers (FRPs) for Reinforcing or Strengthening Concrete Structures.* Report No. 440 3R-04, Farmington Hills MI.

Al-Sulaimani, G.J., Sharif, A.M., Basunbul, I.A., Baluch, M.H., and Ghaleb, B.N. (1994). Shear repair for reinforced concrete by fiberglass plate bonding. *ACI Struct. J.* 91(3), pp. 458–464.

Barros, J.A.O. and Dias, S.J.E. (2005). Near surface mounted CFRP laminates for shear strengthening of concrete beams. *Cement Concr. Compos.* 28, pp. 289–94.

Bousselham, A. and Chaallal, O. (2004). Shear strengthening reinforced concrete beams with fiber-reinforced polymer: assessment of influencing parameters and required research. *ACI Struct. J.* 101(2), pp. 219–227.

CAN/CSA-S806-02 (2002). *Design and construction of building components with fiber-reinforced polymer.* Canadian Standards Association, Rexdale, Canada.

Chaallal, O., Nollet, M.-J., and Perraton, D. (1998). Shear strengthenig of RC beams by externally bonded side CFRP strips. *J. Compos. Constr.* 2(2), pp. 111–113.

Chaallal, O., Shahawy, M., and Hassan, M. (2002). Performance of reinforced concrete T-girders strengthened in shear with CFRP fabrics. *ACI Struct. J.* 99(3), pp. 335–343.

De Lorenzis, L and Nanni, A. (2001). Shear strengthening of reinforced concrete beams with NSM fiber-reinforced polymer rods. *ACI Struct J*, 98(1), pp. 60–68.

fib-TG 9.3 (2001). *Externally Bonded FRP Reinforcement for RC Structures.* International Federation for Structural Concrete, Lausanne, Switzerland.

Khalifa, A., Gold, W.J., Nanni, A. and Aziz, A. (1998). Contribution of externally bonded FRP to shear capacity of RC flexural members. *J. Compos. Constr.* 2(4), pp. 195–203.

Mofidi, A. and Chaallal, O. (2011-a). Shear strengthening of RC beams with EB FRP—influencing factors and conceptual debonding model. *J. Compos. Constr.* 15(1), pp. 62–74.

Pellegrino, C. and Modena, C. (2002). Fiber reinforced polymer shear strengthening of RC beams with transverse steel reinforcement. *J. Compos. Constr.* 6(2), pp. 104–111.

Rizzo, A. and De Lorenzis, L. (2009). Behavior and capacity of RC beams strengthened in shear with NSM FRP reinforcement. *Constr. and Building Materials.* 23, pp. 1555-1567.

Triantafillou, T.C. (1998). Shear strengthening of reinforced concrete beams using epoxy-bonded FRP composites. *ACI Struct. J.* 95(2), pp. 107–115.

Uji, K. (1992). Improving shear capacity of existing reinforced concrete members by applying carbon fiber sheets. *Trans. Jpn. Concr. Institute*, 14(253), pp. 66.

Valerio P. and Ibell T.J. (2003) Shear strengthening of existing concrete bridges, *Proc. Institution of Civil Engineers-Structures and Buildings*, 156(1), 75-84. Valerio P., Ibell T.J., and Darby A.P. (2009) Deep embedment of FRP for concrete shear strengthening. *Proc. Institution of Civil Engineers-Structures and Buildings* 162(5), pp. 311-321.

CHAPTER 5

SHEAR STRENGTHENING OF RC BEAMS WITH EXTERNALLY BONDED FRP COMPOSITES: EFFECT OF STRIP-WIDTH TO STRIP-SPACING RATIO

Amir Mofidi and Omar Chaallal

Department of Construction Engineering, École de Technologie Supérieure 1100 Notre-Dame Ouest, Montréal, Québec, Canada H3C 1K3

5.1   Abstract

This paper presents the results of an experimental and analytical investigation of shear strengthening of reinforced concrete (RC) beams with externally bonded (EB) fibre-reinforced polymer (FRP) strips and sheets, with emphasis on the effect of the strip-width to strip-spacing ratio on the contribution of FRP (V_f). In all, 14 tests were performed on 4520-mm-long T-beams. RC beams strengthened in shear using carbon FRP (CFRP) strips with different width-to-spacing ratios were considered, and their performance was investigated. In addition, these results are also compared with those obtained for RC beams strengthened with various numbers of layers of continuous CFRP sheet. Moreover, various existing equations which express the effect of FRP-strip width and concrete-member width and which have been proposed based on single or double FRP-to-concrete direct pull-out tests are checked for RC beams strengthened in shear with CFRP strips. The objectives of this study are to investigate: 1) the effectiveness of EB discontinuous FRP sheets (FRP strips) compared with that of EB continuous FRP sheets; 2) the optimum strip-width to strip-spacing ratio for FRP

(i.e., the optimum FRP rigidity); 3) the effect of FRP strip location with respect to internal transverse-steel location; 4) the effect of FRP strip width; and 5) the effect of internal transverse-steel reinforcement on the CFRP shear contribution.

5.2   Introduction and background

Significant interest has been shown in the use of externally bonded (EB) fibre-reinforced polymer (FRP) sheets and laminates for strengthening and repair of existing reinforced concrete (RC) beams and slabs, especially for bridges and buildings. Because of its intricacy, shear strengthening of RC beams with FRP is somewhat less well documented than FRP strengthening of beams in flexure and of columns (Bousselham and Chaallal 2004). Research studies carried out during the last decade have provided valuable outcomes, especially concerning the effect of FRP axial rigidity on the shear-strength enhancement of RC beams (Triantafillou 1998; Khalifa et al. 1998). On the basis of these research studies, many codes and design guidelines (hereafter called "the guidelines") for RC structures strengthened with EB FRP have been published worldwide (e.g., ACI 440.2R-08, *fib*-TG 9.3-01, CAN/CSA S806-02, CAN/CSA S6-06, CNR-DT200-04, and HB 305-08). However, in a statistical comparison with available experimental results, Lima and Barros (2007) have revealed that some of the guideline equations (ACI 440 and CNR-DT200) lead to unduly conservative designs which use quantities of FRP materials well in excess of what is required. Efficient and accurate FRP strengthening design equations will greatly benefit the economic aspects of FRP strengthening projects.

Based on available experimental data, Triantafillou (1998) discovered that FRP effective strain decreases as FRP rigidity increases. Khalifa and Nanni (2000) realized that increasing the amount of CFRP may not always result in a proportional increase in shear resistance. They noted the existence of an FRP quantity threshold beyond which further strengthening effectiveness is questionable. In addition, their experimental tests showed that CFRP strips can outperform continuous CFRP sheets. Other experimental tests by Khalifa and Nanni (2002) and Zhang and Hsu (2005) confirmed these observations.

Unlike shear-strengthening methods which use FRP continuous sheets, with discontinuous FRP sheets the quantity of FRP present varies with the strip-width to strip-spacing ratio (w_f/s_f). The FRP rigidity parameter (R_f) can be used to quantify the amount of FRP used with respect to the FRP-strip-width to FRP-strip-spacing ratio. The FRP rigidity parameter can be expressed as a function of (w_f/s_f) as follows:

$$R_f = \rho_f \times E_f \qquad (5.1a)$$

where

$$\rho_f = \frac{2t_f}{b_w} \times \frac{w_f}{s_f} \qquad (5.1b)$$

In the calculation of FRP rigidity, the only variable is the FRP-strip-width to FRP-strip-spacing ratio (assuming that the FRP sheet characteristics and the RC beam cross-sectional dimensions are constants). Based on the authors' updated database which encompasses the test results available in the literature up to 2010 on RC beams strengthened with FRP strips (see Bousselham and Chaallal (2004) for the original database), the relationship of FRP rigidity and shear-capacity increase has been investigated and is presented in Figure 5.1. It can be seen that increasing the FRP rigidity (i.e. the FRP-strip-width to FRP-strip-spacing ratio) does not necessarily lead to a gain in shear resistance. This result is in agreement with previous findings by Triantafillou (1998) and Khalifa and Nanni (2000).

In most current design models, the FRP contribution to shear resistance is assumed to be linearly related to FRP rigidity (or w_f/s_f). Clearly, this assumption is not in agreement with Figure 5.1 of the current research study, nor with the results of previous research studies (Triantafillou 1998; Khalifa and Nanni 2000). Therefore, to enhance current design guidelines, further consideration of the effect of the w_f/s_f ratio (i.e., FRP rigidity) seems reasonable.
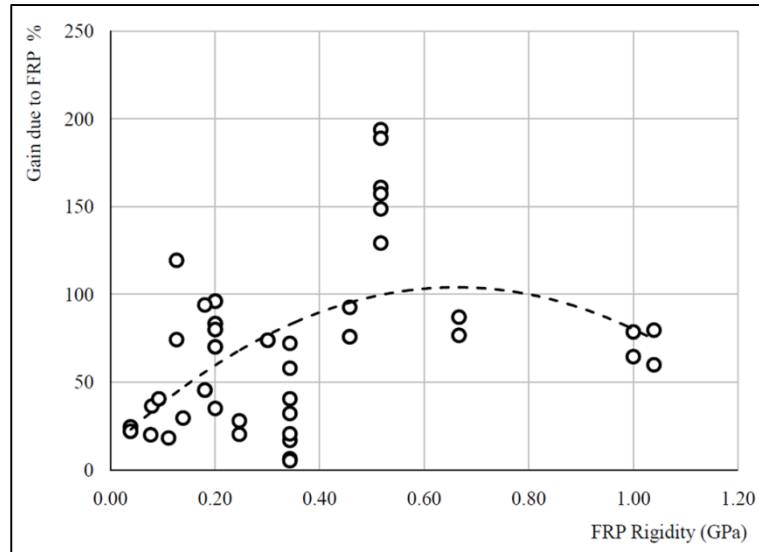
Figure 5.1   FRP rigidity versus shear resistance gain.

FRP-to-concrete direct pull-out tests (e.g., Bizindavyi and Neale 1999, Brosens and Van Gemert 1999) have demonstrated that the width of the FRP sheets, b_f, and the width of the concrete block, b_c, have a significant effect on the maximum bond strength of the FRP. Kamel et al. (2000) observed that the maximum load per unit width of the FRP strip can be significantly reduced in wide FRP sheets because of strain concentrations at the edges. To express this phenomenon, Holzenkämpfer (1994) introduced the term k_f for steel plates bonded to concrete blocks, as follows:

$$k_f = \sqrt{1.125 \times \frac{2 - \dfrac{b_f}{b_c}}{1 + \dfrac{b_f}{400}}} \qquad (5.2)$$

Neubauer and Rostásy (1997) confirmed Holzenkämpfer's (1994) equation for FRP sheets bonded to concrete. Brosens and Van Gemert (1999) modified Eq. (2) as follows:

$$k_f = \sqrt{1.5 \times \frac{2 - \dfrac{b_f}{b_c}}{1 + \dfrac{b_f}{100}}} \qquad (5.3)$$

Later, Brosens (2001) proposed a modification of Holzenkämpfer's (1994) equation as follows:

$$k_f = \sqrt{1.47 \times \frac{2 - \dfrac{b_f}{b_c}}{1 + \dfrac{b_f}{85}}} \qquad (5.4)$$

Using a regression analysis of available experimental results, Chen and Teng (2001) extended the effect of FRP-plate width and concrete-block width to the effect of the FRP-strip-width to FRP-strip-spacing ratio for RC beams strengthened in shear. The role of k_f in the FRP shear contribution is also described by the authors. In their equation, b_f is replaced by w_f and b_c by s_f, yielding:

$$k_f = \sqrt{\frac{2 - \dfrac{w_f}{s_f}}{1 + \dfrac{w_f}{s_f}}} \qquad (5.5)$$

The objectives of this research study are: (i) to study the effectiveness of CFRP strips compared with that of CFRP sheets for shear strengthening of RC beams; (ii) to test the applicability of available equations for the effect of strip width and concrete-block width on FRP sheets applied to concrete-block joints in RC beams strengthened in shear with different strip-width to strip-spacing ratios; (iii) to investigate the performance of RC beams strengthened in shear with EB CFRP composites, in terms of the CFRP and the transverse-steel reinforcement ratios; and (iv) to check the effect of certain details such as CFRP strip location or CFRP strip width on improving the efficiency and performance of the strengthening system.

5.3   **Description of the Experimental Program**

5.3.1   **Test specimens**

The experimental program included 14 tests performed on seven full-size T-beams (Table 5.1). The specimens are 4,520 mm long and have an effective cross-sectional beam depth $d = 350$ mm (Figure 5.2). Series S0 consists of specimens with no internal transverse-steel stirrups, hereafter called transverse steel. Series S1 consist of specimens with transverse steel spaced at $s = d/2$. The transverse-steel reinforcements were 8 mm in diameter (area=50 mm^2) and were spaced at $s=d/2$ (see Figure 5.2). The distance of the first stirrup from the support was $d/4$.

The control specimens not strengthened with CFRP are labelled as "0R", whereas the specimens retrofitted with CFRP are labelled according to their respective CFRP sheet rigidity as calculated using Eq. (1b). For example, the FRP rigidity of a beam labelled 0.23R is 0.23 GPa. The specimen details are provided in Table 5.1, together with the identification codes used hereafter.
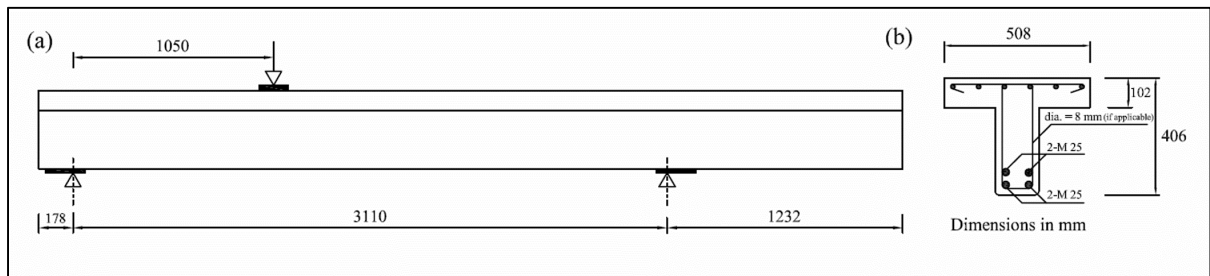
Figure 5.2   Details of concrete beams: (a) elevation; (b) cross section.

A commercially available concrete delivered to the ÉTS laboratory by a local supplier was used in this project. The 28-day concrete compressive strength achieved an average value of 29 MPa, which is very close to the average compressive strength of 31 MPa reached during the tests. In addition, the scatter between the results of compression tests of the cylinder specimens was insignificant.

Table 5.1   Experimental results

Specimen	FRP Configu ration	w_f/s_f	Load at rupture kN	Total resistance kN	Resistance due to concrete kN	Resistance due to steel kN	Resistance due to CFRP kN	Gain due to CFRP %	Deflection loading point mm
S0-0.0R	-	0	122.7	81.2	81.2	0.0	0.0	0	2.60
S0-0.12R	Strips	40/115	182.6	120.9	81.2	0.0	39.7	49	6.95
S0-0.17R1	Strips	87.5/175	203.1	134.5	81.2	0.0	53.3	66	6.16
S0-0.17R2	Sheet	1	154.7	102.4	81.2	0.0	21.2	26	4.90
S0-0.20R1	Strips	53/87.5	204.9	135.7	81.2	0.0	54.5	67	5.85
S0-0.20R2	Strips	30/50	197.9	131.1	81.2	0.0	49.9	61	8.03
S0-0.23R	Strips	87.5/125	227.3	150.6	81.2	0.0	69.3	85	7.23
S0-0.33R	Sheet	1	181.2	120.0	81.2	0.0	38.7	48	4.20
S0-0.66R	Sheet	1	183.8	121.7	81.2	0.0	40.4	50	4.10
S1-0.0R	-	0	350.6	232.2	81.2	151.0	0.0	0	11.9
S1-0.17R1	Strips	87.5/175	365.9	242.3	81.2	151.0	10.1	4	17.19
S1-0.17R2	Strips	87.5/175	372.5	246.7	81.2	151.0	14.5	6	15.93
S1-0.23R	Strips	87.5/125	383.4	253.9	81.2	151.0	21.7	9	15.73
S1-0.33R	Sheet	1	378.3	250.6	81.2	151.0	18.4	8	15.24

The composite material is a unidirectional carbon-fibre fabric epoxy-bonded over the test zone in a U-shape around the web. The CFRP sheet has an ultimate tensile strength of 3,450 MPa, an elastic modulus of 230 GPa, and an ultimate strain of 1.5%. For specimens S0-0.17R2 and S1-0.17R2, the fabric was prepared by manually removing three out of six carbon-fibre yarns (over a 1-in. width) from the original fabric. Table 5.2 presents the mechanical and elastic properties of the CFRP fabric as provided by the manufacturers.

Table 5.2   Mechanical properties of CFRP strips and sheets.

Property	Fibre properties
Modulus of elasticity, GPa	230
Ultimate elongation, %	1.50
Ultimate stress, MPa	3450
Density, g/cm^3	1.8
Basis weight, g/m^3	230

5.3.2   Experimental procedure

All fourteen tests were conducted in three-point load flexure. This loading configuration was chosen because it enabled two tests to be performed on each specimen. Specifically, while one end zone is being tested, the other end zone is overhung and unstressed (see Figure 5.2). The load is applied at a distance $a = 3d$ from the nearest support, which is representative of a slender beam (see Figure 5.2). The measuring device used for the project was carefully designed to meet the objective and the scope of this study. The vertical displacement was measured at the position under the applied load and at mid-span, using a linear variable differential transformer (LVDT) with a 100-mm stroke. In addition, LVDTs were installed on each side of the supports perpendicular to the web plane to monitor any undesired sway or tilt effects.

Various types of strain gauges were installed on the longitudinal reinforcement on the steel stirrups or embedded in concrete to measure the strains experienced by different materials as the loading increased and to monitor thereby the yielding of the steel and the onset of concrete cracking and crushing (Figure 5.3).
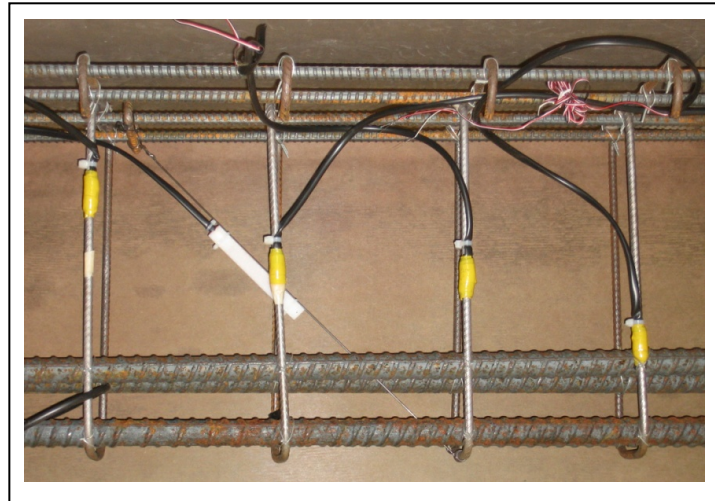
Figure 5.3   Strain gauges on transverse steel and embedded in concrete.

The strain gauges on the stirrups were installed along the anticipated plane of shear fracture. Displacement sensors, also known as crack gauges, were used to measure the deformations in the CFRP sheet. These gauges were fixed vertically on the lateral faces of the specimens at

the same location along the longitudinal axis as the strain gauges on the transverse steel. In this way, the strains in the CFRP and in its corresponding steel stirrups can be conveniently compared during the various loading stages. To measure concrete deformation, crack gauges were glued onto the concrete surface, midway between the support and the point of application of loading, at mid-height of the beam web with a 45° inclination with respect to the longitudinal axis. The load was applied using a 2000 kN-capacity MTS hydraulic jack. All tests were performed under displacement-control conditions at a rate of 2 mm/min.

5.4   Analysis of results

5.4.1   Overall response

Table 5.1 presents the loads attained at rupture, the contributions to the shear resistance of the concrete, the transverse steel, and the CFRP, the gain in capacity due to the CFRP, defined as (gain = V_f / (V_{tot}−V_f), and the maximum deflection at failure under the load point. It should be mentioned that the shear contribution of the concrete and the steel are calculated based on the results gained from the un-strengthened specimens. Note that the following assumptions, implicitly admitted in the guidelines, are considered in deriving some of the values provided in Table 5.1: (i) the shear resistance due to concrete is the same whether the beam is retrofitted in shear with FRP or not and whether the retrofitted beam is reinforced with transverse steel or not; and (ii) the contribution of the transverse steel is the same for both strengthened and un-strengthened beams. Figures 5.4 and 5.5 show the shear force versus mid-span deflection curves for Series S0 and S1 respectively.

The curves presented are typical of a shear test. In the first phase of loading, before concrete cracking, these curves are very similar. The cracking incident and its propagation resulted in a loss of stiffness, which is indicated by the observed decrease in the slopes of the curves. This also led to a redistribution of internal forces and initiated the contributions of the transverse steel and the CFRP reinforcement. In Series S0 (Figure 5.4), beams strengthened with continuous CFRP U-jacket sheets (S0-0.33R and S0-0.66R) exhibited a slightly higher overall stiffness than beams strengthened with CFRP U-jacket strips.
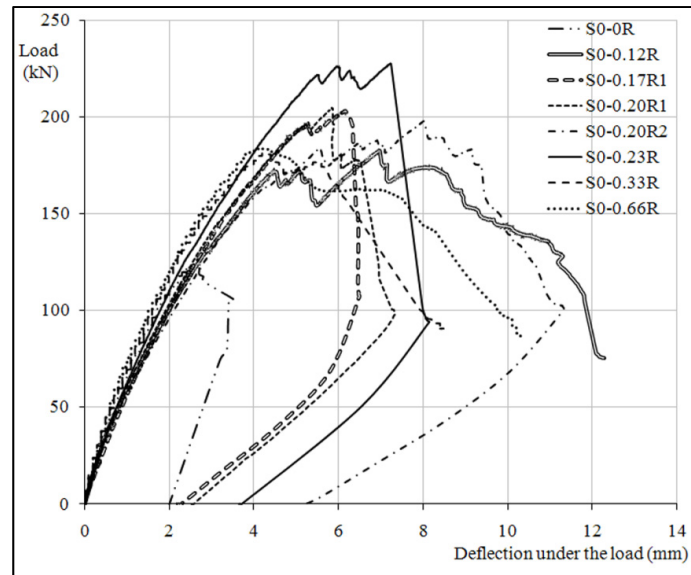
Figure 5.4   Load versus maximum deflection – Series S0.

However, for Series S0 (this was also true for Series S1), the gain due to CFRP in beams strengthened with CFRP U-jacket strips was greater on average than in beams strengthened with a continuous FRP U-jacket. For specimen S0-0.33R, for example, the load at failure was 181.2 kN, compared with 227.3 kN for S0-0.23R.
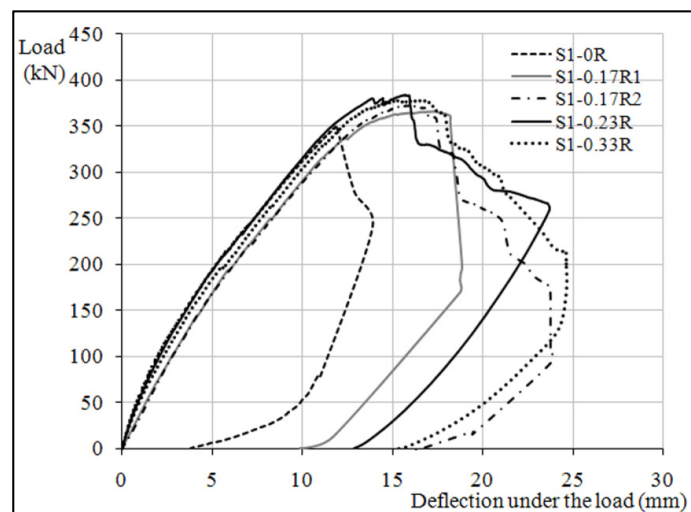
Figure 5.5   Load versus maximum deflection – Series S1.

As for the influence of CFRP thickness on the gain in shear capacity, the addition of a second layer of CFRP (i.e., going from one to two layers; see S0-0.33R versus S0-0.66R) resulted in a modest gain in shear capacity in the S0 specimens. In Series S0, the maximum deflection ratio between the retrofitted and the corresponding control specimen is greater for beams strengthened with CFRP strips than for beams strengthened with continuous CFRP sheets. On average, this ratio is 2.63 for beams strengthened with CFRP strips and only 1.69 for beams strengthened with CFRP sheets.

In Series S1 (Figure 5.5), the addition of transverse-steel reinforcement resulted in a drastic decrease of the gain in shear capacity due to CFRP. As for the gain in stiffness, the observed slope deviations between the curves for the retrofitted specimens and those for the control specimens are not significant. The maximum deflection at failure was slightly greater for specimens strengthened with CFRP strips, with an average value of 16.28 mm. By comparison, the specimens strengthened with CFRP continuous sheet experienced a maximum deflection of 15.24 mm.

5.4.2   Cracking and failure mode

All the test specimens failed in shear. The specimens strengthened with CFRP failed by premature FRP debonding followed by crushing of concrete struts, with a wide-open crack in the RC beam flange (Figures 5.6-a to 5.6-d). Local CFRP fracture was observed in some specimens (S0-0.12R, S0-0.20R1, S0-0.20R2, S0-0.23R), but that was attributable mostly to stress concentration at the web corners (Figure 5.6-b). Control specimen S0–0R exhibited a single shear-crack pattern. The shear crack initiated on the beam web, midway between the support and the point load, and propagated simultaneously toward both the beam flange and the support. As the crack reached the flange, it triggered an immediate failure of the specimen. The cracking propagated at an angle of approximately 42° in the web and became almost horizontal as it reached the beam flange.
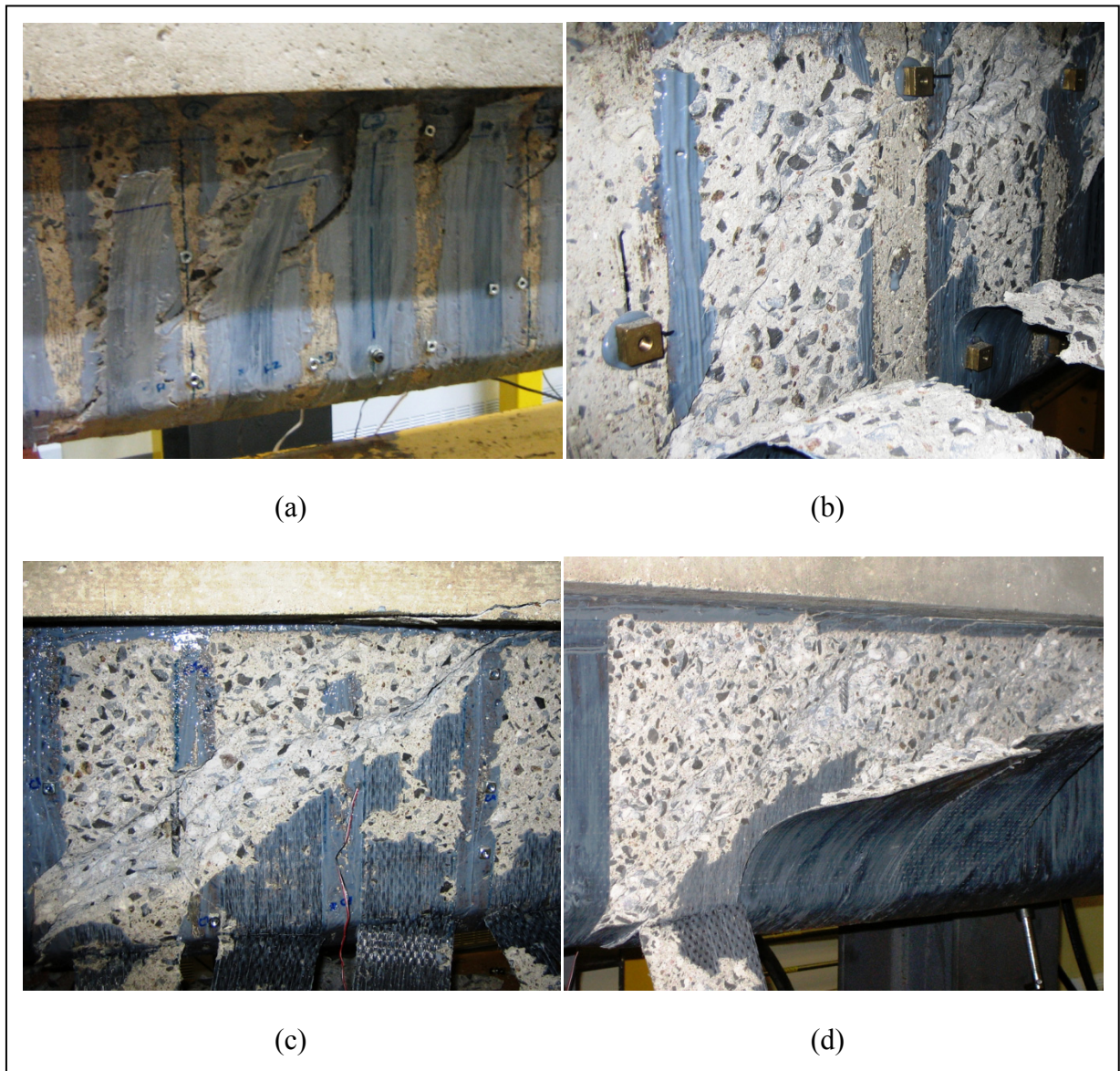
Figure 5.6   Failure mode in strengthened beams: a) S0-0.12R; b) S0-0.17R1;
c) S1-0.23R; and d) S1-0.33R.

Because of the presence of the transverse-steel reinforcement, control specimen S1-0R exhibited a cracking pattern different from that of control specimen S0-0R; its cracking pattern was more widespread and propagated at an average angle of approximately 39°.

In Series S0, cracking initiated at more or less the same load level, approximately 80 kN, for all beams of the series. After cracking, the stiffness of the beams decreased, as expected.

However, in retrofitted specimens, this reduction in stiffness was more pronounced in beams strengthened with CFRP U-jacket strips than in beams strengthened with continuous CFRP sheets. In the retrofitted specimens, only one principal crack was observed in the specimens in Series S0. For the beams strengthened with U-shaped strips, the gain in shear capacity due to CFRP was 66% on average, compared to 31% for specimens strengthened with continuous CFRP sheets.

In strengthened beams in Series S1, two parallel diagonal cracks formed between 78 and 81 kN and propagated with increasing load from the support to the flange at an average angle of approximately 38°. As the load was reaching its ultimate value, these two diagonal cracks merged into a single crack which progressed horizontally in the RC beam flange. The Series S1 beams strengthened by U-shaped strips achieved an average gain of 6% in shear capacity due to FRP, compared to 8% for specimens strengthened with continuous CFRP sheets.

5.4.3 CFRP strains

Figures 5.7 and 5.8 present the shear force versus CFRP strain curves for Series S0 and S1 respectively. All the curves presented in these figures show that the CFRP did not contribute to the load-carrying capacity in the initial stage of loading, i.e., up to an applied shear force between 70 and 80 kN. Thereafter, the strain in the CFRP started to increase steadily up to a maximum value (Figures 7 and 8), the level at which the CFRP U-jackets started to debond locally. In Series S0, the maximum measured strain values for the CFRP strips (4999 $\mu\varepsilon$ on average) are significantly greater than those for the CFRP continuous sheets (3583 $\mu\varepsilon$ on average). For example, in beams strengthened with CFRP strips, the strain attained 5822 μstrains in beam S0-0.12R and 5553 μstrains in S0-0.23R. In specimens strengthened with CFRP U-jacket sheet, the strain reached 2478 μstrains in S0-0.33R and 4688 μstrains in SB-0.66R. Finally, a comparison of Figure 5.7 with Figure 5.8 reveals that the maximum strains achieved in the CFRP were somewhat similar for corresponding beams of both series (except for specimen S0-0.33R where the strain gauges might not have captured the maximum attained CFRP strain).
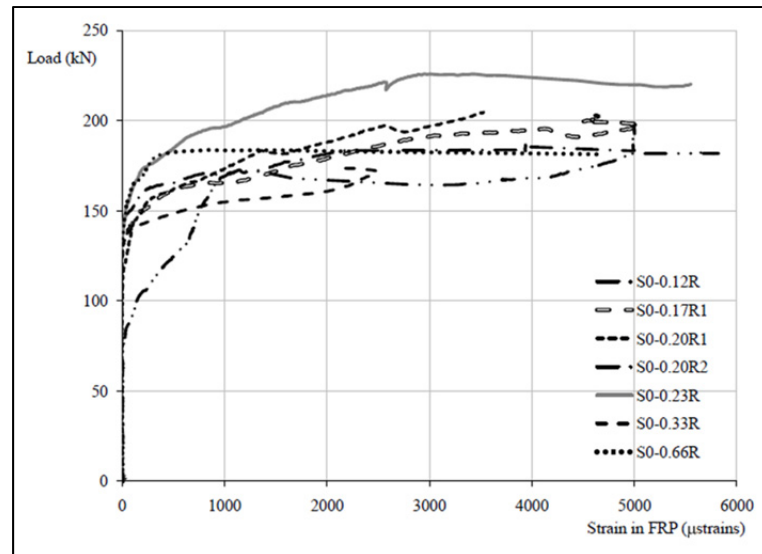
Figure 5.7 Load versus maximum strain in FRP – Series S0.

However, the contribution of FRP to shear resistance is significantly greater for beams in Series S0 (with no transverse-steel reinforcement) than for beams in Series S1 (with transverse-steel reinforcement) (45.9 kN versus 16.2 kN on average).
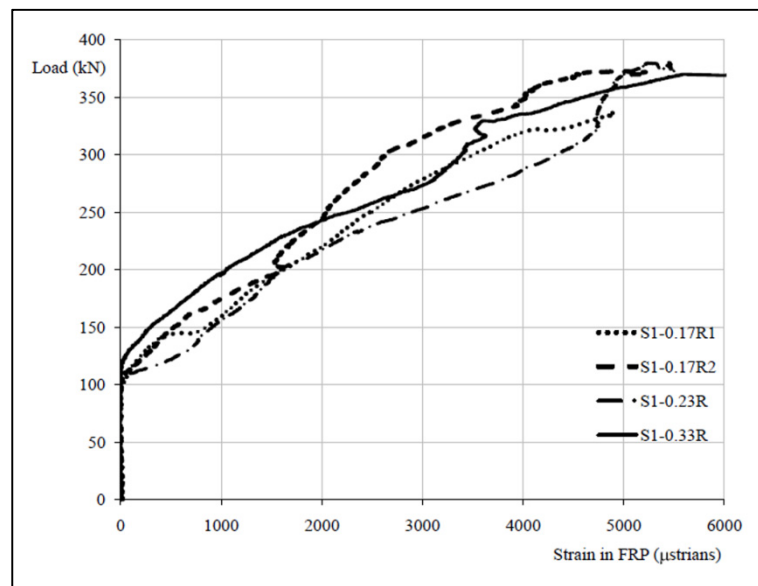
Figure 5.8 Load versus maximum strain in FRP – Series S1.

It must be pointed out that this strain value, like all those reported in this paper, is the maximum measured value, but not necessarily the absolute maximum value, experienced by the CFRP U-jackets. The two values may differ in cases where the strain gauges did not intercept the main cracks.

5.4.4 Transverse-steel strains

Curves representing the applied shear force versus the strains in the transverse-steel reinforcement are presented in Figure 5.9 for specimens of Series S1. It should be noted that the reported transverse steel strain is the measured strain in the steel stirrup that achieved the maximum strain during loading.
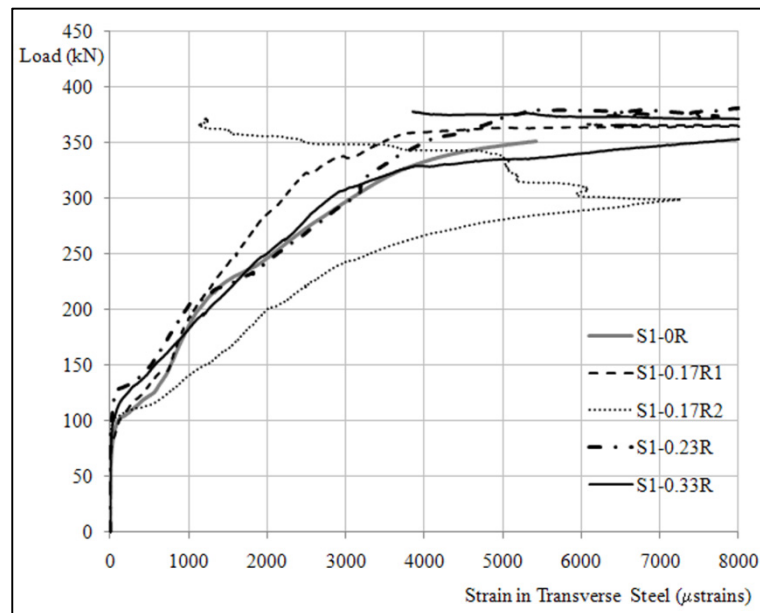
Figure 5.9   Load versus maximum strain in steel stirrup – Series S1.

As for CFRP, it can be observed that the steel stirrups did not contribute to the load-carrying capacity in the initial stage of loading. The transverse-steel contribution to shear resistance initiated after the formation of diagonal cracking. In the un-strengthened control specimen S1-0R, for example, this initiation occurred at an applied shear force of approximately 77 kN, whereas for the retrofitted specimens (S1-0.17R1, S1-0.17R2, S1-0.23R, and S1-0.33R), it occurred at an applied shear force of approximately 85 kN. The transverse-steel strain continued to increase with increasing load. For all specimens in Series S1, the transverse-steel reinforcement yielded well ahead of general failure. For specimen S1-0.17R2 (CFRP strips between the steel-stirrup locations), the strain value was significantly greater than for specimen S1-0.17R1 (CFRP strips at the same locations along the longitudinal axis as the steel stirrups). Moreover, the strain started to increase at an earlier loading stage in specimen S1-0.17R2 than in specimen S1-0.17R1.

5.5 Discussion and Analysis of Experimental Results

The first part of this section compares the efficiency of the strengthened beams. Then the effects of certain details on the shear strengthening of RC beams with CFRP, including CFRP strip widths, presence of transverse steel, and CFRP strip locations, are successively presented and analyzed. A comparison of the effectiveness of CFRP strips and CFRP sheets is then presented. Finally, the applicability of available equations describing the effect of strip width and concrete-block width on FRP sheets applied to concrete-block joints in RC beams strengthened in shear with different strip-width to strip-spacing ratios is examined.

5.5.1 Efficiency of strengthening systems

As shown in Table 5.1, the strengthened beams showed a significant increase in shear capacity compared with the control beams. In particular, the beams strengthened with externally bonded U-jacket CFRP strips and sheets were on average 43% and 33% stronger respectively than their corresponding control beam.

Table 5.3   Efficiency of FRP using different strengthening methods

Specimen	Area of CFRP	Ultimate tensile capacity per unit length	V_f	ψ_f Efficiency of FRP
	mm²/m	kN/m	kN	%
S0-0.12R	77	266	39.7	14.9
S0-0.17R1	110	380	53.3	14.0
S0-0.17R2	120	414	21.2	5.1
S0-0.20R1	133	459	54.5	11.9
S0-0.20R2	132	455	49.9	11.0
S0-0.23R	154	531	69.3	13.1
S0-0.33R	220	759	38.7	5.1
S0-0.66R	440	1518	40.4	2.7
S1-0.17R1	110	380	10.1	2.7
S1-0.17R2	110	380	14.5	3.8
S1-0.23R	154	531	21.7	4.1
S1-0.33R	220	759	18.4	2.4

This result confirms that externally bonded continuous CFRP sheets and CFRP strips can be used effectively to strengthen RC beams that are deficient in shear. Table 5.3 compares the efficiencies achieved by the various strengthened beams. The FRP efficiency ratio is defined as the contribution of FRP to shear resistance divided by the maximum FRP tensile strength per unit length.

It can be seen that the FRP efficiency ratio is superior (9.7% versus 3.3%) for the beams of Series S0 (without transverse steel) compared to that for Series S1 (beams with transverse steel). In addition, the FRP efficiency ratio is greater for beams strengthened with CFRP strips than for beams strengthened with CFRP sheets for both series (Table 5.3).

5.5.2   Effect of CFRP strip width (for constant w_f/s_f)

The effect of strip width (for a given w_f/s_f ratio) can be observed by comparing the response of beams S0-0.2R1 and S0-0.2R2. These beams have a similar width-to-spacing ratio, but

different FRP strip widths. The FRP in specimen S0-0.2R2 with narrow FRP strips (w_f =30 mm) reached higher strains than did specimen S0-0.2R1 (5738 με versus 3530 με). Conversely, specimen S0-0.2R1 with wide FRP strips (53 mm) achieved a greater contribution of FRP to shear resistance than did specimen S0-0.2R2 (54.5 kN versus 49.9 kN).

The last observation is in contrast with the findings of Kamel et al. (2000) from direct-tension tests conducted to investigate the effect of CFRP-strip-width to concrete-block-width ratio for CFRP sheets bonded to concrete blocks. Those tests revealed that for wide FRP sheets, the maximum load per unit width of the FRP strip can be considerably reduced by strain concentrations at the edges. It can be concluded that the effect of the strip-width to concrete-block-width ratio observed in the direct-tension test for CFRP strips bonded to concrete blocks does not seem to be valid for beams strengthened in shear with CFRP strips. It follows that the applicability of the equations that were proposed based on direct-tension tests of CFRP strips bonded to concrete blocks (Equations 5.2 to 5.5) to beams strengthened in shear with CFRP strips is questionable.

5.5.3 Effect of the presence of internal transverse steel

The effect of the presence of transverse steel on the contribution of FRP to shear resistance can be examined by comparing the results for Series S0 with those for Series S1 (Table 5.1). The average gain in shear resistance due to FRP in the specimens of Series S0 is 57%, compared to 7% for the beams of Series S1. In particular, the presence of transverse steel resulted in a significant decrease in the contribution of FRP to shear resistance for specimens S0-0.17R1, S0-0.23R, and S0-0.33R, from 53.3, 69.3, and 38.7 kN to 14.5, 21.7, and 18.4 kN respectively. This result corroborates once again the findings of previous research studies on the effect of transverse steel (Chaallal et al. 2002; Pellegrino and Modena 2002; Bousselham and Chaallal 2006 and Pellegrino and Modena 2006).

5.5.4   Effect of CFRP-strip location with respect to steel stirrup location

The effect of FRP-strip location with respect to steel-stirrup location can be examined by comparing the test results for beams S1-0.17R1 and S1-0.17R2 (Figure 5.10).
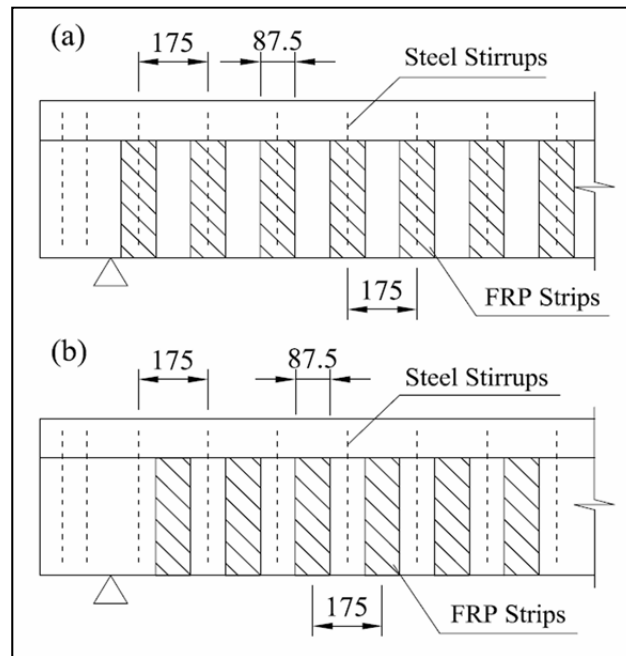
Figure 5.10   Elevation of: a) specimen S1-0.17R1 with CFRP strips placed in the same locations along the longitudinal axis as the steel stirrups and b) specimen S1-0.17R2 with CFRP placed mid-way between the steel-stirrup locations (dimensions in mm).

The width and spacing of the CFRP strips in both specimens are similar. In beam S1-0.17R1, the FRP strips are placed at the same locations along the longitudinal axis as the steel stirrups, whereas in beam S1-0.17R2, the FRP strips are located mid-way between the steel stirrups. Figure 5.5 shows that the two beams exhibited similar stiffness until the load reached 330 kN. Thereafter, the stiffness of beam S1-0.17R1 dropped slightly compared to that of beam S1-0.17R2. At failure, the contribution to shear resistance due to FRP for specimen S1-0.17R2 was 1.43 times that of specimen S1-0.17R1 (14.5 kN versus 10.1 kN). The mid-span deflection of beam S1-0.17R1 just before failure was 1.08 times the deflection of beam S1-0.17R2 at failure (17.2 mm at load 365.9 kN versus 15.9 mm at 372.5 kN). Therefore, it can be concluded that installing FRP strips mid-way between steel stirrups can

enhance the overall performance of the strengthened beam. On the other hand, it was experimentally observed that beam S1-0.17R1 with FRP strips bonded in the same place as the steel stirrups was more flexible than beam S1-0.17R2 with FRP strips bonded mid-way between the steel stirrups.

5.5.5 Discontinuous CFRP strips versus continuous CFRP sheets

To compare the effectiveness of CFRP U-jacket (discontinuous) strips with that of CFRP U-jacket continuous sheets, three pairs of specimens were selected. Specimen S0-0.17R1 is strengthened with CFRP strips, whereas specimen S0-0.17R2 is strengthened with a continuous CFRP sheet; however, both specimens have the same CFRP axial rigidity (0.17 GPa). To create a CFRP sheet with a rigidity of 0.17 GPa, three out of six carbon-fibre yarns (for each 25.4-mm width) were manually removed from the original manufactured fabric. Table 5.1 clearly shows that the contribution of FRP to shear resistance was drastically reduced in specimen S0-0.17R2 compared with specimen S0-0.17R1 (21.2 kN versus 53.3 kN). In addition, the test results for specimens S0-0.23R and S1-0.23R (both strengthened with the same CFRP strips and spacings) can be compared with those for specimens S0-0.33R and S1-0.33R (both strengthened with one layer of CFRP sheet). It can be observed that using CFRP strips instead of CFRP sheets resulted in an increase of 49% on average in the contribution of FRP to shear resistance. The superior performance of CFRP U-jacket strips compared to a continuous CFRP U-jacket could be attributed to the fact that, in a strengthened beam with FRP strips, two adjacent FRP strips can perform independently in the direction perpendicular to the major load-carrying direction of the FRP fibres. Therefore, unlike a continuous FRP U-jacket, local debonding in one FRP strip does not affect the performance of adjacent strips. All the specimens strengthened with FRP strips experienced local strip debonding during loading. Each local strip-debonding event resulted in a noticeable drop in the load-carrying capacity of the beam in question (see Figure 5.4), but the load continued to increase as the cracks propagated, engaging thereby the unloaded CFRP strips in their path. It follows that the beams strengthened with FRP strips feature a rather ductile mode of failure (Figure 5.4). This contrasts with the situation in beams strengthened

with CFRP sheets, which featured a progressive FRP debonding type of failure once local debonding initiated, as illustrated by the load-deflection graphs (see Figures 5.4 and 5.5) for specimens strengthened with CFRP sheets (S0-0.17R2, S0-0.33R, and S1-0.33R).

It can be seen in Figure 5.4 that the flexural stiffness of specimens S0-0.33R and S0-0.66R, which were strengthened with continuous CFRP sheets, is slightly greater than that of both the control beam and the beams strengthened with CFRP strips. The greater flexural stiffness in these beams can be attributed to the effect of the continuity of the CFRP sheets. Although uniaxial, the CFRP sheet used in this research can still carry some load in the direction perpendicular to its fibre orientation. In fact, the CFRP sheet in question has a tensile strength of 27 MPa and a tensile modulus of 5876 MPa in the minor direction (90°). During the three-point loading test (before beam failure), the RC beams starts to bend as flexural cracks propagate in the concrete tension zone. Meanwhile, no signs of separation (unzipping) of the fibres were observed in the CFRP U-jacket sheet. This shows that the CFRP U-jacket sheet (unlike the FRP strips) contributes to the RC beam's bending resistance. It is believed that, although the longitudinal tensile force in the U-jacket sheet adds to the RC beam's flexural stiffness, it also facilitates the progressive debonding process in the U-jacket once local debonding has taken place in a particular FRP band. As the RC concrete beam strengthened with CFRP sheet bends and flexural cracks open up, the FRP sheet and the epoxy layer can no longer accommodate the RC beam's deformability. At the same time as the shear cracks start to grow, local debonding takes place in the CFRP sheet. The horizontal strain left in the CFRP bonded layer due to the difference in flexibility of the RC beam and the CFRP sheet causes the local debonding to migrate from one fibre band to another. This causes overall CFRP U-jacket debonding, followed by failure of the RC beam. In this way, a local CFRP debonding event can trigger overall CFRP U-jacket debonding. Therefore, the RC beam's failure is due to progressive CFRP debonding (Figure 5.6-d).

On the other hand, as mentioned earlier, the CFRP strips debond independently from each other because the FRP fibres in one strip cannot transfer forces to adjacent FRP strips in the FRP minor direction. Moreover, the FRP strips do not interfere with the RC beam's flexural

behavior. Therefore, the load-carrying capacity of the RC beam continues to increase even after local debonding has taken place in some FRP strips (Figure 5.4).

5.5.6   Effect of strip-width to strip-spacing ratio

To investigate the effect of the FRP strip-width to strip-spacing ratio, five beams strengthened in shear using CFRP strips in Series S0 were considered: S0-0.12R, S0-0.17R1, S0-0.20R1, S0-0.20R2, and S0-0.23R (see Table 5.1 for details). The only variable among the selected beams is the width-to-spacing ratio (FRP rigidity). As discussed earlier, various equations (Equations 5.2 to 5.5) have been proposed by researchers (Holzenkämpfer 1994, Brosens and Van Gemert 1999, Brosens 2001, Chen and Teng 2001) to express the effect of the strip-width to strip-spacing ratio based on direct pull-out test results for FRP bonded to concrete. The validity of the proposed equations for retrofitted beams is examined here using the results of RC beams strengthened in shear with different strip-width to strip-spacing ratios. The experimental V_f results ($V_{f exp}$) are compared with the calculated V_f results ($V_{f cal}$) as predicted by the ACI 440.2R-08 model. The ACI 440 model is selected as a reference model since it was proven to be one of the most accurate predictive models among current well-known design codes (Lima and Barros 2007). This holds true despite the fact that ACI 440 uses a bond model which is not correctly related to FRP stiffness (Chen and Teng 2001, Mofidi and Chaallal 2011-a). Therefore, predictions of the ACI 440.2R-08 model were multiplied to the k_f coefficients proposed by different researchers and compared in Figures 5.11 to 5.12. Figures 5.11 and 5.12 reveal that the coefficients proposed by Holzenkämpfer (1994) and Chen and Teng (2001) show a better correlation ($R^2 = 0.80$ and 0.84 respectively) with experimental results than those proposed by Brosens and Van Gemert (1999) and Brosens (2001) ($R^2 = 0.54$ and 0.50 respectively). However, it can be seen that the predicted V_f without considering the effect of the abovementioned coefficients achieves the best correlation ($R^2 = 0.89$) with the experimental results. This indicates that the abovementioned coefficients do not reflect the correct approach to characterization of the strip-width to strip-spacing ratio effect on RC beams strengthened in shear with FRP strips.

Figure 5.13 illustrates the trend of experimental values of coefficient k_f on the one hand, and on the other hand the values of k_f calculated using the coefficient equations proposed by researchers (Equations 5.2 to 5.5) versus the w_f/s_f ratio.
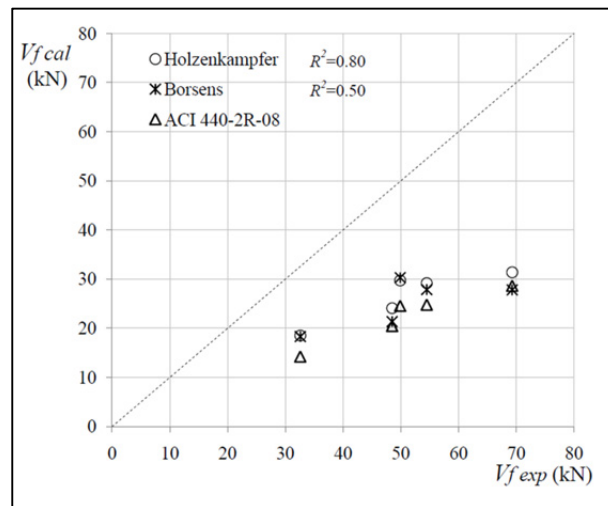
Figure 5.11   Predicted versus experimental FRP contribution: a) ACI 440 2R-08; b) ACI 440 2R-08 multiplied by Holzenkämfper (1994) coefficient; and c) ACI 440 2R-08 multiplied by Brosens (2001) coefficient.
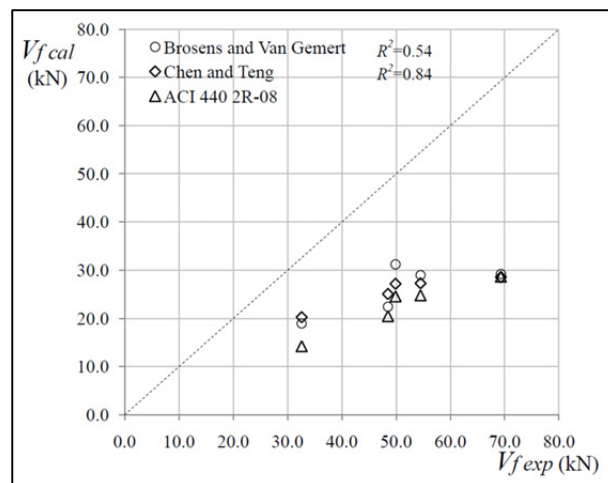
Figure 5.12: Predicted versus experimental FRP contribution: a) ACI 440 2R-08; b) ACI 440 2R-08 multiplied by Brosens and Van Gemert (1999) coefficient; and c) ACI 440 2R-08 multiplied by Chen and Teng (2001) coefficient.
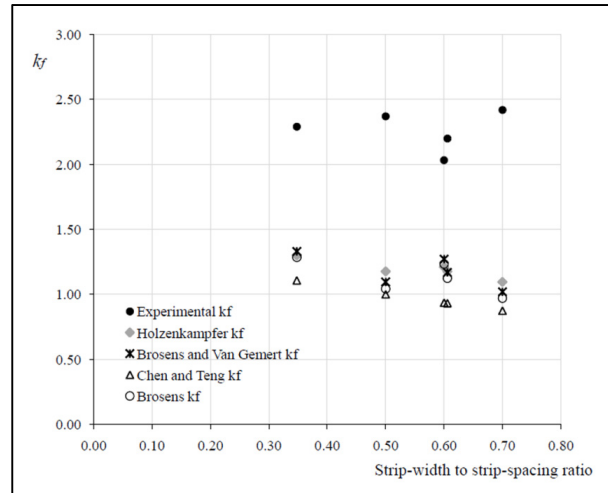
Figure 5.13 Experimental k_f ($V_{f\ exp}$ / $V_{f\ cal}$) of the test specimens and k_f proposed by Holzenkämfper (1994), Brosens and Van Gemert (1999), Brosens (2001), and Chen and Teng (2001) versus strip-width to strip-spacing ratio.

It is seen that, unlike the experimental values of k_f, the coefficients proposed by the researchers show a decreasing trend with increasing w_f / s_f ratio. This implies that the suggested coefficients, which are based on direct pull-out tests of FRP sheets bonded to concrete blocks, might not be valid for RC beams strengthened in shear with FRP strips. To investigate this phenomenon further by considering more experimental results, 42 RC beams strengthened in shear with U-jacket and side-bonded FRP strips were selected from the authors' database and their experimental k_f values plotted versus w_f / s_f ratio, as shown in Figure 5.14. In addition, the calculated k_f coefficients based on the equations proposed by the four researchers mentioned above are also shown in Figure 5.14. Unlike the calculated k_f values, the experimental k_f values from the database do not exhibit a clear decreasing trend as the w_f / s_f ratio increases. This result is in agreement with the experimental results presented in this paper (Figure 5.13). Regression of the test data, as plotted in Figure 5.14, shows that the w_f / s_f ratio is well correlated with k_f, as shown in the following equation:

$$k_f = \frac{1+(\dfrac{w_f}{s_f}-\dfrac{1}{2})^2}{1-(\dfrac{w_f}{s_f}-\dfrac{1}{2})^2} \tag{5.6}$$
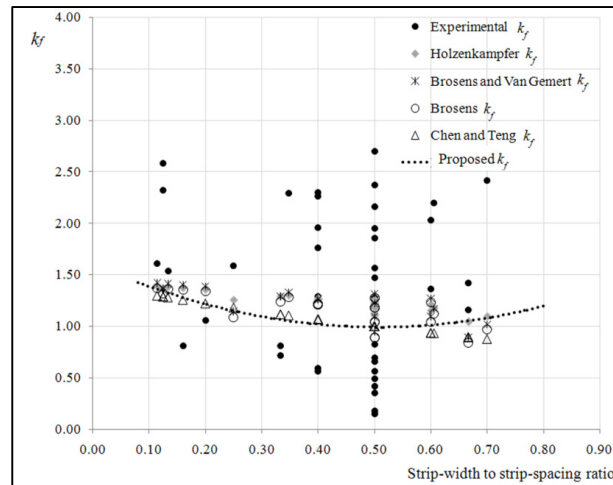
Figure 5.14   Experimental k_f ($V_{f\,exp}$ / $V_{f\,cal}$) from database and k_f proposed by Holzenkämfper (1994), Brosens and Van Gemert (1999), Brosens (2001), and Chen and Teng (2001) versus strip-width to strip-spacing ratio.

It should be mentioned that Figure 5.14 shows a wide range of experimental k_f for certain strip-width to strip-spacing ratios. This is attributed to the presence of few unacceptable experimental results in the database, where the available experimental data are extracted as reported in the original articles. The proposed k_f is applicable for all the beams (Rectangular and T-sections) strengthened with U-jacket or side-bonded EB FRP composites.

5.6   Comparison of test results with shear design equations

The contribution of CFRP to shear-resistance test results (see Table 5.1) is compared with the nominal shear resistance predicted by the guidelines (ACI 440.2R 2008 (based on Khalifa et al. 1998), *fib*-TG 9.3 2001 (based on Triantafillou 1998), CAN/CSA-S806 2002, HB 305 2008 (based on Chen and Teng 2003), and CNR-DT200 2004) and with predictions from a model proposed by the authors (see Mofidi and Chaallal 2011-a). To check the accuracy of each model in predicting the contribution of CFRP strips to the shear resistance of beams strengthened with CFRP strips, the results for beams strengthened with continuous CFRP sheet were excluded from this comparison.

Table 5.4, which presents the coefficients of determination (R^2) between the calculated $V_{f\,cal}$ for each of the models and the experimental $V_{f\,exp}$, clearly shows that the proposed model is superior to the design guidelines (without considering the new k_f: $R^2 = 0.67$, considering the new k_f: $R^2 = 0.78$). It also shows the lack of accuracy of the current guidelines in predicting the shear resistance due to FRP in presence of the transverse steel.

The low R^2 reported in Table 5.4 is mainly due to the fact that the guidelines fail to consider the effect of the transverse steel. In Series S1 (specimens with transverse steel), the test results showed that the shear resistance due to FRP is significantly reduced compared to corresponding specimens with no transverse steel, whereas the guidelines produce similar values for similar RC beams with and without transverse steel. For example, in specimen S0-0.23R, the shear resistance due to FRP is 69.3 kN, compared to 21.7 kN for specimen S1-0.23R. ACI-4402R-08 predicted a shear resistance of 28.6 kN for both specimens. Unlike the design guidelines, the model by Mofidi and Chaallal (2011-a) predicted V_f with a reasonable correlation for both Series S0 and S1 (Table 5.4).

Table 5.4   Coefficient of determination (R^2) between the calculated $V_{f\,cal}$ for each of the guidelines and the experimental values of $V_{f\,exp}$ (considering Series S0 and Series S1).

FRP design model	Year	R^2
Mofidi & Chaallal model	2010	0.67
CSA-S806	2002	0.21
ACI 440-2R	2008	0.20
fib-TG 9.3	2001	0.22
CNR-DT 200	2004	0.18
HB 305	2008	0.18

In order to consider the effect of strip-width to strip-spacing in the current guidelines in a more precise way, it was deemed useful to evaluate the effect of k_f (dimensionless

coefficient) on the values of $V_{f\,cal}$ calculated using the guidelines. The specimens in Series S1 (with transverse steel) were not considered for this evaluation, since the guidelines produce significantly more accurate results when the effect of transverse steel is not considered. To consider the effect of strip-width to strip-spacing, k_f was multiplied by $V_{f\,cal}$, which was calculated based on the ACI 440.2R 2008, *fib*-TG 9.3 2001, and CAN/CSA-S806 2002 codes (Table 5.5). For the HB 305 2008 and CNR-DT200 2004 guidelines, the k_f coefficients (Eq. 5.6) were substituted for the strip-width to strip-spacing ratio included in the models.

Table 5.5   Coefficient of determination (R^2) between the calculated V_f
$_{cal}$ for each of the guidelines and the experimental values
of $V_{f\,exp}$ (considering only Series S0, units are in kN).

	Specimen	S0-0.12R	S0-0.17R1	S0-0.20R1	S0-0.20R2	S0-0.23R	R^2
	$V_{f\,exp}$	39.7	53.3	54.5	49.9	69.3	-
Without considering the proposed k_f	CSA-S806	24.1	34.6	41.9	41.5	48.4	0.78
	ACI 440-2R	15.4	22.1	26.8	26.5	30.9	0.78
	fib-TG 9.3	25.8	30.3	32.9	32.8	35.1	0.76
	CNR-DT 200	13.1	17.9	21.7	21.8	24.16	0.72
	HB 305	25.0	32.5	36.7	36.4	39.8	0.75
Considering the proposed k_f	CSA-S806	25.2	34.6	42.9	42.4	52.5	0.83
	ACI 440-2R	16.1	22.1	27.3	27.0	33.5	0.83
	fib-TG 9.3	27.0	30.3	33.7	33.5	38.0	0.84
	CNR-DT 200	11.2	16.1	20.0	19.5	25.3	0.87
	HB 305	23.7	32.5	40.2	39.8	49.2	0.83

It is apparent that incorporating k_f into the current guidelines resulted in enhanced accuracy of the calculated results for all the guidelines mentioned (Table 5.5). It should be noted that incorporating the effect of k_f into the proposed model by Mofidi and Chaallal (2011-a) resulted in a significant level of accuracy in predicting the experimental V_f ($R^2 = 0.78$ when considering Series S0 and Series S1, $R^2 = 0.84$ when considering only Series S0). This shows

the relevance of the proposed equation for calculating the effect of the CFRP strip-width to strip-spacing ratio for beams strengthened in shear using CFRP strips.

The current design guidelines models produced a significantly low coefficient of determination. This is mainly due to the fact that the current design models fail to consider the effect of the transverse steel. As can be seen in Table 5.1, the presence of the transverse steel has a significant effect on the shear resistance of RC beams strengthened with FRP, and therefore, should ultimately be considered in the design models, as was recently proposed by the authors elsewhere (Mofidi and Chaallal 2011-a).

5.7   Conclusions

This paper presents the results of an experimental investigation involving fourteen tests on RC T-beams strengthened in shear with externally bonded CFRP strips and sheets. The parameters of the study are: (i) the effectiveness of the externally bonded CFRP strips compared to that of externally bonded CFRP sheets, (ii) the optimum strip-width to strip-spacing ratio for FRP (optimum FRP rigidity), (iii) the effect of FRP strip location with respect to transverse-steel location, (iv) the effect of FRP strip width, and (v) the effect of internal transverse-steel reinforcement on CFRP shear contribution. The main findings of this research are as follows:

- the maximum measured strain values with CFRP strips, and hence the gain in strength due to CFRP strips, are significantly greater than with CFRP continuous sheets. However, the maximum deflection is slightly greater for beams retrofitted with CFRP strips than for beams strengthened with continuous CFRP sheets;

- the addition of internal transverse steel resulted in a significant decrease in the gain due to FRP in the tested specimens. The maximum strains achieved in the CFRP were somewhat similar for the beams in Series S0 and S1. However, the contribution of FRP to shear resistance is significantly greater for beams with no transverse-steel

reinforcement (Series S0) than for beams with transverse-steel reinforcement (Series S1);

- given a strengthened beam and the CFRP strip-width to strip-spacing ratio, beams strengthened with wider CFRP strips achieved greater V_f values than beams with narrower strips;

- installing EB FRP strips mid-way between steel stirrups results in an increase in the maximum failure load as well as in the stiffness of the RC beam compared to installing FRP strips in the same location along the longitudinal axis as steel stirrups. Beams with CFRP strips installed in the same location along the longitudinal axis as steel stirrups exhibited more flexible behaviour than beams with CFRP strips installed mid-way between steel stirrups;

- the current equations proposed by Holzenkämpfer (1994), Brosens and Van Gemert (1999), Brosens (2001), and Chen and Teng (2001), which are based on tension tests, fail to predict the correct trend of variation of k_f versus w_f / s_f for $w_f / s_f > 0.5$, and therefore their applicability to RC beams strengthened in shear with EB FRP is questionable;

- a new coefficient, k_f, is proposed to address the effect of the strip-width to strip-spacing ratio on beams strengthened in shear with CFRP strips. Incorporating k_f into the equations of other models resulted in a better correlation of experimental results with the design equations of all guidelines.

Finally, comparison of shear resistance values as predicted by the ACI 440.2R (2008), *fib*-TG 9.3 (2001), CAN/CSA-S806 (2002), HB 305 (2008), and CNR-DT200 (2004) guidelines with test results has indicated that the guidelines fail to capture the influence of the parameters under study. The model proposed by Mofidi and Chaallal (2011-a) showed the best correlation with experimental results compared with the current guidelines. Incorporating k_f into the current guidelines resulted in an increase in the accuracy of the predicted values for all the guidelines mentioned. In addition, introducing k_f into the

proposed model resulted in enhanced accuracy ($R^2 = 0.84$) in predicting the experimental values of V_f. The current design guidelines models produced a significantly low coefficient of determination. This is mainly due to the fact that the current design models fail to consider the effect of the transverse steel. The presence of the transverse steel has a significant effect on the shear resistance of RC beams strengthened with FRP, and therefore, should ultimately be considered in the design models, as was recently proposed by the authors elsewhere (Mofidi and Chaallal 2011-a).

5.7   References

American Concrete Institute (ACI) (2008). *Guide for the Design and Construction of Externally Bonded FRP Systems for Strengthening Concrete Structures.* Report No. 440 2R-08, Farmington Hills MI.

Bizindavyi, L. and Neale, K. W., (1999). Transfer lengths and bond strengths for composites bonded to concrete. *J. Compos. Constr.* 3(4), pp. 153–160.

Bousselham, A. and Chaallal, O. (2004). Shear strengthening reinforced concrete beams with fiber-reinforced polymer: assessment of influencing parameters and required research. *ACI Struct. J.* 101(2), pp. 219–227.

Bousselham, A. and Chaallal, O. (2006). Behavior of reinforced concrete T-beams strengthened in shear with carbon fiber-reinforced polymer—An experimental study. *ACI Struct. J.* 103(3), pp. 339–347.

Brosens, K. and Van Gemert, D. (1999). Anchorage Design for Externally Bonded Carbon Fiber

Polymer Laminates, *Proc. of the 4th Int. Symp. on Fiber Reinforced Polymer Reinforcement for Concrete Structures*, Baltimore, USA, pp. 635–645.

Brosens, K. (2001). Anchorage of Externally Bonded Steel Plates and CFRP Laminates for the Strengthening of Concrete Elements. PhD Dissertation, Department of Civil Engineering, Katholieke Universiteit Leuven.

CAN/CSA-S6-06 (2006). *Canadian Highway Bridge Design Code.* Canadian Standards Association, Mississauga, Canada.

CAN/CSA-S806-02 (2002). *Design and construction of building components with fiber-reinforced polymer.* Canadian Standards Association, Rexdale, Canada.

Chen, J.F. and Teng, J.G., (2001). Anchorage strength models for FRP and steel plates bonded to concrete. *J. Struct. Eng.* 127(7), pp. 784–791.

Chen, J.F. and Teng, J.G. (2003). Shear capacity of FRP strengthened RC beams: FRP debonding. *Const. and Building Materials*, 17(1), pp. 27-41.

Chaallal, O., Shahawy, M. and Hassan, M. (2002). Performance of reinforced concrete T-girders strengthened in shear with CFRP fabrics. *ACI Struct. J.* 99(3), pp. 335–343.

CNR-DT200 (2004). *Guidelines for Design, Execution, and Control of Strengthening Interventions by means of Fiber-Reinforced Composites.* National Research Council, Italy.

fib-TG 9.3 (2001). *Externally Bonded FRP Reinforcement for RC Structures.* International Federation for Structural Concrete, Lausanne, Switzerland.

Holzenkämpfer, O. (1994). *Ingenieurmodelle des Verbundes Geklebter Bewehrung für Betonbauteile.* Dissertation, TU Braunschweig, Germany.

Kamel, A.S., Elwi, A.E. and Cheng, J.J.R. (2000). Experimental study of the behavior of CFRP sheets bonded to concrete. *Proc., 3rd Int. Conf. on Advanced Composite Materials for Bridges and Structures*, Canadian Society for Civil Engineering, Ottawa, pp. 61–68.

Khalifa, A., Gold, W.J., Nanni, A., and Aziz, A. (1998). Contribution of externally bonded FRP to shear capacity of RC flexural members. *J. Compos. Constr.* 2(4), pp. 195–203.

Khalifa, A. and Nanni, A. (2000). Improving shear capacity of existing RC T-section beams using CFRP composites. *Cem. Concr. Compos.* 22, pp. 165–174.

Khalifa, A. and Nanni, A. (2002). Rehabilitation of rectangular simply supported RC beams with shear deficiencies using CFRP composites. *Constr. and Building Materials.* 16, pp. 135–146.

Lima, J.L.T. and Barros, J.A.O. (2007). Design models for shear strengthening of reinforced concrete beams with externally bonded FRP composites: A statistical versus reliability approach. *Proc. 8th Int. Symp. on Fiber Reinforced Polymer Reinforcement for Concrete Structures*, Patras, Greece.

Mofidi, A. and Chaallal, O. (2011). Shear Strengthening of RC Beams with Epoxy Bonded FRP—Influencing Factors and Conceptual Debonding Model. *ASCE, J. of Composites for Construction.* 15(1), pp. 62-74.

Neubauer, U. and Rostásy, F.S. (1997). *Design Aspects of Concrete Structures Strengthened with Externally Bonded CFRP Plates.* ECS Publications, Edinburgh, pp. 109–118.

Oehlers, D.J., Seracino, R. and Smith, S.T. (2008) *Design Guideline for RC Structures Retrofitted with FRP and Metal Plates: Beams and Slabs*, HB 305-2008, Standards Australia, Sydney, Australia, ISBN 0 7337 7831 3, 73 pp.

Pellegrino, C. and Modena, C. (2002). Fiber reinforced polymer shear strengthening of RC beams with transverse steel reinforcement. *J. Compos. Constr.* 6(2), pp. 104–111.

Pellegrino C. and Modena C. (2006). FRP shear strengthening of RC beams: experimental study and analytical modeling. *ACI Struct. J.* 103(5), pp. 720-728.

Triantafillou, T.C. (1998). Shear strengthening of reinforced concrete beams using epoxy-bonded FRP composites. *ACI Struct. J.* 95(2), pp. 107–115.

Zhang, Z., Hsu, C.-T. and Moren, J. (2004). Shear strengthening of reinforced concrete deep beams using carbon fiber reinforced polymer laminates. *J. Compos. Constr* 8(5), pp. 403–414.

CHAPTER 6

PERFORMANCE OF END-ANCHORAGE SYSTEMS FOR RC BEAMS STRENGTHENED IN SHEAR WITH EPOXY-BONDED FRP

Amir Mofidi and Omar Chaallal

Department of Construction Engineering, École de Technologie Supérieure 1100 Notre-Dame Ouest, Montréal, Québec, Canada H3C 1K3

6.1   **Abstract**

This paper presents the results of an experimental investigation on the performance of full-scale reinforced concrete (RC) T-girders strengthened in shear using externally bonded FRP (EB FRP) U-jackets end-anchored with different systems. Debonding of FRP, particularly in shear, is a major failure mode when using FRP sheets to strengthen concrete structures. Design code provisions and guidelines related to shear strengthening of RC beams using EB FRP suggest the use of end-anchorage systems to prevent FRP debonding. However, no guidelines are available for the design and effectiveness of end-anchorage systems. The main objective of this study is to evaluate the effectiveness of different end-anchorage systems for RC beams strengthened using EB FRP methods. To this end, nine tests were performed on 4520-mm-long RC T-beams. Four specimens were strengthened in shear using EB FRP methods with various end-anchorage systems, and their performance was compared with similar specimens strengthened with: (i) EB FRP with no anchorage; (ii) near-surface-mounted (NSM) FRP rods; and (iii) embedded through-section (ETS) FRP rods. The results of this study reveal that specimens retrofitted with EB FRP methods and properly designed

end-anchorage systems can achieve a superior contribution to shear resistance compared with specimens strengthened using EB FRP with no anchorage, NSM, or ETS methods.

6.1　　　Introduction

Externally bonded (EB) fibre-reinforced polymer (FRP) is increasingly used to strengthen existing reinforced concrete (RC) structures. International recognition and widespread application of this method in recent years are mainly the result of extensive and valuable research efforts implemented in recent years (e.g., Sato et al. 1997; Khalifa & Nanni 2000 and Bousselham & Chaallal 2008). However, debonding of FRP sheet or laminate has been a major issue for concrete structures strengthened in shear using EB FRP methods (Mofidi and Chaallal 2011-a). For RC beams strengthened in shear with EB FRP, failure by debonding of FRP is generally a brittle type of failure. Therefore, for such beams, debonding is considered to be an undesirable failure mode which should be avoided. Debonding of FRP sheets or laminates is generally caused by concrete-cover delamination due to the low tensile strength of the concrete, which limits the bonding force between the FRP and the concrete (Chaallal et al. 2011). When the bond length of the FRP sheet or laminate is limited because of the RC beam's geometry, an end-anchorage can be used to achieve the full design capacity of the FRP sheet (Eshwar et al. 2008). The European *fib* TG9.3 (2001) code recommends that FRP transverse reinforcement be attached to the compressive zone of the RC member by means of end-anchorage systems when full FRP wrap is not feasible. Without giving further details, ACI 440.2R-08 recommends using mechanical anchorages at the termination points of the FRP transverse reinforcement to develop larger tensile forces.

Different anchorage systems have been investigated for shear strengthening of RC beams using EB FRP methods. Sato et al. (1997) used steel plates and mechanical anchors to increase the shear capacity of RC members strengthened using EB FRP methods through different anchorage systems. Khalifa and Nanni (2000) investigated a form of bonded anchored U-jacketing FRP application. The anchor consisted of a bent portion of the end of the FRP reinforcement embedded into a preformed groove in concrete. Meanwhile, *fib* TG9.3

(2001) recommends anchorage for shear strengthening of RC beams with FRP strips using simple mechanical anchors or by bonding the ends of the strips into core holes through the flange of a T-beam. Schuman (2004) used a GFRP/steel anchorage system in an FRP-concrete double-shear bond test series. Mofidi (2008) successfully explored the possibility of using an unbonded CFRP U-jacket anchorage system to strengthen RC T-beams in shear. In this method, dry CFRP sheets were wrapped around and bonded to two steel rods. The steel rods were anchored to the corners of the web-flange intersection of the T-beam with mechanical bolts. Eshwar et al. (2008) investigated the performance of spike anchors and near-surface mounted (NSM) end-anchorage systems in a series of FRP-concrete shear bond tests. A spike anchor consists of a bundle of carbon or glass fibres. One end of the fibers takes the form of a fan which is sandwiched between the two FRP sheets to be anchored. The other end of the bundle is fully bonded and inserted into a hole through the RC beam. In a research study by Eshwar et al. (2008), many of the spike anchors failed prematurely and did not add to the FRP-concrete bond resistance. The NSM end-anchorage system used by Eshwar et al. (2008) was similar to one proposed by Khalifa and Nanni (2000) and had been successfully tested in FRP-concrete shear bond tests. Ceroni et al. (2008) compared the effectiveness of different anchorage systems in a series of double-tension tests on CFRP sheets epoxy-bonded to T-shaped concrete specimens. Among the different anchorage systems considered in their research study, EB FRP laminates, EB steel plates, and NSM FRP end-anchorage systems showed superior performance. Based on the research studies described above and on recommendations from various guidelines, the use of end-anchorage systems for shear strengthening of RC beams using EB FRP methods can result in a greater FRP contribution to shear resistance. Several end-anchorage systems have been proposed by researchers, but their effectiveness has not yet been well documented. In addition, few experimental research studies comparing different anchorage systems under similar test conditions exist in the literature (Ceroni et al. 2008).

In this research study, results of four end-anchorage systems for RC beams strengthened in shear using EB FRP methods are presented. The results for specimens strengthened with different end-anchored EB FRP sheets are compared with those for specimens strengthened using other effective shear-strengthening techniques such as NSM (De Lorenzis and Nanni

2001; Barros and Dias 2005) and embedded through-section (ETS) methods (Chaallal et al. 2011).

6.2 Test program

The RC beam specimens were tested in three-point load flexure. Overall, the experimental program (Table 6.1) involved nine tests performed on full-scale RC T-beams. The control specimen, not strengthened with carbon FRP (CFRP), is labelled CON, whereas the specimens retrofitted with a layer of EB CFRP sheet are labelled EB. The specimens strengthened with U-jacketed EB CFRP sheets are labelled as follows: NA for specimens strengthened with a CFRP U-jacket with no end-anchorage; SBFA for specimens strengthened with a CFRP U-jacket with a surface-bonded flat CFRP bar end-anchorage; DAMA for specimens strengthened with a CFRP U-jacket with a double-aluminum-plate mechanical anchorage; ERBA for specimens strengthened with a CFRP U-jacket with an embedded round CFRP bar end-anchorage; and EFLA for specimens strengthened with a CFRP U-jacket with an embedded flat CFRP laminate end-anchorage. Moreover, specimens strengthened with NSM FRP rods are labelled NSM, and specimens strengthened using the ETS FRP method are labelled ETS.

Table 6.1   Experimental results.

Specimen	Load at rupture	Total shear resistance	Resistance due to concrete	Resistance due to steel	Resistance due to CFRP	Gain due to CFRP	Deflection at load point	Failure mode
	kN	kN	kN	kN	kN	%	mm	
S0-CON	122.7	81.3	81.3	0.0	0.0	0	2.6	Shear
S3-CON	294.0	194.7	94.4	100.3	0.0	0	11.2	Shear
S3-EB-NA	367.3	243.2	94.4	100.3	48.5	25	14.4	Shear
S3-EB-SBFA	381.6	252.7	94.4	100.3	58.0	30	12.2	Shear
S3-EB-DAMA	421.6	279.2	94.4	100.3	84.5	43	17.6	Flexure
S3-EB-ERBA	417.0	276.2	94.4	100.3	81.5	42	18.2	Shear
S3-EB-EFLA	431.4	285.7	94.4	100.3	91.0	48	21.3	Flexure
S3-NSM	381.0	252.3	94.4	100.3	57.6	30	11.7	Shear
S3-ETS	425.5	281.8	94.4	100.3	87.1	45	15.2	Shear

All the beams tested in this study are labelled S3 except for the S0-CON beam, which has no transverse steel reinforcement. All the specimens in the S3 series have internal transverse steel stirrups spaced at $s = 260$ mm ($\approx 3d/4$), where $d = 350$ mm and represents the effective depth of the cross-section of the beam (Figure 6.1). Thus, for instance, specimen S3-EB-EFLA features a beam with internal steel stirrups spaced at $s = 260$ mm, which has been retrofitted with an EB CFRP U-jacket with an embedded flat CFRP laminate end-anchorage. The labels used for the specimens are provided in Table 6.1.

6.2.1   Description of specimens

The cross-section and dimensions of each specimen are shown in Figure 6.1. A 4520-mm-long T-beam with a web width of 152 mm and a flange depth of 102 mm was chosen for study. The top flange width of the beam is 508 mm, and the total depth of the beam's cross-section is 406 mm. The longitudinal steel reinforcement consists of four 25M bars (diameter 25.2 mm, area 500 mm^2) laid in two layers at the bottom and six 10M bars (diameter 10.3 mm, area 100 mm^2) laid in one layer at the top (Figure 6.1). The internal steel stirrups are 8 mm in diameter (area 50 mm^2 per leg). The specimens are chamfered at the outer soffit corners to ease the high stress concentrations in the CFRP at those sharply pointed locations. Details of the specimens are provided in Table 6.1.

The following parameters are studied in this investigation:

- effectiveness of end-anchorage systems for beams strengthened in shear with EB FRP. This is measured by comparing results for RC beams strengthened with one layer of EB CFRP U-jacket. The results for strengthened beams with EB U-jackets that use end-anchorage systems (i.e., S3-EB-SBFA, S3-EB-DAMA, S3-EB-ERBA and S3-EB-EFLA), are compared with those of the strengthened beam with EB U-jacket but with no end-anchorage system (i.e., S3-EB-NA);

- efficiency of strengthening methods. This is measured by comparing results for beams strengthened with anchored and unanchored EB U-jackets with those for beams strengthened using NSM and ETS methods.
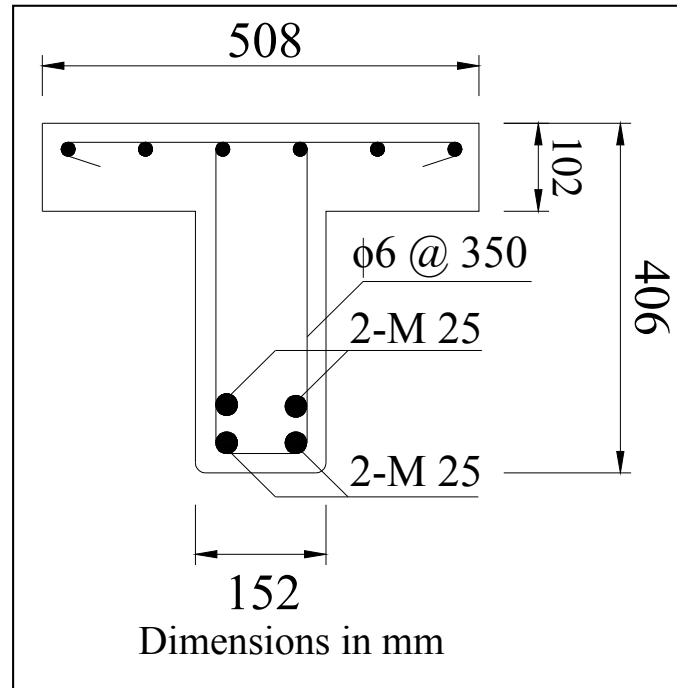
Figure 6.1: Cross section of RC T-beams used in the research study.

6.2.2 Materials

The internal flexural and shear-steel reinforcements have a nominal yield strength of 650 MPa. A commercially available concrete was used in this project and was delivered to the laboratory by a local supplier. The 28-day concrete compressive strength for 152-mm diameter by 305-mm long concrete cylinders achieved an average value of 29.6 MPa. This is close to the average concrete compressive strength of 33.7 MPa reached the day the testing of the RC beams was performed. The scatter of the compression test results was negligible. A lower concrete compressive strength, 25.0 MPa, was obtained only for the S0-CON specimen, which was made from a different concrete batch.

The CFRP sheet used for the EB specimens was a unidirectional carbon-fibre sheet which was applied continuously over the test zone in a U-shaped envelope around the web. The CFRP sheet (SikaWrap Hex 230C) was then epoxy-bonded to the beam surface with a two-component adhesive made of a resin and a hardener, both of which are engineered primarily for structural applications and were supplied by the manufacturer. CFRP rods with a nominal diameter of 9.5 mm (area: 71 mm^2) and 12.7 mm (area: 127 mm^2) were used for the NSM and ETS strengthening methods respectively. The tensile strength and modulus of elasticity of the CFRP rods were 1870 MPa and 143.9 GPa respectively. The mechanical properties of the epoxy paste used for embedding the rods, as specified by the manufacturer, were: 21 MPa bond strength, 1% elongation at breakage, 75 MPa compressive strength, and 3656 MPa compressive modulus. The mechanical and elastic characteristics of the CFRP round and flat bars (Sika) and the aluminum plates used for different end-anchorage systems are provided in Table 6.2, as are those of the other CFRP fabrics and rods used in this research study. An epoxy paste similar to that used to bond the CFRP bars in the NSM and ETS methods was used for the end-anchorage systems of the beams strengthened using the EB method.

Table 6.2   Mechanical properties of CFRP sheets, laminates, and rods.

Property	Dry fibre sheet	CFRP laminate	9.5-mm diameter CFRP rod
Modulus of elasticity, GPa	231	165	155
Ultimate elongation, %	1.40	1.69	1.80
Ultimate stress, MPa	3650	3100	2800

6.2.3   Test setup and procedure

All beams were tested in three-point load flexure. The load was applied at a distance $a = 3d$ from the nearest support (shear span equal to 1050 mm), which corresponds to a slender beam test. An extensive and carefully detailed measuring device was chosen for the project. Using a linear variable differential transformer (LVDT), the vertical displacement was measured at the position under the applied load and at the mid-span. Horizontal LVDTs were also installed at each side of the supports to capture any undesirable sway or tilt effects.

Strain gauges were glued onto the transverse and longitudinal steel reinforcements, and CFRP rods to measure their respective deformations at different loading phases. Displacement sensors, known as crack gauges, were used to measure the deformations experienced by the CFRP U-jacket. These gauges were installed vertically onto the web of RC beams at the same positions along the longitudinal axis as the strain gauges on the internal transverse steel. This ensured that the transverse steel and CFRP responses could be compared at the same positions during the different phases of loading. All tests were conducted under displacement control conditions at a rate of 2 mm/minute.

6.2.4   Strengthening systems

The following steps were taken to implement the EB strengthening system with no end-anchorage: (1) the area of the specimen where the continuous CFRP sheet was to be glued was sand-blasted to remove any surface cement paste and to round off the beam edges; (2) the bond area was ground to remove any possible irregularities and to achieve a desirable smooth bond surface; (3) residues were removed using compressed air; and (4) a layer of U-shaped continuous CFRP sheet was glued to the bottom and lateral faces of the RC beam using a two-component epoxy resin.

To apply the SBFA end-anchorage system for beams strengthened using the EB method, the following two steps were carried out in addition to the four steps implemented as described above: (1) a thin layer of epoxy paste was applied continuously to the two ends of the CFRP U-jacket; and (2) a CFRP laminate with a cross-section of 20 mm × 2.5 mm was epoxy-bonded to the two ends of the CFRP U-jacket along the shear span (Figure 6.2).

To implement the DAMA end-anchorage system for beams strengthened using the EB method, the following steps were carried out: (1) 12-mm-diameter horizontal holes spaced at 175 mm were drilled perpendicular to the RC beam's web surface. The centre line of the holes was 55 mm below the bottom of the flange; (2) a thin layer of epoxy paste was applied around 10-mm-diameter, 60-mm-long, threaded steel rods; (3) the 10-mm-diameter stainless-
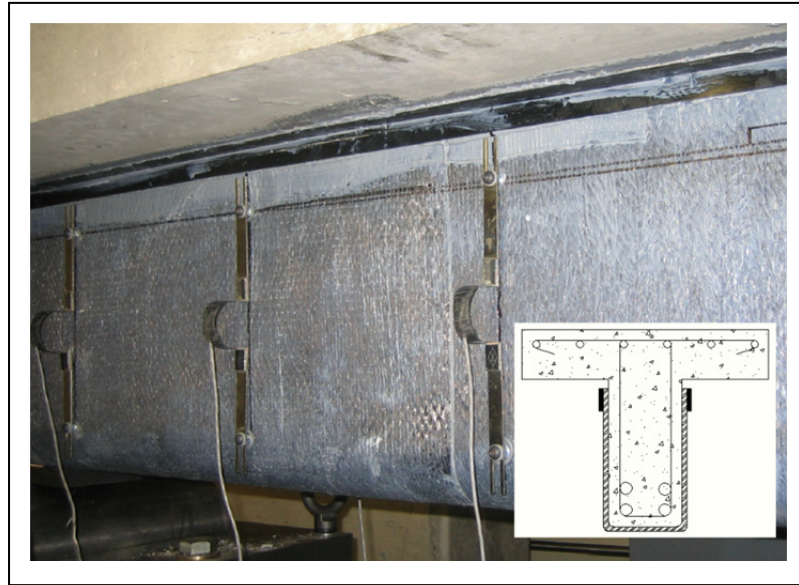
Figure 6.2   Elevation of specimen S3-EB-SBFA with surface
bonded CFRP laminate end-anchorage system

steel threaded rods were installed into the holes; (4) a CFRP U-jacket was epoxy-bonded to
the RC beam's shear span in the same way as previously described for the specimen with no
end-anchorage; (5) a layer of epoxy paste was applied continuously to the two ends of the

(a)   (b)

Figure 6.3   Elevation of specimen S3-EB-DAMA; a) first aluminum
plate installed; and b) second aluminum plate installed

CFRP U-jacket; (6) a 3/8-in.-thick aluminum plate with matching pre-drilled holes and embedded threaded stainless-steel rods was bonded onto the two ends of the CFRP U-jacket along the shear span; (7) the free ends of the CFRP sheet were wrapped around the aluminum plate (Figure 6.3-a); and (8) a similar aluminum plate was installed on top of the free ends of the CFRP sheet, and the two aluminum plates were tightened to each other using stainless-steel nuts on the embedded threaded steel mechanical anchor (Figure 6.3-b).

To install the ERBA end-anchorage system for beams strengthened using the EB method, the following procedures were carried out: (1) grooves 15 mm in width and 15 mm in depth were made along the shear span in the beam's flange at the flange-web intersection; (2) the beam was then prepared in the same way as previously described for the specimen with no end-anchorage; (3) a thin layer of epoxy paste was applied along the grooves; (4) the free ends of the CFRP sheets bonded to the beam's web were bonded around the groove's surface; (5) the grooves were filled up to two-thirds of their volume with the epoxy paste; (6) 9.5-mm CFRP rods were installed into the grooves in both sides of the beam's flange; and (7) the excess epoxy paste was removed (Figure 6.4).
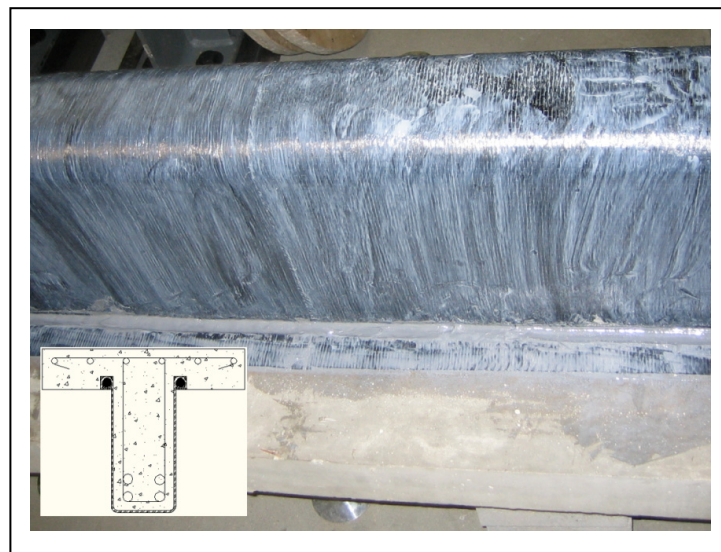
Figure 6.4   Specimen S3-EB-ERBA after the embedded round FRP
bar end-anchorage system is installed.

To implement the EFLA end-anchorage system for beams strengthened using the EB method, the following steps were carried out: (1) grooves 5 mm in width and 22 mm in depth

were made along the shear span in the beam's flange at the flange-web junction; (2) the beam was then prepared in the same way as previously described for the specimen with no end-anchorage; (3) a thin layer of epoxy paste was applied along the grooves; (4) the free ends of the CFRP sheets bonded to the beam's web were installed inside the grooves using a 20 mm × 2.5 mm CFRP laminate (the CFRP sheet ends were wrapped around the CFRP laminate); and (5) the grooves were filled with epoxy paste (Figure 6.5). For each of the end-anchorage systems mentioned above, the CFRP sheet must be cut to an exact length.
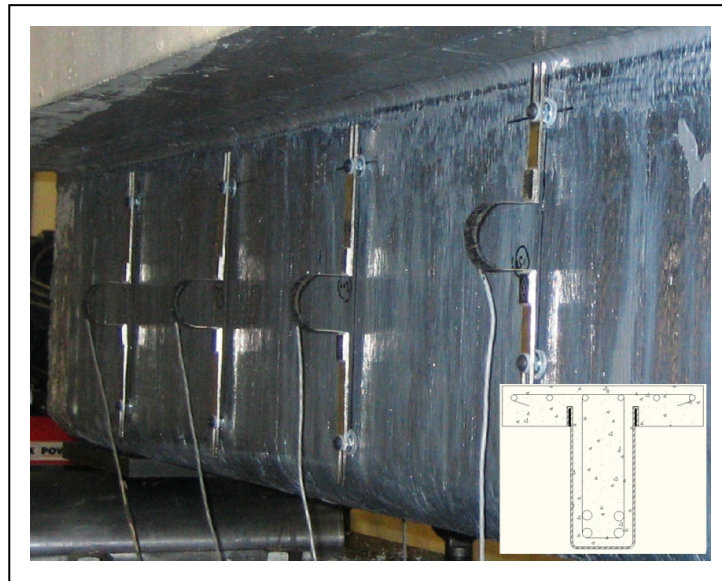
Figure 6.5   Specimen S3-EB-EFLA after the embedded
FRP laminate is installed.

6.3   Presentation of results

6.3.1   Overall response

Table 6.1 summarizes the experimental test results for all the specimens. The results are presented in terms of the loads attained at failure; the experimental shear resistance due to concrete, transverse steel, and CFRP; and the shear capacity gain due to CFRP. The shear contributions of concrete and steel were calculated based on the results obtained from the

unstrengthened specimens, i.e., S0-CON and S3-CON. Some of the values provided in Table 6.1 were derived on the basis of the following assumptions which are implicitly mentioned in the guidelines: a) for both strengthened and unstrengthened beams, with and without transverse steel, it is assumed that the shear resistance due to concrete is constant, implying that the presence of the transverse steel does not affect the contribution of concrete to the shear resistance. However, the shear contribution of concrete is calculated separately for different concrete strengths on the basis of results achieved by the control beams; and b) for both strengthened and unstrengthened beams, the contribution of the transverse steel is assumed to be constant.

The results show that the shear capacity gain due to CFRP for the EB-strengthened specimen with no end-anchorage was 25%, compared to 41% on average for the four specimens strengthened with end-anchored EB. The shear capacity gain due to CFRP for the specimens strengthened using the NSM and ETS methods was 30% and 45% respectively. This clearly confirms the effectiveness of the end-anchorage systems proposed in this research study for RC beams strengthened using the EB method.

For beams strengthened using EB FRP end-anchorage systems, the embedded CFRP laminate end-anchorage system (EFLA) and the double-aluminum-plate mechanical end-anchorage system (DAMA) showed the highest shear-capacity gain compared to the other two anchorage systems. Specimens S3-EB-EFLA and S3-EB-DAMA reached a 48% and 43% gain respectively, whereas specimens S3-EB-ERBA and S3-EB-SBFA reached 42% and 30% shear capacity gain respectively under corresponding conditions.

6.3.2   Failure mode

All the tested specimens failed in shear except for specimens S3-EB-DAMA and S3-EB-EFLA, which failed in flexure (Table 6.1). For the specimens with transverse steel, shear failure occurred after the transverse steel intersecting the shear crack had yielded. Similar results have been observed by the authors in more than 30 RC beams strengthened with

CFRP sheets in previous research studies (e.g., Bousselham and Chaallal 2008, Mofidi and Chaallal 2011-a, Mofidi and Chaallal 2011-b, Chaallal et al. 2011). These results contradict the outcomes of certain recent finite-element model studies which concluded that for RC beams strengthened in shear with FRP, the internal steel stirrups do not reach the yield point and therefore cannot be fully used. Some researchers (e.g., Chen et al. 2010) believe that by strengthening RC beams with EB FRP, the transverse steel does not reach its yield strength at failure. Therefore, shear contribution of transverse steel to the shear resistance decreases in strengthened beams compared to the control beam. In this research study, it has been shown experimentally that the transverse steel reaches its yield strength at failure which is in agreement with the assumption made in the present article.

During loading of specimen S0-CON, diagonal shear cracks formed at a load of 77.6 kN. A crack initiated at the support and progressed rapidly towards the compression zone until failure.

In beam S3-CON strengthened with transverse steel, diagonal shear cracks formed at a load (78.6 kN) similar to the load at which the shear crack appeared in S0-CON. The cracking in the S3-CON specimen was fairly widespread and propagated at a greater angle than that in the S0-CON specimen.

Beam S3-EB-NA had transverse steel similar to S3-CON, but was externally strengthened with an EB CFRP U-jacket with no end-anchorage. In specimen S3-EB-NA, failure was initiated by debonding of the CFRP sheets (with a layer of concrete adhered to them) over the main shear crack, which occurred at the same location as in the control beam, S0-CON (Figure 6.6-a). The CFRP debonding was followed by shear compression failure.

In specimen S3-EB-SBFA, a popping noise throughout the test revealed the progressive cracking of the epoxy adhesive into which the CFRP flat bars were bonded. Failure eventually occurred due to debonding of the CFRP sheet following end-anchorage failure (Figure 6.6-b). In specimen S3-EB-DAMA, no signs of debonding, delamination, fracture of the CFRP sheet, or failure of the anchorage were observed. Moreover, there were no signs of local CFRP sheet fracture due to stress concentration at the corners of the aluminum plates.
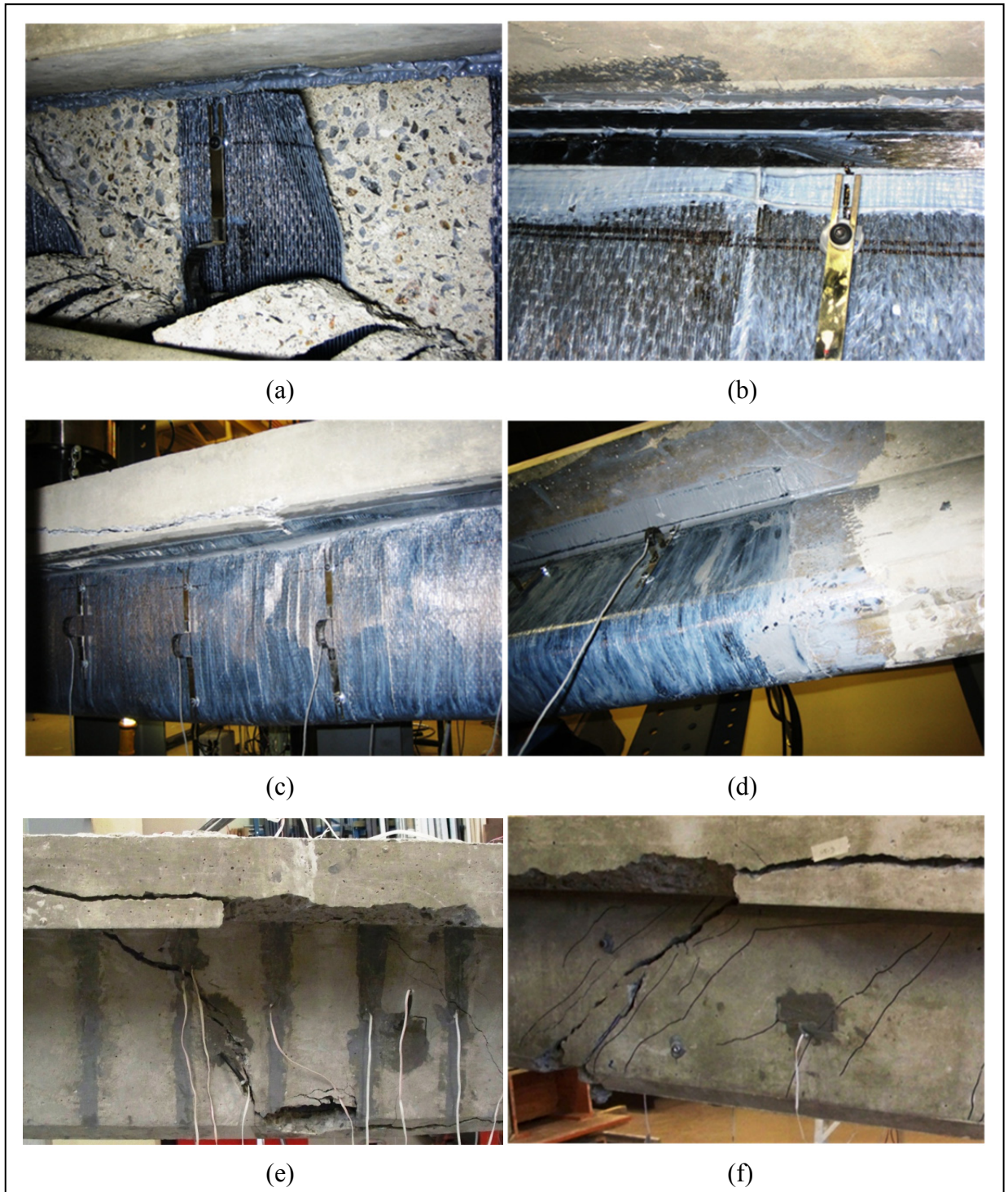
Figure 6.6   Strengthened specimens after failure: a) S3-EB-NA; b) S3-EB-SDMA; c) S3-EB-ERBA; d) S3-EB-EFLA; e) S3-NSM; and f) S3-EST.

Failure eventually occurred when the beam reached its maximum flexural capacity. In specimen S3-EB-ERBA, no end-anchorage failure was observed. Failure eventually occurred due to shear diagonal tension failure (Figure 6.6-c). At the moment of ultimate failure, local CFRP delamination occurred at the centre of the beam's web. Specimen S3-EB-EFLA achieved the maximum shear resistance of all the specimens tested in this research study. Similarly to S3-EB-DAMA, specimen S3-EB-EFLA exhibited no signs of debonding, delamination, fracture of the CFRP sheet, or failure of the anchorage. It should be emphasized that there were no signs of local CFRP sheet fracture due to stress concentration at the corners of the CFRP laminate in the anchorage system. Failure eventually occurred when the beam reached its maximum flexural capacity (Figure 6.6-d). In beam S3-NSM failure was eventually triggered by splitting of the concrete cover, which resulted in shear diagonal tension failure of the beam (Figure 6.6-e). In beam S3-ETS, shear diagonal tension failure occurred following yielding of the longitudinal steel (Figure 6.6-f).

6.3.3   Deflection response

Figure 6.7-a shows the load versus maximum deflection curves for beams strengthened using the EB method (with and without end-anchorage systems) and for the control beams. The figure shows the total applied load versus deflection under a point load for the two control beams as well as for the five beams strengthened using the EB method with different end-anchorage systems.

Figure 6.7-a reveals that the S3-EB-SBFA and S3-EB-DAMA specimens exhibited a greater overall stiffness than the other beams. The greater overall stiffness of specimens S3-EB-SBFA and S3-EB-DAMA could be attributed to the effect of bonded longitudinal rectangular CFRP and aluminum bars, respectively. Specimens S3-EB-DAMA and S3-EB-EFLA failed in a more ductile manner at their flexural capacity limits (Figures 6.7-a and 6.7-b) than the other strengthened and unstrengthened specimens. The maximum load at failure and the maximum deflection attained at the loading point for each specimen are provided in Table 6.1. Meanwhile, the S3-EB-DAMA, S3-EB-ERBA, and S3-EB-EFLA specimens exhibited a

higher deflection at the loading point and a higher maximum load at failure than the other strengthened and unstrengthened specimens (Table 6.1). The end-anchorage systems greatly enhanced the overall behaviour of the RC beams strengthened using the EB method because they resulted in a higher load at failure and a greater maximum deflection than for the corresponding beam without an end-anchorage system (Figures 6.7-a and 7-b).
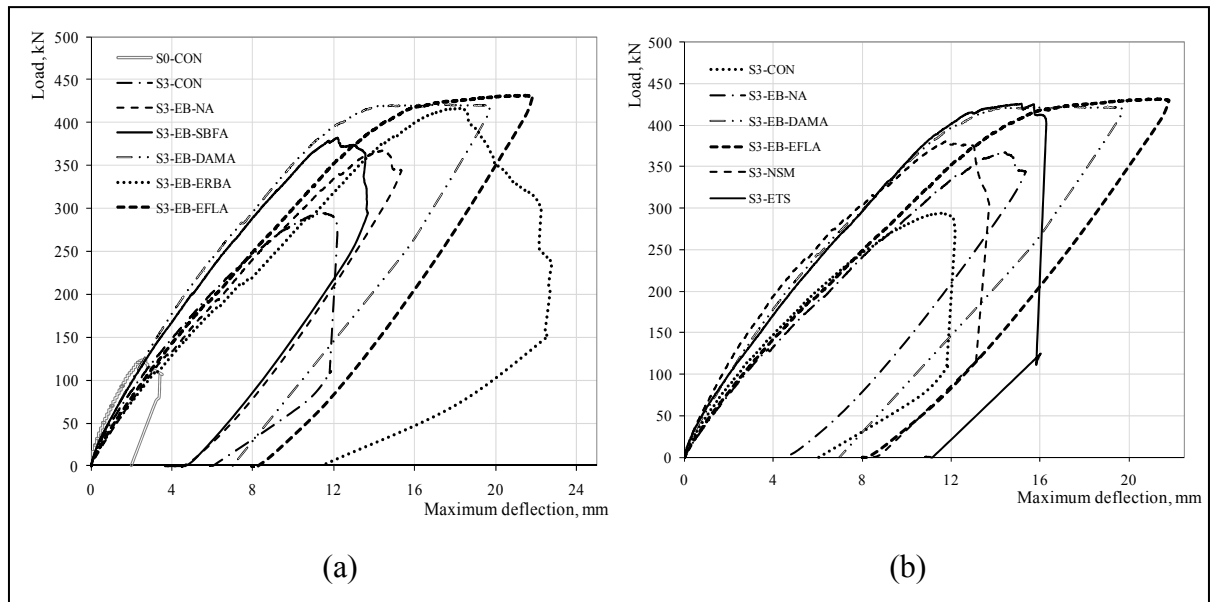
Figure 6.7 Load versus maximum deflection: a) beams strengthened with EB method (with and without end-anchorage systems and the control beams; and b) beams strengthened with EB, NSM and ETS methods.

Figure 6.7-b compares the deflection response for beams strengthened using the EB method (with and without end-anchorage systems) and beams strengthened using the NSM and ETS methods. Among the beams strengthened using the anchored EB FRP method only, beams S3-EB-DAMA and S3-EB-EFLA were considered. Figure 6.7-b shows that the S3-EB-DAMA, S3-NSM, and S3-ETS specimens exhibited a greater overall stiffness than the other beams illustrated in Figure 6.7-b. Specimens S3-EB-DAMA and S3-EB-EFLA exhibited a higher deflection at the loading point and a higher maximum load at failure than the other specimens (Figure 6.7-b). The beams strengthened with end-anchorage systems exhibited a more ductile behaviour than beams strengthened with other effective shear-strengthening methods using FRP, such as the NSM and ETS methods.

For example, the deflection under point load of beam S3-EB-EFLA at its maximum load was 1.40 times that of the S3-ETS beam at its maximum load (21.3 mm at 431.4 kN load versus 15.2 mm at 425.5 kN) and 1.82 times that of the S3-NSM beam at its maximum load (21.3 mm at 431.4 kN load versus 11.7 mm at 381.0 kN), whereas the S3-EB beam failed at a maximum load of 294.0 kN corresponding to a 14.4-mm deflection. All the beams in the S3 series, except for S3-EB-DAMA, S3-EB-EFLA, and S3-ETS (Figures 6.7-a and 6.7-b), exhibited a somewhat brittle type of behaviour characterized by a sudden drop in the load-displacement curves after the peak load. In contrast, beams S3-EB-DAMA, S3-EB-EFLA, and S3-ETS featured a ductile behaviour.

6.3.4   Strain response

This part of the study analyzes the strain readings of CFRP and transverse steel for all the tested specimens. As mentioned earlier, the use of a comprehensive measuring device enabled the collection of valuable data which are much needed for better understanding of the shear-resistance behaviour of beams strengthened with FRP using different methods.

CFRP strain: Figure 6.8-a presents the load versus maximum FRP strain curves for the beams strengthened using the EB method (with and without end-anchorage systems). As can be seen in Figure 6.8-a, all these curves feature a similar three-phase pattern. In the first phase, as the load increases, the CFRP does not contribute significantly to the load-carrying capacity. In the second phase, the CFRP begins to strain at an applied load of approximately 100 kN to 150 kN for all specimens (Figure 6.8-a). Under increasing load, the CFRP strain continues to increase at a relatively high rate up to a certain threshold, the value of which differs from one specimen to another depending on the strengthening method. In specimens strengthened using the EB method with end-anchorage systems (Figure 6.8-a), the maximum strain in the second phase reached 1842 $\mu\varepsilon$ and 2450 $\mu\varepsilon$ for specimens S3-EB-SBFA and S3-EB-DAMA respectively. In the third phase, the rate of increase of the CFRP strain starts to increase significantly as the load increases. This can be attributed to local CFRP debonding, the effect of which can be seen in the curve reversals in Figure 6.8-a. For strengthened beams with

more effective anchorage systems, the third phase is shorter than the second phase with respect to strain. Specimens S3-EB-DAMA, S3-EB-ERBA, and S3-EB-EFLA, with more than 40% gain due to CFRP, are the specimens which were strengthened more effectively with EB anchorage systems compared to the other specimens. In Figure 6.8-a, considering the constant slope of the strain increase from start to finish for the S3-EB-ERBA and S3-EB-EFLA specimens, it can be said that debonding of the FRP was prevented by the anchorage systems. For specimens S3-EB-NA and S3-EB-SBFA, debonding of FRP resulted in a longer phase 3 compared to the other specimens illustrated in Figure 6.8-a. It should be noted that all the reported strain values in this paper are the maximum measured values, but not necessarily the absolute maximum values experienced by the FRP. This can be the case when the strain gauges do not intercept the main cracks.
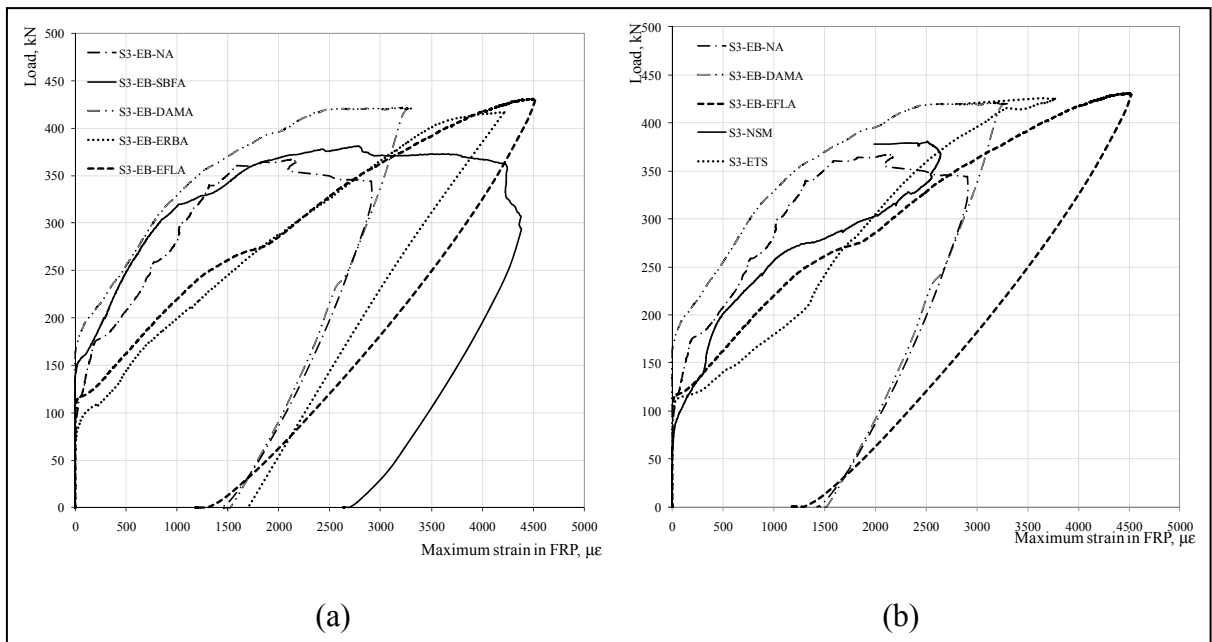
Figure 6.8   Load versus maximum strain in FRP: a) beams strengthened with EB method (with and without end-anchorage systems and the control beams; and b) beams strengthened with EB, NSM and ETS methods.

Figure 6.8-b shows the load versus FRP strain curves for the beams strengthened using the EB method and for the beams strengthened using the NSM and ETS methods. In Figure 6.8-

b, considering the relatively constant slope of the strain increase for the S3-ETS specimen, it can be concluded that debonding of the FRP rods did not take place in the S3-ETS specimen. In addition, in specimen S3-NSM, the strain in the FRP rods decreased significantly at failure due to splitting of the concrete cover (Figure 6.8-b).

Transverse steel strain: Figures 6.9-a and 6.9-b represent the applied load versus maximum strain curves in transverse steel for each of the specimens. These curves show that the behaviour of the transverse steel went through three phases during loading. In the first phase, the contribution of the transverse steel to shear resistance is negligible. In the second phase, the transverse steel starts to strain as the first diagonal cracks initiate. In the beams strengthened using the EB method with end-anchorage systems, for instance, this phase starts when the applied load reached 50 kN to 100 kN. In the third stage, with increasing load, the transverse-steel strain continues to increase at a relatively high rate until either the transverse steel yields or rupture of the specimen occurs. In all beams, the transverse steel crossing the crack lines yielded.

At a given applied load, the strain in the transverse steel is substantially greater in the control specimen with no CFRP than in the strengthened specimens (Figures 6.9-a and 6.9-b). Similarly, the strain in the transverse steel is greater in the specimen strengthened using the EB method with no anchorage (S3-EB-NA) than in the specimens strengthened using the EB method with end-anchorage systems (Figure 6.9-a). Overall, for the specimens with greater shear capacity gain due to CFRP, the transverse steel experienced lower strain during the tests. Thus, it can be concluded that the presence of an effective CFRP strengthening system eases the strains in the transverse steel. Therefore, yielding of the transverse steel is postponed in specimens with effective CFRP strengthening systems compared to corresponding specimens with no strengthening system or a less-effective strengthening system. Eventually, for all the tested specimens, yielding of transverse steel occurred for all the stirrups crossing the major shear crack at the maximum load.
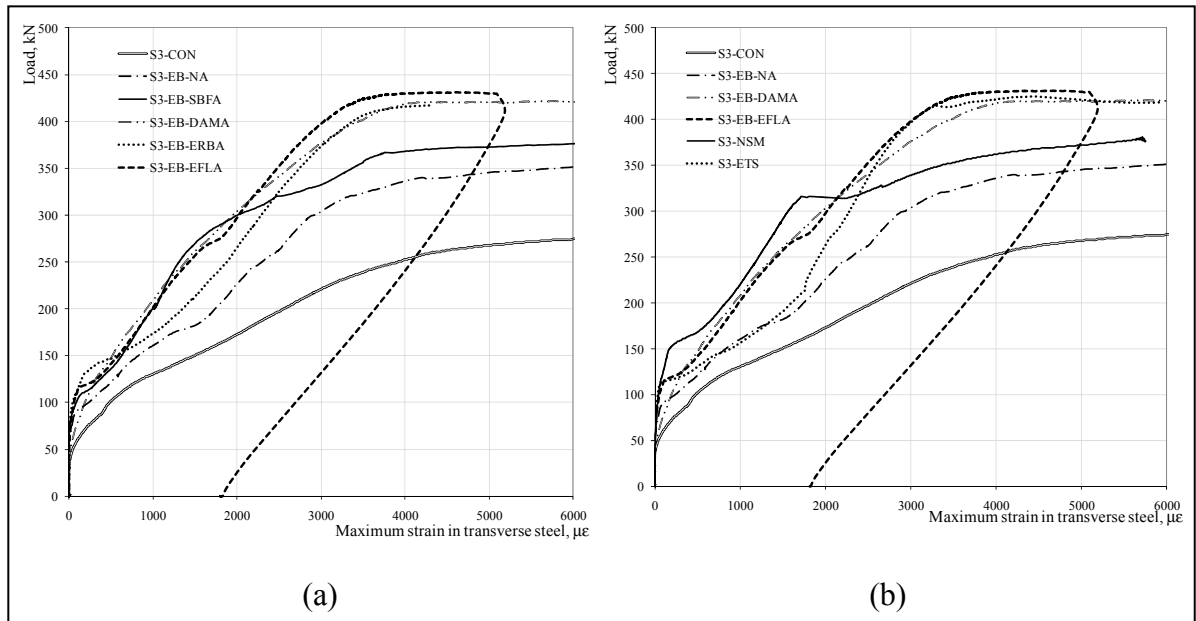
Figure 6.9 Load versus maximum strain in transverse steel: a) beams strengthened with EB method and the control beams; and b) beams strengthened with EB method (with and without end-anchorage systems) and beams strengthened with NSM and ETS methods.

Figure 6.10 shows the measured strain distribution at failure in the transverse steel for all the tested specimens. The strain curves are drawn to scale and represented on the monitored stirrups. The horizontal line indicates the yield point of the transverse steel as obtained the by tests (ε_y = 3250 με). All the stirrups are highly strained, which is clearly reflected in the widespread cracking patterns observed in the beams with transverse steel (e.g., Figure 6.6-a). However, the stirrups crossing the principal shear crack are the most strained. Yielding of transverse steel is observed for all the steel stirrups crossing the principal shear crack, which is in agreement with the assumptions of the design guidelines (ACI 440.2R-08; CSA S806-02; *fib* TG 9.3-01).

6.4   Discussion of results

6.4.1   Efficiency of the end-anchorage Systems

In this section, the effectiveness of the proposed strengthening method for beams retrofitted using the EB FRP method with different anchorage systems is compared to that of the EB

FRP sheet method with no anchorage, the NSM FRP method, and the ETS FRP method. To define the effectiveness of CFRP for each of these methods, the amount of FRP per unit length was taken into account. The sectional area of CFRP per metre of shear span used in all beams strengthened using the EB method (with or without anchorage systems) was 214 mm^2/m. For beams strengthened using the NSM and ETS methods, the sectional area of CFRP per metre of shear span was 1090 mm^2/m and 974 mm^2/m, respectively. The ultimate tensile capacity per unit length of the strengthening systems in all beams strengthened using the EB method (with or without anchorage systems) was 781 kN/m. For beams strengthened using the NSM and ETS methods, the ultimate tensile capacity per unit length was 2055 kN/m and 1807 kN/m respectively.
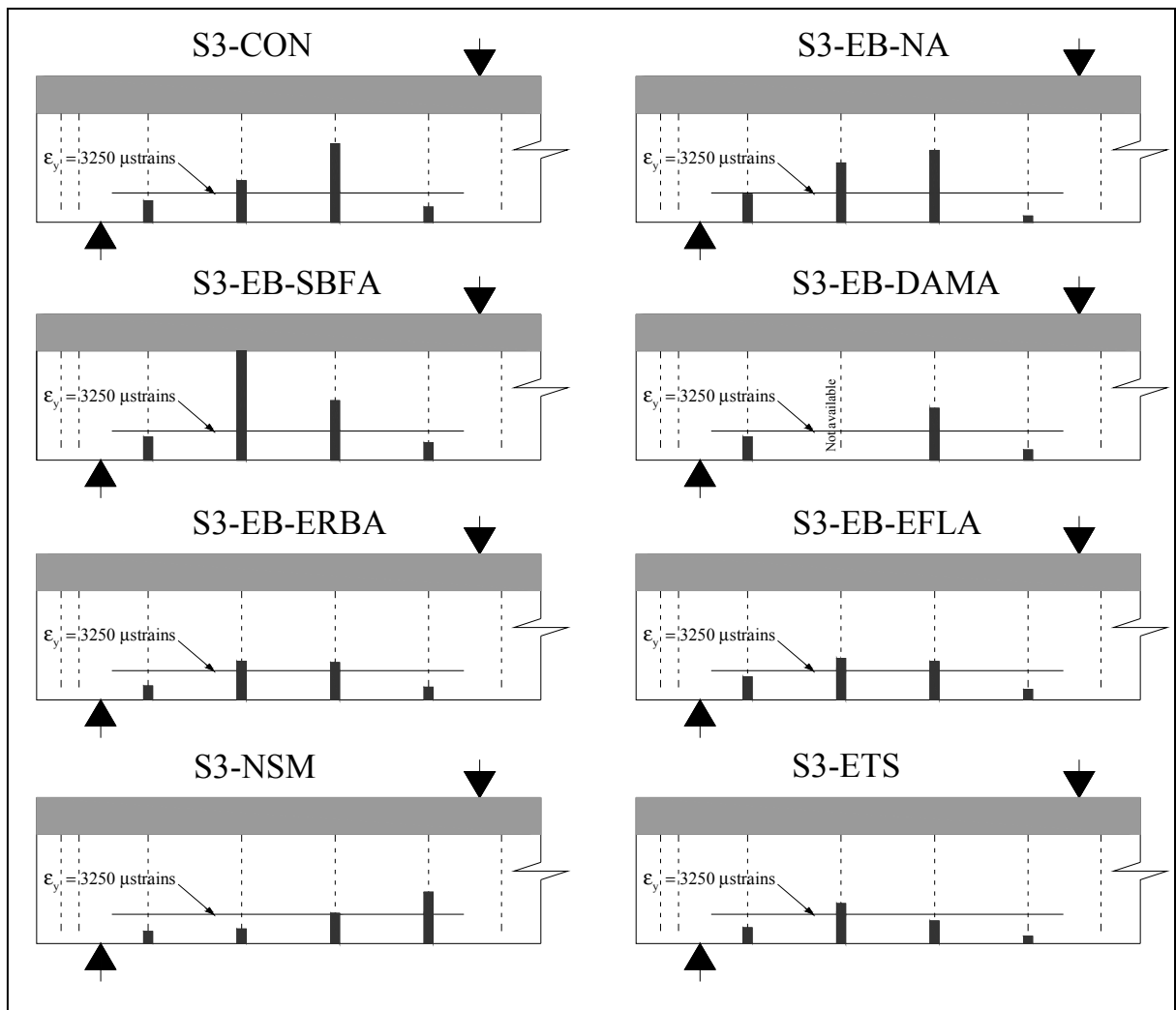
Figure 6.10   Distribution of maximum strains in the transverse steel at failure.

In this study, CFRP characteristics are calculated based on dry-fibre material properties as reported by the manufacturer. To compare the efficiency of CFRP for each strengthening method, an efficiency measure ψ_f has been defined. The efficiency of the FRP strengthening system (ψ_p) for each specimen is equal to the FRP contribution to the shear strength, V_f, divided by the ultimate tensile capacity per unit length of the FRP used in each specimen. The efficiency of the FRP strengthening method for each specimen is shown in Table 6.3. It can be seen that beams strengthened using the EB method with the DAMA, ERBA, and EFLA anchorage systems achieved the highest FRP efficiency of all the strengthened beams considered in this study.

Table 6.3   Efficiency of FRP for different strengthening methods.

Specimen	Area of dry fibre used, mm^2/m	Ultimate tensile capacity per unit length kN/m	V_f, kN	ψ_f, Efficiency of FRP % m
S3-EB-NA	214	781	48.5	6.2
S3-EB-SBFA	214	781	58.0	7.4
S3-EB-DAMA	214	781	84.5	10.8
S3-EB-ERBA	214	781	81.5	10.4
S3-EB-EFLA	214	781	91.0	11.7
S3-NSM	1090	2055	57.6	2.8
S3-ETS	974	1807	87.1	4.8

6.4.2   Anchorage factor

Based on computational analysis, Deniaud and Cheng (2004) showed that the anchorage factor has an inverse relationship with the FRP effective strain. According to their study, the anchorage factor should be set to 1 or 2 for unanchored FRP U-jackets and unanchored side-bonded FRP sheets respectively. In the current research study, the anchorage factor for each end-anchorage system used to strengthen RC beams with EB U-jackets was calculated based on experimental results (Table 6.4).

Table 6.4   Anchorage factor and shear contribution of FRP calculations.

Specimen	End-Anchorage system	Experimental shear contribution of CFRP	Anchorage Factor, k_a	Calculated V_{frp} by Mofidi and Chaallal (2011-a)
S3-EB-NA	No End-Anchorage	48.5	1.00	27.2
S3-EB-SBFA	Surface Bonded Flat CFRP Bar	58.0	0.84	32.4
S3-EB-DAMA	Aluminum Mechanical Anchorage	84.5	0.57	47.7
S3-EB-ERBA	Embedded Round CFRP Bar	81.5	0.60	45.3
S3-EB-EFLA	Embedded Flat CFRP Laminate	91.0	0.53	51.3

The anchorage factor for unanchored FRP U-jackets was set to 1 (specimen S3-EB-NA). The shear contribution of the FRP for each of the end-anchorage methods can then be calculated using any design model proposed for FRP U-jacket strengthening methods with no anchorage, assuming the given anchorage factor in the equations. For example, the design proposals by Mofidi and Chaallal (2011-a) for calculating the shear contribution of FRP for beams strengthened with EB FRP with no anchorage can be modified for beams strengthened using EB FRP with an anchorage system as follows:

$$\varepsilon_{fe} = 0.31 \frac{k_c \cdot k_L \cdot k_w}{k_a} \sqrt{\frac{\sqrt{f_c'}}{t_f E_f}} \leq \varepsilon_{fu} \qquad \text{Eq. (6.1)}$$

$$V_f = \frac{2t_f \cdot w_f \cdot \varepsilon_{fe} \cdot E_f \cdot (\cot\theta + \cot\alpha) \cdot \sin\alpha \cdot d_f}{s_f} \qquad \text{Eq. (6.2)}$$

For details on the calculations of k_c, k_L, and k_w, see Mofidi and Chaallal (2011-a). The anchorage factor, k_a, and the calculated shear contribution of FRP for the four end-anchorage systems used in the current research study can be obtained from Table 6.4. Obviously, more

experimental results are needed to verify fully the calculated anchorage factors for the end-anchorage systems used in this research study.

6.5   Conclusions

Based on the results of the current research study, the following major conclusions can be drawn:

- end-anchorage systems can significantly enhance the shear capacity of RC beams strengthened using the EB FRP sheet method. In this study, the average increase in shear capacity was as high as 41% for the beams strengthened using an EB U-jacket sheet with end-anchorage. In contrast, the increase in shear capacity was 25% for beams strengthened using EB FRP with no anchorage, 30% for beams strengthened with NSM FRP rod, and 45% for beams strengthened with ETS FRP rods;

- beams strengthened with a double-aluminum-plate mechanical end-anchorage system (DAMA) and an embedded CFRP laminate end-anchorage system (EFLA) attained the highest gains in shear due to FRP strengthening among all the shear-strengthening methods considered in this research study (except for beams strengthened using ETS method);

- for specimens S3-EB-DAMA, S3-EB-EBRA, and S3-EB-EFLA, debonding was prevented by the end-anchorage systems. The failure mode of the mentioned specimens was mainly flexural (except for specimen S3-EB-EBRA);

- the S3-EB-DAMA and S3-EB-EFLA specimens achieved the highest gains in shear due to FRP strengthening of all the shear-strengthening methods considered in this research study;

- at a given load, the strain in transverse steel was significantly smaller in specimens with end-anchorage systems. Nevertheless, the transverse steel yielded in most cases, as assumed by design codes and standards. Therefore, the shear contribution of transverse steel can be calculated using the equations in the design guidelines;

- specimens strengthened using the EB method with the DAMA, ERBA, and EFLA anchorage systems achieved the highest efficiency among the end-anchorage systems tested in this research study;

- based on the experimental results of this research study, the anchorage factor for each end-anchorage system used to strengthen RC beams with EB U-jackets was calculated. The shear contribution of the FRP for each end-anchorage system can be calculated using the proposed design equations. More experimental results are needed to verify the proposed anchorage factors.

6.6   References

American Concrete Institute (ACI) (2008). *Guide for the Design and Construction of Externally Bonded FRP Systems for Strengthening Concrete Structures.* Report No. 440 2R-08, Farmington Hills MI.

Barros, J.A.O., Dias, S.J.E. (2005). Near-surface-mounted CFRP laminates for shear strengthening of concrete beams. *Cement Concr. Compos.* 28, pp. 289–294.

Bousselham, A. and Chaallal, O. (2008). Mechanisms of shear resistance of concrete beams strengthened in shear with externally bonded FRP. *J. Compos. Constr.* 12(5), pp. 499–512.

Ceroni, F., Pecce, M., Matthys, S. and Taerwe, L. (2008). Debonding strength and anchorage devices for reinforced concrete elements strengthened with FRP sheets. *Compos. Part B: Eng.* 39, pp. 429-441.

Chaallal, O., Mofidi, A., Benmokrane, B. and Neale, K. (2011). Embedded Through-Section FRP Rod Method for Shear Strengthening of RC Beams: Performance and Comparison with Existing Techniques. *ASCE, J. Compos. Constr.* 15(3), pp. 374-383.

Chen, G.M., Teng, J.G., Chen J.F. and Rosenboom, O.A. (2010) Interaction between steel stirrups and shear-strengthening FRP strips in RC beams. *J. Compos. Constr.* 14(5), pp. 498–509.

De Lorenzis, L. and Nanni, A. (2001). Shear strengthening of reinforced concrete beams with NSM fiber-reinforced polymer rods. *ACI Struct J.* 98(1), pp. 60–68.

Deniaud, C. and Cheng, J.J.R. (2004). Simplified shear design method for concrete beams strengthened with fiber-reinforced polymer sheets. *J. Compos. Constr.* 8(5), pp. 425–433.

Eshwar, N., Nanni, A. and Ibell, T.J. (2008). Performance of two anchor systems of externally bonded fiber-reinforced polymer laminates. *ACI Materials J.* 105(1), pp. 72–80.

fib-TG 9.3 (2001). *Externally Bonded FRP Reinforcement for RC Structures.* International Federation for Structural Concrete, Lausanne, Switzerland.

Khalifa, A. and Nanni, A. (2000). Improving shear capacity of existing RC T-section beams using CFRP composites. *Cem. Concr. Compos.* 22, pp. 165–174.

Mofidi A. (2008). Strengthening RC T-beams in flexure and shear using new mechanically-anchored FRP and dry fibre systems. M.A.Sc. Thesis. Concordia University, Montreal, Canada. 160 pp.

Mofidi, A. and Chaallal, O. (2011-a). Shear strengthening of RC beams with EB FRP: influencing factors and conceptual debonding model. *J. Compos. Constr.* 15(1), pp. 62–74.

Mofidi, A. and, Chaallal, O. (2011-b). Shear Strengthening of RC Beams with Externally Bonded FRP Composites: Effect of Strip-Width to Strip-Spacing Ratio. *ASCE, J. of Composites for Construction.* 15(5), pp. 732-742.

Sato, Y., Katsumata, H. and Kobatake, Y. (1997) Shear strengthening of existing reinforced concrete beams by CFRP sheet. *Proc. of the 3rd Int. Symp. on Non-Metallic (FRP) Reinforcement for Concrete Structures*, Sapporo, Japan, pp. 507–514.

Schuman, P. (2004). Mechanical anchorage for shear rehabilitation of reinforced concrete structures with FRP: an appropriate design approach. Ph.D. Thesis, University of California, San Diego. 528 pp.

CHAPTER 7

EXPERIMENTAL TESTS AND DESIGN MODEL FOR RC BEAMS STRENGTHENED IN SHEAR USING THE EMBEDDED THROUGH-SECTION FRP METHOD

Amir Mofidi and Omar Chaallal

Department of Construction Engineering, École de Technologie Supérieure 1100 Notre-Dame Ouest, Montréal, Québec, Canada H3C 1K3

7.1 Abstract

This paper presents results of an analytical and experimental investigation on reinforced concrete (RC) T-beams retrofitted in shear with embedded through-section (ETS) fiber-reinforced polymer (FRP). The ETS FRP rod method is a promising method to increase the shear strength of RC beams. As this method develops, the structural behavior of RC beams strengthened with the ETS method needs to be thoroughly characterized and the influencing parameters addressed. In this research study, nine tests were performed on 4520-mm-long RC T-beams. The parameters of this study are: (i) the effect of the surface coating on the FRP bars; (ii) the effect of internal transverse-steel reinforcement on the FRP shear contribution; (iii) the effect of FRP bar spacing; (iv) the effect of FRP rod diameter; and (v) the efficiency of the embedded through-section FRP rod method. The main objective of the study is to analyze the behaviour of RC T-beams strengthened in shear with ETS FRP rods by varying the parameters just mentioned. New design equations are proposed to calculate

the shear contribution of FRP for beams strengthened using the ETS FRP method. The design equations are validated against results collected from the experimental part of the current research study. The proposed model shows an acceptable correlation with the experimental results.

7.2   Introduction

Strengthening of existing reinforced-concrete (RC) structures has gained increasing attention around the world. In the last two decades, fiber-reinforced polymer (FRP) has become an attractive subject for researchers and engineers as an alternative strengthening and reinforcing material (ACI 440R 2007, ACI 440.2R 2008, NCHRP Report 514 2008 and NCHRP Report 655 2010). Several research studies on shear strengthening of RC beams with FRP composites have been conducted and have provided valuable results (ACI 440.2R 2008). However, shear strengthening of RC beams with FRP composites is still insufficiently documented, with many questions yet to be answered (Bousselham and Chaallal 2004; Mofidi and Chaallal 2011a-b).

Externally bonded (EB) FRP is the most commonly used method for strengthening RC beams using FRP material. Many research studies on shear strengthening of RC beams with EB FRP sheets or laminate have been carried out (e.g., Uji 1992; Chaallal et al. 1998; Triantafillou 1998; Khalifa et al. 1998; Bousselham and Chaallal 2008; Chaallal et al. 2011).

De Lorenzis and Nanni (2001) successfully used near-surface-mounted (NSM) FRP rods to increase the shear resistance of RC beams. In the NSM method, FRP rods are embedded into pre-cut grooves on the concrete cover of both sides of an RC beam. Research has proven the effectiveness of the NSM method for increasing the shear resistance of RC beams (De Lorenzis and Nanni 2001; Barros and Dias 2005; Rizzo and De Lorenzis 2009; Chaallal et al. 2011). However, the tedious surface and groove preparation required, as well as the occurrence of debonding of the FRP rods (delamination of the concrete cover), still remain the main disadvantages of EB FRP and NSM methods (Chaallal et al. 2011). The debonding

occurs mainly because in EB and NSM methods, the FRP sheets or rods rely on the concrete cover of the RC beams. Therefore, the effectiveness of these methods is limited by the low tensile strength of the concrete.

The embedded-through-section (ETS) method is a recently developed technique for strengthening RC beams in shear using FRP rods (Valerio and Ibell 2003; Valerio et al. 2009; Chaallal et al. 2011). In the ETS method, FRP rods are epoxy-bonded to pre-drilled holes through the cross section of the RC beam. Previous research has shown the superior performance of the ETS method over EB and NSM methods (Chaallal et al. 2011). This improvement is achieved because in the ETS method, unlike the EB and NSM methods, the FRP relies on the concrete core of the RC beam, which offers better confinement and therefore improves bond performance.

The objective of this research study is to investigate the effect of the following variables on RC beams strengthened in shear using the ETS method: (i) FRP rod surface coating; (ii) internal transverse-steel; (iii) FRP rod spacing; and (iv) FRP rod diameter. Moreover, using the BPE (Bertero, Popov, and Eligehausen) modified shear-slip law (Cosenza et al. 1997), new equations are proposed to calculate the shear contribution of FRP for RC beams strengthened in shear using the ETS method.

7.3   Experimental program

The experimental program (Table 7.1) involves nine tests performed on full-scale RC T-beams. The control specimens, not strengthened with carbon FRP (CFRP) rods, are labeled as CON. The specimens labeled S0 are RC beams with no internal transverse-steel reinforcement (that is, no stirrups). The specimens labeled S1 and S3 have internal transverse-steel stirrups, hereafter called transverse-steel, spaced at $s = d/2$ for S1 and $s = 3d/4$ for S3, where $d = 350$ mm and represents the effective depth of the cross section of the beam. The specimens strengthened with 12.7-mm-diameter rods are labeled 12d, and the specimens strengthened with 9.5-mm-diameter rods are labeled 9d. All the specimens

strengthened using the ETS method with CFRP rod spacings of 130 mm and 260 mm are labeled 130 and 260 respectively. Finally, the specimens strengthened using sand-coated CFRP rods are labeled "s," and the specimens strengthened using CFRP rods with a plain (smooth) surface are labeled "p." Thus, for instance, specimen S1-9d260s features a T-beam with transverse-steel spaced at $d/2 = 175$ mm which is retrofitted using 9.5-mm-diameter sand-coated ETS CFRP rods spaced at 260 mm.

Table 7.1   Description of test specimens.

Specimen	FRP Surface coating	Transverse steel	FRP rod spacing, mm	FRP rod diameter, mm
S0-CON	-	S0	-	-
S1-CON	-	S1	-	-
S3-CON	-	S3	-	-
S0-12d130s	Sand-coated	S0	130	12.7
S1-9d260s	Sand-coated	S1	260	9.5
S1-12d260s	Sand-coated	S1	260	12.7
S1-12d130s	Sand-coated	S1	130	12.7
S1-9d260p	Plain surface	S1	260	9.5
S3-12d130s	Sand-coated	S3	130	12.7

7.3.1   Description of specimens

The specimens tested in this study were 4520-mm-long RC T-beams. The T-section had overall dimensions of 508 mm (flange width) by 406 mm (total depth). The thicknesses of the web and the flange were 152 and 102 mm respectively (Figure 7.1). The longitudinal-steel reinforcement consisted of four 25M bars (diameter 25.2 mm, area 500 mm^2) laid in two layers at the bottom and six 10M bars (diameter 10.3 mm, area 100 mm^2) laid in one layer at the top. The bottom bars were anchored at the support with 90-degree hooks to prevent premature anchorage failure. The internal steel stirrups (where applicable) were 8 mm in diameter (area 50 mm^2).
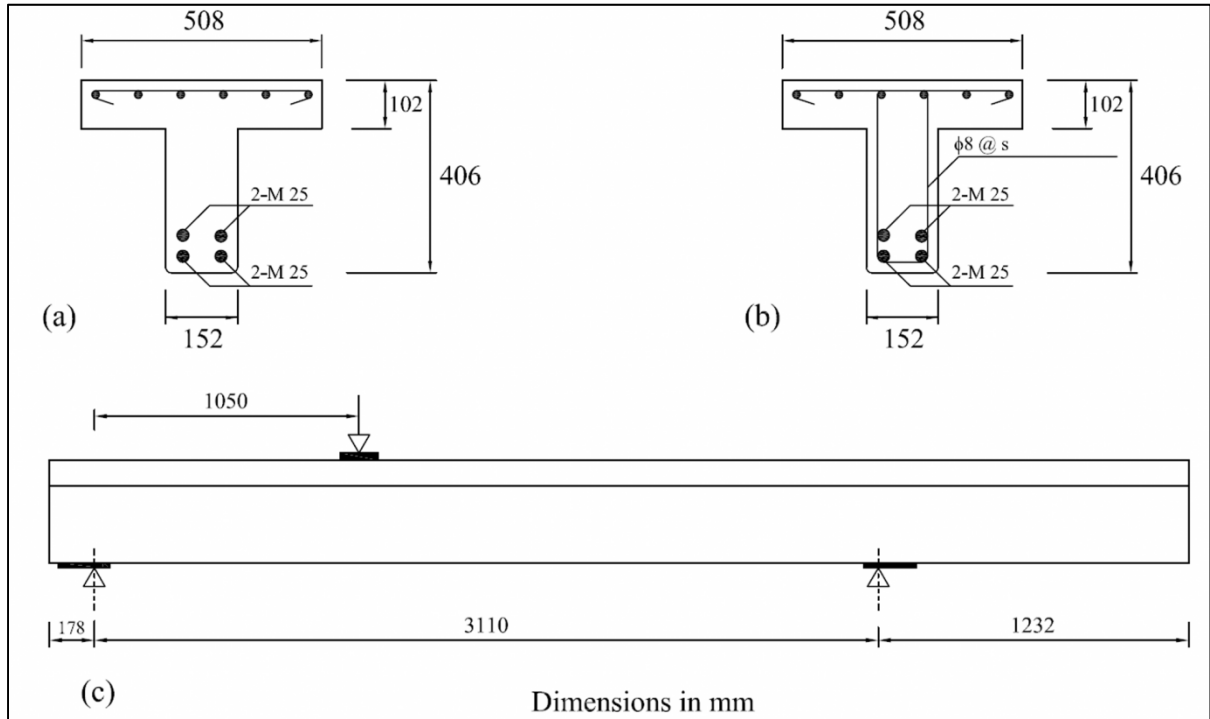
Figure 7.1 Details of concrete beams: a) cross section with no transverse-steel;
b) cross section with transverse-steel; and c) elevation.

In order to install CFRP rods used in the ETS method the following steps are performed: (1) vertical holes, with a diameter 1.5 times the diameter of the CFRP rods, spaced at designated distances are made through the middle of the cross-section of the RC beam and the beam's longitudinal axis; (2) the holes are cleaned by compressed air and water; (3) one end of the holes is blocked using epoxy and the holes are filled with 2/3 of the needed epoxy adhesive volume; (4) a thin layer of the adhesive is applied around CFRP rods; (5) the CFRP rods are installed into the holes all the way through the cross-section of the RC beams. The rods can be inserted either from the top or the bottom of the RC beams, whichever is more practical. It should be noted that when using the ETS method, special care should be taken to avoid damaging the existing steel reinforcement. In normal conditions, the position of the existing steel bars is readily available using either existing drawings or rebar detectors. In addition, it should be mentioned that the tools typically used to drill concrete are not able to damage the steel reinforcement. Further details on the ETS strengthening technique can be found elsewhere (Chaallal et al. 2011).

7.3.2   Materials

A commercially available concrete delivered to the laboratory by a local supplier was used. The specimens were cast in two phases using separate concrete batches of the same mix design and supplier. Specimens S0-CON, S1-CON, S0-12d130s, and S1-12d130s were cast in the first phase. The rest of the specimens were cast in the second phase. Standard compression tests on control cylinders yielded an average 28-day concrete compressive strength of 25.0 MPa and 29.6 MPa for the first and the second phases respectively. Note that for each concrete batch, the scatter among the compression test results for the cylinder specimens was negligible.

Sand-coated CFRP rods and plain-surfaced CFRP rods were used to strengthen the RC beams. The tensile strength and modulus of elasticity of the sand-coated CFRP rods were 1885 MPa and 148 GPa respectively. The tensile strength and modulus of elasticity of the plain-surfaced CFRP rods were 2800 MPa and 155 GPa respectively. It should be mentioned that sand-coated and plain-surfaced CFRP rods used in this study are produced by different manufacturers. Table 7.2 presents the mechanical and elastic properties of the CFRP rods as provided by the manufacturer. The CFRP rods were bonded into pre-drilled holes with an adhesive made of a resin and a hardener, both of which are specifically engineered for structural applications. The mechanical properties of the adhesive as specified by the manufacturer were as follows: 21 MPa bond strength, 1% elongation at break, 75 MPa compressive strength, and 3656 MPa compressive modulus.

Table 7.2   Mechanical properties of CFRP rods.

Property	Plain-surfaced CFRP rod	Sand-coated CFRP rod
Modulus of elasticity, GPa	155	148
Ultimate elongation, %	1.80	1.27
Ultimate stress, MPa	2800	1885

Note that the sand-coated rod is primarily used as a reinforcing bar for non-prestressed or prestressed concrete members. In contrast, the plain-surface rod is primarily used as an epoxy

bonded bar for retrofit. The purpose of comparison of these two rods was to generate test data and evaluate their performance for strengthening purposes.

7.3.3   Test setup and procedure

The beam specimens were tested in three-point bending as shown in Figure 7.1. The load was applied at a distance $a = 3d$ from the nearest support, which corresponds to the case of a slender beam in which the shear resistance is governed by the beam action mechanism (i.e., combined bending and shear stress). Hence, no extra strength due to arch action was expected.

7.3.4   Instrumentation

The vertical displacement was measured at the position under the applied load using linear variable differential transformers (LVDT) 150 mm in length. The longitudinal-steel reinforcement was instrumented with a strain gauge at the point load location. Strain gauges were also installed on the transverse-steel located in the loading zone along the anticipated plane of shear failure. The deformations experienced by the CFRP rods were measured using strain gauges installed on the rods. These gauges were fixed vertically on the CFRP rods before the rods were epoxy-bonded into pre-drilled holes. The deformations of the concrete were measured using 45° inclined embedded strain gauges installed midway between the support and the loading point, at the mid-height of the beam's web. The load was applied using a 2000-kN capacity hydraulic actuator. All tests were conducted under displacement control conditions at 2 mm/minute.

7.4   Discussion of experimental results

7.4.1   Overall response

Table 7.3 shows the maximum loads attained at rupture, the contributions to shear resistance of the concrete, the transverse-steel, and the CFRP, the gain in capacity due to the CFRP, and

the maximum deflection under the load point at failure. Note that the contributions of concrete and steel to shear are calculated based on the results obtained for unstrengthened beams. The following assumptions were made when calculating the values provided in Table 7.3: (i) the shear resistance due to concrete was assumed constant for beams with or without transverse steel reinforcement; (ii) the shear resistance due to concrete was assumed constant for both retrofitted and unstrengthened specimens; and (iii) the contribution of the transverse-steel was assumed constant for both retrofitted and unstrengthened specimens.

Table 7.3   Experimental results.

Specimen	Load at ruptur	Total resistance	Resistance due to	Resistance due to steel	Resistance due to CFRP	Gain due to CFRP	Deflection loading point
	kN	kN	kN	kN	kN	%	mm
S0-CON	122.7	81.3	81.3	0.0	0.0	0	2.6
S1-CON	350.6	232.2	81.3	150.9	0.0	0	11.9
S3-CON	294.0	194.7	88.5	106.2	0.0	0	11.2
S0-12d130s	273.0	180.8	81.3	0.0	99.5	122	8.9
S1-9d260s	393.0	260.3	88.5	157.8	14.0	6	21.3
S1-12d260s	402.6	266.6	88.5	157.8	20.3	8	15.4
S1-12d130s	398.0	263.6	81.3	150.9	31.4	14	18.6
S1-9d260p	423.8	280.7	88.5	157.8	34.4	14	24.7
S3-12d130s	425.5	281.8	88.5	106.2	87.1	45	16.6

Figures 7.2 and 7.3 show the curves for applied load versus maximum deflection at the point load for the control and strengthened beams. The curves represent typical behavior during a shear test. In the initial phase of loading (before the concrete starts to crack), these curves show similar characteristics. The observed decrease in the slopes of the curves is an indication of a loss of beam's stiffness as a result of crack propagation. This loss of stiffness led to a redistribution of internal stresses and triggered the contribution of the transverse-steel and the CFRP reinforcement to the shear resistance.
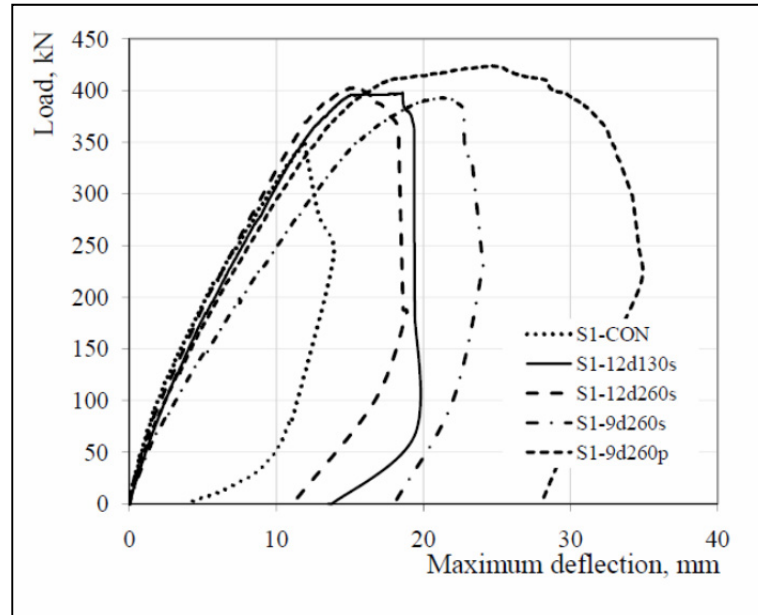
Figure 7.2   Load versus maximum deflection: specimens S1-CON, S1-12d130s,
          S1-12d260s, S1-9d260s, and S1-9d260p.

In series S1 (Figure 7.2), the beams strengthened with 12.7-mm-diameter rods (S1-12d130s and S1-12d260s) exhibited a slightly higher overall stiffness than the beams strengthened with 9.5-mm-diameter rods (S1-9d260s and S1-9d260p). However, in series S1, the ultimate load at failure in specimens S1-9d260p and S1-12d130s was greater than that in S1-9d260s and S1-12d260s (Figure 7.2). For specimen S1-9d260p, for example, the load at failure was 423.8 kN, compared with 393.0 kN for S1-9d260s. In series S1, the maximum deflection ratio between the strengthened beams and the corresponding control beams was greater for beams retrofitted with 9.5-mm-diameter rods than for beams retrofitted with 12.7-mm-diameter rods. On average, the maximum deflection ratio was 1.93 for beams retrofitted with 9.5-mm-diameter rods and 1.43 for beams retrofitted with 12.7-mm-diameter rods.

Figure 7.3 shows the curves of applied load versus maximum deflection at the point load for beams with similar FRP reinforcement but different internal steel reinforcement (i.e., S0, S1, and S3). Figure 7.3 reveals that the addition of transverse-steel reinforcement resulted in a significant decrease of the gain in shear capacity due to CFRP. As for the gain in stiffness,

the slope variations between the curves for the strengthened beams and those for the control beams were not significant.
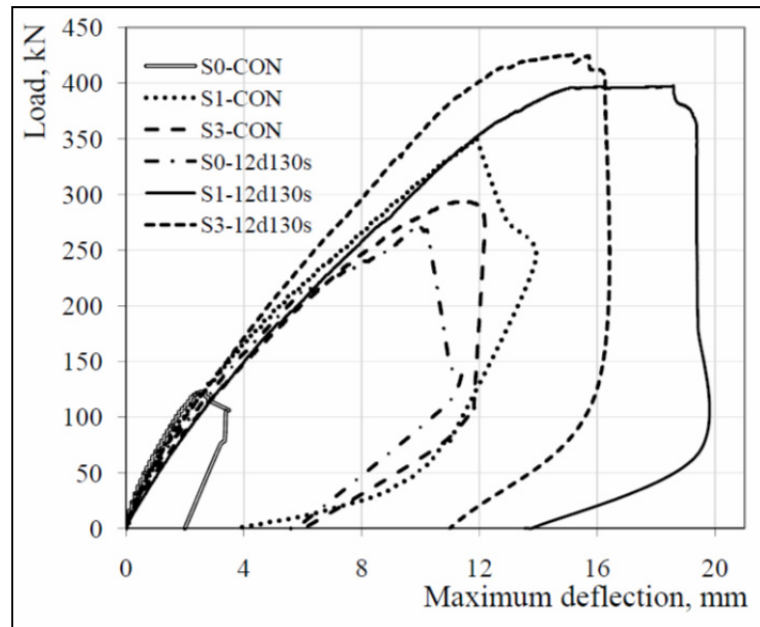
Figure 7.3 Load versus maximum deflection: specimens S0-CON, S1-CON, S3-CON, S0-12d130s, S1-12d130s, and S3-12d130s.

The maximum deflection at failure was slightly greater (18.6 mm) for the strengthened specimen with S1 transverse-steel (S1-12d130s) than for the specimen with S3 transverse-steel (S3-12d130s), which had a value of 16.6 mm. The strengthened specimen without transverse-steel (S0-12d130s) experienced a maximum deflection of 8.9 mm.

7.4.2   Cracking and failure mode

All the test specimens except S1-12d130s failed in shear. For specimens S1-9d260p and S3-12d130s, failure occurred by diagonal tension after the longitudinal steel yielded. For specimen S1-12d130s, the failure was mainly flexural. No signs of debonding of FRP rods were observed in any of the test specimens.

The load at which the first diagonal cracks occurred was of a similar magnitude for all specimens. In addition, the crack pattern was comparable in all retrofitted specimens in the same series. Parallel diagonal cracks started to open up with a relatively equal spacing from each other at an angle with respect to the beam axis varying between 37° and 42°. Figures 7.4 and 5 show the spacing between the initial shear cracks.
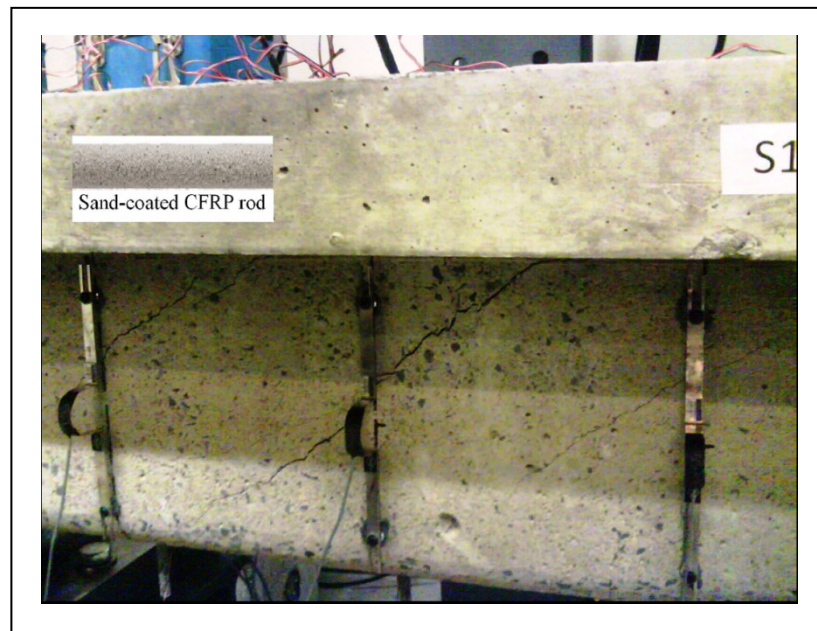
Figure 7.4   Parallel diagonal shear cracks, specimen S1-9d-260s.

In this stage of loading, as the load increased, the major shear crack grew faster and wider compared to other diagonal cracks. The major shear crack initiated on the beam's web, midway between the support and the point load, and propagated simultaneously toward both the beam flange and the support. As the crack reached the flange, it triggered an immediate failure with a quasi-horizontal crack angle (except for specimen S1-12d130s).

Figure 7.5   Parallel diagonal shear cracks, specimen S1-9d-260p.

For the beams without transverse-steel (Series S0), cracking started at more or less the same load level, approximately 78 kN. A loss of rigidity was observed after cracking initiated, followed by an increase in the beam's deflection. However, in the retrofitted specimen (S0-12d130s), this reduction in stiffness was more pronounced (Figure 7.3). Only one principal crack was observed in the specimens of series S0.

In the series S1 specimens, three parallel diagonal cracks initiated between 81 and 84 kN and propagated with increasing load. As the load reached its ultimate value, the principal diagonal crack became wider (Figure 7.6) and progressed horizontally in the RC beam flange (except for specimen S1-12d130s). Specimens S1-9d260p and S1-12d130s, which reached their flexural capacity limit, exhibited more ductile behavior compared to the other strengthened and control specimens in series S1 (Figure 7.7). In fact, specimen S1-12d130s did not fail in shear, but rather in flexure (Figure 7.8).

In series S3, the control beam started to crack diagonally at a load of 85 kN. The failure was due to rupture of a steel stirrup. Specimen S3-12d130s failed with a major shear crack at an angle of 38° after the longitudinal steel had yielded (Figure 7.9).
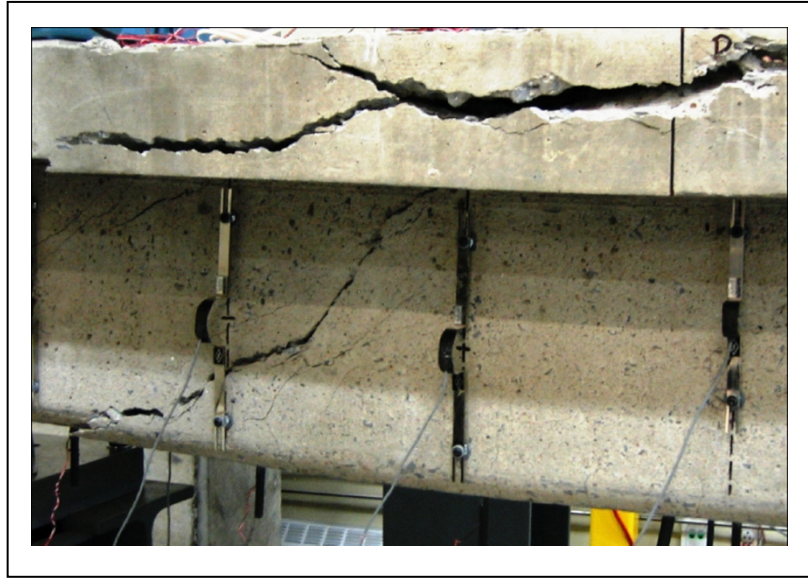
Figure 7.6   Failure mode of specimen S1-9d260s.

Figure 7.7   Failure mode of specimen S1-9d260p.

Figure 7.8   Failure mode of specimen S1-12d130s.

Figure 7.9   Failure mode of specimen S3-12d130s.

7.4.3   CFRP strains

Figure 7.10 presents curves of applied load versus CFRP strain for all the strengthened specimens. Examination of these curves reveals that the CFRP rods did not contribute to the load-carrying capacity in the initial stage of loading, i.e., before the formation of the concrete struts. It must be noted that all the strain values reported in this paper are the maximum measured (i.e., captured) values. These values are not necessarily the absolute maximum values experienced by the ETS CFRP rods (i.e., in cases where the strain gauges did not intercept the principal cracks).

Figure 7.10   Load versus maximum strain in FRP.

After the applied load increased beyond 85 kN, the strain in the CFRP rods started to increase to a maximum value (Figure 7.10), the level at which the beam ultimately failed. In series S0 (specimen S0-12d130s), the maximum measured strain value in the CFRP rods was 2286 $\mu\epsilon$. The CFRP rods in specimen S0-12d130s started to contribute to the shear resistance in an earlier stage of loading (Figure 7.10) compared to those of the retrofitted specimens with transverse-steel (series S1 and S3). This shows that after the formation of the concrete

struts and in the presence of the transverse-steel, the CFRP rods contribute to shear resistance later than the steel stirrups. In the specimens with transverse-steel (series S1 and S3), the CFRP rods started to contribute to the shear resistance at a similar load. After the FRP rods start to contribute to the shear resistance until the failure of the beam, the strain in all the specimens mentioned (except specimen S1-9d260p) increased with a constant slope. Specimen S1-9d260p was strengthened with CFRP rods having a plain surface. The increase in the FRP strain is significantly greater in specimen S1-9d260p compared to the rest of the specimens. This shows that plain surface CFRP rods epoxy-bonded to the concrete holes exhibited a superior bond behaviour compared to that of the CFRP rods with a sand-coated surface for RC beams strengthened in shear with ETS method.

On average, specimens strengthened with CFRP rods spaced at 260 mm reached higher strains than those strengthened with CFRP rods spaced at 130 mm (Figure 7.10). The maximum measured strain among all CFRP rod-strengthened specimens was 5933 μstrains in S1-9d260p. The maximum measured strain among the specimens strengthened with sand-coated CFRP rods was 3767 μstrains in S3-12d130s. The smallest maximum measured strain in the CFRP rods among all specimens was 2286 μstrains in S0-12d130s. In contrast, the smallest maximum measured strain in the CFRP rods among the specimens with transverse-steel was 2936 μstrains in S1-9d260s. Note that even though the strain in the CFRP rods is the smallest in the beam without transverse-steel, the contribution of CFRP to the shear resistance (V_{frp}) is greater for that beam (Table 7.3) than for the rest of the specimens (99.5 kN for S0-12d130s versus 87.1 kN for S3-12d130s, which reached the second highest V_{frp}).

7.4.4   Transverse-steel strain

The curves representing applied force versus strain in the transverse-steel reinforcement are presented in Figure 7.11 for all the specimens. Similarly to the situation of the strain in the CFRP rods, the transverse-steel did not contribute to the load-carrying capacity in the initial stage of loading.
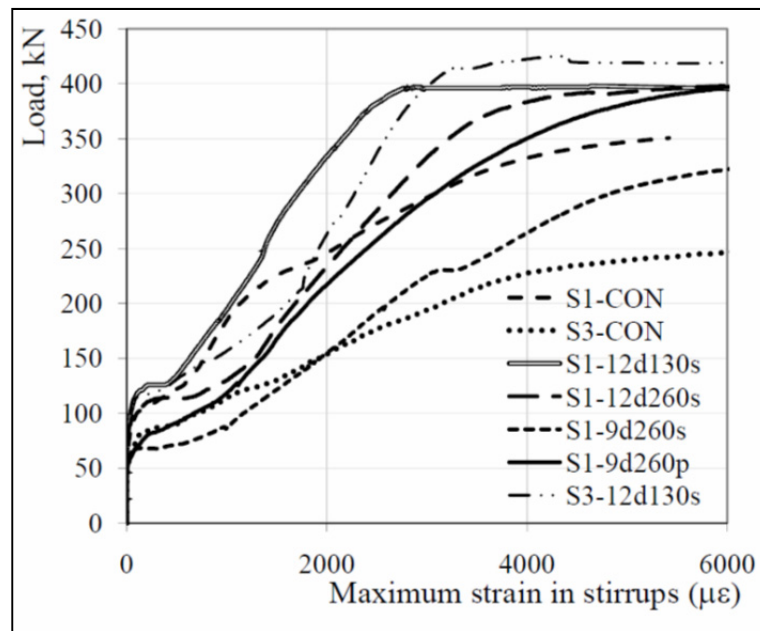
Figure 7.11   Load versus maximum strain in internal transverse-steel.

The contribution of steel stirrups to shear resistance started after the formation of diagonal cracks. In the S3-CON, S1-9d-260s, and S1-9d-260p specimens, the cracking initiated at an average applied load of 70 kN, whereas for the rest of the specimens, it started at an average applied load of 85 kN. This difference can be attributed to the wider spacing between the transverse reinforcement (steel and CFRP) in S3-CON, S1-9d-260s, and S1-9d-260p compared to the rest of the specimens. Specimen S1-9d-260p exhibited the greatest strain increase in transverse-steel among all the retrofitted specimens. This can be attributed to the greater strain increase in the matching CFRP rods, as mentioned previously (Figure 7.10). The smallest strain increase was observed in specimen S1-12d130s, due to the large amount of transverse-steel and CFRP reinforcement in that specimen. For all the specimens in this study, the transverse-steel reinforcement yielded well before final failure. Note that in Figure 7.11, the strains in the transverse-steel beyond 6000 μstrains are not reported.

7.5   Effect of experimental parameters

The various parameters investigated for beams strengthened in shear using the ETS method are analyzed in this section. The effects of the targeted parameters described earlier on the shear strengthening of RC beams using the ETS method are consecutively presented and analyzed in this section. Based on those findings, a new design approach is proposed in the next section for calculating the shear contribution of FRP for RC beams strengthened using the ETS FRP method.

7.5.1   Effect of CFRP rod surface coating

The effect of CFRP rod surface coating can be observed by comparing the response of beams S1-9d260s and S1-9d260p. These beams were strengthened with CFRP rods with similar diameter (9.5 mm) and similar spacing (260 mm), but having different surface coatings (see Figures 7.4 and 7.5). Specimen S1-9d260s was retrofitted using sand-coated CFRP rods, whereas specimen S1-9d260p was strengthened using CFRP rods with a plain surface. The CFRP rods with a plain surface finish in specimen S1-9d260p reached significantly higher strains than did specimen S1-9d260s (5933 $\mu\varepsilon$ versus 2936$\mu\varepsilon$). Furthermore, specimen S1-9d260p exhibited a greater contribution of FRP to shear resistance than did specimen S1-9d260s (34.4 kN versus 14.0 kN). It is evident that CFRP rods with a plain surface can be more efficient than sand-coated CFRP rods for beams strengthened using the ETS method. The superior performance of plain surface CFRP rods indicates a better shear transfer in the FRP-epoxy-concrete interface compared to sand-coated surface rods. This was corroborated by the results of a preliminary investigation undertaken by the authors and involving direct pull-out tests for CFRP rods epoxy-bonded to pre-drilled holes of concrete cylinders. This is attributed to the fact that FRP rods with plain surface finish offer a significant chemical bond within the FRP-epoxy-concrete interface, since the epoxy and the FRP rod contain similar polar molecular groups which are mutually attractive and chemically compatible. Sand-coating of FRP rods may inhibit the full compatibility between the adhesive and the rod matrix, reducing thereby the chemical bond within the FRP-epoxy-concrete interface compared to the case with FRP rods with plain surface.

It may be worth noting that for the FRP rods embedded in concrete (FRP-concrete bond, i.e., no epoxy at the FRP-concrete interface), research studies showed that rough-surfaced (including sand-coated) FRP bars achieved a better FRP-concrete bond behavior compared to plain surface FRP bars (e.g., Cosenza et al. 1997). This could be due to the fact that the mechanical bond holds a significant role in FRP-concrete interface when the FRP rods are directly embedded in concrete (i,e., without epoxy interface).

7.5.2   Effect of internal transverse-steel

The effect of the presence of transverse-steel on the FRP contribution to shear resistance for beams strengthened using the ETS method can be examined by comparing the results for specimens S0-12d130s, S1-12d130s, and S3-12d130s (Table 7.3). Specimen S0-12d130s had no internal transverse-steel reinforcement. Specimen S1-12d130s was reinforced with 8-mm-diameter stirrups spaced at $s = d/2$. Specimen S3-12d130s had 8-mm-diameter transverse-steel spaced at $s = 3d/4$.

The attenuating effect of transverse-steel on the shear contribution of externally bonded CFRP has already been established for RC beams strengthened in shear with CFRP sheets or fabrics (Chaallal et al. 2002; Bousselham and Chaallal 2008). In the current study, the presence of internal transverse-steel significantly decreased the gain due to FRP. Specimen S0-12d130s attained a 122% gain due to FRP strengthening, while specimens S1-12d130s and S3-12d130s showed 13% and 45% gain, respectively. The shear resistance due to FRP in specimen S0-12d130s was 99.5 kN, compared to 87.1 kN for specimen S3-12d130s (Table 7.3). In addition, the shear resistance due to ETS strengthening in specimen S1-12d130s ($V_f =$ 31.4 kN) with narrowly spaced transverse-steel would have been higher had flexural failure been avoided. In general, it can be said that the effect of transverse-steel in reducing the shear contribution of FRP for RC beams with widely spaced transverse-steel is less pronounced than the effect in beams with closely spaced transverse-steel. This highlights the importance of access to the amount and the spacing of internal transverse steel for the practicing engineers prior to shear retrofitting of RC beams with FRP.

7.5.3 Effect of CFRP rod spacing

To investigate the effect of CFRP rod spacing for beams strengthened in shear using the ETS method, specimens S1-12d130s and S1-12d260s are considered. Specimen S1-12d130s was strengthened with 12.7-mm-diameter rods spaced at 130 mm, whereas specimen S1-12d260s was retrofitted using similar CFRP rods spaced at 260 mm. The shear resistance due to FRP in specimen S1-12d130s was 31.4 kN, compared to 20.3 kN for specimen S1-12d260s. Decreasing the spacing of the rods from 260 mm to 130 mm, which corresponds to a 100% increase in the amount of FRP material present, led to an increase in shear resistance of 55%. As mentioned earlier, if specimen S1-12d130s had not failed by flexure, the shear contribution of the FRP would have been greater. Figure 7.10 shows that the maximum measured CFRP rod strain for specimen S1-12d130s reached 2967 με before flexural failure occurred. For design, the strain in the CFRP can reach 4000 με before the concrete cross section loses its coherence due to loss of aggregate interlocking and may fail in shear (ACI 440.2R 2008). It was thought that for a typical case where flexural failure could be avoided and specimen S1-12d130s would fail in shear after the strain in the CFRP rod had reached 4000 με, then V_f for specimen S1-12d130s could reach 41.9 kN. In this case, decreasing the spacing of the CFRP rods when using the ETS method could proportionately increase the shear contribution of FRP. For the current case, because of the particular failure mode, it can only be concluded that decreasing the spacing of the CFRP rods resulted in a higher shear resistance due to FRP.

7.5.4 Effect of CFRP rod diameter

To investigate the effect of CFRP rod diameter for beams strengthened in shear using the ETS method, specimens S1-9d260s and S1-12d260s are considered. Specimen S1-9d260s was strengthened with 9.5-mm-diameter rods spaced at 260 mm, whereas specimen S1-12d260s was retrofitted using 12.7-mm-diameter rods with a similar spacing between the rods. The shear resistance due to FRP in specimen S1-9d260s was 14.0 kN, compared to 20.3 kN for specimen S1-12d260s. Hence, increasing the diameter of the rods from 9.5 mm to

12.7 mm, which corresponds to a 79% increase in the amount of FRP material present, led to an increase in shear resistance of 45%.

Therefore, it can be said that increasing the diameter of the CFRP rods to strengthen RC beams in shear using the ETS method resulted in a higher shear resistance due to FRP. However, the increase in the resistive force of the FRP rods was not proportional to the increase in the amount of FRP (i.e., the increase in the CFRP rod area).

Research studies have revealed that other parameters such as bond stress are influenced by changes in the diameter of embedded FRP rods in concrete. Cosenza et al. (1997) gathered available experimental results of direct pull-out tests on embedded FRP rods in concrete blocks. According to their study, the maximum bond strength decreases as the FRP diameter increases. Subsequently, Cosenza et al. (1997) proposed a modification to the bond-slip model for deformed steel bars presented by Eligehausen, Popov, and Bertero (1983), also known as the BPE model. The modified BPE model was thus made applicable to FRP rods. According to the modified BPE model, the stress in FRP rods corresponding to maximum bond stress and maximum slip is inversely related to $\sqrt{D_{frp}}$ as follows:

$$f\left(s_m\right) = \sqrt{\frac{8E_{frp}}{D_{frp}} \cdot \frac{\tau_m \cdot s_m}{1+\alpha}} \qquad (7.1)$$

where $f(s_m)$ is the stress in FRP rods corresponding to maximum bond stress, s_m is the slip at maximum bond stress, τ_m is the maximum bond stress, α is a curve-fitting parameter that modifies the ascending branch, E_{frp} and D_{frp} are the modulus of elasticity and cross-section diameter of FRP rod, respectively.

On the other hand, the shear contribution of FRP can be calculated using the strut-and-tie model (STM). Based on this model, V_f is directly related to the stress in the FRP rod and the cross-sectional area of the FRP rod (Khalifa et al. 1998). As mentioned in the previous paragraph, the stress in embedded FRP rods in concrete is inversely related to $\sqrt{D_{frp}}$.

Assuming that the cross-sectional area of the FRP rod is a product function of $D_{frp}{}^2$, it can be concluded that V_f for RC beams strengthened using ETS method is directly related to $D_{frp}{}^{3/2}$. A more detailed analysis is provided in the section describing the proposed design equations.

7.5.5   Effect of the FRP rigidity ratio

The FRP rigidity ratio (R_{frp}) can be used to quantify the amount of FRP used for each strengthened specimen. The FRP rigidity parameter can be expressed as follows (Triantafillou 1998):

$$R_{frp} = \frac{A_{frp}}{b_w \cdot s_{frp}} \times E_{frp} \qquad (7.2)$$

The effect of the FRP rigidity ratio can be observed by comparing the response of specimens S1-9d260s, S1-12d260s, and S1-12d130s. The FRP rigidity ratios for specimens S1-9d260s, S1-12d260s, and S1-12d130s are 0.26, 0.46, and 0.92 GPa respectively.
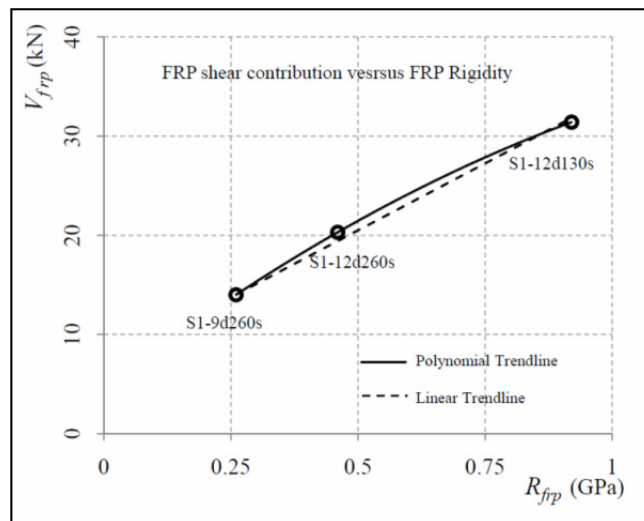

Figure 7.12   Shear contribution of FRP versus FRP rigidity ratio for specimens S1-9d260s, S1-12d260s, and S1-12d130s.

7.5.6   Efficiency of FRP

Table 7.4 compares the efficiencies achieved by the strengthened specimens using several variables investigated in this study for the ETS method. The efficiency of the FRP ratio (ψ_f) is defined as the FRP contribution to shear capacity, V_f, divided by the ultimate tensile capacity per unit length of FRP used in each specimen (Rizzo and De Lorenzis 2009). Table 7.4 shows that, compared to the specimen without transverse-steel (S0-12d130s), the efficiency decreased only slightly in the specimen with widely spaced transverse-steel (S3-12d130s). However, the efficiency of the ETS method significantly decreased in the specimen with narrowly spaced transverse-steel (S1-12d130s). Moreover, it can be seen that, for the specimens of series S1, the FRP efficiency ratio becomes greater when the FRP rod diameter is decreased, the rod spacing is increased, or both. In addition, the FRP efficiency ratio is greater for beams strengthened with CFRP rods with a plain surface than for beams strengthened with sand-coated CFRP rods (Table 7.4).

Table 7.4   Efficiency of FRP for the strengthened specimens.

	Area of CFRP used per unit length, mm²/m	Ultimate tensile capacity per unit length, kN/m	V_f, kN	ψ_f, Efficiency of FRP %
S0-12d130s	977	1827	99.5	5.0
S1-9d260s	273	510	14.0	2.7
S1-12d260s	488	913	20.3	2.2
S1-12d130s	977	1827	31.4	1.7
S1-9d260p	273	764	34.4	4.5
S3-12d130s	977	1827	87.1	4.7

7.6   Proposed shear design equations

In this section, a new design model is proposed for RC beams strengthened in shear using the ETS method. To analyze the behavior of epoxy-bonded FRP rods in pre-drilled holes in the concrete cross section, the BPE modified bond-slip model (Cosenza et al. 1997) was used. The original BPE bond-slip analytical law was proposed by Eligehausen, Popov, and Bertero (Eligehausen et al. 1983) to model the interaction between concrete and steel reinforcement.

Cosenza et al. (1997) successfully modified the BPE model so that it can be applied to FRP rebars. The BPE modified bond-slip model (Figure 7.13) mainly features an ascending branch (for $s < s_m$), and a descending branch (for $s_m < s < s_u$). In the BPE modified model, the ascending branch of the bond-slip relationship is given by:

$$\tau = \tau_m \cdot \left(\frac{s}{s_m}\right)^\alpha \tag{7.3}$$

However, the descending branch exhibits a linear behaviour with a slope of $\dfrac{p \cdot \tau_m}{s_m}$, which is given by:

$$\tau = \tau_m \left(1 + p - p\frac{s}{s_m}\right) \tag{7.4}$$

where s, s_m, and s_u are the slip, the slip at maximum bond stress, and the slip at the end of the BPE modified model descending branch respectively, and τ and τ_m are the bond stress and the maximum bond stress respectively. Moreover, α and p are curve-fitting parameters that modify respectively the ascending branch and the descending branch.
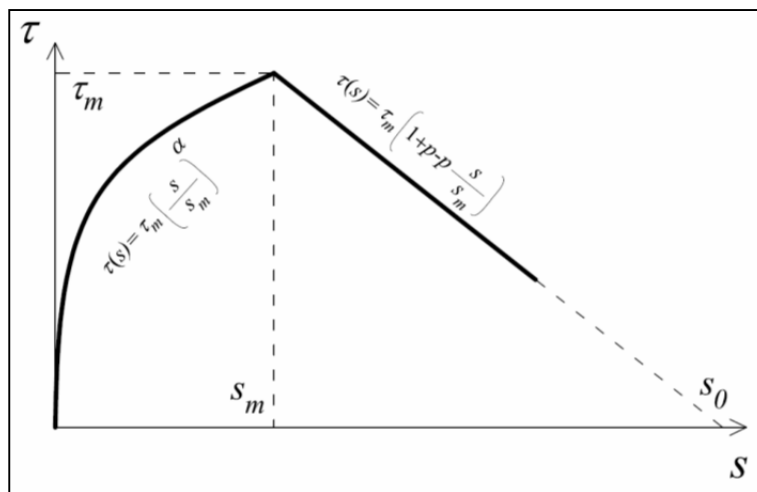

Figure 7.13 BPE modified bond stress-slip model.

Cosenza et al. (2002) calculated the stress in the FRP bar at maximum slip, $f(s_m)$, and the effective length of the FRP rod corresponding to the maximum slip, $L_{eff}(s_m)$, by considering the ascending branch of the BPE modified shear-slip model as follows:

$$f(s_m) = \sqrt{\frac{8E_{frp}}{D_{frp}} \cdot \frac{\tau_m \cdot s_m}{1+\alpha}} \tag{7.5}$$

$$L_{eff}(s_m) = \frac{f(s_m) \cdot D_{frp}}{4\tau_m} \cdot \frac{1+\alpha}{1-\alpha} \tag{7.6}$$

It should be noted that the value of the effective length is defined as the length beyond which the transferred stress will no longer increase. On the other hand, for the descending branch of the BPE modified shear-slip model, the stress in the FRP bar corresponding to the ultimate slip, $f(s_0)$, can be expressed as:

$$f(s_0) = \sqrt{\frac{8E_{frp}}{D_{frp}} \left(\frac{\tau_m \cdot s_m (1+\alpha+2p)}{2p(1+\alpha)} \right)} \tag{7.7}$$

Cosenza et al. (2002) used a procedure proposed by Pecce et al. (2001) to calculate the mean values and the coefficient of variation (c.o.v.) of the curve-fitting parameters using available experimental bond-test results. They recommended that only the ascending branch of the BPE modified bond-slip model be used for design because the descending branch showed unstable (i.e., large c.o.v.) results compared to experimental test results. Therefore, in the current study, Eqs. (7.5) and (7.6) are used for the calculation of V_{frp} in RC beams strengthened using the ETS method.

A series of direct pull-out tests for CFRP rods epoxy-bonded to pre-drilled holes in a concrete block was conducted in the laboratory of the École de Technologie Supérieure of the University of Quebec. The results of this experimental study showed that the behavior of the CFRP rods epoxy-bonded to pre-drilled holes in a concrete block (ETS rods) can be modeled using the BPE modified shear-slip constitutive law. Figure 7.14 shows the analytical

and experimental bond shear-slip relations for ETS FRP rods with a plain surface and a sand-coated surface epoxy-bonded in a concrete block.
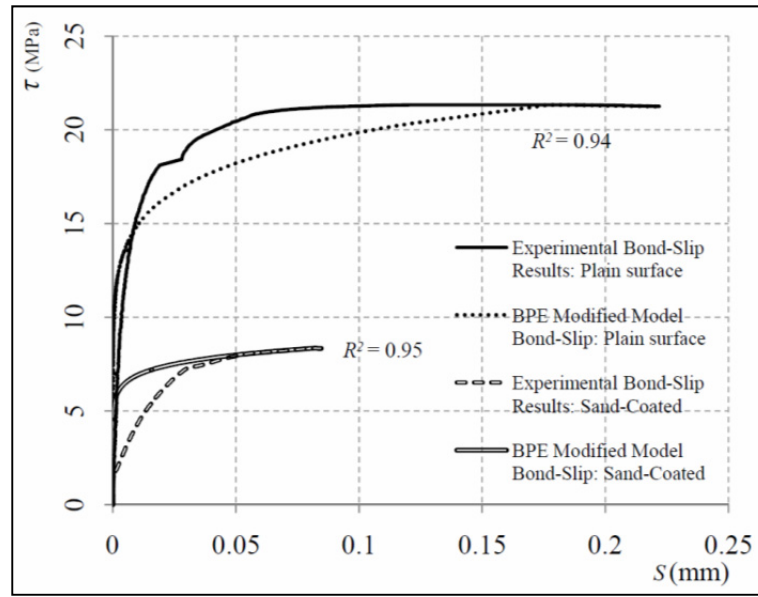
Figure 7.14   Analytical and experimental bond shear-slip relation for ETS FRP rods with plain surface and sand-coated surface epoxy-bonded to a concrete block.

Based on these experimental results, the bond parameters τ_m, s_m, and α for an FRP rod with a plain surface were derived as 21.3 MPa, 0.176 mm, and 0.125 respectively. For an FRP rod with a sand-coated surface, the bond parameters τ_m, s_m, and α were determined as 8.4 MPa, 0.08 mm, and 0.09 respectively (Figure 7.14).

Using the BPE modified shear-slip constitutive law and the bond parameters obtained from the pull-out test result for the ETS rods epoxy-bonded to concrete blocks, the strain in the ETS FRP rods can be calculated for RC beams strengthened in shear. Assuming that the FRP rods used to strengthen RC beams in shear using the ETS method carry only normal stresses in the principal FRP material direction, the strain in the CFRP rods can be calculated using the strut-and-tie model. In this case, all the FRP rods intersected by the selected shear crack are assumed to contribute the same amount to the FRP effective strain. The effective strain, ε_{frp}, in the principal material direction is in general limited to 0.004 (ACI 440.2R 2008). The

effective strain limit for the CFRP strengthening material is based on limiting the crack opening to ensure proper aggregate interlocking of the concrete. The effective strain in the FRP rods for RC beams strengthened in shear using the ETS method can be calculated as follows:

$$\varepsilon_{frp} = \sqrt{\frac{8}{D_{frp} \cdot E_{frp}} \left(\frac{\tau_m \cdot s_m}{1+\alpha} \right)} \leq 0.004 \tag{7.8}$$

The calculated FRP strain is equal to 1893 με, 1633 με and 4254 με for RC beams strengthened with the ETS method using 9.5 mm diameter sand-coated rods, 12.7 mm diameter sand-coated rods and 9.5 mm diameter rods with plain surface, respectively.

Thus, for RC beams retrofitted using the ETS method, the FRP contribution to the shear resistance can be written in the following form:

$$V_{frp} = k_L \cdot k_S \frac{A_{frp} \cdot E_{frp} \cdot \varepsilon_{frp} \cdot d_{frp} \left(\sin\alpha + \cos\alpha \right)}{s_{frp}} \tag{7.9}$$

where A_{frp}, d_{frp}, α, and s_{frp} are the FRP rod cross-sectional area, effective shear depth (the greater of 0.72h and 0.9d), FRP rod inclination angle, and spacing between the CFRP rods respectively. Note that Eq. (9) is generalized for inclined FRP rods on the basis of analytical assumptions. In addition, k_L is a decreasing coefficient ($0 \leq k_L \leq 1$) which represents the effect of FRP rods having an anchorage length shorter than the minimum anchorage length needed (L_{eff}). The effective anchorage length coefficient (k_L) can be determined using the following equations:

$$k_L = \begin{cases} 1 & \dfrac{d_{frp}}{2} \geq L_{eff} \\[3mm] \dfrac{d_{frp}}{\sqrt{\dfrac{E_{frp} \cdot D_{frp}}{2} \cdot \dfrac{s_m}{\tau_m} \cdot \dfrac{1+\alpha}{(1-\alpha)^2}}} & \dfrac{d_{frp}}{2} < L_{eff} \end{cases} \tag{7.10}$$

Moreover, k_S accounts for the effect of the internal transverse-steel on the effective strain in the FRP rods used in the shear strengthening of RC beams using the ETS method. Until

further data are available, it is recommended that k_S be set to 0.6 for RC beams having internal transverse-steel with a spacing less than ⅔ d. For RC beams strengthened using the ETS method and which have no internal transverse steel or internal transverse steel with a spacing equal to or greater than ⅔ d, k_S can be set to 1.

Note that the proposed design model can be used for FRP-reinforced concrete beams with an appropriate choice of bond parameters. These parameters can be obtained from Cosenza et al. (1997) for FRP-reinforced concrete beams.

The experimental contribution of FRP to shear resistance (see Table 7.3) is then compared with the nominal shear resistance predicted by the proposed model. Table 7.5 presents the calculated contribution of FRP to shear resistance, V_{fcal}, and the experimental contribution, $V_{f\,exp}$, for each of the specimens. The coefficient of determination (R^2) between the calculated $V_{f\,cal}$ and the experimental $V_{f\,exp}$ is 0.93 (Figure 7.15). R^2 is equal to 0.57 when the effect of transverse steel is not considered (i.e., $k_S = 1$). This shows that the proposed equations produce reasonably accurate results compared to the experimental results. However, more experimental tests should be conducted to verify fully the soundness of the proposed equations.

Table 7.5   Calculated shear contribution of FRP, V_{fcal}, (for $k_S = 1$ and proposed k_S) versus the experimental values of V_{fexp}.

Specimen	V_{fcal} $(k_S{=}1)$, kN	V_{fcal} $(k_S{=}0.6)$, kN	V_{fexp}, kN	$\dfrac{V_{f\,exp}}{V_{f\,cal}}$
S0-12d130s	72.3	72.3	99.5	1.38
S1-9d260s	23.4	14.0	14.0	1.00
S1-12d260s	36.2	21.7	20.3	0.94
S1-12d130s	72.3	43.4	31.4	0.72
S1-9d260p	53.3	32.0	34.4	1.08
S3-12d130s	72.3	72.3	87.1	1.21
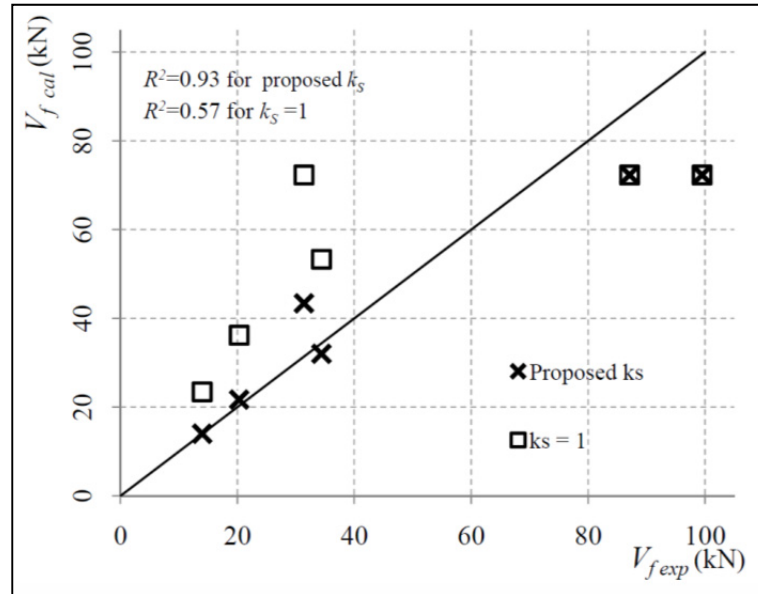
Figure 7.15   Predicted versus experimental FRP contribution for RC beam
strengthened using the ETS method.

7.7   Conclusions

This paper presents the results of an experimental investigation involving nine tests on RC T-beams strengthened in shear using the embedded through-section (ETS) method. A new design model using the BPE modified shear-slip law is proposed for calculating the shear contribution of FRP for RC beams strengthened using the ETS method. The accuracy of the proposed method has been verified using experimental results obtained in the current study. The proposed model showed a reasonable correlation with experimental results ($R^2 = 0.93$). In addition, the main findings of this research are as follows:

- the ETS FRP strengthening method has proven to be an effective way to increase the shear capacity of RC beams even in the presence of a limited amount of internal transverse-steel reinforcement. In this study, the average increase in shear capacity was 35% for specimens retrofitted using the ETS method;

- the shear contribution of FRP drastically decreased for RC beams with narrowly spaced internal steel reinforcement (series S1). The contribution of FRP to shear resistance and

the gain due to FRP were significantly greater for beams with no transverse-steel reinforcement (series S0) and with widely spaced internal steel reinforcement (series S3) compared to series S1;

- for the rods considered in this study, CFRP rods with a plain surface were more effective than sand-coated CFRP rods. The superior performance of CFRP rods with a plain surface is due to a better shear transfer between plain-finished CFRP rods and epoxy, compared to that between sand-coated CFRP rods and epoxy;

- for beams strengthened in shear using the ETS method, decreasing the CFRP rod spacing resulted in a higher contribution of FRP to shear resistance;

- beams strengthened in shear using the ETS method with a greater rod diameter achieved greater V_f values than beams with a smaller rod diameter. It can be said that the shear contribution of FRP is directly related to $D_{frp}{}^{3/2}$;

- the shear contribution of FRP and the gain due to FRP increased as the FRP rigidity ratio increased, even with the presence of narrowly spaced internal steel reinforcement;

- the FRP efficiency ratio is greater when the FRP rod diameter is decreased, the spacing between FRP rods is increased, or both. In addition, the FRP efficiency ratio is greater for beams strengthened with plain-surfaced CFRP rods than for beams strengthened with sand-coated CFRP rods.

7.7   References

American Concrete Institute (ACI) (2007). *State of the Art Report on FRP for Concrete Structures*. Report No. 440 R-07, Farmington Hills. MI.

American Concrete Institute (ACI) (2008). *Guide for the Design and Construction of Externally Bonded FRP Systems for Strengthening Concrete Structures.* Report No. 440 2R-08, Farmington Hills. MI.

Barros, J.A.O. and Dias, S.J.E. (2005). Near-surface-mounted CFRP laminates for shear strengthening of concrete beams. *Cement Concr. Compos.* 28, pp. 289–294.

Bousselham, A. and Chaallal, O. (2004). Shear strengthening reinforced concrete beams with fiber-reinforced polymer: assessment of influencing parameters and required research. *ACI Struct. J.* 101(2), pp. 219–227.

Bousselham, A. and Chaallal, O. (2008). Mechanisms of shear resistance of concrete beams strengthened in shear with externally bonded FRP. *J. Compos. Constr.* 12(5), pp. 499–512.

Chaallal, O., Nollet, M.J., and Perraton, D. (1998). Strengthening of reinforced concrete beams with externally bonded fiber-reinforced-plastic plates: design guidelines for shear and flexure. *Can. J. Civil Eng.* 25(4), pp. 692–704.

Chaallal, O., Shahawy, M., and Hassan, M. (2002). Performance of reinforced concrete T-girders strengthened in shear with CFRP fabrics. *ACI Struct. J.* 99(3), pp. 335–343.

Chaallal, O., Mofidi, A., Benmokrane, B., and Neale, K. (2011). Embedded Through-Section FRP Rod Method for Shear Strengthening of RC Beams: Performance and Comparison with Existing Techniques. *ASCE, J. of Composites for Construction.* 15(3), pp. 374-383.

Cosenza, E., Manfredi, G., and Realfonzo, R. (1997). Behaviour and modeling of bond of FRP rebars to concrete. *J. Compos. Constr.* 1(2), pp. 40–51.

Cosenza, E., Manfredi, G., and Realfonzo, R. (2002). Development length of FRP straight rebars. *Compos. Part B: Eng.* 33, pp. 493–504.

De Lorenzis, L. and Nanni, A. (2001). Shear strengthening of reinforced concrete beams with NSM fiber-reinforced polymer rods. *ACI Struct J.* 98(1), pp. 60–68.

Eligehausen, R., Popov, E.P., and Bertero. V.V. (1983). Local bond stress-slip relationships of deformed bars under generalized excitations. Report no. 83/23, EERC, University of California, Berkeley, USA.

Khalifa, A., Gold, W.J., Nanni, A., and Aziz, A. (1998). Contribution of externally bonded FRP to shear capacity of RC flexural members. *J. Compos. Constr.* 2(4), pp. 195–203.

Mofidi, A. and Chaallal, O. (2011-a). Shear strengthening of RC beams with EB FRP—influencing factors and conceptual debonding model. *J. Compos. Constr.* 15(1), pp. 62–74.

Mofidi, A. and, Chaallal, O. (2011-b). Shear Strengthening of RC Beams with Externally Bonded FRP Composites: Effect of Strip-Width to Strip-Spacing Ratio. *ASCE, J. of Composites for Construction.* 15(5), pp. 732-742.

National Cooperative Highway Research Program (NCHRP) (2008). *Bonded Repair and Retrofit of Concrete Structures Using FRP Composites.* Report No. 514, Washington. DC.

National Cooperative Highway Research Program (NCHRP) (2010). *Recommended Guide Specification for the Design of Externally Bonded FRP Systems for Repair and Strengthening of Concrete Bridge Elements.* Report No. 655, Washington. DC.

Pecce, M., Manfredi, G., Realfonzo, R., and Cosenza, E. (2002). Experimental and analytical evaluation of bond properties of GFRP bars. *J. Mater. Civil Eng.* 13(4), pp. 280–290.

Rizzo, A. and De Lorenzis, L. (2009). Behavior and capacity of RC beams strengthened in shear with NSM FRP reinforcement. *Constr. and Building Materials.* 23, pp. 1555-1567.

Triantafillou, T.C. (1998). Shear strengthening of reinforced concrete beams using epoxy-bonded FRP composites. *ACI Struct. J.* 95(2), pp. 107–115.

Uji, K. (1992). Improving shear capacity of existing reinforced concrete members by applying carbon fiber sheets. *Trans. Jpn. Concr. Institute* 14, pp. 253–266.

Valerio, P. and Ibell, T.J. (2003). Shear strengthening of existing concrete bridges. *Proc., Institution of Civil Engineers: Structures and Buildings* 156(1), pp. 75–84.

Valerio, P., Ibell, T.J., and Darby, A.P. (2009). Deep embedment of FRP for concrete shear strengthening. *Proc., Institution of Civil Engineers: Structures and Buildings* 162(5), pp. 311–321.

CONCLUSIONS AND RECOMMENDATIONS

Conclusions

This PhD program is based on experimental and analytical investigations of shear strengthening of RC beams with externally-bonded fibre-reinforced polymer strips, sheets and rods. Due to its intricacy, the shear strengthening of RC members with EB FRP still has numerous research problems that require further investigation to be entirely solved. Recent findings have revealed that major aspects related to shear strengthening with EB FRP are still not fully captured. During this PhD program these aspects were investigated experimentally and analytically as follows:

1) influencing factors and conceptual debonding model in shear strengthening of RC beams with EB FRP: The main objective of this study is to analyze the effect of the parameters that have the greatest influence on the shear behaviour of RC members strengthened with EB FRP and the role of these parameters in current design codes. A new design approach is proposed for calculating the shear contribution of FRP, taking into consideration the effect of transverse steel on the EB FRP contribution in shear. The effectiveness of the proposed method was validated using experimental results available in the literature. The result of this study is published in the journal of composites for construction of American society of civil engineering (ASCE);

2) embedded Through-Section FRP rod method for shear strengthening of RC beams: and Comparison with Existing Techniques. The Embedded Through-Section FRP Rod method presents many advantages over existing methods such EB FRP sheets and near surface mounted FRP rods (NSM FRP). Unlike EB and NSM methods where the FRP relies on the concrete cover of RC beams, in the ETS method the FRP relies on the concrete core of the RC beam which offers a greater confinement and hence improves bonding performance. The significant results of this research study are published as a journal paper to the journal of composites for construction of ASCE;

3) effect of strip-width to strip-spacing ratio in shear strengthening of RC beams with externally bonded FRP composites. This study critically reviews the available equations in current international design codes and guidelines which consider the effect of strip-width to strip-spacing of FRP strips in RC beam strengthened in shear. Current equations used in codes and guidelines to take into account the effect of strip-width to strip-spacing of FRP strips are proposed based on FRP-to-concrete direct pull-out tests on FRP strips bonded to concrete blocks. The applicability of such equations for RC beams strengthened in shear with FRP strips was not validated. The results of this study reveals that these equations do not predict well the experimental results when the strip-width to strip-spacing ratio is greater than 0.5. New equations with enhanced accuracy were proposed that consider the effect of strip-width and strip-spacing of FRP strips. To check the accuracy of the proposed equations in predicting the contribution of CFRP strips to the shear resistance of beams strengthened with CFRP strips, the results of the experimental part of this study on beams strengthened with CFRP strips were considered. The study showed that the proposed equations were superior to the design guidelines equations;

4) performance of end-anchorage systems for RC beams strengthened in shear with epoxy-bonded FRP: This part of the Ph.D program is based on experimental investigations on different anchorage methods of CFRP sheets in shear strengthening of RC beams. Debonding problem remains the main disadvantage of EB FRP sheets in shear strengthening of RC beams. This research study proposes new end-anchorage methods to prevent FRP debonding in EB FRP strengthening systems. The results of this research study are published in journal of composites for construction of ASCE;

5) tests and design equations for RC beams strengthened in shear using Embedded Through-Section Method: The effect of different variables on the shear contribution of RC beams strengthened using the ETS method was investigated in this study. The parameters of this study are: (i) the effect of the surface coating on the FRP bars; (ii) the effect of internal transverse-steel reinforcement on the FRP shear contribution; (iii) the effect of FRP bar spacing; (iv) the effect of FRP rod diameter; and (v) the

efficiency of the ETS FRP rod method. A new design model using the BPE modified shear-slip law is proposed for calculating the shear contribution of FRP for RC beams strengthened using the ETS method. The accuracy of the proposed method was validated using experimental results obtained in the current study. The results of this research study were gathered in an article that was accepted for publication in the journal of composites for construction of ASCE.

Recommendations

The results achieved on the shear strengthened RC beams using ETS FRP method are preliminary and therefore comprehensive analytical and experimental investigations are required to completely understand the behaviour of RC beams strengthened with the ETS method. As this method develops, the structural behaviour of RC beams strengthened in shear with the ETS FRP rods should be analyzed by varying the influencing parameters, including: (i) the type of FRP bars, (ii) type of adhesive used, (iii) RC beams tested under fatigue loading conditions, and (iv) RC beams considered to check the environmental effect on durability of the beams strengthened with ETS method.

Future work is required to precisely focus on those required investigations to make the highly effective ETS method for shear strengthening of RC beams a method widely used in practice.

BIBLIOGRAPHY

Adhikary, B.B., Mutsuyoshi, H. and Ashraf, M. (2004). Shear strengthening of reinforced concrete beams using fibre-reinforced polymer sheets with bonded anchorage. *ACI Struct. J.* 101(5), pp. 660–668.

American Concrete Institute (ACI) (2004). *Guide Test Methods for Fiber-Reinforced Polymers (FRPs) for Reinforcing or Strengthening Concrete Structures.* Report No. 440 3R-04, Farmington Hills MI.

American Concrete Institute (ACI) (2007). *State of the Art Report on FRP for Concrete Structures*. Report No. 440 R-07, Farmington Hills. MI.

American Concrete Institute (ACI) (2008). *Guide for the Design and Construction of Externally Bonded FRP Systems for Strengthening Concrete Structures.* Report No. 440 2R-08, Farmington Hills MI.

Al-Sulaimani, G.J., Sharif, A.M., Basunbul, I.A., Baluch, M.H. and Ghaleb, B.N. (1994). Shear repair for reinforced concrete by fibreglass plate bonding. *ACI Struct. J.* 91(3), pp. 458–464.

Araki, N., Matsuzaki, Y., Nakano, K., Kataoka, T. and Fukuyama, H. (1997). Shear capacity of retrofitted RC members with continuous fiber sheets. *Proceedings of the 3rd International Symposium on Non-Metallic (FRP) Reinforcement for Concrete Structures*, Sapporo, Japan, 14-16 Oct, 1, Japan Concrete Institute, pp. 515-522.

Barros, J.A.O. and Dias, S.J.E. (2005). Near surface mounted CFRP laminates for shear strengthening of concrete beams. *Cement Concr. Compos.* 28, pp. 289–94.

Berset, J.-D. (1992). *Strengthening of Reinforced Concrete Beams for Shear Using FRP Composites.* MSc Thesis, Department of Civil and Environmental Engineering, Massachusetts Institute of Technology, Boston MA. USA: 105 pp.

Bizindavyi, L. and Neale, K. W. (1999). Transfer lengths and bond strengths for composites bonded to concrete, *J. Compos. Constr.* 3(4), pp. 153–160.

Blaschko, M. Niedermeier, R. and Zilch, K. (1998). Bond failure modes of flexural members strengthened with FRP. *Proceedings Fibre Compos. in Infrastruct., 2nd Int. Conf. on Compos. In Infrastruct.*, Tucson. Arizona, pp. 315–327.

Bousselham, A. and Chaallal, O. (2004). Shear strengthening reinforced concrete beams with fibre-reinforced polymer: assessment of influencing parameters and required research. *ACI Struct. J.* 101(2), pp. 219–227.

Bousselham, A. and Chaallal, O. (2006a). Behavior of reinforced concrete T-beams strengthened in shear with carbon fiber-reinforced polymer—An experimental study. *ACI Struct. J.* 103(3), pp. 339–347.

Bousselham, A. and Chaallal, O. (2006b). Effect of Transverse Steel and Shear Span on the Performance of RC Beams Strengthened in Shear with CFRP. *Composites: Part B*, Elsevier, 37, pp. 37-46.

Bousselham, A. and Chaallal, O. (2008). Mechanisms of shear resistance of concrete beams strengthened in shear with externally bonded FRP. *J. Compos. Constr.* 12(5), pp. 499–512.

Brosens, K. and Van Gemert, D. (1999). Anchorage design for externally bonded carbon fibre polymer laminates, *Proceedings of the 4th International Symposium on Fibre Reinforced Polymer Reinforcement for Concrete Structures*, Baltimore, MD, pp. 635–645.

Brosens, K. (2001). Anchorage of Externally Bonded Steel Plates and CFRP Laminates for the Strengthening of Concrete Elements. PhD Dissertation, Department of Civil Engineering, Katholieke Universiteit Leuven.

CAN/CSA-S806-02 (2002). *Design and construction of building components with fibre-reinforced polymer.* Canadian Standards Association, Rexdale, Canada.

CAN/CSA-S6-06 (2006). *Canadian Highway Bridge Design Code.* Canadian Standards Association, Mississauga, Canada.

Carolin, A. and Täljsten, B. (2005-a). Theoretical study of strengthening for increased shear bearing capacity. *J. Compos. Constr.* 9(6), pp. 497–506.

Carolin, A., Taljsten, B. (2005-b). Experimental Study of Strengthening for Increased Shear Bearing Capacity. *Journal of Composites for Construction*, 9(6), pp. 488-496

Cao, S. Y., Chen, J. F., Teng, J. G., Hao, Z. and Chen, J. (2005). Debonding in RC Beams Shear Strengthened with Complete FRP Wraps. *J. Compos. Const.*, ASCE, 9(5), pp. 417-428.

Chaallal, O., Mofidi, A., Benmokrane, B. and Neale, K. (2011). Embedded Through-Section FRP Rod Method for Shear Strengthening of RC Beams: Performance and Comparison with Existing Techniques. *ASCE, J. of Composites for Construction.* 15(3), pp. 374-383.

Chaallal, O., Nollet, M.J. and Perraton, D. (1998). Strengthening of reinforced concrete beams with externally bonded fibre-reinforced-plastic plates: design guidelines for shear and flexure. *Can. J. Civil Eng.* 25(4), pp. 692–704.

Chaallal, O., Shahawy, M. and Hassan, M. (2002). Performance of reinforced concrete T-girders strengthened in shear with CFRP fabrics. *ACI Struct. J.* 99(3), pp. 335–343.

Chajes, M.J., Januszka, T.F., Mertz, D.R., Thomson, T.A. Jr. and Finch W.W. Jr. (1995). Shear strengthening of reinforced concrete beams using externally applied composite fabrics. *ACI Struct. J.* 92(3), pp. 295–303.

Chen, J.F. and Teng, J.G., (2001). Anchorage strength models for FRP and steel plates bonded to concrete. *J. Struct. Eng.* 127(7), pp. 784–791.

Chen, J.F. and Teng, J.G. (2003). Shear capacity of FRP-strengthened RC beams: FRP debonding. *Construction and Building Materials* 17(1), pp. 27–41.

Chen, G.M., Teng, J.G., Chen J.F. and Rosenboom, O.A. (2010) Interaction between steel stirrups and shear-strengthening FRP strips in RC beams. *J. Compos. Constr.* 14(5), pp. 498–509.

Ceroni, F., Pecce, M., Matthys, S. and Taerwe, L. (2008). Debonding strength and anchorage devices for reinforced concrete elements strengthened with FRP sheets. *Compos. Part B: Eng.* 39, pp. 429-441.

CIDAR (2006). *Design Guideline for RC Structures Retrofitted with FRP and Metal Plates: Beams and Slabs.* Draft 3 - submitted to Standards Australia, The University of Adelaide, Australia.

CNR-DT200 (2004). *Guidelines for Design, Execution, and Control of Strengthening Interventions by means of Fibre-Reinforced Composites.* National Research Council, Italy.

Cosenza, E., Manfredi, G. and Realfonzo, R. (1997). Behaviour and modeling of bond of FRP rebars to concrete. *J. Compos. Constr.* 1(2), pp. 40–51.

Cosenza, E., Manfredi, G. and Realfonzo, R. (2002). Development length of FRP straight rebars. *Compos. Part B: Eng.* 33, pp. 493–504.

Czaderski, C. (2002). Shear Strengthening with Prefabricated CFRP L-Shaped plates. Test Beams S1 to S6, EMPA. Report No. 116/7, Switzerland, 78 pp.

De Lorenzis, L. and Nanni, A. (2001). Shear strengthening of reinforced concrete beams with NSM fiber-reinforced polymer rods. *ACI Struct J*; 98(1), pp. 60–8.

De Lorenzis, L. and Nanni, A. (2002). Bond between near-surface mounted fiber-reinforced polymer rods and concrete in structural strengthening. *ACI Struct J*; 99(2), pp. 123–132.

De Lorenzis, L. and Teng, J.G. (2007). Near-surface mounted FRP reinforcement: An emerging technique for strengthening structures. *Composites: Part B* 38, 119– pp. 43.

Deniaud, C. and Cheng, J.J.R. (2001). Shear behavior of reinforced concrete T-beams with externally bonded fibre-reinforced polymer sheets. *ACI Struct. J.* 98(3), pp. 386– 394.

Deniaud, C. and Cheng, J.J.R. (2004). Simplified shear design method for concrete beams strengthened with fibre-reinforced polymer sheets. *J. Compos. Constr.* 8(5), pp. 425–433.

Diagana, C., Li, A., Gedalia, B. and Delmas, Y. (2003). Shear strengthening effectiveness with CFRP strips. *Engineering Structures* 25(4), pp. 507–516.

Dias, S.J.E. and Barros, J.A.O., (2008). Shear strengthening of T cross section reinforced concrete beams by near-surface mounted technique. *J. Compos. Constr.* 12(3), pp. 300–11.

Dussek, I. J., (1980). Strengthening of Bridge Beams and Similar Structures by Means of Epoxy-Resin-Bonded External Reinforcement, *Transportation Research Record* 785, *Transportation Research Board,* pp. 21-24.

Eligehausen, R., Popov, E.P. and Bertero. V.V. (1983). Local bond stress-slip relationships of deformed bars under generalized excitations. Report no. 83/23, EERC, University of California, Berkeley, USA.

Eshwar, N., Nanni, A. and Ibell, T.J. (2008). Performance of two anchor systems of externally bonded fiber-reinforced polymer laminates. *ACI Materials J.* 105(1), pp. 72–80.

fib-TG 9.3 (2001). *Externally Bonded FRP Reinforcement for RC Structures.* International Federation for Structural Concrete, Lausanne, Switzerland.

Funakawa, I., Shimono, K., Watanabe, T., Asada, S. and Ushijima, S. (1997). Experimental Study on Shear Strengtheninig with Continuous Fiber Reinforcement Sheet and Methyl Methacrylate Resin. *Proceedings of the 3rd International Symposium on Non-Metallic (FRP) Reinforcement for Concrete Structures*, Japan Concrete Institute. Sapporo, Japan, 1, pp. 491-498.

Hassan Dirar, S.M.O., Hoult, N.A., Morley, C.T. and Lees, J.M. (2006). Shear Strengthening of Precracked Reinforced Concrete Beams Using CFRP Straps. *Fédération Internationale de Béton (fib), Proceedings of the 2nd International Congress*, Naples, Italy. ID 10- pp. 70.

Hassan Dirar. S., Morley. C. and Lees. J. (2007). Effect of Effective Depth and Longitudinal Steel Ratio on the Behaviour of Precracked Reinforced Concrete T- Beams

Strengthened in Shear with CFRP Fabrics. *8ʰ International Symposium on Fiber Reinforced Polymer Reinforcement for Concrete Structures.* Patras. Greece.

Hiroyuki, Y. and Wu, Z. (1997). *Analysis of Debonding Fracture Properties of a CFS-Strengthened Member Subject to Tension.* Japan Concrete Institute, Sapporo, Japan: pp. 287–294.

Holzenkämpfer, P. (1994). *Ingenieurmodelle des Verbundes Geklebter Bewehrung für Betonbauteile.* Dissertation, TU Braunschweig, Germany.

Hsu, C.T.T., Punurai, W. and Zhang, Z. (2003). *Flexural and Shear Strengthening of RC Beams Using Carbon Fibre Reinforced Polymer Laminates.* SP 211-5, ACI, pp. 89–114.

Kamel, A.S., Elwi, A.E. and Cheng, J.J.R. (2000). Experimental study of the behavior of CFRP sheets bonded to concrete. *Proceedings, 3ʳᵈ Int. Conf. on Advanced Composite Materials for Bridges and Structures*, Canadian Society for Civil Engineering, Ottawa, pp. 61–68.

Kamiharako, A., Maruyama, K., Takada, K. and Shiomura, T. (1997). Evaluation of Shear Contribution of FRP Sheets Attached to Concrete Beams. *Proceedings of the Third International Symposium on Non-Metallic (FRP) Reinforcement for Concrete Structures*, October, 1997, 1, pp. 467-474.

Karbhari, V. M., Niu, H. and Sikorsky, C. (2006). Review and comparison of fracture mechanics-based bond strength models for FRP-strengthened structures. *J. Reinf. Plastics Compos.* 25, pp. 17.

Khalifa, A., Gold, W.J., Nanni, A. and Aziz, A. (1998). Contribution of externally bonded FRP to shear capacity of RC flexural members. *J. Compos. Constr.* 2(4), pp. 195–203.

Khalifa, A. and Nanni, A. (1999). Rehabilitation of Rectangular Simply Supported RC Beams with Shear Deficiencies Using CFRP Composites. *Construction and Building Materials*, 16(3), pp. 135-146.

Khalifa, A., Tumialian, G., Nanni, A. and Belarbi, A. (1999). Shear Strengthening of Continuous RC Beams Using Externally Bonded CFRP Sheets. SP-188, ACI, pp. 995-1008.

Khalifa, A. and Nanni, A. (2000-a). Improving shear capacity of existing RC T-section beams using CFRP composites. *Cem. Concr. Compos.* 22, pp. 165–174.

Khalifa, A., Nanni, A. and De Lorenzis, L. (2000-b). FRP composites for shear strengthening of RC beams. *Proceedings, 3rd Int. Conf. on Advanced Compos. Materials in Bridges and Structures (ACMBS)*, Ottawa, Canada, pp. 137–144.

Khalifa, A. and Nanni, A. (2002). Rehabilitation of rectangular simply supported RC beams with shear deficiencies using CFRP composites. *Constr. and Building Materials*. 16, pp. 135–146.

Khalifa, A., Nanni, A. and De Lorenzis L. (2000). FRP Composites for Shear Strengthening of RC Beams. *Proceedings of the 3rd International Conference on Advanced Composite Materials in Bridges and Structures* (ACMBS), Ottawa, Canada, pp. 137-144.

Klaiber, F.W., Dunker, K.F. ,Wipf, T.J. and Sanders, W.W.Jr. (1987). Methods of Strengthening Existing Highway Bridges, *NCHRP Research Report No. 293*, *Transportation Research Report Board*. 114 pp.

Lees, J. M., Winistöfer, A. U., Meier, U. (2002). External Prestressed Carbon Fiber-Reinforced Polymer Straps for Shear Enhancement of Concrete. *J. of Composites for Construction*, ASCE, 6(4), pp. 249-256.

Li, A., Diagana, C. And Delmas, Y. (2002). Shear Strengthening Effect by Bonded Composite on RC Beams. *Composites: Part B*, Elsevier, 33, pp. 225-239.

Li, A., Assih, J. and Delmas, Y. (2001). Shear Strengthening of RC Beams with Externally Bonded CFRP Sheets. *J. of Structural Engineering*, ASCE, 27(4), pp. 374-380.

Lima, J.L.T. and Barros, J.A.O. (2007). Design models for shear strengthening of reinforced concrete beams with externally bonded FRP composites: A statistical versus reliability approach. *Proc. 8th Int. Symp. on Fiber Reinforced Polymer Reinforcement for Concrete Structures*, Patras, Greece.

Maeda, T., Asano, Y., Sato, Y., Ueda, T. and Kakuta, Y. (1997). A study on bond mechanism of carbon fibre sheet. Maeda, T., Asano, Y., Sato, Y., Ueda, T., and Kakuta, Y. (1997). *Proc. of the 3rd Int. Symp. on Non-Metallic (FRP) Reinforcement for Concrete Structures*, Sapporo, Japan, 1, pp. 279-286.

Micelli, F., Annaiah, R.H. and Nanni, A. (2002). Strengthening of short shear span reinforced concrete T-joists with fibre-reinforced plastic composites. *J. Compos. Constr* 6(4), pp. 264–271.

Miller, B. (1999). Bond Between Carbon Fiber Reinforced Polymer Sheets and Concrete. Ma.Sc. Thesis, Department of Civil Engineering, University of Missouri, Rolla.

Ministère des Transports Québec. (2011). Pre-feasibility Study Concerning the Replacement of the Existing Champlain Bridge. *JCCBI Contract No. 61100.* Februrary 2011. 82 pp.

Mirza, S., MacGregor, J. and Hatzinikolas, M. (1979). Statistical descriptions of strength of concrete. *J. Struct. Div.* 105(6), pp. 1021–1037.

Mitsui, Y., Murakami, K0., Takeda, K. and Sakai, H. (1998). A Study on Shear Reinforcement of Reinforced Concrete Beams Externally Bonded with Carbon Fiber Sheets. *Composites Interface*, 5(4), pp. 285-295.

Miyauchi, K., Inoue, S., Nishibayashi, S. and Tanaka, Y. (1997). Shear Behaviour of Reinforced Concrete Beam Strengthenedwith CFRP Sheet. *Transactions of the Japan Concrete Institute*, Vol.19, pp. 97-104.

Mofidi A. (2008). Strengthening RC T-beams in flexure and shear using new mechanically-anchored FRP and dry fibre systems. M.A.Sc. Thesis. Concordia University, Montreal, Canada. 160 pp.

Mofidi, A. and Chaallal, O. (2011-a). Shear strengthening of RC beams with EB FRP—influencing factors and conceptual debonding model. *J. Compos. Constr.* 15(1), pp. 62–74.

Mofidi, A. and, Chaallal, O. (2011-b). Shear Strengthening of RC Beams with Externally Bonded FRP Composites: Effect of Strip-Width to Strip-Spacing Ratio. *ASCE*, *J. of Composites for Construction.* 15(5), pp. 732-742.

Monti, G., Renzelli, M. and Luciani, P. (2003). FRP Adhesion in uncracked and cracked concrete zones. *FRPRCS-6*, Singapore, pp. 183-192.

Monti, G. and Liotta, M. (2006). Tests and design equations for FRP strengthening in shear. *Construction and Building Materials* 21, pp. 799–809.

National Cooperative Highway Research Program (NCHRP) (2008). *Bonded Repair and Retrofit of Concrete Structures Using FRP Composites.* Report No. 514, Washington. DC.

National Cooperative Highway Research Program (NCHRP) (2010). *Recommended Guide Specification for the Design of Externally Bonded FRP Systems for Repair and Strengthening of Concrete Bridge Elements.* Report No. 655, Washington. DC.

Neubauer, U. and Rostásy, F.S. (1997). *Design Aspects of Concrete Structures Strengthened with Externally Bonded CFRP Plates.* ECS Publications, Edinburgh: pp. 109–118.

Pellegrino, C. and Modena, C. (2002). Fibre reinforced polymer shear strengthening of RC beams with transverse steel reinforcement. *J. Compos. Constr.* 6(2), pp. 104–111.

Pellegrino C. and Modena C. (2006). FRP shear strengthening of RC beams: experimental study and analytical modeling. *ACI Struct. J.* 103(5), pp. 720-728.

Oehlers, D.J., Seracino, R. and Smith, S.T. (2008) *Design Guideline for RC Structures Retrofitted with FRP and Metal Plates: Beams and Slabs*, HB 305-2008, Standards Australia, Sydney, Australia, ISBN 0 7337 7831 3, 73 pp.

Pecce, M., Manfredi, G., Realfonzo, R. and Cosenza, E. (2002). Experimental and analytical evaluation of bond properties of GFRP bars. *J. Mater. Civil Eng.* 13(4), pp. 280–290.

Rizzo, A. and De Lorenzis, L. (2009). Behavior and capacity of RC beams strengthened in shear with NSM FRP reinforcement. *Constr. and Building Materials.* 23, pp. 1555-1567.

Sato, Y., Ueda, T., Kakuta, Y. and Tanaka, T. (1996). Shear Reinforcing Effect of Carbon Fiber Sheet Attached to Side of Reinforced Concrete Beam. *Proceeding of the 2nd Int. Conf, on Advanced Composite Materials in Bridges*, ACMBS II, Montreal, August 1996, Ed. M.M.El-Badry. CSCE. pp. 621-637.

Sato, Y., Ueda, T., Kakuta, Y. and Ono, S. (1997). Ultimate Shear Capacity of Reinforced Concrete Beams with Carbon Fiber Sheet. *Proceedings of the 3rd International Symposium on Non-Metallic (FRP) Reinforcement for Concrete Structures*, Sapporo, Japan, 14-16 Oct, 1, Japan Concrete Institute, pp. 499-506.

Sato, Y., Katsumata, H. and Kobatake, Y. (1997). Shear strengthening of existing reinforced concrete beams by CFRP sheet. *Proc. of the 3rd Int. Symp. on Non-Metallic (FRP) Reinforcement for Concrete Structures*, Sapporo, Japan, pp. 507–514.

Schuman, P. (2004). Mechanical anchorage for shear rehabilitation of reinforced concrete structures with FRP: an appropriate design approach. Ph.D. Thesis, University of California, San Diego. 528 pp.

Taerwe, L., Khalil, H. and Matthys, S. (1997). Behaviour of RC beams strengthened in shear by external CFRP sheets. *Proceedings, 3rd Int. Symp. on Non-Metallic (FRP) Reinforcement for Concrete Structures*, Sapporo, Japan, Vol. 1, pp. 507–514.

Tanaka, T. (1996). *Shear-Resisting Mechanism of Reinforced Concrete Beams with CFS as Shear Reinforcement.* Graduation thesis, Hokkaido University, Japan.

Täljsten, B. (1997). Strengthening of concrete structures for shear with bonded CFRP fabrics. *Proceedings, US-Canada-Europe Workshop on Bridge Engineering,* organized by EMPA, Zurich, Switzerland, pp. 57–64.

Täljsten, B. (2003). Strengthening of Concrete Beams for Shear with CFRP Sheets. *Construction and Building Materials*, Elsevier, 17, pp. 15-26.

Triantafillou, T.C. (1998). Shear strengthening of reinforced concrete beams using epoxy-bonded FRP composites. *ACI Struct. J.* 95(2), pp. 107–115.

Triantafillou, T.C. and Antonopoulos, C.P. (2000). Design of concrete flexural members strengthened in shear with FRP. *J. Compos. Constr.* 4(4), pp. 198–205.

Statistics Canada, (2012) Age of Public Infrastructure: A Provincial Perspective. http://www.statcan.gc.ca/pub/11-621-m/11-621-m2008067-eng.htm. retrieved June 2012.

Uji, K. (1992). Improving shear capacity of existing reinforced concrete members by applying carbon fibre sheets. *Trans. Jpn. Concr. Institute* 14(253), pp. 66.

Umezu, K., Fujita, M., Nakai, H. and Tamaki,K. (1997). Shear Behaviour of RC Beams with Aramid Fiber Sheet. *Proceedings of the 3rd International Symposium on Non-Metallic (FRP) Reinforcement for Concrete Structures*, Sapporo, Japan, 14-16 Oct, Vol. 1, Japan Concrete Institute, pp. 491-498.

Zhang, Z., Hsu, C.-T. and Moren, J. (2004). Shear strengthening of reinforced concrete deep beams using carbon fibre reinforced polymer laminates. *J. Compos. Constr* 8(5), pp. 403–414.

Valerio, P. and Ibell, T.J. (2003). Shear strengthening of existing concrete bridges. *Proc., Institution of Civil Engineers: Structures and Buildings* 156(1), pp. 75–84.

Valerio, P., Ibell, T.J. and Darby, A.P. (2009). Deep embedment of FRP for concrete shear strengthening. *Proc., Institution of Civil Engineers: Structures and Buildings* 162(5), pp. 311–321.